ON THE DESIGN OF PLATE-SPRING MECHANISMS

Proefschrift

ter verkrijging van de graad van doctor in de
technische wetenschappen aan de Technische Hogeschool Delft,
op gezag van de Rector Magnificus,
prof.dr. J.M. Dirken,
in het openbaar te verdedigen
ten overstaan van het College van Dekanen op
dinsdag 16 april 1985 om 16.00 uur.

door

JAN VAN EIJK
werktuigkundig ingenieur
geboren te Amsterdam

Dit proefschrift is goedgekeurd door de promotor
PROF.DR. D. DE JONG

TABLE OF CONTENTS

SUMMARY

Plate-springs are construction elements with interesting properties which may be used to construct accurate guiding mechanisms. Good reproducibility of the relative motion of the parts of the mechanism may be obtained due to the lack of play and high stiffnesses in the direction of the "fixed" degrees of freedom.
These high stiffnesses will generally depend upon the magnitude of the deformations of the plate-springs and thus a limit to the maximum deflections will in many practical cases be imposed.

Apart from the different advantages of plate-spring constructions one of the main drawbacks might be the absence of a "technical infrastructure" for their application. Practical experience in the design of plate-spring mechanisms is limited and has not been documented extensively. Also the information about the behaviour of the mechanisms under influence of different loading conditions is not available, or in some instances, not easily accessible.

In this thesis additional information about the behaviour of plate-spring mechanisms will be derived. In addition this information will be combined with information obtained in previous researches in three chapters in an attempt to make it accessible for designers of plate-spring mechanisms.

To obtain additional information an elastic-line model for a plate-spring under three dimensional loading is developed in chapter 2. In chapter 3 and 4 an approximating analytical method is described which may be used to obtain solutions for the equations found from the mathematical model. Comparison of calculated and measured results, obtained with experimental set-ups discussed in chapter 8, indicated that the elastic-line model had to be extended. Two additional effects had to be considered. The first effect has been noted earlier and is related with the transition from the stress distribution as found in bending of beams to the one found in the bending of plates.
The second effect is related to the restrictions imposed by the clamped ends upon the torsional deformation of a plate-spring. This effect of the "constrained warping" of the cross-section has been incorporated into the mathematical model.

In chapter 5 to 7 the main properties of different plate-spring mechanisms is

discussed. In chapter 5 the most complete description of the effects encountered in the design of plate-spring mechanisms is given, as applied to the design of plate-spring parallel guidings. Chapter 6 contains additional information as might be used in the design of cross-spring pivots. A selection of different plate-spring applications is discussed in chapter 7. Also in this chapter a discussion about the possible advantages of the use of "reinforced" plate-spring elements in parallel guiding mechanisms.

In a separate appendix to this thesis the hysteresis in plate-spring mechanisms is briefly discussed. Generally it is considered as an advantage of plate-spring mechanisms that "almost no" hysteresis is present. To quantify the magnitude of hysteresis to be expected in these mechanisms measurement of some of the factors influencing the hysteresis have been started. The preliminary results will be discussed in Appendix A.

INDEX OF GLOBAL SYMBOLS

The main symbols used in this thesis will be defined here. Symbols used only in a single part of the text will be defined in the text.

Decimal point, Multiplication sign.

In the text the comma-sign, ",", will be used to mark the decimal point in numbers. A dot at the middle of the character line will be used as multiplication sign.

Symbol	Definition	Dimension
A	Cross-sectional area of plate-spring ($b \cdot h$)	(m^2)
a	Geometrical parameter in cross-spring pivots (fig. 6.3)	(-)
b	Width of plate-spring (fig. 1.1)	(m)
c	Stiffness	
	c_x, c_y, c_z, linear stiffness	(N/m)
	c_ψ, c_ϕ, c_θ, rotation stiffness	(Nm/rad)
E	Young's modulus	(N/m^2)
F	Force	(N)
G	Shear modulus	(N/m^2)
h	Plate-spring thickness (fig. 1.1)	(m)
$I = I_z$	Moment of inertia of the cross-sectional area of the plate-spring around the z-axis ($= \frac{1}{12} \cdot b \cdot h^3$)	(m^4)
I_x	Moment of isertia of the cross-sectional area of the plate-spring around the x-axis ($= \frac{1}{12} \cdot h \cdot b^3$)	(m^4)
J	Polar moment of inertia of the cross-sectional area of the plate-spring around the y-axis (for $b > h$ follows $J \simeq \frac{1}{3} \cdot b \cdot h^3$)	(m^4)
K_x, K_y, K_z	Compliance factors of the plate-spring cross-section ($K_x = \frac{12}{E \cdot h \cdot b^3}$, $K_y \simeq \frac{3}{G \cdot b \cdot h^3}$, $K_z = \frac{12}{E \cdot b \cdot h^3}$)	($1/Nm^2$)
L	Length of reinforced plate-spring element	(m)

ℓ	Length of elastic part of plate-spring	(m)
m	Mass	(kg)
q	Rate of reinforcement of reinforced plate-spring element (fig. 7.11)	(-)
s	Length coordinate measured along the axis of the plate-spring (fig. 2.1)	(m)
u, u(s), u(ℓ) v, v(s), v(ℓ) w, w(s), w(ℓ)	Displacements in the directions of the x, y and z-axis (fig. 2.2)	(m)
x y z	Coordinate-axes of the plate-springs (fig. 2.1)	(-)
$\psi, \psi(s), \psi(\ell)$	Rotation around the x-axis	(rad)
$\theta, \theta(s), \theta(\ell)$	Rotation around the y-axis	(rad)
$\phi, \phi(s), \phi(\ell)$	Rotation around the z-axis	(rad)
μ	Coefficient related with the effect of the constrained warping, (para. 4.5) (for plate-springs with b > h $\mu \simeq \frac{\ell}{b} \cdot \sqrt{\frac{24}{1+\nu}}$)	(-)
Γ	"Warping constant" for the plate-spring cross-section (for b > h follows $\Gamma \simeq \frac{1}{144} \cdot b^3 \cdot h^3$)	(m^6)
ν	Poisson's constant (for steel $\nu \cong$ 0,3 is used in this text)	(-)

Chapter 1

Introduction

1.1 General remarks, advantages and applications

Plate-springs are construction elements with a number of interesting properties. Two parts connected to each end of a plate-spring, figure 1.1, are rigidly connected to each other in the direction of the three "in-plane" degrees of freedom. In the remaining three degrees of freedom small relative movements may be made without exceeding the elastic stress limits of the plate-spring material. The extremely large ratios, up to 10^4 - 10^6, between the stiffnesses in the "in-plane" and "out-of-plane" directions yield interesting possibilities for the design of mechanisms.

Different combinations of plate-springs may be used to construct mechanisms. The most commonly known mechanisms are the plate-spring parallel guiding and the double symmetric orthogonal cross-spring pivot shown in figure 1.2. In these mechanisms two parts of the construction are connected by two plate-springs. Generally these two plate-springs will allow one of the two parts to move with one degree of freedom relatively to the other. As will be discussed later there will generally be one degree of freedom that is determined twice (see ch. 5).
In the mechanisms shown in figure 1.2 two plate-springs are acting parallel and one degree of freedom remains "free". Another possibility is to make constructions using two plate-springs in series. In that case only one degree of freedom is determined. Thus simple elastic shaft couplings and other mechanisms may be devised (see ch. 7).

The advantage of plate-spring mechanisms have been discussed by different authors (J1, H1, B1, Y1, etc.).
The main advantages noted are :

* Relative motion is performed without any sliding or rolling contacts. This results in a lack of friction and wear.

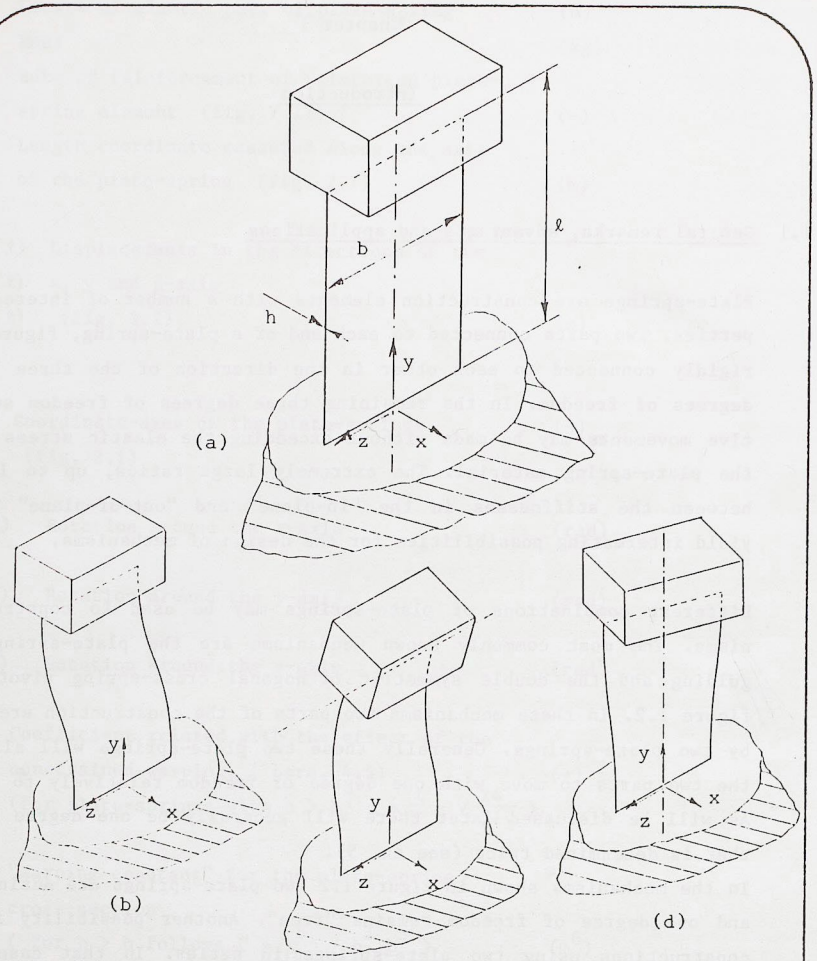

Figure 1.1.

A plate-spring fixes the relative motion of its two clamped ends in three of the degrees of freedom with relatively high stiffness. In the remaining three degrees of freedom limited displacements of the ends can be made. These displacements may be described as,

(b) - Linear motion in the direction of the x-axis

(c) - Rotation around an axis parallel to the z-axis and located in the plane of the plate-spring and

(d) - Rotation around an axis parallel to the y-axis and located in the plane of the plate-spring.

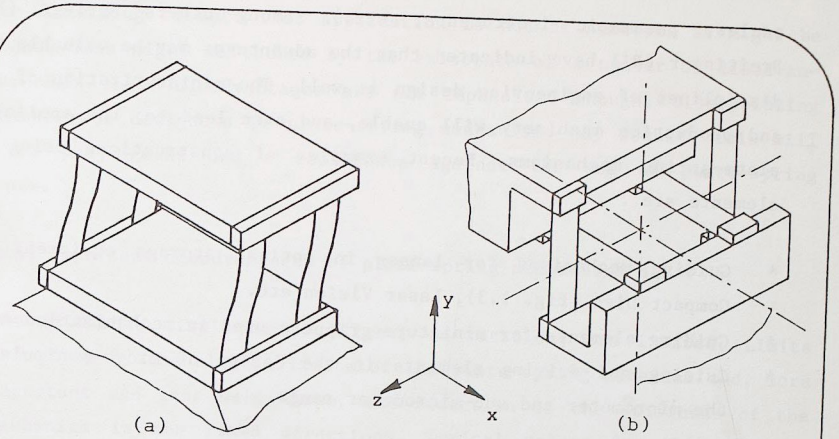

Figure 1.2

Two of the most well known plate-spring mechanisms are the plate-spring parallel guiding (a) and the cross-spring pivot (b). In these mechanisms the deformation of the plate-springs is restricted to bending around axes parallel to the z-axis. Therefore every point of the mechanisms will move in a plane parallel to the x-y-planes of the plate-springs. The x-y-plane is therefore called "the plane-of-motion".

* The two parts to be connected are solidly connected in the degrees of freedom which are to be fixed. This results in a total absence of "play" and high stiffnesses in these directions. Together these two facts lead to a highly reproducible movement of the two parts relative to each other.
* Plate-spring mechanisms are highly insensitive to the influence of dust, moisture, heat and other environmental conditions.
* To obtain a certain displacement a force should be applied and this opens the possibility to use the plate-springs both as a guiding and as a measuring element.
* Accurate guiding mechanisms may be produced without expensive parts or production processes.

These advantages have been used extensively in the field of instrument design. The reproducible motion is used to guide elements, such as optical parts, relative to each other. The lack of friction and the small magnitude of the hysteresis is used to guide parts in measuring devices (weighing

scales, pneumatic instruments, etc.). Among others Haringx (H1) and Breitinger (B1) have indicated that the advantages may be valuable in other disciplines of engineering design as well. The miniaturization of products and production machinery will enable, and even lead to, the application of plate-spring mechanisms. Recent examples of constructions using elastic elements are :

* Guiding mechanisms for lenses in optical storage equipment such as Compact Disc (fig. 1.3), Laser Vision etc.
* Guiding elements for miniature grippers used in mechanisation machines.
* Guiding and driving elements in the design of micro-manipulators for the micrometer and sub-micrometer range.

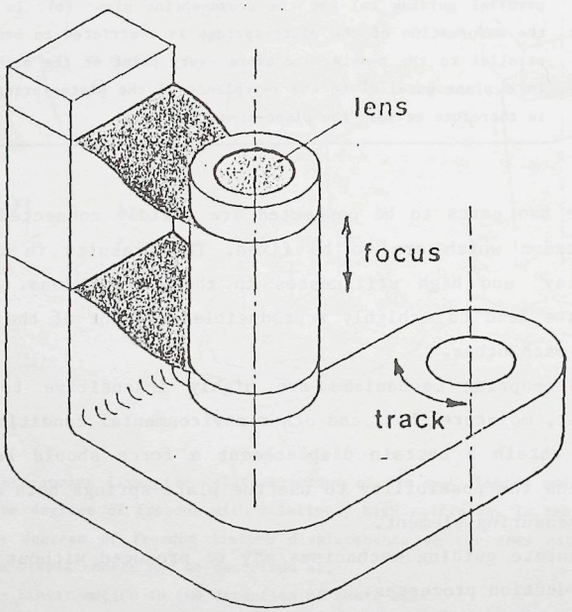

Figure 1.3

An example of application of a plate-spring parallel guiding is found in Philips' Compact Disc player.Here plate-springs are used to connect the lens body with the track-following mechanism.

It is surprising to note that application is not as numerous as might be expected. This might be caused by the existence of a number of disadvantages. When these disadvantages are not emphasized enough, disappointing experiences of designers of plate-spring mechanisms may result. This will lead to prejudgment and a resistance against the use of plate-spring elements.

The most important disadvantages of plate-spring mechanisms are :

* The allowable displacements, linear or rotation, are limited. Limits are given by the elastic limits of the plate-spring material and, more important and less well known, the reduction of the stiffness of the mechanism in the fixed directions. Typical values for the range of displacements are ± 0,2 rad for rotations and ± 10 mm for translations.

* To maintain a certain displacement a driving force should be applied. In some mechanisms such a force might be undesirable, in other cases the force may be considered to be an advantage. Different possibilities exist to reduce the magnitude of the driving force (D1, E1), but such solutions are only used in special applications (W2).

* The relative movement prescribed by the plate-springs will in general not be a pure rotation or translation of the two parts.

* In plate-spring guiding mechanisms as shown in figure 1.2 one degree of freedom is overdetermined. Upon assembly or during the lifetime the two plate-springs may apply internal loads to each other. Due to these unknown and unpredictable stresses the behaviour of the mechanism may be unpredictable, or time and temperature dependent.
  Once the existence of this over-determination of the one degree of freedom is recognized relatively simple methods are available to avoid the internal stresses (see also ch. 5 and 6).

* For the design of plate-spring mechanisms there exists no "technical infra-structure". Therefore designers will first invent a solution to their problem, using conventional elements, that satisfies an assumed set of requirements. Attempts to introduce plate-spring elements afterwards are generally in vain due to the different geometrical requirements. When the use of plate-springs would have been considered at an

early stage in the design process their application might have been an advantage.
Another result of the lacking "infra-structure" is the limited experience and know-how about reliable and simple methods to connect plate-spring to machine parts. The presence of dead-lines in the design process will thus favour the use of conventional solutions.

* The behaviour of plate-spring elements is not generally known. Different authors have studied the behaviour in different respects. The results are however not always easily accessible for designers.

The first two disadvantages are elementary. The second one will be a drawback only in special cases. The existence of the remaining disadvantages may be considered as problems to be solved. Time and effort should be dedicated to the development of a "technical infra-structure". The information about the behaviour of plate-spring mechanisms may be collected, additional information may be searched for and a translation of the information to a form easily accessible and easily used by designers may be made.
In the following it will be attempted to contribute to the solution of these problems. Main attention will be given to the summarizing and the supplementing of the available information about the behaviour of plate-spring mechanisms. This will be discussed in chapter 2, 3 and 4. In the chapter 5, 6 and 7 information for designers will be given.

1.2 Aim and scope of present work

Previous research about plate-spring mechanisms has been directed to the analysis of the behaviour of the plate-springs under loading in the x-y-plane. For the mechanisms shown in figure 1.2 this plane is called the "plane-of motion". Every point of the mechanism moves in a plane parallel to the x-y-planes of the two plate-springs. The deformations considered in these researches are restricted to bending of the plate-springs around the z-axis.

In first instance the results of such researches are :

* The stiffness of the guiding mechanism in the desired direction of motion.
* The maximum value of the bending stresses at a certain deflection in the mechanism.

These results could be obtained with a linearized form of the differential equation which may be used to describe the bending of long and slender beams. They are only valid for relatively small displacements.
The next parameter of interest is the loading capacity of the guiding mechanism. To estimate this the buckling load of long slender beams loaded in the plane-of-motion was calculated.

As the guiding mechanisms were mainly used in measuring instruments the non-linearity of the force-displacement relation and the accurate description of the relative motion of the two parts of the mechanisms were important characteristics. The linear theory had to be abandonned and different ways to solve the non-linear equations were developed (for a brief review, see para. 3.2). The results obtained from investigations with regard to a single plate-spring are ,

* Description of the geometrical non-linearity in the force-displacement characteristics at relatively large displacements.
* Expressions for the stiffness of deformed plate-springs in the direction of the y-axis.

With regard to the behaviour of mechanisms information about the relative movement of the two parts of the mechanism was obtained.

These results were all derived using an "elastic-line" model for the plate-springs. Basically this model is known from general theory about elastic deformation described by Love, Kirchhoff, Kelvin and others in the nineteenth century (lit. L1). Applications of these theories to plate-spring mechanisms were reported by, (among others), Eastman (1937, E1), Young (1944, Y1), Haringx (1949, H1), Hasselmeier (1954, H2), Lotze (1964, L2) and Zenov (1970, Z1). More recently Dijksman (1979, D1) has developed a non-linear analysis of cross-spring pivots.

Apart from the theoretical observations about plate-spring mechanisms different authors have attempted to describe practical applications. An interesting summary of possibilities to make practical and impractical mechanisms was given by Breitinger (1976,B1). His description is restricted to qualitative remarks only.

Although information about relatively large deflections is derived by different authors the deflection in practical applications of plate-springs in guiding mechanisms is relatively small. Only for small deflections the advantages of plate-springs (reproducible motion, high stiffness) are fully utilized. This is illustrated in figure 1.4 where the ratio between the stiffness c_y and c_x of a plate-spring used in a parallel guiding is shown as a function of the relative displacement of the guiding. In this thesis it will generally be assumed that the plate-spring deflections are relatively small.

It may be concluded that all previous publications are based upon observations about the "elastic-line" model for the plate-spring and are restricted to loading forces in the plane-of-motion. For practical applications this model may prove to be insufficient.
Dijksman (D1) for instance noted that a considerable contribution to the non-linearity in the force-displacement characteristics may be expected when the plate-spring is considered as a plate with a finite width. Unfortunately he does not quantify this effect in his analysis and only describes the magnitude of the geometrical non-linearity.

In applications of plate-spring mechanisms it is also not practical to assume that loading forces are restricted to act in one plane. Loading forces and moments in the other directions will also influence the behaviour of the mechanisms. In such cases other deformations in the plate-springs, such as shear , bending around the x-axis and torsion around the y-axis should be taken into consideration.

In this work it has been attempted to summarize the relevant information known from earlier research and to derive additional information that may be considered necessary for the design of mechanisms. Two separate parts in this work may therefore be distinguished,

* One part describes the development of a mathematical model describing

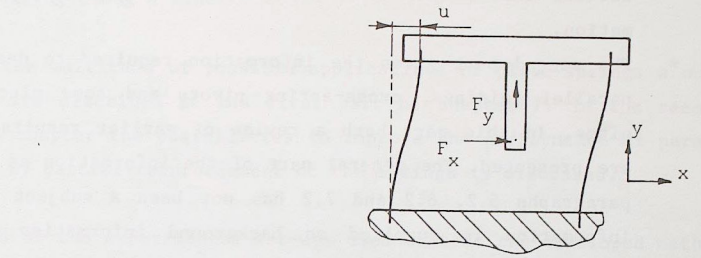

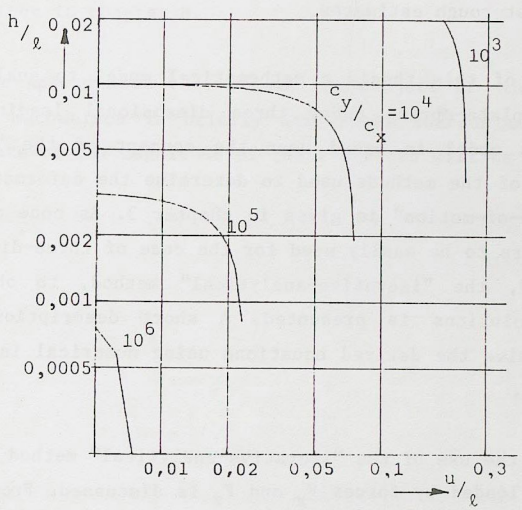

Figure 1.4

One of the advantages of plate-spring mechanisms is the large ratio between driving (c_x) and guiding stiffnesses. The ratio between c_y and c_x for a plate-spring parallel guiding is given by

$$\frac{c_y}{c_x} = \frac{\ell^2}{h^2 + \frac{12}{700} \cdot u^2}$$

which relation is derived in chapter 5. From this expression it is clear that a large ratio, for instance more than 10^4, is only obtainable for small deflections u of the mechanism. Therefore application of plate-spring mechanisms is restricted to relatively small displacements.
In the graph the relation between $\frac{u}{\ell}$ and $\frac{h}{\ell}$ needed to obtain a certain stiffness ratio is shown.

the deformations of plate-springs under three-dimensional loading conditions This model is subsequently used to derive the desired information.

* The second part gives the information required to design plate-spring parallel guidings, cross-spring pivots and some miscellaneous mechanisms. In this part both a review of earlier results and new results are presented. The general part of the information as presented in the paragraphs 5.2, 6.2 and 7.2 has not been a subject of research. The information is supplied as background information usefull for the design of plate-spring mechanisms. The expressions given in these parts may be just rough estimates.

In chapter 2 of this thesis a mathematical model to analyse the deformations of a plate-spring under three dimensional loading conditions is derived. This model is based upon the concept of the "elastic-line". A short review of the methods used to determine the deformations under loads in the "plane-of-motion" is given in chapter 3. As none of the analytical methods appears to be easily used for the case of three-dimensional loading a new method, the "iterative-analytical" method, to obtain approximate analytical solutions is presented. A short description of a computer program to solve the derived equations using numerical integration techniques is given.

In chapter 4 the use of the "iterative-analytical" method for the case of a plate-spring loaded by forces F_x and F_z is discussed. From results of measurements it proves that the elastic-line concept is not adequate to describe the main charasteristics of the plate-springs. An improved model taking into account the effects of the warping of the cross-section is developed in this chapter.

Application of the results of this analysis to the case of plate-spring parallel guidings is described extensively in chapter 5. In the same chapter relevant information about parallel guidings is given. In this chapter almost all theoretical aspects about the behaviour of plate-spring mechanisms are discussed and, where needed, compared with results from measurements.

In chapter 6 the main characteristics of cross-spring pivots are discussed. The kinematic motion of the two parts of the mechanism relative to each other is described in second-order approximation using the equivalent model of a wheel rolling along a line.

To indicate the multitude of possible applications of plate-springs a number of them are described in the first part of chapter 7. In the second half of this chapter the posibilities to improve the performance of parallel guidings by partial reinforcement of the springs is discussed.

A description of the experimental set-ups used to test the developed mathematical models and of a number of important factors in the design of these set-ups is given in chapter 8.

In a separate Appendix to this thesis the subject of static hysteresis in plate-spring mechanisms is briefly discussed. Sources of this hysteresis and an estimate of the magnitude of their effects will be indicated.

Chapter 2

Derivation of a general set of equations.

2.1 Introduction.

To obtain a set of equations that determine the deformations of plate-springs they may be treated as long thin rods. In this case it is assumed that only deformations due to bending and torsion need to be considered. It is assumed that the stress distribution in a cross-section is a superposition of the stress-distributions due to the pure bending of the central line about two axis and due to pure torsion about the central-line. In this case the stress at the central-line will be equal to zero and the central-line is also referred to as "neutral-line".

In this approach the plate-spring with its rectangular cross-section is represented only by its central-line having two bending and one torsion stiffness. Therefore this approach is also referred to as the "elastic-line"-concept.

The following assumptions will be made in this analysis.

- The center line is considered to be inextensible. Deformations due to transverse shear will not be taken into account.
- As a generalization of the "Bernoulli-hypothesis" it will be assumed that linear relations exist between the bending and torsion moments and the respective curvatures and twist of the plate-spring.
- The deformations will be restricted in order to avoid stress levels above the elastic limit of the material.

These assumptions are justified in most applications of plate-spring mechanisms. In general they allow for a good approximation of the first order effects. However there will be deviations between theory and measurement due to a number of additional effects. Such effects, which will be discussed in more detail in following chapters, are,

- Non-linearities in the relations between the moments and curvature and twist which may occur due to transition from plane-strain to plane-

stress bending or due to the constrained warping of the cross-section of the plate-spring.

- Additional stress components due to the influence of clamping and loading of the plate-spring. The assumption about the stress distribution is valid "at a distance" from points of clamping or loading. In the neighbourhood of such places a more detailed analysis may be required.

As a result the equations developed in the rest of this chapter offer a good approximation of the deformations of loaded plate-springs when the loads remain sufficiently small and when the length of the plate spring is sufficiently large to allow for neglecting the end-effects.

2.2 Selection of coordinate systems.

To determine the deformations of a plate-spring clamped at one end and loaded at the other end a general set of equations will be developed. To describe the position of the plate-spring an orthogonal coordinate system with its origin at the clamped end and the y-axis along the center-line of the, originally straight, plate-spring will be used. The remaining axes are directed along the principal axes of the cross-section.

In figure 2.1 this coordinate-system and the line-coordinate s along the center-line are indicated. At the free end the plate-spring is loaded by a force and a torque which can be developed in components along the three coordinate-axes. The force components are F_x, F_y, and F_z respectively, while the torque components are M_x, M_y and M_z.

When the plate-spring is deformed the position and orientation of a cross-section at a distance s from the clamped end can be described by six parameters. The position of the center of the cross-section is determined by the displacements u, v and w in the directions of the x, y and z-axis. For the orientation a set of three angular coordinates can be used to describe the rotations of a local orthogonal coordinate system. This local coordinate system has its origin at the center of the cross-section, the y-axis along the tangent to the center-line and x- and z-axis along the principal axes of the cross-section.

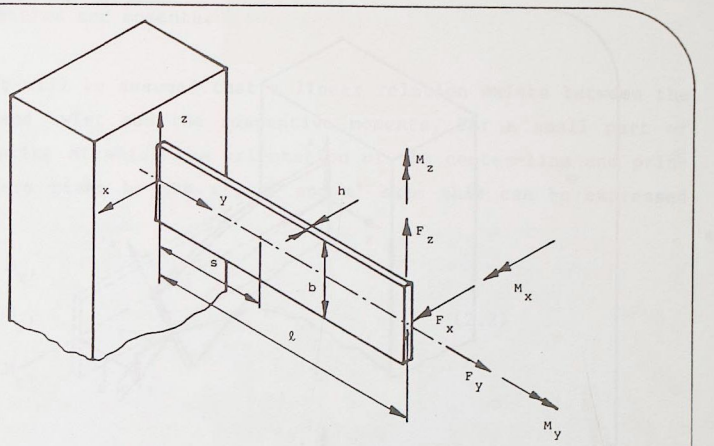

Figure 2.1 Selection of the fixed coordinate system with the origin at the clamped end. The y-axis coincides with the undeformed center-line and the x- and z-axes with the principal axes of the cross-section. The definitions of the positive directions of the loading components and the dimensions of the plate-spring are indicated.

Different definitions of the angular coordinates have been proposed. For plate-spring mechanisms where angular deformations are moderately large (less than one radian) the modified angular coordinates as suggested by Euler can be used. The definitions of the angular coordinates, ψ, θ and ϕ are given in figure 2.2.

The definitions of the angular coordinates allow for the transformation of a vector $\underline{r}$ in the original coordinate system to a vector $\underline{r}'$ in the new coordinate system. The total transformation matrix for the orientation of the orthogonal axes is a result of multiplying the three transformation matrices for each rotation indicated in figure 2.2. This results in:

$$\underline{r}' = \begin{bmatrix} x' \\ y' \\ z' \end{bmatrix} = \begin{bmatrix} 1 & 0 & 0 \\ 0 & \cos\psi & \sin\psi \\ 0 & -\sin\psi & \cos\psi \end{bmatrix} \cdot \begin{bmatrix} \cos\theta & 0 & -\sin\theta \\ 0 & 1 & 0 \\ \sin\theta & 0 & \cos\theta \end{bmatrix} \cdot \begin{bmatrix} \cos\phi & \sin\phi & 0 \\ -\sin\phi & \cos\phi & 0 \\ 0 & 0 & 1 \end{bmatrix} \cdot \begin{bmatrix} x \\ y \\ z \end{bmatrix} =$$

$$= R \cdot \underline{r} \qquad (2.1)$$

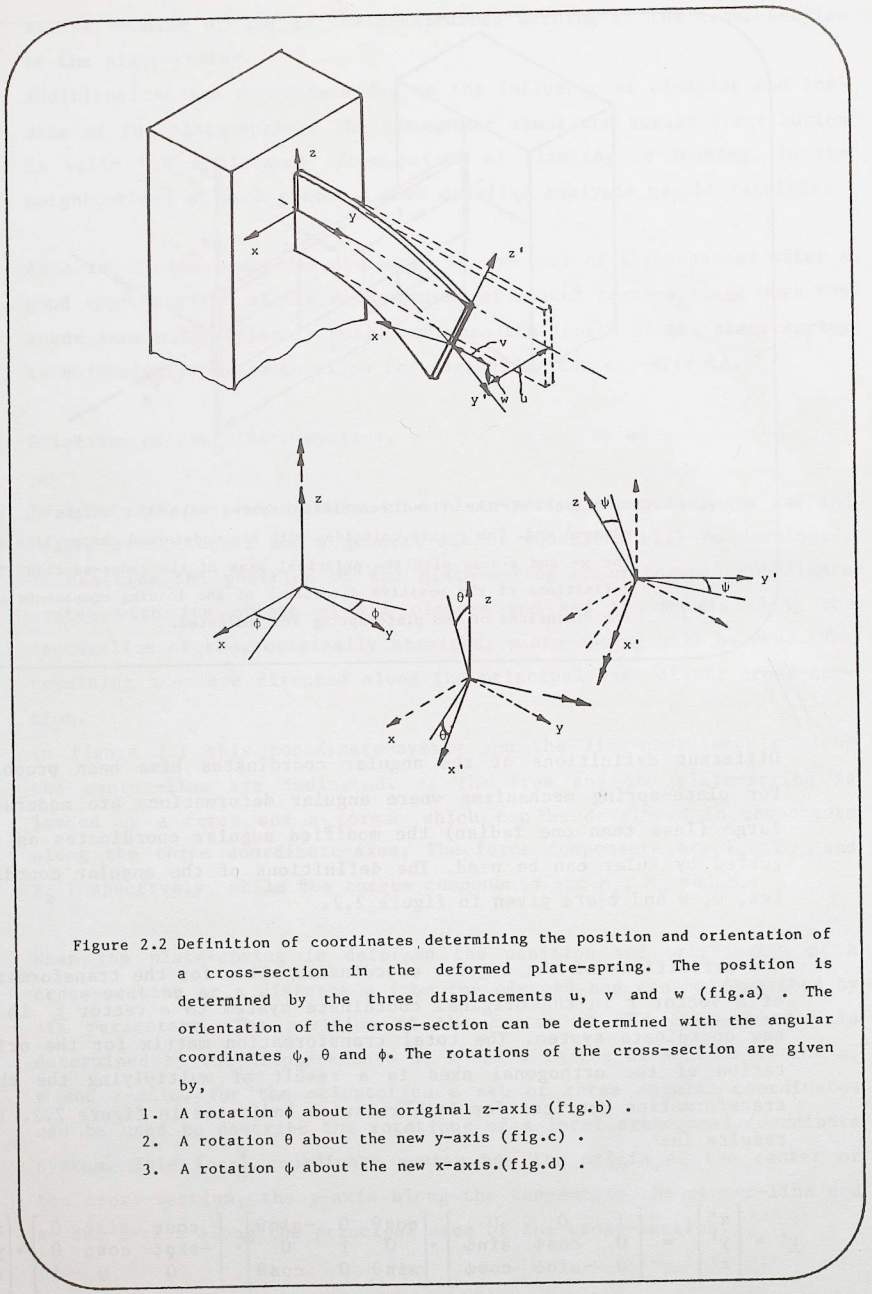

Figure 2.2 Definition of coordinates determining the position and orientation of a cross-section in the deformed plate-spring. The position is determined by the three displacements u, v and w (fig.a) . The orientation of the cross-section can be determined with the angular coordinates ψ, θ and ϕ. The rotations of the cross-section are given by,

1. A rotation ϕ about the original z-axis (fig.b) .
2. A rotation θ about the new y-axis (fig.c) .
3. A rotation ψ about the new x-axis.(fig.d) .

2.3 Global curvatures and moments.

As stated it will be assumed that a linear relation exists between the curvatures and twist and the respective moments. For a small part of the plate-spring of which the orientation of the center-line and principal axes are given by the x', y' and z' axes this can be expressed as:

$$\begin{aligned} \kappa_{x'} &= K_x \cdot M_{x'} \\ \kappa_{y'} &= K_y \cdot M_{y'} \\ \kappa_{z'} &= K_z \cdot M_{z'} \end{aligned} \qquad (2.2)$$

where $\kappa_{x'}$ and $\kappa_{z'}$ are the curvatures about x' and z'-axes. $\kappa_{y'}$ is the twist about the center-line. $M_{x'}$, $M_{y'}$ and $M_{z'}$ are the applied moments about the axes x', y' and z'. The coefficients K_x, K_y and K_z are the compliance factors which are determined by the dimensions of the cross-section and the properties of the material.

The expressions (2.2) relate the local curvatures and twist of the beam to the applied torque decomposed into components about the local axes. The shape of a deformed plate-spring will, however, be described with respect to the fixed, or global, system of coordinates. Similarly the loading forces will generally be specified with respect to the fixed system of coordinates as shown in figure 2.1.

An expression relating global curvatures to global moments can be derived from equation (2.2). Therefore it is usefull to write (2.2) in the form of a matrix equation,

$$\underline{\kappa}' = \begin{bmatrix} \kappa_{x'} \\ \kappa_{y'} \\ \kappa_{z'} \end{bmatrix} = \begin{bmatrix} K_x & 0 & 0 \\ 0 & K_y & 0 \\ 0 & 0 & K_z \end{bmatrix} \cdot \begin{bmatrix} M_{x'} \\ M_{y'} \\ M_{z'} \end{bmatrix} = K \cdot \underline{M}' \qquad (2.3)$$

In this expression $\underline{M}'$ is the torque-vector with respect to the local system of coordinates. Transformation of this vector to the global system is easily achieved with the transformation expressions specified

in equation (2.1). This yields,

$$\underline{\kappa}' = K \cdot R \cdot \underline{M} \qquad (2.4)$$

Transformation of the vector κ' to expressions containing the derivatives of the angular coordinates is not as simple. The rotation axis for ψ , θ and ϕ are not orthogonal and correct expressions can be obtained mathematically (lit. B2, L1) or can be taken from figure 2.3. From figure 2.3. follows

$$\underline{\kappa}' = \begin{bmatrix} \kappa_{x'} \\ \kappa_{y'} \\ \kappa_{z'} \end{bmatrix} = \begin{bmatrix} 1 & 0 & -\sin\theta \\ 0 & \cos\psi & \sin\psi.\cos\theta \\ 0 & -\sin\psi & \cos\psi.\cos\theta \end{bmatrix} \cdot \begin{bmatrix} \frac{d\psi}{ds} \\ \frac{d\theta}{ds} \\ \frac{d\phi}{ds} \end{bmatrix} = R' \cdot \begin{bmatrix} \frac{d\psi}{ds} \\ \frac{d\theta}{ds} \\ \frac{d\phi}{ds} \end{bmatrix} \qquad (2.5)$$

From (2.4) and (2.5) a set of equations relating the global curvatures and torques is obtained as

$$\begin{bmatrix} \frac{d\psi}{ds} \\ \frac{d\theta}{ds} \\ \frac{d\phi}{ds} \end{bmatrix} = R'^{-1} \cdot K \cdot R \cdot \underline{M} \qquad (2.6)$$

With the known matrices R', K and R solutions for ψ , θ and ϕ as functions of the coordinate s may be obtained by integration when the loading vector $\underline{M}$ is known as function of s.

2.4 Relation between end-loads and local moments.

For an end-loaded plate-spring an expression for the three moments at a cross-section at s can be obtained with the help of the equilibrium equations for the part of the plate-spring between s and the end. From figures 2.1 and 2.2 the following expressions are obtained:

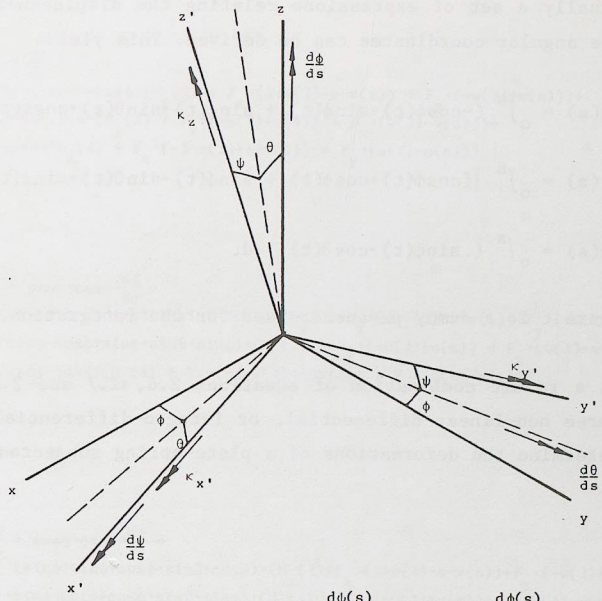

$$\kappa_{x'} = \frac{d\psi(s)}{ds} - \sin\theta(s) \cdot \frac{d\phi(s)}{ds}$$

$$\kappa_{y'} = \cos\psi(s) \cdot \frac{d\theta(s)}{ds} + \cos\theta(s) \cdot \sin\psi(s) \cdot \frac{d\phi(s)}{ds}$$

$$\kappa_{z'} = -\sin\psi(s) \cdot \frac{d\theta(s)}{ds} + \cos\theta(s) \cdot \cos\psi(s) \cdot \frac{d\phi(s)}{ds}$$

Figure 2.3. The local curvatures and the twist, $\kappa_{x'}$, $\kappa_{z'}$ and $\kappa_{y'}$,can be expressed in terms of the derivatives of the angular coordinates. These equations can be directly derived from the drawing or may be obtained along formal mathematical lines (lit.B2)

$$M_x(s) = M_x(\ell) + F_z \cdot (\ell + v(\ell) - s - v(s)) + F_y \cdot (-w(\ell) + w(s))$$
$$M_y(s) = M_y(\ell) + F_z \cdot (-u(\ell) + u(s)) + F_x \cdot (w(\ell) - w(s)) \qquad (2.7)$$
$$M_z(s) = M_z(\ell) + F_x \cdot (-\ell - v(\ell) + s + v(s)) + F_y \cdot (u(\ell) - u(s))$$

Finally a set of expressions relating the displacements u, v and w to the angular coordinates can be derived. This yields

$$u(s) = \int_0^s (-\cos\psi(t) \cdot \sin\phi(t) + \sin\psi(t) \cdot \sin\theta(t) \cdot \cos\phi(t)) \cdot dt$$

$$v(s) = \int_0^s \{(\cos\psi(t) \cdot \cos\phi(t) + \sin\psi(t) \cdot \sin\theta(t) \cdot \sin\phi(t)) - 1\} \cdot dt$$

$$w(s) = \int_0^s (\sin\psi(t) \cdot \cos\theta(t)) \cdot dt \qquad (2.8)$$

where t is a dummy parameter used for the integration.

As a result combination of equations 2.6, 2.7 and 2.8 yields a set of three non-linear differential, or integro-differential, equations which determine the deformations of a plate-spring subjected to end loads.

2.5 Conclusion.

The analysis given in this chapter leads to a set of equations that describe the behaviour of a plate-spring under end-loads. Each of the three equations is a second-order non-linear differential equation. The boundary conditions needed to solve the equations are available at two different places and the three equations are strongly coupled. The total set of equations is shown in figure 2.4. For such a set of equations no general analytical solution has yet been obtained.
A set of equations as shown in figure 2.4 may be solved with numerical techniques for different combinations of loading forces. Due to the triple boundary value problem a rather complex computing program will be required while a thorough understanding of the behaviour of the plate-spring will be needed to devise a suitable iteration strategy. Examples of the use of numerical techniques to solve the equations will

$$\frac{d\psi}{ds} - \sin\theta \cdot \frac{d\phi}{ds} =$$
$$= K_x \cdot \{ \cos\theta \cdot \cos\phi \cdot (M_x(\ell) + F_z \cdot (\ell + v(\ell) - s - v(s)) + F_y \cdot (-w(\ell) + w(s))) +$$
$$+ \cos\theta \cdot \sin\phi \cdot (M_y(\ell) + F_z \cdot (-u(\ell) + u(s)) + F_x \cdot (w(\ell) - w(s))) +$$
$$- \sin\theta \cdot (M_z(\ell) + F_x \cdot (-\ell - v(\ell) + s + v(s)) + F_y \cdot (u(\ell) - u(s))) \}$$

$$\cos\psi \cdot \frac{d\theta}{ds} + \sin\psi \cdot \cos\theta \cdot \frac{d\phi}{ds} =$$
$$= K_y \cdot \{ (-\cos\psi \cdot \sin\phi + \sin\psi \cdot \sin\theta \cdot \cos\phi) \cdot (M_x(\ell) + F_z \cdot (\ell + v(\ell) - s - v(s)) + F_y \cdot (-w(\ell) + w(s))) +$$
$$+ (\cos\psi \cdot \cos\phi + \sin\psi \cdot \sin\theta \cdot \sin\phi) \cdot (M_y(\ell) + F_z \cdot (-u(\ell) + u(s)) + F_x \cdot (w(\ell) - w(s))) +$$
$$+ \sin\psi \cdot \cos\theta \cdot (M_z(\ell) + F_x \cdot (-\ell - v(\ell) + s + v(s)) + F_y \cdot (u(\ell) - u(s))) \}$$

$$-\sin\psi \cdot \frac{d\theta}{ds} + \cos\psi \cdot \cos\theta \cdot \frac{d\phi}{ds} =$$
$$= K_z \cdot \{ (\sin\psi \cdot \sin\phi + \cos\psi \cdot \sin\theta \cdot \cos\phi) \cdot (M_x(\ell) + F_z \cdot (\ell + v(\ell) - s - v(s)) + F_y \cdot (-w(\ell) + w(s))) +$$
$$+ (-\sin\psi \cdot \cos\phi + \cos\psi \cdot \sin\theta \cdot \sin\phi) \cdot (M_y(\ell) + F_z \cdot (-u(\ell) + u(s)) + F_x \cdot (w(\ell) - w(s))) +$$
$$+ (\cos\psi \cdot \cos\theta) \cdot (M_z(\ell) + F_x \cdot (-\ell - v(\ell) + s + v(s)) + F_y \cdot (u(\ell) - u(s))) \}$$

$$u(s) = \int_0^s (-\cos\psi \cdot \sin\phi + \sin\psi \cdot \sin\theta \cdot \cos\phi) \cdot dt$$
$$v(s) = \int_0^s (\cos\psi \cdot \cos\phi + \sin\psi \cdot \sin\theta \cdot \sin\phi - 1) \cdot dt$$
$$w(s) = \int_0^s (\sin\psi \cdot \cos\theta) \cdot dt$$

Figure 2.4 Total set of equations relating the angular coordinates and displacements to the end loads applied to the plate-spring.

be given in chapters 3 and 4.

Another way to use the general equations is to attempt to simplify them in a way suitable for the loading case under investigation. The simplified form that has been studied most intensively is the one where loads are only applied in a plane through the center-line and one of the principal axis. In such a case only pure bending around the z-axis occurs. The relevant equations for this case are:

$$\frac{d\phi}{ds} = K_z \cdot \{ M_z + F_x \cdot(-\ell - v(\ell) + s + v(s)) + F_y \cdot(u(\ell) - u(s)) \}$$

$$u(s) = \int_0^s -\sin\phi(t) \cdot dt \quad \text{and} \quad v(s) = \int_0^s (\cos\phi(t) - 1) \cdot dt \qquad (2.9)$$

These equations can be differentiated with respect to s yielding

$$\frac{d^2\phi(s)}{ds^2} = K_z \cdot \{ -F_x \cdot\cos\phi + F_y \cdot\sin\phi \}$$

$$\text{with} \quad \frac{d\phi(\ell)}{ds} = K_z \cdot M_z \qquad (2.10)$$

These two forms of expressions for the deformation of a plate-spring loaded in its "plane of motion" have been used extensively. In chapter 3 a glossary of analyzing methods and a new suggestion to obtain approximate solutions will be presented.

In chapter 4 solutions of simplified forms of the general equations will be obtained. It will be shown that loading forces perpendicular to the "plane of motion" have considerable influence on the properties of plate-spring mechanisms.

Finally it must be emphasized that the obtained equations are just approximations. Their derivation has been based upon the elastic line concept, a number of assumptions which restrict their applicability. In the following chapters some examples of additional effects will be discussed. It will be attempted to obtain additional expressions to incorporate such effects in the calculations.

Chapter 3.

Deformations in the plane of loading.

3.1 Introduction.

When a plate-spring, clamped at one end, is loaded at its free end by forces in the x-y-plane its deformation can be described with the following equations :

$$\frac{d\phi(s)}{ds} = K_z \cdot(-F_x \cdot(\ell + v(\ell) - s - v(s)) + F_y \cdot(u(\ell) - u(s)) + M_z(\ell)$$

$$u(s) = \int_0^s \sin\phi(t) \cdot dt \qquad v(s) = \int_0^s (1 - \cos\phi(t)) \cdot dt \qquad (3.1)$$

which were derived in chapter 2. In order to determine the behaviour of plate-spring mechanisms solutions for this equation have to be obtained. Many different methods to obtain solutions have been developed. In many cases equation (3.1) is differentiated with respect to the arc length s to obtain the following equations:

$$\frac{d^2\phi(s)}{ds^2} = K_z \cdot (-F_x \cdot \cos\phi(s) + F_y \cdot \sin\phi(s))$$

$$\left\{ \frac{d\phi(s)}{ds} \right\}_{s=\ell} = K_z \cdot M_z \qquad (3.2)$$

Due to the absence of the displacements u and v these equations allow for somewhat simpler solutions.

A review of different methods for solution will be given in the following section. As most of the analytical methods do not enable simple application to the general case of three-dimensional loading another approach will be developed in section 3.3.

All methods described are based upon the assumption that the compliance factor, K_z, is independent of the curvature of the plate-spring. The magnitude of K_z is determined by the Young's modulus, E, of the material and the dimensions of the cross-section, b and h. Two relations for K_z are in use. When the width, b, is much larger than the thickness, h, the plate-spring is treated as a plate. For smaller values of b the plate-spring is considered to be a narrow beam. This results in:

$$K_z = \frac{12}{E \cdot b \cdot h^3} \qquad \text{for } b \simeq h$$

and $$K_z = \frac{12 \cdot (1 - \nu^2)}{E \cdot b \cdot h^3} \qquad \text{for } b > h$$

where ν is the Poisson's ratio of the material. Dijksman (D1) and Schuller (S4) have indicated that the influence of contraction effects does not only depend upon the ratio b/h but also upon the radius of curvature. A range of transition between plane-stress and plane-strain bending has been described by these authors. This transition may have considerable effects upon the linearity of force-displacement characteristics of plate-spring mechanisms. Therefore the equations described by Dijksman have been used in a numerical method to solve equations (3.1) or (3.2). This method will be described in section 3.4.
In section 3.5 the results of some of the methods of solutions wil be compared with each other and with results from measurements. From the comparison an indication of the range of validity of each method can be obtained.

3.2 Review of methods to solve equation (3.1).

-Exact analytical solution.
Exact solutions of equations (3.1) or (3.2) may be obtained using the concept of elliptic integrals. Such solutions have been obtained by Frisch-Fay, Haringx and many others.
Although it is attractive to obtain an exact solution it has occurred to different authors that the use of elliptic functions is extremely tedious. As a result different approximating analytical solutions were sought.
A good description of the use of elliptic functions to describe the behaviour of plate-springs is given by Frisch-Fay (F1).

-Linear beam theory.
The first of a number of approximating methods for solution is the linear beam theory which is used widely to determine strength and stiffness of structures. When the deformations are very small the following simplifications and differential equations are used:

$$\cos \phi(s) \simeq 1 \qquad \sin \phi(s) \simeq 0$$

$$\frac{d^2\phi(s)}{ds^2} \simeq -K_z \cdot F_x \qquad \text{with } \left\{\frac{d\phi(s)}{ds}\right\}_{s=\ell} = K_z \cdot M_z \qquad (3.3)$$

Although this method is not suitable to study all aspects of the behaviour of mechanisms the simple expressions which may be obtained can be used to study the main characteristics of different plate-spring mechanisms.

-Quasi-linear beam theory.
In the linear beam theory the influence of the loading force F_y is neglected. When the approximation $\sin\phi(s) \simeq \phi(s)$ is used a differential equation results which can be solved analytically and which allows to determine the behaviour of loaded plate-spring mechanisms. The estimated errors in this method are of the order $\frac{1}{2} \cdot \phi(s)^2$ and for technical applications angles upto about 0,3 radians might be allowable.
The resulting expressions for the quasi-linear beam theory are:

$$\cos \phi(s) \simeq 1 \qquad \sin \phi(s) \simeq \phi(s)$$

$$\frac{d^2\phi(s)}{ds^2} = K_z \cdot (-F_x + F_y \cdot \phi(s)) \qquad \text{with } \left(\frac{d\phi(s)}{ds} \right)_{s=\ell} = M_z \cdot K_z \qquad (3.4)$$

For these equations solutions of the form:

$$\phi(s) = A \cdot e^{k \cdot s} + B \cdot e^{-k \cdot s} + C$$
$$\text{with } k = \sqrt{F_y \cdot K_z}$$

can be found.

-Power-series development.
The previous two approximative techniques were based upon the assumption that $\phi(s) \ll 1$ and the first terms of the power series for $\cos \phi(s)$ and $\sin \phi(s)$ were used. Another way to use power series, as developed by Dijksman (D1) and Zenov (Z1), is based upon the assumption that the loading forces remain relatively small. This leads to the requirements:

$$F_x \cdot \ell^2 \cdot K_z < 1 \quad , \quad F_y \cdot \ell^2 \cdot K_z < 1 \quad \text{and} \quad M_z \cdot \ell \cdot K_z < 1 \quad .$$

In this case the solution for $\phi(s)$ may be expressed as an expansion in

power series with terms of different degree of loading forces. On this basis results for $\phi(s)$ including third order terms in the loading forces have been obtained (D1, Z1). But in principal there are no problems in obtaining higher order solutions.

With this method expressions describing the behaviour of plate-spring mechanisms for values of $\phi(s) < 0{,}6$ rad. under the mentioned restrictions for the loading forces can be obtained. For practical purposes this maximum angle is more than sufficient. However the restrictions to low loading conditions might be a disadvantage.

-"Iterative"-analytical solution.

When $u^*(s)$ and $v^*(s)$ are estimates for the functions u(s) and v(s) for a particular case of loading of a plate-spring, an approximate value of $\phi(s)$ can be found from

$$\frac{d\phi(s)}{ds} = K_z \cdot (F_x \cdot (-\ell - v^*(\ell) + s + v^*(s)) + F_y \cdot (u^*(\ell) - u^*(s)) + M_z)$$

This equation can be solved analytically provided that $u^*(s)$ and $v^*(s)$ can be directly integrated. This solution yields an estimated function $\phi^*(s)$ which can be used to obtain new estimates for u(s) and v(s) using the relations

$$u(s) = -\int_0^s \sin \phi(t) \cdot dt \quad \text{and} \quad v(s) = \int_0^s (\cos \phi(t) - 1) \cdot dt$$

Whith these new estimates the process of solving equation 3.1 can be restarted. When the differences between subsequent expressions for $\phi(s)$ are small enough a solution for equation 3.1 has been obtained.

The success of this iterative method depends upon the convergence of the process. This again depends strongly upon the suitability of the initial estimates, $u^*(s)$ and $v^*(s)$. When these functions are chosen with care it may be possible to obtain a solution for $\phi(s)$ in only <u>one</u> iteration step.

In the section 3.3 it will be shown that it is possible to create good estimates and that this process forms a powerfull tool in studying the behaviour of plate-springs.

-Numerical methods.

With different methods for numerical integration solutions of equations (3.1) or (3.2) for a particular case can be obtained. Such a solution is comparable with the results from measurements of deformations of real plate-springs. The advantage of the numerical method is that results are obtained easily and with a good accuracy. The disadvantage is that the "numerical experiment" can only describe the reactions of the <u>model</u> assumed to derive the differential equations. Like the experimental approach the numerical technique is useful to estimate the validity of expressions obtained with analytical methods. In addition results of numerical solutions may be used to derive "empirical" expressions describing the behaviour of plate-spring mechanisms.

As the numerical integration method is capable of treating any sort of differential equation it also allows to estimate the influence of the transition from plane-stress to plane-strain bending. With the expressions given by Dijksman (D1) describing this transition the behaviour of real plate-spring may be estimated. This will be discussed further in section 3.4.

The main difficulty in solving equation (3.1) numerically results from the boundary conditions which are specified in two different points of the plate-spring. At the clamped end the angle $\phi(s)$ is equal to zero while values for $u(\ell)$ and $v(\ell)$ are needed to start an integration procedure. This problem can be solved by an iterative process. Estimates of $u(\ell)$ and $v(\ell)$ are used and improved after every cycle. In this process it is also important to start with well estimated values to improve convergence of the iterative process.

-Finite Element Method.

Another method to perform numerical experiments on models of the physical plate-springs is the finite element method. In this method the plate-spring is considered as a system containing a number of smaller parts. For each small part relatively simple relations between the relative motion of the ends and the forces applied at these ends can be obtained. Solutions for the complete plate-spring are obtained when the resulting set of linear algebraic equations is solved. For larger deflections different iterations are required to arrive at sufficiently accurate solutions.

In this method the set of differential equations derived in chapter 2 is not used. As this method will give results that are similar and equivalent to those obtainable with the numerical integration method it has not been used in this research.
Examples of the application of the finite element method can be found in literature (W1) and (W2). In the first report van der Werff (W1) describes calculations of the behaviour of the doubly symmetric cross-spring pivot under different loading conditions.In the second report (W2) a finite element program is described that may be used to calculate the main properties of different sorts of plate-spring mechanisms in the plane of motion.
An advantage of the finite element method is that without further complications the calculations can be performed on complete mechanisms containing more than one or two plate-springs and rigid links.

3.3 Iterative analytical solution.

As stated in the previous section equation (3.1) could be solved when suitable estimates for u(s) and v(s) are available. Such estimates can be found using the fact that a plate-spring, when considered in the plane of motion, has only two degrees of freedom. This indicates that the shape for a plate-spring is, to a high degree of accuracy, determined by two parameters. Suitable parameters are the displacement and angular deflection at the end of the plate-spring, $u(\ell)$ and $\phi(\ell)$.

This assumption about the plate-spring having only two degrees of freedom is correct when the deflections are not too large and no buckling occurs. As plate-springs are used in the design of mechanisms because they have only two degrees of freedom this assumption will not be a restriction to the field of application of this method.

To illustrate the iterative analytical solution the case of a plate-spring loaded only by the force F_x will be discussed here. The full solution of equation (3.1) will be given in Annex 3.I to this chapter.

For this particular case equation (3.1) reduces to

$$\frac{d\phi(s)}{ds} = -K_z \cdot F_x \cdot (\ell + v(\ell) - s - v(s))$$

$$\text{with} \quad v(s) = \int_0^s (\cos \phi(t) - 1) \cdot dt \qquad (3.5)$$

To obtain estimates for u(s) and v(s) it is assumed that $\phi(s)$ is described by

$$\phi(s) = a_0 + a_1 \cdot s + a_2 \cdot s^2 + a_3 \cdot s^3$$

and that good estimates for u(s) and v(s) are obtained using the linearized expressions

$$u(s) \simeq - \int_0^s \phi(t) \cdot dt \qquad \text{and} \qquad v(s) \simeq - \frac{1}{2} \cdot \int_0^s \phi(t)^2 \cdot dt$$

The values of the coefficients a_0 to a_3 are determined from the boundary conditions

$\phi(0) = 0 \qquad u(0) = 0$

$\phi(\ell) = \phi(\ell) \qquad u(\ell) = u(\ell)$

As a result the following estimate for $\phi(s)$ is obtained.

$$\phi(s) \simeq \left(-2\cdot\phi(\ell) - 6\cdot\frac{u(\ell)}{\ell} \right)\cdot\left(\frac{s}{\ell}\right) + \left(3\cdot\phi(\ell) + 6\cdot\frac{u(\ell)}{\ell}\right)\cdot\left(\frac{s}{\ell}\right)^2$$

Putting $\phi(\ell) = \phi_\ell$, $\frac{u(\ell)}{\ell} = u_\ell$ and $\xi = \frac{s}{\ell}$ this expression becomes

$$\phi(s) = \left(-2\cdot\phi_\ell - 6\cdot u_\ell \right)\cdot\xi + \left(3\cdot\phi_\ell + 6\cdot u_\ell \right)\cdot\xi^2 \qquad (3.6)$$

Expression (3.6), which is a general expression for the first estimate of the plate-spring shape as a function of $\phi(\ell)$ and u_ℓ, may be simplified for this particular case since M_z=0. This yields

$$M_z\cdot K_z = \left\{ \frac{d\phi(s)}{ds} \right\}_{s=\ell} = 0 \quad \text{and thus}$$

$$\phi(s) \simeq 2\cdot\phi_\ell\cdot\xi - \phi_\ell\cdot\xi^2 \qquad (3.7)$$

Using this expression to obtain an estimate for v(s) yields

$$\frac{v^*(s)}{\ell} \simeq -\phi_\ell^2\cdot\left\{ \frac{2}{3}\cdot\xi^3 - \frac{1}{2}\cdot\xi^4 + \frac{1}{10}\cdot\xi^5 \right\}$$

and $$\frac{v^*(\ell)}{\ell} \simeq -\frac{4}{15}\cdot\phi_\ell^2$$

When these results are substituted in the differential equation (3.5) this yields

$$\frac{d\phi(s)}{ds} \simeq -K_z\cdot F_x\cdot\ell\cdot\left\{ 1 - \frac{4}{15}\cdot\phi_\ell^2 - \xi + \phi_\ell^2\cdot\left(\frac{2}{3}\cdot\xi^3 - \frac{1}{2}\cdot\xi^4 + \frac{1}{10}\cdot\xi^5 \right) \right\}$$

Through direct integration this can be solved, leading to

$$\phi(s) \simeq -K_z\cdot F_x\cdot\ell^2\cdot\left\{ \xi - \frac{1}{2}\cdot\xi^2 + \phi_\ell^2\cdot\left(-\frac{4}{15}\cdot\xi + \frac{1}{6}\cdot\xi^4 - \frac{1}{10}\cdot\xi^5 + \frac{1}{60}\cdot\xi^6 \right) \right\} \qquad (3.8)$$

Expression (3.8) gives a new estimate for the shape of the deformed plate-spring. To compare this shape with the original estimate in equation (3.7) the loading force F_x should be expressed in the angular deflection of the end of the plate-spring.
This leads to

$$F_x \simeq -\phi_\ell\cdot\frac{2}{K_z\cdot\ell^2}\cdot\frac{1}{\left(1 - \frac{11}{30}\cdot\phi_\ell^2 \right)} \qquad (3.9)$$

and, after some rearringing,

$$\phi(s) \simeq \left(2\cdot\phi_\ell\cdot\xi - \phi_\ell\cdot\xi^2 \right)\cdot \qquad (3.10)$$
$$\cdot\left\{ 1 + \frac{\phi_\ell^2}{\left(1 - \frac{11}{30}\cdot\phi_\ell^2 \right)}\cdot\left(\frac{6 - 11\cdot\xi + 10\cdot\xi^3 - 6\cdot\xi^4 + \xi^5}{60 - 30\cdot\xi} \right) \right\}$$

The first factor in (3.10) is equivalent to expression (3.7). The difference between the two expressions can be easily estimated. When $\phi(s)$ is smaller than 0,5 rad., the difference along the plate-spring is nowhere more than 0,005 rad. This indicates that, for most practical purposes, the result obtained after one iterative step is accurate enough. To illustrate this the relation between F_x and ϕ_ℓ as given in expression (3.9) is compared with similar results from other techniques in figure 3.1.

The fact that the technique described above is sufficiently convergent in one step is due to the selection of ϕ_ℓ and u_ℓ as parameters to estimate the shape of the plate-spring. It would be equally possible to use the loading force F_x as parameter to describe the estimated shape. Using results from the linear beam theory the first estimate would be

$$\phi(s) \simeq -K_z\cdot F_x\cdot\ell^2\cdot\left(\xi - \frac{1}{2}\cdot\xi^2 \right)$$

and along similar lines as described before the following expression relating ϕ_ℓ and F_x is obtained

$$\phi_\ell \simeq -K_z\cdot F_x\cdot\ell^2\cdot\left(\frac{1}{2} - \frac{11}{240}\cdot\left(F_x\cdot K_z\cdot\ell^2 \right)^2 \right) \qquad (3.11)$$

A result that was also obtained by Dijksman (D1), and can be used only for small values of F_x as can be concluded from figure 3.1.

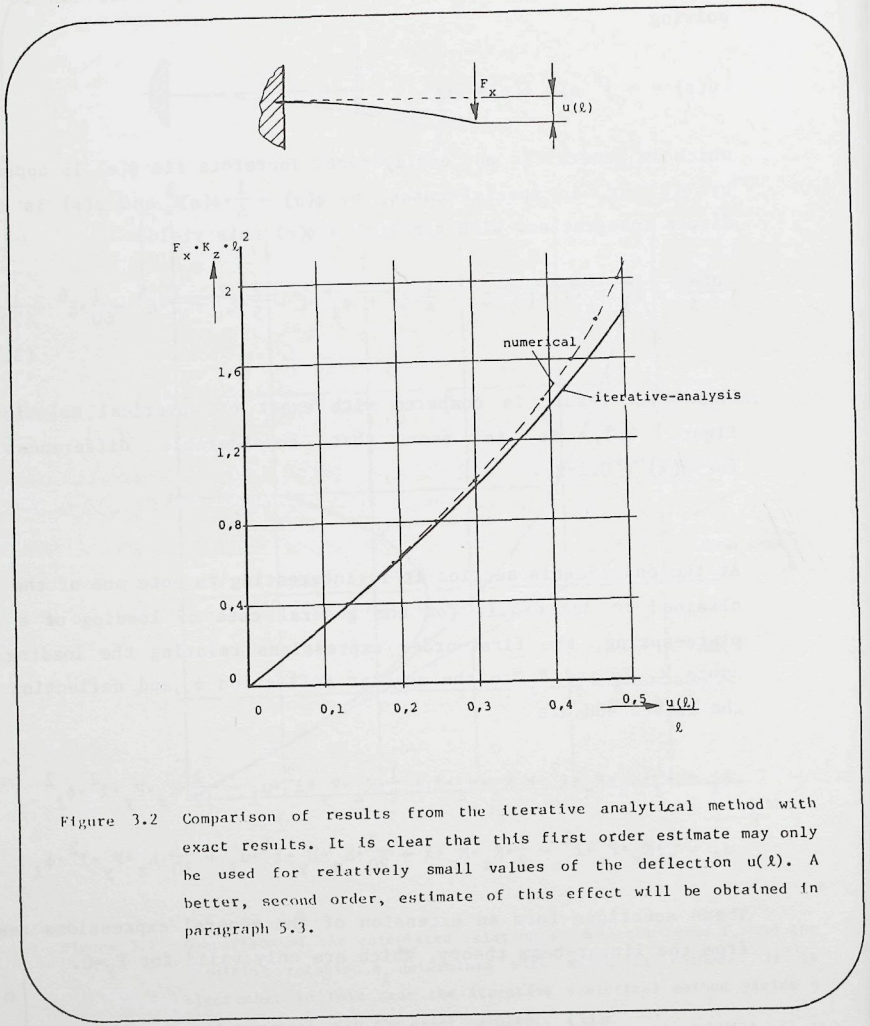

Figure 3.2 Comparison of results from the iterative analytical method with exact results. It is clear that this first order estimate may only be used for relatively small values of the deflection u(ℓ). A better, second order, estimate of this effect will be obtained in paragraph 5.3.

3.4 Numerical integration.

The expressions for u(s) and v(s) may be differentiated and equations 3.1 may thus be written as

$$\frac{d\phi(s)}{ds} = K_z \cdot \{ -F_x \cdot (\ell + v(\ell) - s - v(s)) + F_y \cdot (u(\ell) - u(s)) + M_z \}$$

$$\frac{du(s)}{ds} = \sin \phi(s) \qquad (3.12)$$

$$\frac{dv(s)}{ds} = \cos \phi(s) - 1$$

Equations (3.12) form a set of first-order differential equations. With standard methods for numerical integration solutions for such a set of equations can be obtained with sufficient accuracy. Examples of such standard methods are Eulers' method, Heun's method and, in different forms, Runge-Kutta methods. In the following the fourth-order Runge-Kutta integration method will be used (see also Annex 3.II).

When solving equations (3.12) the simultaneous numerical integration will be started from s=0. As can be seen from the first of equations (3.12) it will be necessary to know the value of u(ℓ) and v(ℓ) to determine $\frac{d\phi(s)}{ds}$. However u(ℓ) and v(ℓ) are only known when the equations have been solved.

As a result it will be necessary to perform an iterative process of estimating u(ℓ) and v(ℓ), solving equations 3.I2, improving the estimates for u(ℓ) and v(ℓ) etc., until they have been estimated with sufficient accuracy. For this iterative process different strategies may be developed in order to assure convergence to the desired solution without excessive computing efforts. This is not trivial since for given end displacements expression (3.12) can have an indefinite number of solutions.

The most straight-forward strategy appears to be the one described in figure 3.3. After choosing a first estimate for u(ℓ) and v(ℓ) the equations are integrated. The values of u(ℓ) and v(ℓ) determined by the integration are directly used as new estimates and this continues untill the differences in the successive estimates are less than the allowed inaccuracy.

This simple strategy is, however, not "globally convergent". For the loading cases, combined with initial estimates, where no convergence occurs more refined strategies to determine new estimates can be developed.

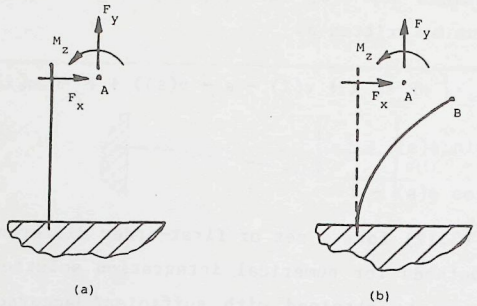

To start the iteration process an estimate for the position of the loaded end is made, point A. Upon integration the shape of a loaded plate-spring is determined. The newly calculated end position is point B. The determined shape is the correct solution for the loading case shown in c and d.

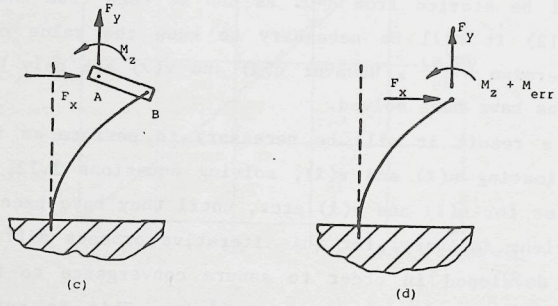

The magnitude of the extra bending moment, M_{err}, which is added to the desired loading M_z, can be easily determined from the equilibrum equations for the bar AB in figure c.

Figure 3.3 Iterative "shooting" process used to determine the deformed shape of a loaded plate-spring through numerical integration.

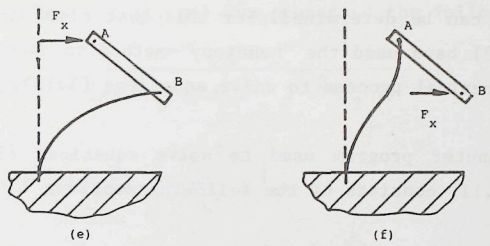

In the following step the new estimate for the position of the loaded end might be point B. Upon integration a new position for the loaded end of the plate-spring is obtained. In order to find the desired solution it is hoped that after every step the magnitude of M_{err} will decrease.

The described process proves to be suitable for many practical loading situations. As shown in figures e and f there may occur diffículties.

When point A is selected as estimate the point B will result. Using point B will again generate point A and this will continue forever. In such cases the process as described here is not convergent. Other strategies to obtain new estimates can be chosen. A simple variation would be to select a point "somewhere" on the line connecting A and B as a new estimate. Variations of the distance from point A supplies a tool that may be used to make the process convergent.

Figure 3.3. Continued

For most practical cases the strategies as described in figure 3.3 are sufficient. With these methods it turns out that even "exotic"-cases as the post-buckling of the Euler-strut and large deformations of C-shaped springs can be determined. For this last class of problems Watsong and Wang (W3) have used the "homotopy"-method to develop a globally-convergent numerical process to solve equations (3.12).

The computer program used to solve equations (3.12) as described in Annex 3.II, consists of the following sections :

-Main program, controlling input and output and the "shooting"-strategy to determine new estimates. To perform integration this program calls to,

-Subroutine RKSTEP, which performs one step of the integration process on an arbitrary number of first-order differential equations. This routine calls to,

-Subroutine FUNK, which returns the values of the different derivatives at the specified point of the plate-spring. This subroutine contains the three differential equations (3.12).

The numerical method to determine solutions for the differential equations has different applications in the analysis of plate-spring mechanisms. Firstly it is possible to determine highly accurate solutions even for larger deflections. Such solutions can be used to test the validity of simple expressions obtained with approximative methods. Still the solutions can only describe the behaviour of the model used to describe the plate-springs and differences between calculated and measured values can be expected.
This comparison of calculation and measurements, when both are sufficiently reliable, may enable to improve the model describing the plate-spring.

When such improvements of the model are incorporated in the differential equations the numerical method enables solution of complex sets of equations which cannot be treated with exact or approximative tools.

An interesting example of this second application is formed by the

analysis of the influence of the transition between plane-strain and plane-stress bending. To describe the relation between the bending compliance factor K_z, the dimensions of the plate-springs and the curvature κ_z Dijksman (lit. D1) has presented the following equations

$$K_z = \frac{12\cdot(1-\nu^2)}{E\cdot b\cdot h^3} \cdot \left\{ \frac{1}{\frac{1}{2}\cdot\nu^2\cdot f_1(\eta) + 1 - 2\cdot\nu^2\cdot f_2(\eta)} \right\}$$

where $$\eta = \left\{ 3\cdot(1-\nu^2)\cdot b^4 \cdot \frac{\kappa_z^2}{h^2} \right\}^{\frac{1}{4}}$$

$$f_1(\eta) = \frac{\frac{1}{2}\cdot\sinh(2\cdot\eta)-\frac{1}{2}\cdot\sin(2\cdot\eta)-2\cdot\eta\cdot\sinh(\eta)\cdot\sin(\eta)+\cosh(\eta)\cdot\sin(\eta)-\sinh(\eta)\cdot\cos(\eta)}{\eta\cdot(\sinh(\eta)+\sin(\eta))^2}$$

$$f_2(\eta) = \frac{\cosh(\eta)-\cos(\eta)}{\eta\cdot(\sinh(\eta)+\sin(\eta))}$$

(E is Youngs modulus and ν the Poisson ratio of the material).
As can be seen the bending stiffness is a function of the curvature κ_z. This is graphically represented, for different values of Poisson's ratio, in figure 3.4 . (See also Ashwell (A1))

When these equations are incorporated in the FUNCTION-subroutine part of the computerprogram a new value of K_z will be calculated at every step in the integration process. A slight complication is that K_z is known as a function of the curvature. When only the applied torque is known K_z can be determined in a few iterative-steps. The nature of the curves as shown in figure 3.4 assures that a good estimate can be obtained, even when the curvature, κ_z, is replaced by,

$$\kappa_z(s) \approx 12\cdot M_z(s)\cdot \frac{1-\nu^2}{E\cdot b\cdot h^3}$$

as a first estimate in the iterative process.
The new FUNCTION-subroutine is shown in Annex 3.II. This new model of the plate-spring can be used to determine whether observed differences between calculated and measured values are due to this effect of variation of the bending stiffness. This will be discussed further in the following section.

As discussed in section 3.3 for larger values of the loading force F_x the relations derived by the linear-beam theory are no longer valid. With the power-series method (Dijksman (D1)/Zenov (Z1)) and the iterative analytical method the following relations can be derived:

Linear beam , $u_\ell \simeq \frac{1}{3} \cdot f_x$

Power series , $u_\ell \simeq \frac{1}{3} \cdot f_x \cdot (1 - \frac{4}{35} \cdot f_x^{\,2})$ (Zenow,Z1)

Iterative analysis $\dfrac{u_\ell}{(1 - \frac{324}{420} \cdot u_\ell^{\,2})} \simeq \frac{1}{3} \cdot f_x \cdot (1 - \frac{1}{35} \cdot f_x^{\,2})$

where $f_x = F_x \cdot K_z \cdot \ell^2$ and $u_\ell = \frac{u(\ell)}{\ell}$.

The result from the iterative-analysis contains the result from equation (3.11) and, in addition, an estimate of the third-order term in the approximation for sin $\phi(s)$.

To make the differences between the different methods visible the magnitude of the force F_x as predicted or measured is divided by F_{xo}, the force as calculated with the linear beam theory. The results are given in figure 3.6.

In figure 3.6 two results from measurements are shown. For the relatively "narrow" plate-spring the results agree well with these obtained through numerical calculation. The measured results for the "wide" plate-spring differ consiberally from the calculated results.
These differences result from the fact that the wide plate-spring will experience a transition from plane-stress to plane-strain at the places that are most heavily loaded. With the numerical method the influence of this effect can be calculated and the results are shown in figure 3.7. It is seen that a good agreement for both the narrow and the wide plate-spring is obtained with Poisson's ratio of 0,3.
(Note: The actual value of the Poisson ratio for the material of the plate-spring has not been measured and the value of 0,3 is an estimate. Due to the anisotropy in the thin sheet of rolled material the actual value might be slightly different. The inaccuracy resulting from this uncertainty is considered to be negligible.)

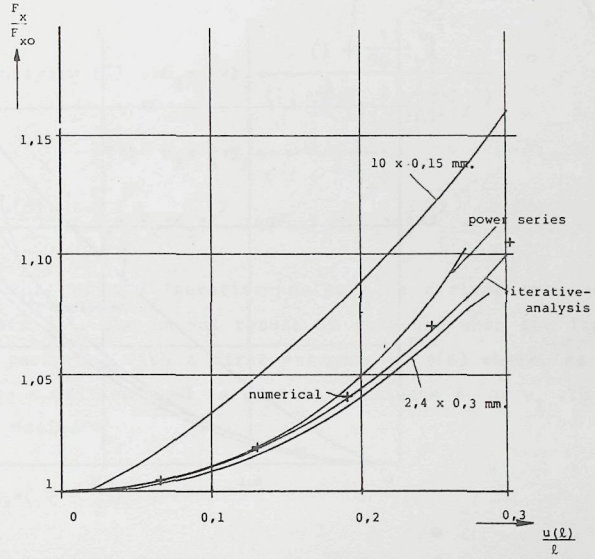

Figure 3.6 *Comparison of results from different methods to determine the* relation between the force F_x and the deflection $u(\ell)$ with results from measurements. The result from the numerical analysis was obtained without the consideration of the variation of the bending stiffness. The measured results were obtained through measurements at plate-spring parallel guidings with spring dimensions 80*2,5*0,4 mm. and 80*20*0,25 mm.

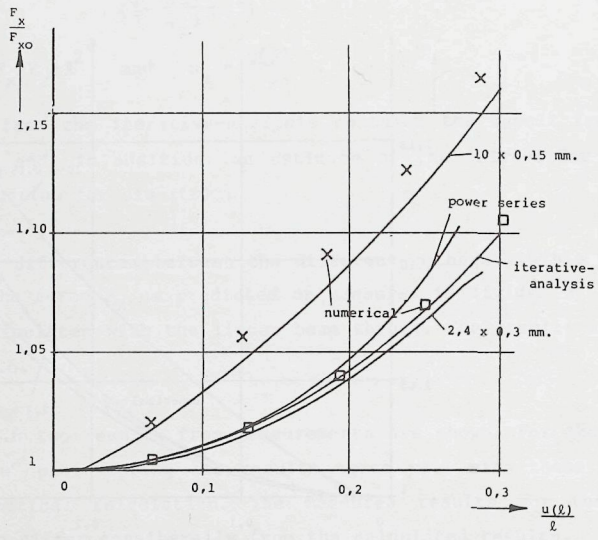

Figure 3.7 To determine the influence of the transition from plane-stress to plane-strain the effect of the variation of the bending stiffness can be incorporated in the computer program for the numerical solution of the differential equation. With this improved model the obtained results show a good agreement with the measured results. (For the calculations a Poisson's constant of 0,3 was used.)

When the plate-spring is loaded by a force F_y the stiffness in the direction of the x-axis will differ from the result obtained with the linear-beam theory. In this case the influence of F_y will also be noticed for small deflections. To analyse this influence it is sufficient to consider only the linear terms of the force F_x and deflection $u(\ell)$. The relations between $u(\ell)$, F_x and F_y from the different methods are

Linear-beam theory $$u_\ell = \frac{1}{3} \cdot f_x$$

Power-series $$u_\ell = \frac{1}{3} \cdot f_x \cdot \left(1 - \frac{2}{5} \cdot f_y + \frac{17}{105} \cdot f_y^2 \right)$$ (litt.Z1)

Iterative analysis (I) $$u_\ell \simeq \frac{1}{3} \cdot f_x \cdot \frac{\left(1 + \frac{1}{90} \cdot f_y\right)}{\left(1 + \frac{5}{12} \cdot f_y + \frac{7}{240} \cdot f_y^2\right)}$$

(II) $$u_\ell \simeq \frac{1}{3} \cdot f_x \cdot \frac{1}{\left(1 + \frac{2}{5} \cdot f_y\right)}$$

where $u_\ell = \frac{u(\ell)}{\ell}$, $f_x = F_x \cdot K_z \cdot \ell^2$ and $f_y = F_y \cdot K_z \cdot \ell^2$.

The first result of the iterative-analysis is derived from equations 3.I.2 in Annex 3.I. The second result is obtained when the iterative-analysis is performed with a first estimate of $\phi(s)$ where, as in section 3.3, the condition $M_z=0$ is used to eliminate ϕ_ℓ or u_ℓ .This leads to the first estimate

$$\phi(s) \simeq -3 \cdot u_\ell \cdot \left(\xi - \frac{1}{2} \cdot \xi^2 \right)$$

These results are graphically represented in figure 3.8 where the normalized stiffness, the ratio between F_x and u_ℓ , as a function of F_y is plotted. It can be clearly seen that the stiffness as predicted by the power-series method is only valid for small values of F_y, as was indicated by Dijksman (D1) whose power-series derivation required that f_x, $f_y < 1$.

Conclusion:

The examples of the application of the iterative analytical method to solve the differential equations (3.1) indicate that this method yields relatively simple expressions for the main characteristics of loaded plate-springs. The obtained results are sufficiently accurate for most practical applications and they are equivalent to the results obtained with other analytical methods. In addition the iterative analysis may be used to study the behaviour of plate-springs under the influence of spatial loading. In the following chapters it will be shown that this method is efficient when the deformations of plate-spring mechanisms under various loading conditions must be determined.

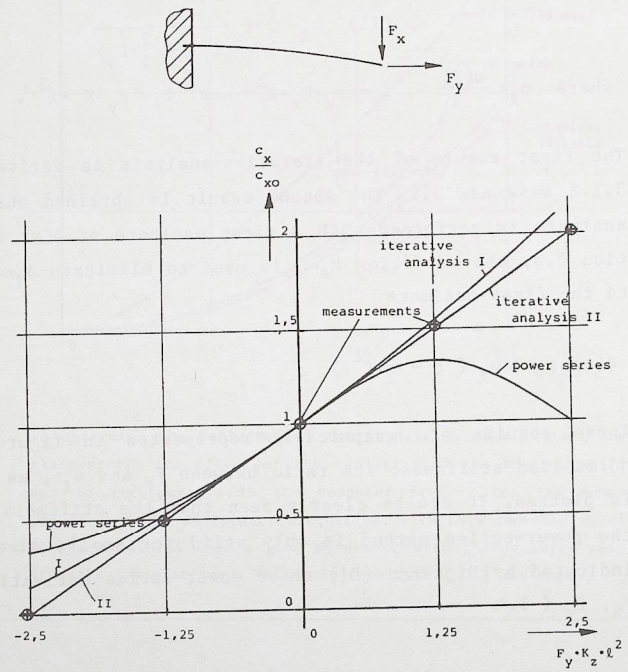

Figure 3.8 Application of a force F_y to the plate-spring influences the stiffness c_x .The magnitude of this influence can be estimated with different analytical methods. The obtained results are compared with results from measurements performed by Grentzius (G1).

3.I Annex. Calculation of general expressions for end-loaded plate-spring.

The analysis of the deformation of the end-loaded plate-spring is based upon the following expressions

$$\frac{d\phi(s)}{ds} = K_z \cdot \{ -F_x \cdot (\ell + v(\ell) - s - v(s)) + F_y \cdot (u(\ell) - u(s)) + M_z \}$$

$$u(s) = \int_0^s -\sin \phi(t) \cdot dt \qquad \text{and} \qquad v(s) = \int_0^s (\cos \phi(t) - 1) \cdot dt$$

For practical applications in plate-spring mechanisms it may be assumed that $\phi(s) < 0.5$. To simplify the given expressions the following definitions are introduced

$$\xi = \frac{s}{\ell} \quad , \quad v_\ell = \frac{v(\ell)}{\ell} \quad , \quad v(\xi) = \frac{v(s)}{\ell} \quad , \quad u_\ell = \frac{u(\ell)}{\ell} \quad , \quad u(\xi) = \frac{u(s)}{\ell}$$

$$\text{and} \quad f_x = F_x \cdot K_z \cdot \ell^2 \quad , \quad f_y = F_y \cdot K_z \cdot \ell^2 \quad , \quad m_z = M(\ell) \cdot K_z \cdot \ell$$

Together with $\phi(s) < 0.5$ the basic equations are reduced to

$$\frac{d\phi(\xi)}{d\xi} = -f_x \cdot (1 + v_\ell - \xi + v(\xi)) + f_y \cdot (u_\ell - u(\xi)) + m_z$$

$$u(\xi) \simeq \int_0^\xi -\phi(\alpha) \cdot d\alpha \quad , \quad v(\xi) \simeq \int_0^\xi (-\frac{1}{2} \cdot \phi(\alpha)^2) \cdot d\alpha \qquad (3.I.1)$$

Using these definitions the first estimate for $\phi(\xi)$ and $u(\xi)$ can be derived from (3.6), yielding:

$$\phi(\xi) \simeq \phi_\ell \cdot (-2 \cdot \xi + 3 \cdot \xi^2) - u_\ell \cdot (6 \cdot \xi - 6 \cdot \xi^2)$$

$$u(\xi) \simeq \phi_\ell \cdot (\xi^2 - \xi^3) + u_\ell \cdot (3 \cdot \xi^2 - 2 \cdot \xi^3)$$

To obtain a first order solution which incorporates the influence of the loading force F_y equation (3.I.1) may be solved using these estimates and assuming $v(\xi)$ to be equal to zero.
This leads to

$$\frac{d\phi(\xi)}{d\xi} \simeq -f_x \cdot (1 - \xi) + m_z + f_y \cdot u_\ell \cdot (1 - 3 \cdot \xi^2 + 2 \cdot \xi^3) - f_y \cdot \phi_\ell \cdot (\xi^2 - \xi^3)$$

and, upon integration with $\phi(0) = 0$ and $u(0) = 0$,

$$\phi(\xi) \simeq -f_y \cdot (\xi - \tfrac{1}{2}\cdot\xi^2) + m_z \cdot \xi + f_y \cdot u_\ell \cdot (\xi - \xi^3 + \tfrac{1}{2}\cdot\xi^4) + - f_y \cdot \phi_\ell \cdot (\tfrac{1}{3}\cdot\xi^3 - \tfrac{1}{4}\cdot\xi^4)$$

$$u(\xi) \simeq f_x \cdot (\tfrac{1}{2}\cdot\xi^2 - \tfrac{1}{6}\cdot\xi^3) - \tfrac{1}{2}\cdot m_z \cdot \xi^2 - f_y \cdot u_\ell \cdot (\tfrac{1}{2}\cdot\xi^2 - \tfrac{1}{4}\cdot\xi^4 + \tfrac{1}{10}\cdot\xi^5) + + f_y \cdot \phi_\ell \cdot (\tfrac{1}{12}\cdot\xi^4 - \tfrac{1}{20}\cdot\xi^5)$$

With these expressions the following relations between the loading forces and the deflections of the loaded end can be obtained,

$$\begin{aligned} \phi(\ell) &\simeq -\tfrac{1}{2}\cdot f_x + m_z + \tfrac{1}{2}\cdot f_y \cdot u_\ell - \tfrac{1}{12}\cdot f_y \cdot \phi_\ell \\ u_\ell &\simeq \tfrac{1}{3}\cdot f_x - \tfrac{1}{2}\cdot m_z - \tfrac{7}{20}\cdot f_y \cdot u_\ell + \tfrac{1}{30}\cdot f_y \cdot \phi_\ell \end{aligned} \qquad (3.I.2)$$

These relations are similar to those obtained by the linear-beam theory when F_y equals zero. They form a basic set of equation for plate-springs loaded by a tensile or compression force.

In addition to these expressions a relation for $v(\xi)$ or v_ℓ can be obtained using the third of equations (3.I.1). For v_ℓ this yields,

$$v_\ell \simeq -\tfrac{1}{2}\cdot\{ \tfrac{2}{15}\cdot f_x^{\,2} + \tfrac{1}{3}\cdot m_z^{\,2} - \tfrac{5}{12}\cdot f_x \cdot m_z - f_x \cdot f_y \cdot (\tfrac{39}{140}\cdot u_\ell - \tfrac{19}{630}\cdot\phi_\ell) + + m_z \cdot f_y \cdot (\tfrac{13}{30}\cdot u_\ell - \tfrac{1}{20}\cdot\phi_\ell) + f_y^{\,2} \cdot (\tfrac{367}{2520}\cdot u_\ell^{\,2} + \tfrac{1}{504}\cdot\phi_\ell^{\,2} - \tfrac{1}{5040}\cdot u_\ell \cdot \phi_\ell) \} \qquad (3.I.3)$$

These results are first order expressions which are good approximations as long as $v(\xi)$ is negligibly small. This assumption is not satisfied for larger deflections or for compressive loads above the critical buckling force. A more accurate expression for moderately large deflections can be obtained when an estimated function for both $u(\xi)$ and $v(\xi)$ is substituted in the differential equation. Suggestions for such estimates are

$$u(\xi) \simeq \phi_\ell \cdot (-\xi^2 + \xi^3) + u_\ell \cdot (3\cdot\xi^2 - 2\cdot\xi^3)$$

and $$v(\xi) \simeq -\phi_\ell^{\,2} \cdot (\tfrac{2}{3}\cdot\xi^3 - \tfrac{3}{2}\cdot\xi^4 + \tfrac{9}{10}\cdot\xi^5) - u_\ell \cdot \phi_\ell \cdot (4\cdot\xi^3 - \tfrac{15}{2}\cdot\xi^4 + \tfrac{18}{5}\cdot\xi^5) + -u_\ell^{\,2} \cdot (6\cdot\xi^3 - 9\cdot\xi^4 + \tfrac{18}{5}\cdot\xi^5)$$

Solving the equations (3.I.1) with these estimates leads to expressions which allow to estimate non-linear effects in guiding mechanisms in a way similar to the one used in section 3.3. The shape of the plate-spring resulting from this solution is determined by

$$\phi(\xi) \simeq -f_x \cdot \{ \xi - \tfrac{1}{2}\cdot\xi^2 + \phi_\ell^{\,2} \cdot (-\tfrac{1}{15}\cdot\xi + \tfrac{1}{6}\cdot\xi^4 - \tfrac{3}{10}\cdot\xi^5 + \tfrac{3}{20}\cdot\xi^6) + + u_\ell \cdot \phi_\ell \cdot (-\tfrac{1}{10}\cdot\xi + \xi^4 - \tfrac{3}{2}\cdot\xi^5 + \tfrac{3}{5}\cdot\xi^6) + + u_\ell^{\,2} \cdot (-\tfrac{3}{5}\cdot\xi + \tfrac{3}{2}\cdot\xi^4 - \tfrac{9}{5}\cdot\xi^5 + \tfrac{3}{5}\cdot\xi^6) \} + + m_z \cdot \xi + f_y \cdot u_\ell \cdot (\xi - \xi^3 + \tfrac{1}{2}\cdot\xi^4) - f_y \cdot \phi_\ell \cdot (\tfrac{1}{3}\cdot\xi^3 - \tfrac{1}{4}\cdot\xi^4)$$

and

$$\phi(\ell) \simeq -f_x \cdot (\tfrac{1}{2} - \tfrac{1}{20}\cdot\phi_\ell^{\,2} - \tfrac{3}{10}\cdot u_\ell^{\,2}) + m_z + \tfrac{1}{2}\cdot f_y \cdot u_\ell - \tfrac{1}{12}\cdot f_y \cdot \phi_\ell \qquad (3.I.4)$$

With the approximation $\sin\phi(s) \simeq \phi(s)$ the deflection u_ℓ of the end is determined as,

$$u_\ell \simeq f_x \cdot (\tfrac{1}{3} - \tfrac{1}{35}\cdot\phi_\ell^{\,2} - \tfrac{1}{70}\cdot u_\ell \cdot \phi_\ell - \tfrac{3}{14}\cdot u_\ell^{\,2}) - \tfrac{1}{2}\cdot m_z - \tfrac{7}{20}\cdot f_y \cdot u_\ell + \tfrac{1}{30}\cdot f_y \cdot \phi_\ell \qquad (3.I.5)$$

With these expressions it is possible to estimate a part of the non-linearity in plate-spring mechanisms. The non-linearities are, in general, resulting from the non-linear geometry and from non-linear behaviour of the material. In expressions (3.I.4 and 5) the influence of the deflection $v(s)$ is determined. However it has been assumed that $\phi(s)$ is small in order to calculate $u(s)$ with the linearized expression for $\sin\phi(s)$. This means that non-linear effects of the order $\frac{1}{6}\cdot\phi(s)^3$ have been neglected. It is of course possible to derive better approximations for $u(s)$. The resulting expressions are becoming rather complex.

An illustration of the result obtained when a higher order approximation is used has been given in para.3.5. Here the relation between the deflection u and the driving force F_x for a plate-spring has been given.

Annex 3.II.

Computer programs used for the numerical integration of the differential equations

The computer program consists of the following three sections :

Main program	:VEERO1
Integration subroutine	:RKSTEP
Function subroutine with the differential equations	:FUNK

Two versions of the last subroutine are presented. The first one is not accounting for the effect of the anti-clastic curvature of the plate-spring. In the second version a few statements have been added to take this effect into account.

Main program

```
C       Program "VEERO1"
C
C       This is the main program unit used for the numerical
C       integration of differential equations describing the
C       behaviour of plate-springs loaded at the free end.
C       Here the input of the data about the loading case and
C       spring dimensions may be entered. The program will then
C       perform numerical integration of the equations.
C       This process is started with initial estimates
C        provided interactively and after each cycle the new
C       values for the end deflections are returned. The user
C       may specify whether a new
C        integration cycle should be started and this will
C       continue untill the user indicates that the end
C       deflections have been determined with sufficient
C       accuracy.
C
        PROGRAM VEERO1
        DIMENSION STO(100,6),A(6),AN(6)
        COMMON /FUNV/XM,YM,ZM,FD,FN,FP,RKX,RKY
        COMMON /FUNV2/UL,VL,WL
        COMMON /EDEV/ LTR,LTW,LLP,LTX
        LOGICAL*1 EDJA,LEXT
        DATA LTR/5/,LTW/7/,LLP/6/,LTX/4/
        DATA STO/600*0./
C
C
C       Input section for the relative compliances Kx
C       and Ky, the magnitude of the normalized
C        loading components, the number of integration
C       intervals along the plate-spring and an estimate
C       for the deflection u(1) of the loaded end.
C
        WRITE(LTW,*) 'GEEF RKX EN RKY'
        READ(LTR,100) RKX,RKY
        WRITE(LLP,102) RKX,RKY
102     FORMAT(' COMPLIANTIES ZIJN : ',2F12.5)
```



```
40      WRITE(LTW,*) 'GEEF MX,MY,MZ,D,N,P '
        READ(LTR,100) XM,YM,ZM,FD,FN,FP
        WRITE(LLP,103)
103     FORMAT(' BELASTINGEN ZIJN : (MX,MY,MZ,D,N,P)')
        WRITE(LLP,100) XM,YM,ZM,FD,FN,FP
        WRITE(LTW,*) 'HOEVEEL STAPPEN? (INTEGER)'
        READ(LTR,101) NSTEP
100     FORMAT(6F12.5)
101     FORMAT(2I8)
        WRITE(LTW,*) 'GEEF SCHATTER VOOR UL:'
        READ(LTR,100) UL
        VL=0.
        WL=0.
        H=1./FLOAT(NSTEP)
50      DO 41 J=1,6
        A(J)=0.
41      CONTINUE
        S=0.
        DO 200 K=1,NSTEP
C
C       For each integration interval a standard
C       integration routine, "RKSTEP", is called
C        that will perform the integration
C       of the differential equations.
C
        CALL RKSTEP(A,S,H,6,AN)
        DO 55 J2=1,6
        STO(K,J2)=AN(J2)
        A(J2)=AN(J2)
55      CONTINUE
C       WRITE(LLP,100) (AN(I),I=1,6)
        S=S+H
200     CONTINUE
        UL=AN(4)
        VL=AN(5)
        WL=AN(6)
C
C       The resulting values of the end deflections are presented at
C       the user-terminal and he is asked whether a new integration cycle
C       is desired.
C
        WRITE(LTW,110) UL,VL,WL
110     FORMAT(' NIEUWE WAARDEN ZIJN:  ',3F12.5)
        WRITE(LTW,*) 'NIEUWE ITERATIE? '
        IF (EDJA()) GOTO 50
        WRITE(LLP,111)
111     FORMAT('^     PSI          THETA          PHI
     1    U(S)          V(S)          W(S) ')
        DO 300 K=1,NSTEP
C
C       When the user is satisfied the results of the numerical
C       integration process are printed and the user may start to
C       specify a new loading case.
C
        WRITE(LLP,100) (1000.*STO(K,J),J=1,6)
300     CONTINUE
        WRITE(LTW,*) 'NIEUWE WAARDEN ?'
        IF (EDJA()) GOTO 40
        CALL EXIT
        END
```

Integration subroutine

```
      SUBROUTINE RKSTEP(A,S,H,NVER,AN)
      DIMENSION A(NVER),A1(20),DA(20),AN(NVER)
      CALL FUNK(A,S,DA)
      DO 10 I=1,NVER
      A1(I)=A(I)+H*DA(I)/2.
      AN(I)=A(I)+H*DA(I)/6.
10    CONTINUE
      CALL FUNK(A1,S+H/2.,DA)
      DO 11 I=1,NVER
      A1(I)=A(I)+H*DA(I)/2.
      AN(I)=AN(I)+H*DA(I)/3.
11    CONTINUE
      CALL FUNK(A1,S+H/2.,DA)
      DO 12 I=1,NVER
      A1(I)=A(I)+H*DA(I)
      AN(I)=AN(I)+H*DA(I)/3.
12    CONTINUE
      CALL FUNK(A1,S+H,DA)
      DO 13 I=1,NVER
      AN(I)=AN(I)+H*DA(I)/6.
13    CONTINUE
      RETURN
      END
```

Function subroutine (Version 1)

```
      SUBROUTINE FUNK(A,S,DA)
      DIMENSION A(6),DA(6)
      COMMON /FUNV/XM,YM,ZM,FD,FN,FP,RKX,RKY
      COMMON /FUNV2/UL,VL,WL
      COSPS=COS(A(1))
      SINPS=SIN(A(1))
      COSTH=COS(A(2))
      SINTH=SIN(A(2))
      COSPH=COS(A(3))
      SINPH=SIN(A(3))
      U=A(4)
      V=A(5)
      W=A(6)
      XMS=XM+FP*(1.+VL-S-V)+FN*(-WL+W)
      YMS=YM+FP*(-UL+U)+FD*(WL-W)
      ZMS=ZM+FD*(-1.-VL+S+V)+FN*(UL-U)
      RX=RKX*(COSTH*COSPH*XMS+COSTH*SINPH*YMS
     1          -SINTH*ZMS)
      RY=RKY*((-COSPS*SINPH+SINPS*SINTH*COSPH)*XMS
     1          +(COSPS*COSPH+SINPS*SINTH*SINPH)*YMS
     2          +SINPS*COSTH*ZMS)
      RZ=(SINPS*SINPH+COSPS*SINTH*COSPH)*XMS
     1    +(-SINPS*COSPH+COSPS*SINTH*SINPH)*YMS
     2    +COSPS*COSTH*ZMS
C
C
      DA(3)=(SINPS*RY+COSPS*RZ)/COSTH
      DA(2)=(RY-DA(3)*SINPS*COSTH)/COSPS
      DA(1)=RX+SINTH*DA(3)
      DA(4)=-COSPS*SINPH+SINPS*SINTH*COSPH
      DA(5)=COSPS*COSPH+SINPS*SINTH*SINPH-1.
      DA(6)=SINPS*COSTH
      RETURN
      END
```


Function subroutine (Version 2)

```
      SUBROUTINE FUNK(A,S,DA)
      DIMENSION A(6),DA(6)
      COMMON /FUNV/XM,YM,ZM,FD,FN,FP,RKX,RKY
      COMMON /FUNV2/UL,VL,WL,B,H,PC
      SINH(X)=(EXP(X)-EXP(-X))*.5
      COSH(X)=(EXP(X)+EXP(-X))*.5
      COSPS=COS(A(1))
      SINPS=SIN(A(1))
      COSTH=COS(A(2))
      SINTH=SIN(A(2))
      COSPH=COS(A(3))
      SINPH=SIN(A(3))
      U=A(4)
      V=A(5)
      W=A(6)
      XMS=XM+FP*(1.+VL-S-V)+FN*(-WL+W)
      YMS=YM+FP*(-UL+U)+FD*(WL-W)
      ZMS=ZM+FD*(-1.-VL+S+V)+FN*(UL-U)
      RX=RKX*(COSTH*COSPH*XMS+COSTH*SINPH*YMS
     1          -SINTH*ZMS)
      RY=RKY*((-COSPS*SINPH+SINPS*SINTH*COSPH)*XMS
     1          +(COSPS*COSPH+SINPS*SINTH*SINPH)*YMS
     2          +SINPS*COSTH*ZMS)
      RZ=(SINPS*SINPH+COSPS*SINTH*COSPH)*XMS
     1    +(-SINPS*COSPH+COSPS*SINTH*SINPH)*YMS
     2    +COSPS*COSTH*ZMS
C
      IF (ABS(RZ).EQ.0.)      GOTO 50
C
      PU=B*(H/ABS(RZ))**(-.5)*(3*(1-PC**2))**.25
      F1=(.5*SINH(2.*PU)-.5*SIN(2.*PU)-
     1     2.*PU*SINH(PU)*SIN(PU)+COSH(PU)*SIN(PU)-
     2     SINH(PU)*COS(PU))/
     3     (PU*(SINH(PU)+SIN(PU))**2)
      F2=(COSH(PU)-COS(PU))/
     1    (PU*(SINH(PU)+SIN(PU)))
      RZ=RZ*(1-PC**2)/(1+PC**2*(F1/2.-2.*F2))
C
50    DA(3)=(SINPS*RY+COSPS*RZ)/COSTH
      DA(2)=(RY-DA(3)*SINPS*COSTH)/COSPS
      DA(1)=RX+SINTH*DA(3)
      DA(4)=-COSPS*SINPH+SINPS*SINTH*COSPH
      DA(5)=COSPS*COSPH+SINPS*SINTH*SINPH-1.
      DA(6)=SINPS*COSTH
      RETURN
      END
```

Chapter 4.

Plate spring deformation under three-dimensional loading.

4.1 Introduction

In chapter 2 a mathematical model has been derived which may be used to determine the shape of a plate-spring under three-dimensional loading of the free end. This derivation resulted in the set of "integro-differential" equations of figure 2.4 (which are also given in figure 4.1) . To find solutions for these equations two independent methods are available. The first method is based upon numerical integration and an iterative process which yields solutions for the complete set of equations. The other method is based on the "iterative-analytical" method for solving the simplified differential equations which was introduced in chapter 3.

At first it will be demonstrated how this method is used to solve the equations as derived in chapter 2 which were based upon the concept of the elastic line. This model is only valid for long and slender beams and the results are only first estimates for the behaviour of plate-springs when the length is not large compared to the width. (This discussion is nevertheless presented here as it clearly illustrates the mathematical operations used in the iterative analytical method.)
The theoretical results will be compared with those from numerical methods and with experimental results. It will be shown that the analytical and numerical results are in good agreement. However the experimental results indicate that the torsional compliance of plate-springs is smaller than expected.
In the final part of this chapter the mathematical model will be further developed to account for the effect of the constrained warping of the cross-section at the clamped ends of the plate-spring. It will be shown that better agreement between experimental and theoretical results is obtained with this extended mathematical model.

$$\frac{d\psi}{ds} - \sin\theta\cdot\frac{d\phi}{ds} =$$
$$= K_x\cdot\{\ \cos\theta\cdot\cos\phi\cdot(M_x(\ell) + F_z\cdot(\ell+v(\ell)-s-v(s)) + F_y\cdot(-w(\ell)+w(s)))+$$
$$+\ \cos\theta\cdot\sin\phi\cdot(M_y(\ell) + F_z\cdot(-u(\ell)+u(s)) + F_x\cdot(w(\ell)-w(s)))+$$
$$-\ \sin\theta\cdot(M_z(\ell) + F_x\cdot(-\ell-v(\ell)+s+v(s)) + F_y\cdot(u(\ell)-u(s)))\ \}$$

$$\cos\psi\cdot\frac{d\theta}{ds} + \sin\psi\cdot\cos\theta\cdot\frac{d\phi}{ds} =$$
$$= K_y\cdot\{\ (-\cos\psi\cdot\sin\phi+\sin\psi\cdot\sin\theta\cdot\cos\phi)\cdot(M_x(\ell)+F_z\cdot(\ell+v(\ell)-s-v(s))+F_y\cdot(-w(\ell)+w(s)))+$$
$$+(\cos\psi\cdot\cos\phi+\sin\psi\cdot\sin\theta\cdot\sin\phi)\cdot(M_y(\ell) + F_z\cdot(-u(\ell)+u(s)) + F_x\cdot(w(\ell)-w(s)))+$$
$$+\ \sin\psi\cdot\cos\theta\cdot(M_z(\ell) + F_x\cdot(-\ell-v(\ell)+s+v(s)) + F_y\cdot(u(\ell)-u(s)))\ \}$$

$$-\sin\psi\cdot\frac{d\theta}{ds} + \cos\psi\cdot\cos\theta\cdot\frac{d\phi}{ds} =$$
$$= K_z\cdot\{\ (\sin\psi\cdot\sin\phi+\cos\psi\cdot\sin\theta\cdot\cos\phi)\cdot(M_x(\ell)+F_z\cdot(\ell+v(\ell)-s-v(s))+F_y\cdot(-w(\ell)+w(s)))+$$
$$+(-\sin\psi\cdot\cos\phi+\cos\psi\cdot\sin\theta\cdot\sin\phi)\cdot(M_y(\ell) + F_z\cdot(-u(\ell)+u(s))+F_x\cdot(w(\ell)-w(s)))+$$
$$+(\cos\psi\cdot\cos\theta)\cdot(M_z(\ell) + F_x\cdot(-\ell-v(\ell)+s+v(s)) + F_y\cdot(u(\ell)-u(s)))\ \}$$

$$u(s) = {}_0\int^s (-\cos\psi\cdot\sin\phi + \sin\psi\cdot\sin\theta\cdot\cos\phi)\cdot dt$$

$$v(s) = {}_0\int^s (\cos\psi\cdot\cos\phi + \sin\psi\cdot\sin\theta\cdot\sin\phi - 1)\cdot dt$$

$$w(s) = {}_0\int^s (\sin\psi\cdot\cos\theta)\cdot dt$$

Figure 4.1 The relations between the deformations of the plate-spring and the load applied to the end can be determined with a mathematical model consisting of a set of "integro-differential" equations. This model has been derived in chapter 2 (figure 2.4).

4.2 Linearization and simplification of the differential equations.

Exact analytical solutions of the three differential equations given in figure 4.1 are not available. To determine the behaviour of plate-spring mechanisms it is however sufficient to find solutions for the range of technically possible or desired deformations. Moreover it is sufficient to obtain "close estimates" of the actual behaviour. As the mathematical model is itself an approximation there is no strict need to find exact solutions for the mathematical model.
In this section it will be attempted to use the information available about the physical plate-spring to reduce the differential equations to a set of simplified, approximating equations.

The first step in this process is to assume that angular deflections in "sound" plate-spring mechanisms will remain small. As upper limit angular deflections of 0.3 radians might be used. For the functions $\sin\alpha$ and $\cos\alpha$ the following power series may be used

$$\sin\alpha \simeq \alpha - \frac{1}{6}\cdot\alpha^3 + \ldots$$

$$\cos\alpha \simeq 1 - \frac{1}{2}\cdot\alpha^2 + \ldots$$

When $\sin\alpha$ is approximated by $\sin\alpha \simeq \alpha$ the maximum relative error will be less than 1.5 % for $\alpha < 0.3$ rad. With $\cos\alpha \simeq 1$ the relative error will then be less than 4.5 %. This magnitude of relative errors is for many applications acceptable and the equations of figure 4.1 may be simplified accordingly.This should however be done carefully. For the expression for v(s) for instance

$$v(s) \simeq {}_0\int^s (\cos\psi\cdot\cos\phi + \sin\psi\cdot\sin\theta\cdot\sin\phi - 1)\cdot dt \qquad (4.1)$$

this would result in

$$v(s) \simeq {}_0\int^s (\ 1 + \psi\cdot\theta\cdot\phi - 1\ )\cdot dt = {}_0\int^s \psi\cdot\theta\cdot\phi\cdot\ dt \qquad (4.2)$$

which is incorrect.Substitution of the first two terms of the power-

series for cos α yields

$$v(s) \simeq {}_0\int^s \left(1 - \tfrac{1}{2}\cdot\phi^2 - \tfrac{1}{2}\cdot\phi^2 + \tfrac{1}{4}\cdot\phi^2\cdot\phi^2 + \psi\cdot\theta\cdot\phi - 1 \right)\cdot dt \simeq$$

$$= {}_0\int^s \left(-\tfrac{1}{2}\cdot\phi^2 - \tfrac{1}{2}\cdot\phi^2 + \psi\cdot\theta\cdot\phi \right)\cdot dt \qquad (4.3)$$

This indicates that the substitution of power-series and the successive approximation should be performed carefully. Following this method the equations of figure 4.1 will result in the set of equations given in figure 4.2.

These results are applicable for long slender beams without restriction to the shape of the cross-section. For plate-springs however the compliance factors K_z and K_y are much larger than the compliance factor K_x. Typically the ratio between K_z,K_y and K_x will be from 10^3 to 10^4. As a result only the angular deflection ϕ en θ and the displacement u may have a significant magnitude. The angular deflection ψ and displacements v and w can be considered as disturbances which are relatively small.

To obtain approximating expressions for the main deformations a first estimate in the iterative-analytical process would be to assume that ψ ,v and w are equal to zero. This leads to the following expressions for ϕ, θ and u

$$\frac{d\theta}{ds} \simeq K_y \cdot \{ -\phi\cdot(M_x(\ell) + F_z\cdot(\ell-s)) + M_y(\ell) + F_z\cdot(-u(\ell) + u(s)) \}$$

$$\frac{d\phi}{ds} \simeq K_z \cdot \{ \theta\cdot(M_x(\ell) + F_z\cdot(\ell-s)) + \theta\cdot\phi\cdot(M_y(\ell) + F_z\cdot(-u(\ell) + u(s))) +$$

$$+ (M_z(\ell) + F_x\cdot(-\ell + s) + F_y\cdot(u(\ell) - u(s))) \}$$

$$u(s) \simeq {}_0\int^s -\phi \cdot dt \qquad (4.4)$$

When the main deformations have been determined the magnitude of the disturbances ψ ,v and w can be estimated with simplified forms of the remaining equations

$$\frac{d\psi}{ds} \simeq \theta \cdot \frac{d\phi}{ds} + K_x \cdot \{ M_x(\ell) + F_z\cdot(\ell-s) \}$$

$$v(s) \simeq {}_0\int^s -\tfrac{1}{2} \cdot \phi^2 \cdot dt$$

$$w(s) \simeq {}_0\int^s \psi \cdot dt \qquad (4.5)$$

$$\frac{d\psi}{ds} - \theta\cdot\frac{d\phi}{ds} =$$
$$= K_x\cdot\{ (M_x(\ell) + F_z\cdot(\ell+v(\ell)-s-v(s)) + F_y\cdot(-w(\ell)+w(s)))+$$
$$+ \phi\cdot(M_y(\ell) + F_z\cdot(-u(\ell)+u(s)) + F_x\cdot(w(\ell)-w(s)))+$$
$$-\theta\cdot(M_z(\ell) + F_x\cdot(-\ell-v(\ell)+s+v(s)) + F_y\cdot(u(\ell)-u(s))) \}$$

$$\frac{d\theta}{ds} + \psi\cdot\frac{d\phi}{ds} =$$
$$= K_y\cdot\{ (-\phi+\psi\cdot\theta)\cdot(M_x(\ell)+F_z\cdot(\ell+v(\ell)-s-v(s))+F_y\cdot(-w(\ell)+w(s)))+$$
$$+(1+\psi\cdot\theta\cdot\phi)\cdot(M_y(\ell) + F_z\cdot(-u(\ell)+u(s)) + F_x\cdot(w(\ell)-w(s)))+$$
$$+ \psi\cdot(M_z(\ell) + F_x\cdot(-\ell-v(\ell)+s+v(s)) + F_y\cdot(u(\ell)-u(s))) \}$$

$$-\psi\cdot\frac{d\theta}{ds} + \frac{d\phi}{ds} =$$
$$= K_z\cdot\{ (\psi\cdot\phi+\theta)\cdot(M_x(\ell)+F_z\cdot(\ell+v(\ell)-s-v(s))+F_y\cdot(-w(\ell)+w(s)))+$$
$$+(-\psi+\theta\cdot\phi)\cdot(M_y(\ell) + F_z\cdot(-u(\ell)+u(s))+F_x\cdot(w(\ell)-w(s)))+$$
$$+ (M_z(\ell) + F_x\cdot(-\ell-v(\ell)+s+v(s)) + F_y\cdot(u(\ell)-u(s))) \}$$

$$u(s) = {}_0\int^s (-\phi + \psi\cdot\theta)\cdot dt$$

$$v(s) = {}_0\int^s (-\tfrac{1}{2}\cdot\phi^2 - \tfrac{1}{2}\cdot\phi^2 + \psi\cdot\theta\cdot\phi)\cdot dt$$

$$w(s) = {}_0\int^s \psi \cdot dt$$

Figure 4.2. Result of the first step of simplification of the differential equations from fig.4.1 used to approximate the behaviour of a plate-spring under three-dimensional loading. The angular deflections ψ, θ and ϕ are a function of the parameter s.

A further simplification of the second of equations (4.4) is possible with respect to the part containing the product $\phi \cdot \theta$. In this part the influence of F_z can be neglected as it is small compared with the influence of F_z in the first term. This leads to

$$\frac{d\phi}{ds} \simeq K_z \cdot \{ \theta \cdot (M_x(\ell) + F_z \cdot (\ell - s)) + \theta \cdot \phi \cdot M_y(\ell) + M_z(\ell) + F_x \cdot (-\ell + s) + F_y \cdot (u(\ell) - u(s)) \} \qquad (4.6)$$

This expression still contains one term which is quadratic in the angular deflections , ϕ and θ . This term can only be neglected when the couple $M_y(\ell)$ has the same order of magnitude as one of the other loading components. This will be true for plate-spring mechanisms which are mainly based upon bending of the plate-springs, such as parallel guides and cross-spring pivots.

For plate-spring mechanisms where torsion of the plate-springs is the main deformation it will in many cases be allowable to neglect this term as the deflection $\phi(s)$ will be very small. It is therefore suggested to neglect the term $\theta . \phi . M_y(\ell)$ in equation (4.6) and to verify at the end of the analysis whether this is justified on the basis of the obtained results.

The result of this process of linearization and approximation is the set of equations presented in figure 4.3. In using these expressions it is necessary to be aware of the assumptions made in this section.

Main deformations:

$$\frac{d\theta(s)}{ds} \simeq K_y \cdot \{ -\phi \cdot (M_x(\ell) + F_z \cdot (\ell - s)) + M_y(\ell) + F_z \cdot (-u(\ell) + u(s)) \}$$

$$\frac{d\phi(s)}{ds} \simeq K_z \cdot \{ \theta \cdot (M_x(\ell) + F_z \cdot (\ell - s)) + M_z(\ell) + F_x \cdot (-\ell + s) + F_y \cdot (u(\ell) - u(s)) \}$$

$$u(s) \simeq \int_0^s -\phi \cdot dt$$

Disturbances:

$$\frac{d\psi(s)}{ds} \simeq \theta \cdot \frac{d\phi(s)}{ds} + K_x \cdot \{ M_x(\ell) + F_z \cdot (\ell - s) \}$$

$$v(s) \simeq \int_0^s -\frac{1}{2} \cdot \phi^2 \cdot dt$$

$$w(s) \simeq \int_0^s \psi \cdot dt$$

Figure 4.3. Simplified set of differential equations which can be used to determine the behaviour of plate-spring mechanisms. Derived using the following additional assumptions :
- Angular deflections will remain small (< 0,5 rad)
- $K_x >> K_y, K_z$
- $M_y(\ell)$ is not large compared to all other loading components.

4.3 Application of the iterative-analytical method.

Solutions for the set of simplified equations may be obtained with the iterative-analytical method described in chapter 3. To illustrate how this method is used for cases of three-dimensional loading a simple case of a plate-spring loaded by two forces F_x and F_z will be discussed (see figure 4.4).

As a first step initial estimates for the main deformations, θ, ϕ and u, as a function of s are made, based on the shape of the plate-spring under influence of only the force F_x. In this case the angular deflection θ is equal to zero and the estimates for ϕ and u are

$$\phi^*(s) \simeq \phi_\ell \cdot (-2\cdot\xi + 3\cdot\xi^2) - \frac{u(\ell)}{\ell} \cdot (6\cdot\xi - 6\cdot\xi^2)$$

$$\frac{u^*(s)}{\ell} \simeq \phi_\ell \cdot (\xi^2 - \xi^3) + \frac{u(\ell)}{\ell} \cdot (3\cdot\xi^2 - 2\cdot\xi^3)$$

where $\xi = \frac{s}{\ell}$

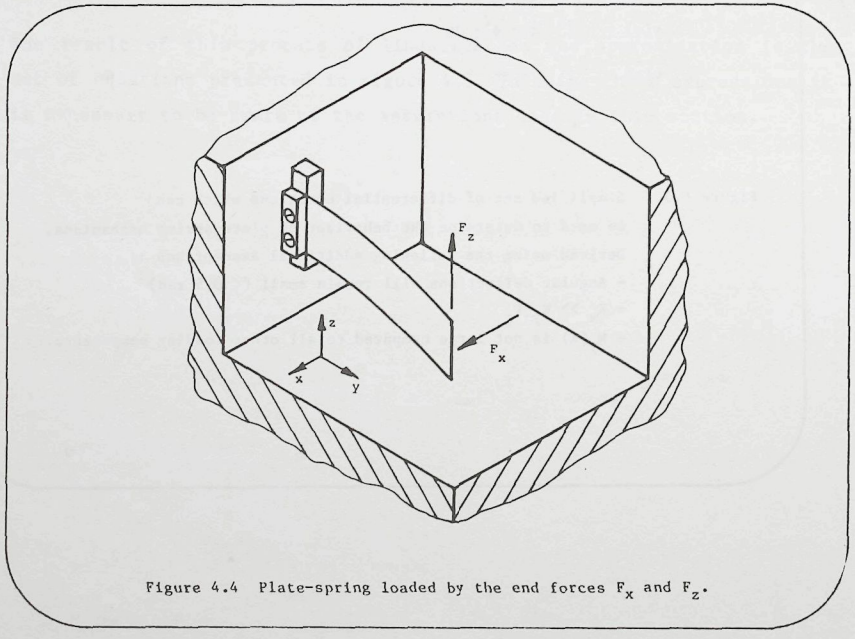

Figure 4.4 Plate-spring loaded by the end forces F_x and F_z.

Using the information that $M_z(\ell)$ equals zero these estimates can be simplified and expressed in either $u(\ell)$ or ϕ_ℓ. Selecting the expression containing $u(\ell)$ yields

$$\phi^*(s) \simeq -\frac{u(\ell)}{\ell} \cdot (3\cdot\xi - \frac{3}{2}\cdot\xi^2)$$

$$\frac{u^*(s)}{\ell} \simeq \frac{u(\ell)}{\ell} \cdot (\frac{3}{2}\cdot\xi^2 - \frac{1}{2}\cdot\xi^3) \qquad (4.7)$$

Substitution of these estimates in the first differential equation of figure 4.3 with M_x and M_y equal to zero leads to

$$\frac{d\theta}{ds} \simeq K_y \cdot \{ \frac{u(\ell)}{\ell} \cdot (3\cdot\xi - \frac{3}{2}\cdot\xi^2)\cdot F_z\cdot(\ell - s) + F_z\cdot u(\ell)\cdot(-1 + \frac{3}{2}\cdot\xi^2 - \frac{1}{2}\cdot\xi^3) \}$$

which can be integrated to estimate the angular deflection θ as

$$\theta^*(s) \simeq K_y\cdot F_z\cdot u(\ell)\cdot\ell\cdot(-\xi + \frac{3}{2}\cdot\xi^2 - \xi^3 + \frac{1}{4}\cdot\xi^4) \qquad (4.8)$$

Substitution of this estimate in the second equation of figure 4.3 and subsequent integration leads to improved estimates of the angular deflection $\phi(s)$ and displacement u(s)

$$\phi^{**}(s) \simeq -K_z\cdot F_x\cdot\ell^2\cdot(\xi - \tfrac{1}{2}\cdot\xi^2) + K_z\cdot K_y\cdot F_z^2\cdot u(\ell)\cdot\ell^3\cdot\{-\tfrac{1}{2}\cdot\xi^2 + \tfrac{5}{6}\cdot\xi^3 - \tfrac{5}{8}\cdot\xi^4 + \tfrac{1}{4}\cdot\xi^5 - \tfrac{1}{24}\cdot\xi^6\}$$

$$u^{**}(s) \simeq K_z\cdot F_x\cdot\ell^3\cdot(\tfrac{1}{2}\cdot\xi^2 - \tfrac{1}{6}\cdot\xi^3) - K_z\cdot K_y\cdot F_z^2\cdot u(\ell)\cdot\ell^4\cdot\{-\tfrac{1}{6}\cdot\xi^3 + \tfrac{5}{24}\cdot\xi^4 - \tfrac{1}{8}\cdot\xi^5 + \tfrac{1}{24}\cdot\xi^6 - \tfrac{1}{168}\cdot\xi^7\} \qquad (4.9)$$

For the relation between the deflection $u(\ell)$ of the end of the plate-spring and the loading forces F_x and F_z the following estimate is thus obtained

$$u(\ell) \simeq \frac{\frac{1}{3}\cdot K_z\cdot F_x\cdot\ell^3}{(1 - \frac{1}{21}\cdot K_z\cdot K_y\cdot F_z^2\cdot\ell^4)} \qquad (4.10)$$

This is the first result of the iterative-analytical analysis giving a first-order estimate of the influence of the loading force F_z on the stiffness of the plate-spring in the direction of the x-axis. This estimate is valid only for relatively small values of F_z. For large values the difference between the two successive estimates for the shape of the plate-spring becomes to large and further iterative steps should be made for such cases.

In order to estimate the difference between the two expressions for the deflection u(s) ,(4.9) and (4.7) , the relative magnitude of the difference for loading with a force $F_z = (\ell^2 \cdot \sqrt{K_z \cdot K_y})^{-1}$ is shown in figure 4. A linear relation exists between the magnitude of the difference and F_z^2 . It is clear that the difference will be less than 5% of u(ℓ) for values of $F_z^2 \cdot K_z \cdot K_y \cdot \ell^4$ upto 10 and for such cases the estimate of (4.7) appears to be sufficiently accurate for most practical cases.

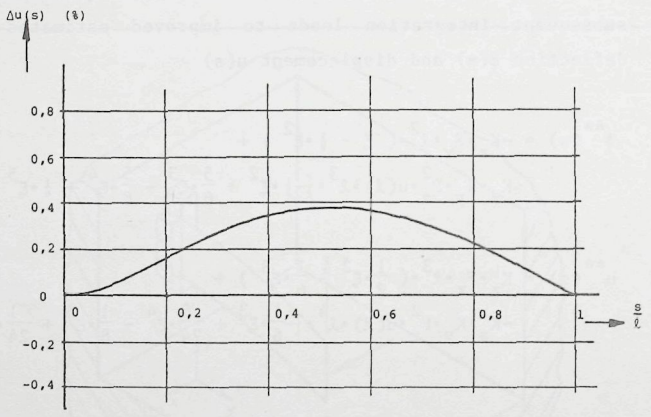

Figure 4.5 During the iterative analytical analysis the shape of the deformed plate-spring is estimated in the subsequent steps. This figure shows the relative difference between the first and second estimate of the deflection u(s) for a loading force where $F_z^2 \cdot K_z \cdot K_y \cdot \ell^4 = 1$.

An interesting aspect of expression (4.10) is that it gives a first-order estimate of the magnitude of the load F_z for which the stiffness c_x of the plate-spring becomes equal to zero. From (4.10) the following expression for F_z is obtained

$$F_z \cdot \ell^2 \cdot \sqrt{K_z \cdot K_y} \simeq 4{,}6$$

This is a first-order estimate and better estimates may be obtained through further steps in the iterative analytical process. From the second step the following estimate for F_z would be obtained

$$F_z \cdot \ell^2 \cdot \sqrt{K_z \cdot K_y} \simeq 4{,}134$$

These results obtained from the relatively simple expressions in the mathematical model may be compared with the result from exact analytical analysis (lit. T1,P1), which yields

$$F_z \cdot \ell^2 \cdot \sqrt{K_z \cdot K_y} \simeq 4{,}013$$

This indicates that the iterative analytical method yields reasonably good estimates.

The next step in the analysis is the determination of the angle $\phi(s)$ and deflection w(s).The relation between F_z and w(s) determines the stiffness of the plate-spring mechanisms perpendicular to the plane of motion. For many applications it will be sufficient to obtain a first order estimate of this stiffness.

Using the fourth of the equations from figure 4.3, the initial estimates for $\phi^*(s)$ and $u^*(s)$ and expression (4.8) the following result for $\phi(s)$ is obtained

$$\phi(s) \simeq F_z \cdot K_y \cdot u(\ell)^2 \cdot \{ \tfrac{3}{2} \cdot \xi^2 - \tfrac{5}{2} \cdot \xi^3 + \tfrac{15}{8} \cdot \xi^4 - \tfrac{3}{4} \cdot \xi^5 + \tfrac{1}{8} \cdot \xi^6 \} + F_z \cdot K_x \cdot \ell^3 \cdot (\xi - \tfrac{1}{2} \cdot \xi^2) \qquad (4.11)$$

where the first part is due to torsion of the plate-spring and the second part results from bending about the x-axis where the compliance K_x is very small.

Integration of (4.11) yields the following estimate for w(s)

$$w(s) \simeq F_z \cdot K_y \cdot u(\ell)^2 \cdot \ell \cdot \{ \frac{1}{2}\cdot\xi^3 - \frac{5}{8}\cdot\xi^4 + \frac{3}{8}\cdot\xi^5 - \frac{1}{8}\cdot\xi^6 + \frac{1}{48}\cdot\xi^7 \} + \\ + F_z \cdot K_x \cdot \ell^3 \cdot (\frac{1}{2}\cdot\xi^2 - \frac{1}{6}\cdot\xi^3) \qquad (4.12)$$

For the deflection $w(\ell)$ of the loaded end this yields

$$w(\ell) \simeq F_z \cdot \ell^3 \cdot \{ K_y \cdot (\frac{u(\ell)}{\ell})^2 \cdot \frac{1}{7} + K_x \cdot \frac{1}{3} \} \qquad (4.13)$$

From this expression it is clear that the deflection due to bending about the x-axis will be dominant for small values of $u(\ell)$. For values of $K_y = 10^3 \cdot K_x$ the two effects are equal in magnitude for $\frac{u(\ell)}{\ell} \simeq 0{,}05$. For larger deflections the influence of the torsional deformation becomes more important.
(Note: This result does not contain the contribution from the shear deformation of the plate-spring which may become relatively important for wide plate-springs, $\ell \leq 2 \cdot b$.)

This analysis of the simple case of loading of the plate-spring illustrates that simple expressions estimating the main properties of the plate-spring are easily obtained with the iterative-analytical method. The derived expressions for the influence of F_z upon the stiffness in the direction of motion ,x-axis direction, and for the stiffness of the deformed plate-spring in the z-direction are first-order estimates which may be used for deflections upto $0{,}2 \cdot \ell$ in x-direction and loading forces F_z upto $2 \cdot (\sqrt{K_z \cdot K_y} \cdot \ell^2)^{-1}$. Depending upon the required accuracy the difference between the estimates and exact solutions of the differential equations may become too large for larger deflections or loading forces.

4.4 Evaluation of experimental and theoretical results.

To investigate whether the iterative-analytical and numerical solutions are acceptable predictions of the actual behaviour of the plate-springs they should be compared with results from reliable experiments.As it is not easily realized to apply two forces to the free end of the spring as described in the preceding paragraph, measurements were carried out with a plate-spring fixed as shown in figure 4.6. The plate-spring is clamped at the two ends. The "free"-end clamping piece is mounted on three steel wires which fix its position in x, ϕ and θ direction. The loading force F_z is applied so as to act along a line through the center of the spring. In this case the loading conditions for each half of the spring will be as discussed in the preceding paragraph (as in figure 4.4). With this measurement the deflection $w(\ell)$ of the free end can be determined.The angular deflection ϕ of the free end will be equal to zero.

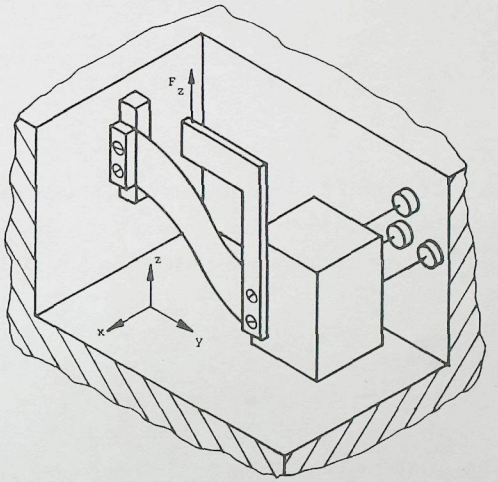

Figure 4.6 In order to realize the loading conditions of a plate-spring shown in figure 4.4 measurements were performed on springs clamped at both ends. Using considerations of the symmetry of the loading when the force F_z is applied at the middle of the plate-spring it can be proved that, apart from a minor effect, each half of the plate-spring is loaded as assumed in the theoretical analysis.
The plate-spring used in measurements thus has a length $2 \cdot \ell$.

Similarly it is possible to determine the influence of the loading force F_z upon the relation between F_x and $u(\ell)$. In this case the stiffness of a plate-spring parallel guide loaded by the force F_z at the center of the guide has been measured. (For more details about the equipment used in measurements see chapter 8)

The measurements were performed with steel plate-springs with the following dimensions, $2 \cdot \ell = 80$ mm.
$b = 20$ mm.
$h = 0.25$ mm.

The magnitude of the compliances were calculated with the expressions,

$$K_x = \frac{12}{E.b^3.h} \quad , \quad K_y = \frac{3}{G.b.h^3} \quad , \quad K_z = \frac{12}{E.b.h^3}$$

where E and G are Young's modulus and shear modulus respectively.

In figure 4.7 the results from measurements are compared with the predicted values from expressions (4.10) and (4.13), and with results from direct numerical integration of the differential equations. In figure 4.7A and B the influence of the shear deformations have been taken into account as well. For the numerical solution an adapted version of the computer program described in chapter 3 was used. As can be seen from figure 4.7 the theoretical results from both methods are in good agreement. This is obvious when the deflections of the plate-springs are small and the approximations made are acceptable. But also for larger values of F_z and $u(\ell)$ both theoretical solutions yield about the same results.There is however a remarkable difference between results from the theory and those from the experiments. These differences could not be attributed to the influence of inaccuracies in the experiments.
This comparison of measured and calculated deformations leads to the conclusion that the mathematical model used to describe the behaviour of the plate-spring is not complete. The differences are expected to be maynly due to the influence of the constrained warping of the cross-section at the clamped ends of the plate-spring.In the following paragraph this will be discussed and the mathematical model will be adjusted accordingly.

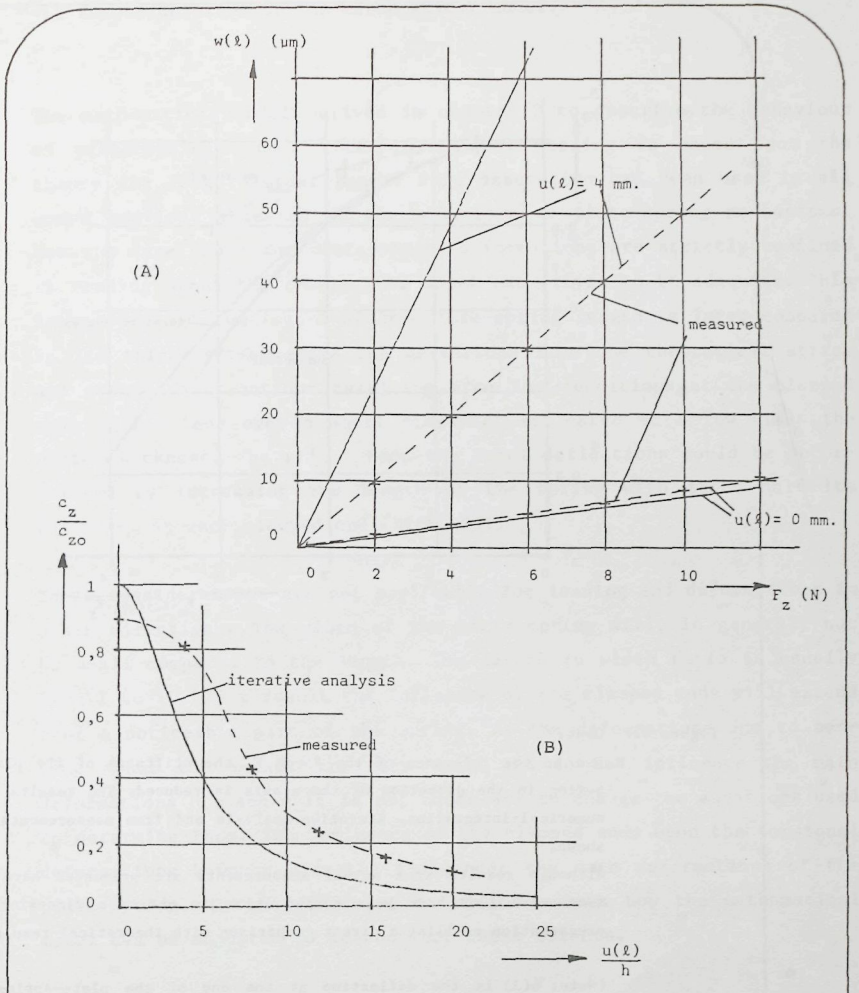

Figure 4.7 Comparison of measured and calculated deformations of a plate-spring loaded by forces F_x and F_z.
A. Measured and calculated deflection $w(\ell)$ as a function of the loading force F_z for displacements $u(\ell)$ of zero and four millimeters.
B. With increasing deflection $u(\ell)$ the stiffness c_z of the plate-spring in the direction of the z-axis decreases.
For these comparisons the influence of the additional deformation of the plate-springs due to the shear deformation has been taken into account.

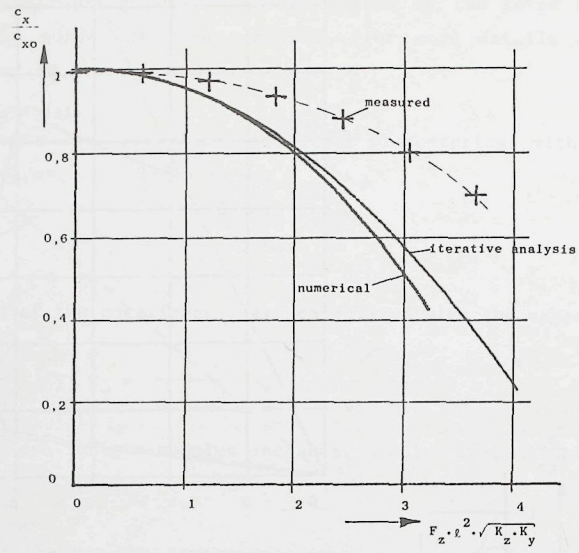

(C)

Figure 4.7 Cont.

C. Due to the influence of the force F_z the stiffness of the plate-spring in the direction of the x-axis is reduced. The results from numerical-integration, iterative-analysis and from measurements are shown.
Although results from actual measurements are presented here the measured values have been scaled so as to obtain a dimensionless presentation enabling a direct comparison with theoretical results.

(Note: $u(\ell)$ is the deflection at the end of the plate-spring as shown in figure 4.4. In the measurements this is the deflection of the middle of the plate-spring (figure 4.6).)

(Plate-spring dimensions: $2 \cdot \ell$ = 80 mm.
b = 20 mm.
h = 0,25 mm.)

4.5 Reconsideration of the mathematical model.

The mathematical model derived in chapter 2 to describe the behaviour of plate-springs under three-dimensional loading is based upon the theory for long, slender beams. This assumption has been used in all known previous research on the behaviour of plate-spring mechanisms. For the case where the plate-spring deformations are strictly confined to bending about the z-axis this model has proven to be adequate. This is a result of the fact that the plate-spring length is large compared to its thickness.Therefore the deviations from the theoretical stress and strain distributions resulting from the conditions at the clamped ends will extend over a short distance, estimated at a few times the plate thickness. The effect upon the total deflections could be incorporated by increasing the length of the spring with about half its thickness at each clamped end (litt. S1).

These considerations are not applicable for loading and deformations in other directions. The width of the plate-spring will, in general, not be small compared to the length. The length to width ratio is usually from 2 to 10. As a result the influence of the clamped ends will extend over a noticeable part of the spring. As the deformations due to bending about the x-axis are very small and do not influence the main deformations θ, ϕ and u it is not necessary to change the equations used to determine them. The influence of the clamped ends upon the torsional deformations however directly influences the main deformations of the plate-spring. In the following it will be shown how the mathematical model can be adjusted to account for these effects.

When a plate-spring is loaded by a torque M_y shear-stresses will occur in the cross-sections. Therefore the cross-sections will be deformed. Points that were initially in one plane of the cross-section will perform a relative displacement perpendicular to this plane. The originally flat cross-section will be deformed as shown in figure 4.8. This deformation is called the "warping" of the cross-section.

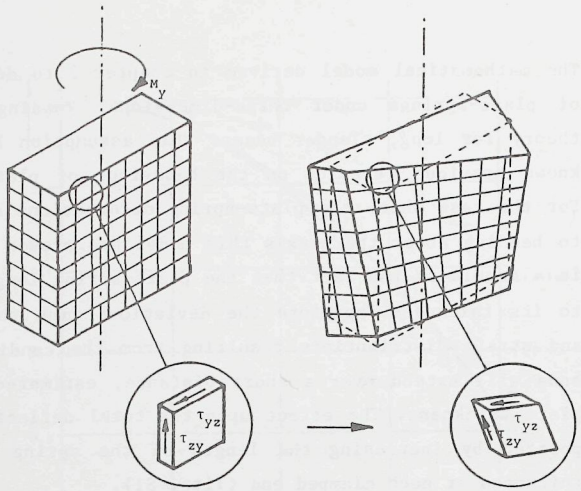

Figure 4.8 Due to the torsion moment M_y shear stresses will be present in every cross-section. Due to these stresses a rectangular part of the undeformed plate-spring will deform into a "diamond" shape. Over the total cross-section this will cause relative motion of different points of the cross-section in the direction of the y-axis. This is called the "warping" of the cross-section.

At the clamping of the plate-spring this warping can not occur. This is due to the fact that a cross-section slightly inside the clamping should then be rotated about the y-axis. As the clamping will inhibit this relative rotation the cross-section located at the edge of the clamping pieces can not be warped.

The torsional deformation of clamped beams can be calculated with a method described among others by Koiter (lit. K1). At first it is necessary to determine the "warping-constant" ,Γ , for the cross-section of the beam. This constant indicates the magnitude of the "out-of-plane" motion of points of the ,initially flat , cross-section.
Using the expressions given in lit.(K1) for plate-springs, with rectangular cross-sections with a large ratio of width to thickness, this constant can be estimated as

$$\Gamma \simeq \frac{1}{144} \cdot b^3 \cdot h^3 \qquad (4.14)$$

From the method described by Koiter it is concluded that the twisting torque, M_y, at a given point of the plate-spring will cause both twist and warping. Whenever the warping is constrained, for instance at the clamped ends, this will mean that an increased torque is required to obtain a certain twist.
This is formalized in the following equation for the curvature

$$\kappa_y(s) \simeq K_y \cdot M_y + K_y \cdot \Gamma \cdot E \cdot \frac{d^2\kappa_y(s)}{ds^2} \qquad (4.15)$$

This expression should replace the second of the equations for the curvatures in chapter 2, the Euler-Bernoulli hypothesis. Also in the final set of equations of chapter 2, figure 2.4, the second differential equation should be adjusted.

To determine the magnitude of the second derivative of the curvature κ_y the expression given in figure 2.3

$$\kappa_y(s) = \cos\phi(s) \cdot \frac{d\theta(s)}{ds} + \sin\phi(s) \cdot \sin\theta(s) \cdot \frac{d\phi(s)}{ds} \qquad (4.17)$$

can be used.The resulting expression for $d^2\kappa_y/ds^2$ will be containing the first and second derivative of $\phi(s)$ and first to third derivative of $\phi(s)$ and $\theta(s)$.As the expressions used to calculate the deformations, (figure 4.3), are obtained by simplification and linearization the expression for $d^2\kappa_y/ds^2$ can also be simplified. This leads to the following result

$$\frac{d^2\kappa_y(s)}{ds^2} \simeq \frac{d^3\theta(s)}{ds^3} \qquad (4.18)$$

With this result the new mathematical model for the plate-spring is formed by the set of equations given in figure 4.9. It is clear that the first equation is now a third-order differential equation. To find solutions for this new mathematical model two additional boundary conditions are required. These conditions are resulting from the situation at the ends of the plate-spring. At a clamped end the warping of the cross-section is inhibited and therefore the first derivative of $\theta(s)$ will be equal to zero.At a free end there are no restrictions imposed upon the deformation of the cross-section. As a result the second derivative of $\theta(s)$ will be equal to zero.

Main deformations:

$$-\frac{d\theta(s)}{ds} - K_y \cdot E \cdot \Gamma \cdot \frac{d^3\theta(s)}{ds^3} =$$

$$\approx K_y \cdot \{-\phi \cdot (M_x(\ell) + F_z \cdot (\ell - s)) + M_y(\ell) + F_z \cdot (-u(\ell) + u(s))\}$$

$$\frac{d\phi(s)}{ds} \approx K_z \cdot \{\theta \cdot (M_x(\ell) + F_z \cdot (\ell - s)) + M_z(\ell) + F_x \cdot (-\ell + s) + F_y \cdot (u(\ell) - u(s))\}$$

$$u(s) \approx \int_0^s -\phi \cdot dt$$

Disturbances:

$$\frac{d\psi(s)}{ds} \approx \theta \cdot \frac{d\phi(s)}{ds} + K_x \cdot \{M_x(\ell) + F_z \cdot (\ell - s)\}$$

$$v(s) \approx \int_0^s -\frac{1}{2} \cdot \phi^2 \cdot dt$$

$$w(s) \approx \int_0^s \psi \cdot dt$$

Figure 4.9 Simplified set of differential equations derived to account for the effect of the warping of the cross-section; this can be used to determine the influence of the constrained warping upon the behaviour of plate-spring mechanisms.

Resuming

-Clamped end → $\frac{d\theta(s)}{ds} = 0$ (4.19)

-Free end → $\frac{d^2\theta(s)}{ds^2} = 0$ (4.20)

This mathematical model can be used to determine the deformations of the plate-spring under the influence of forces F_z and F_x (fig. 4.4). Solutions can be obtained with the iterative analytical method. As in paragraph 4.3 an initial estimate for the deformed shape is used to start calculations. In Annex 4.I this analysis is performed, leading to the following expressions for $u(\ell)$ and $w(\ell)$

$$u(\ell) \approx \frac{1}{3} \cdot K_z \cdot F_x \cdot \ell^3 \cdot \left\{ \frac{1}{1 - K_z \cdot K_y \cdot F_z^2 \cdot \ell^4 \left(\frac{1}{21} - \frac{1}{3 \cdot \mu} + \frac{7}{5 \cdot \mu^2} - \frac{4}{\mu^3} + \frac{8}{\mu^4} - \frac{12}{\mu^5} + \frac{12}{\mu^6} - \frac{12}{\mu^7}\right)} \right\} \quad (4.21)$$

$$w(\ell) \approx \frac{1}{3} \cdot F_z \cdot K_x \cdot \ell^3 + F_z \cdot K_y \cdot u(\ell)^2 \cdot \ell \cdot \left\{ \frac{1}{7} - \frac{1}{\mu} + \frac{21}{5 \cdot \mu^2} - \frac{12}{\mu^3} + \frac{24}{\mu^4} - \frac{36}{\mu^5} + \frac{36}{\mu^6} + \frac{36}{\mu^7} \right\} \quad (4.22)$$

where $\mu^2 = \frac{\ell^2}{E \cdot \Gamma \cdot K_y}$ and with the assumption that $\ell \geq 2 \cdot b$

The magnitude of the influence of the constrained warping depends upon the parameter μ. For long and slender plate-spring this parameter will become very large and expressions (4.21) and (4.22) will give the same results as the earlier results (4.11) and (4.13). For plate-springs with a rectangular cross-section and b > h the parameter μ may be estimated as,

$$\mu \approx \frac{\ell}{b} \cdot \sqrt{\frac{24}{1+\nu}}$$

These results could be compared with the results from experiments and the earlier results as were shown in figure 4.7. In figure 4.10 the results are shown and it is clear that the analytical results with the new mathematical model are better predictions of the experimental results than before. The effect of the constrained warping clearly forms an important factor in the behaviour of plate-spring mechanisms. Still the remaining differences between theoretical and experimental results indicate that other factors are influencing the behaviour of the plate-springs. Possible causes of the remaining differences may be the inaccuracy of the actual dimensions of the plate-springs and the

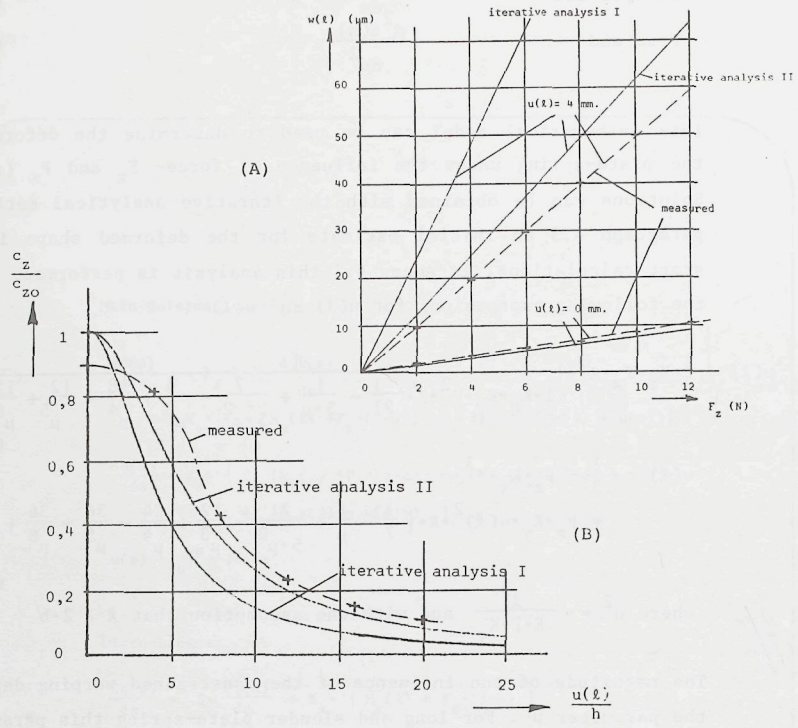

Figure 4.10 Results from calculations based on the new mathematical model compared with the previous results, (fig. 4.7).

A. Measured and calculated deflections $w(\ell)$ as a function of the loading force F_z for displacements $u(\ell)=0$ mm and $u(\ell)=4$ mm.
It is clear that the calculated deflection $w(\ell)$ obtained with the new mathematical model (iterative analysis II) is a better estimate for the measured deflections for $u(\ell) = 4$ mm.

B. The results from calculations with the adjusted mathematical model for the variations of the stiffness c_z of the plate-spring as a function of the deflection of the loaded end compared with the earlier results and the measured values. For practical applications it appears that the new mathematical model yields sufficiently accurate predictions of this variation.

In these comparisons the additional deformation of the plate-spring due to shear has been accounted for.

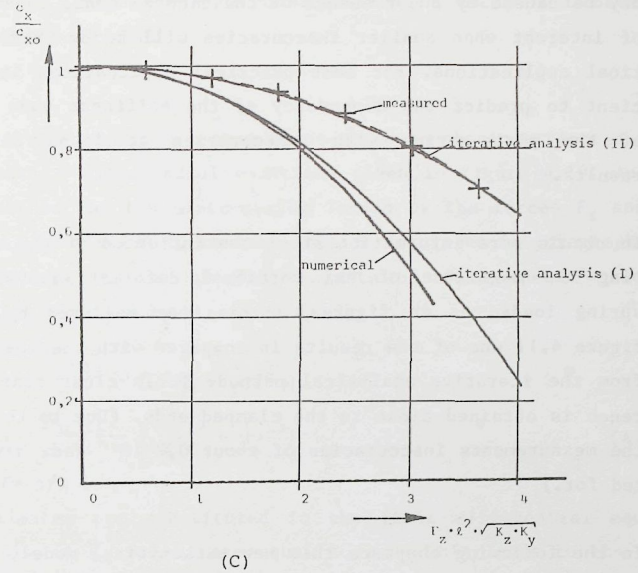

Figure 4.10 Cont.

C. Due to the application of the force F_z the stiffness c_x of the plate-spring decreases. Results from different theoretical methods estimating this effect are shown together with the results from measurements Here a remarkably good agreement between the result obtained with the new mathematical model and the measurement is noticed.
(Note: $u(\ell)$ is the deflection of the end of the plate-spring as shown in figure 4.4. In the measurements this is the deflection of the middle of the plate-spring as shown in figure 4.6)

(Dimensions of the plate-spring, $2\cdot\ell$ = 80 mm
b = 20 mm
h = 0,25 mm.)

an-isotropy of the plate-spring material. In addition other phenomena may be caused by the presence of the clamped ends. These effects may be of interest when smaller inaccuracies will be desired in future practical applications. For most practical applications it will be sufficient to predict the dependency of the stiffness upon the deflections of the plate-spring with inaccuracies as found in the presented results.

To obtain more information about the influence of the constrained warping the magnitude of the torsional deformation $\theta(s)$ of the plate-spring loaded as in figure 4.6 has been measured by Kruit (K2). In figure 4.11 one of the results is compared with the theoretical results from the iterative analytical method. It is clear that a large difference is obtained close to the clamped ends. (Due to the method used in the measurements inaccuracies of about $0{,}2 \cdot 10^{-3}$ rad. have to be accounted for.)

In the following chapters this new mathematical model, given in figure 4.9, will be used to calculate the main properties of different plate-spring mechanisms.

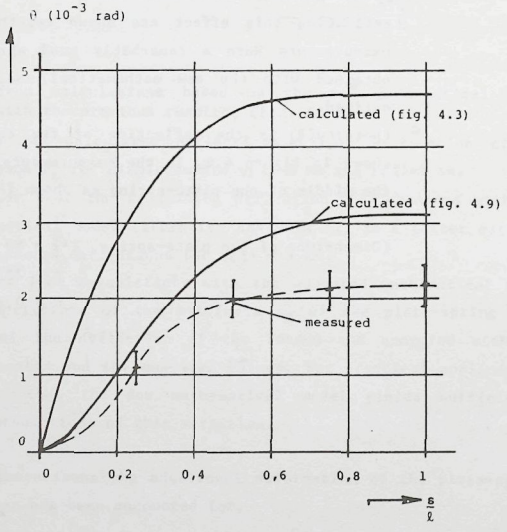

Figure 4.11 Comparison of calculated and measured angular deformations around the y-axis of the plate-spring (as in fig.4.7) under influence of the force F_z. Values given for $u = 0{,}05 \cdot \ell$ and $F_z = 2$ N.

Annex 4.I. Determination of the deformations of a plate-spring due to the forces F_x and F_z, under consideration of the effect of the "constrained" warping.

The iterative-analytical method can be used to obtain estimated solutions for the set of differential equations given in figure 4.10. Application of this method for the plate-spring loaded by the forces F_x and F_z, see figure 4.4, is similar to the application described in paragraph 4.3. The analysis starts with an initial estimate of the shape of the deformed plate-spring as given by equations (4.7)

$$\phi^*(s) \simeq -\frac{u(\ell)}{\ell} \cdot \left(3 \cdot \xi - \frac{3}{2} \cdot \xi^2 \right)$$
$$\frac{u^*(s)}{\ell} \simeq \frac{u(\ell)}{\ell} \cdot \left(\frac{3}{2} \cdot \xi^2 - \frac{1}{2} \cdot \xi^3 \right) \qquad (4.7)$$

where $\xi = s/\ell$.

These estimates are substituted in the first differential equation of figure 4.10. As M_x and M_y are equal to zero this leads to the following equation

$$\frac{d\theta(s)}{ds} - K_y \cdot E \cdot \Gamma \cdot \frac{d^3\theta(s)}{ds^3} =$$
$$\simeq K_y \cdot \left\{ \frac{u(\ell)}{\ell} \cdot \left(3 \cdot \xi - \frac{3}{2} \cdot \xi^2 \right) \cdot F_z \cdot (\ell - s) + F_z \cdot u(\ell) \cdot \left(-1 + \frac{3}{2} \cdot \xi^2 - \frac{1}{2} \cdot \xi^3 \right) \right\} \qquad (4.I.1)$$

The solution of this third-order differential equation can be determined as the sum of a particular solution for the complete equation and a general solution for the reduced equation. In this case the solution will have the following form

$$\theta(s) \simeq K_y \cdot F_z \cdot u(\ell) \cdot \ell \cdot$$
$$\cdot \left(a_1 \cdot \xi + a_2 \cdot \xi^2 + a_3 \cdot \xi^3 + a_4 \cdot \xi^4 + \right. \qquad \text{(particular solution)}$$
$$\left. + A + B \cdot e^{-\mu \cdot \xi} + C \cdot e^{\mu \cdot \xi} \right) \qquad \text{(general solution)} \qquad (4.I.2)$$

where $\mu = \frac{\ell}{\sqrt{K_y \cdot E \cdot \Gamma}}$ which may be estimated as $\mu \simeq \frac{\ell}{b} \cdot \sqrt{\frac{24}{1+\nu}}$ for plate-springs with small thickness compared to the width.

The coefficients a_1-a_4 in the particular solution are determined so as to satisfy equation (4.I.1). The coefficients A, B and C are determined using the boundary conditions for the total solution for $\theta(s)$. For the loading case as shown in figure 4.4 the boundary conditions are

$$s = 0 \rightarrow \quad \theta(0) = 0 \quad , \quad \frac{d\theta(0)}{ds} = 0$$

$$s = \ell \rightarrow \quad \frac{d^2\theta(\ell)}{ds^2} = 0$$

(Note: These boundary conditions are not correct when the plate-spring as used in the measurements, figure 4.7, is analysed. In that case the boundary condition for $s \rightarrow \ell$ should be , $\frac{d\theta(\ell)}{ds} = 0$. This case will be considered in Annex 5.I and the results show no relevant differences for the dimensions of the plate-spring as used in the measurements.)

This leads to the following expressions for the coefficients a_1-a_4 and A, B and C

$$a_1 = -1 - \frac{6}{\mu^2}$$

$$a_2 = \frac{3}{2} + \frac{3}{\mu^2}$$

$$a_3 = -1$$

$$a_4 = \frac{1}{4}$$

$$B = \frac{\left(1 + \frac{6}{\mu^2}\right)\cdot\mu\cdot e^{\mu} + \frac{6}{\mu^2}}{\mu^2\cdot\left(e^{\mu} + e^{-\mu}\right)}$$

$$C = \frac{\left(1 + \frac{6}{\mu^2}\right)\cdot\mu\cdot e^{-\mu} - \frac{6}{\mu^2}}{\mu^2\cdot\left(e^{\mu} + e^{-\mu}\right)}$$

$$A = -B - C \qquad (4.I.3)$$

Having determined this solution for $\theta(s)$, which is a first order estimate, it may be substituted in the second of the equations of figure 4.10. This yields the following equation

$$\frac{d\phi(s)}{ds} \simeq K_z \cdot \left\{ F_z\cdot\ell\cdot(1 - \xi)\cdot\theta(s) + F_x\cdot\ell\cdot(-1 + \xi) \right\} \qquad (4.I.4)$$

where $\theta(s)$ is given by equation (4.I.2). This differential equation can be integrated and leads to the following solution for $\phi(s)$ (with $\phi(0) = 0$)

$$\begin{aligned}\phi(s) \simeq\ & K_z\cdot K_y\cdot F_z^2\cdot\ell^3\cdot u(\ell)\cdot \left\{ a_1\cdot\left(\frac{1}{2}\cdot\xi^2 - \frac{1}{3}\cdot\xi^3\right) + a_2\cdot\left(\frac{1}{3}\cdot\xi^3 - \frac{1}{4}\cdot\xi^4\right) + \right.\\ & + a_3\cdot\left(\frac{1}{4}\cdot\xi^4 - \frac{1}{5}\cdot\xi^5\right) + a_4\cdot\left(\frac{1}{5}\cdot\xi^5 - \frac{1}{6}\cdot\xi^6\right) +\\ & + B\cdot\frac{1}{\mu}\cdot\left(1 - \frac{1}{\mu} + e^{-\mu\cdot\xi}\cdot\left(\xi + \frac{1}{\mu} - 1\right)\right) +\\ & + C\cdot\frac{1}{\mu}\cdot\left(-1 - \frac{1}{\mu} + e^{\mu\cdot\xi}\cdot\left(1 + \frac{1}{\mu} - \xi\right)\right) +\\ & \left. + A\cdot\left(\xi - \frac{1}{2}\cdot\xi^2\right) \right\} + K_z\cdot F_x\cdot\ell^2\cdot\left(-\xi + \frac{1}{2}\cdot\xi^2\right) \qquad (4.I.5)\end{aligned}$$

This result may be used in the third of equations of figure 4.10 and the following expression for u(s) may be obtained through integration (with u(0) = 0)

$$\begin{aligned}u(s) \simeq\ & -K_z\cdot K_y\cdot F_z^2\cdot\ell^4\cdot u(\ell)\cdot \left\{ a_1\cdot\left(\frac{\xi^3}{6} - \frac{\xi^4}{12}\right) + a_2\cdot\left(\frac{\xi^4}{12} - \frac{\xi^5}{20}\right) +\right.\\ & a_3\cdot\left(\frac{\xi^5}{20} - \frac{\xi^6}{30}\right) + a_4\cdot\left(\frac{\xi^6}{30} - \frac{\xi^7}{42}\right) + A\cdot\left(\frac{\xi^2}{2} - \frac{\xi^6}{6}\right) +\\ & + B\cdot\frac{1}{\mu}\cdot\left(\xi - \frac{\xi}{\mu} + \frac{2}{\mu^2} - \frac{1}{\mu} + e^{-\mu\cdot\xi}\cdot\left(\frac{1}{\mu} - \frac{2}{\mu^2} - \frac{\xi}{\mu}\right)\right) +\\ & \left. + C\cdot\frac{1}{\mu}\cdot\left(-\xi - \frac{\xi}{\mu} - \frac{1}{\mu} - \frac{2}{\mu^2} + e^{\mu\cdot\xi}\cdot\left(\frac{2}{\mu^2} + \frac{1}{\mu} - \frac{\xi}{\mu}\right)\right) \right\} +\\ & + K_z\cdot F_x\cdot\ell^3\cdot\left(\frac{\xi^2}{2} - \frac{\xi^3}{6}\right) \qquad (4.I.6)\end{aligned}$$

The relation between the forces F_x and F_z and the displacement $u(\ell)$ of the plate-spring end can thus be obtained by substitution of expressions (4.I.3) and evaluation of (4.I.6) for $s = \ell$.
Thus the following expression is obtained

$$\begin{aligned}u(\ell) \simeq\ & u(\ell)\cdot K_z\cdot K_y\cdot F_z^2\cdot\ell^4\cdot\left\{ \left(\frac{1}{21} + \frac{7}{5\cdot\mu^2} + \frac{8}{\mu^4} + \frac{12}{\mu^6} - \frac{12}{\mu^7}\right) +\right.\\ & - \left(\frac{1}{3\cdot\mu} + \frac{4}{\mu^3} + \frac{12}{\mu^5}\right)\cdot\left(\frac{e^{\mu} - e^{-\mu}}{e^{\mu} + e^{-\mu}}\right) +\\ & \left. + \left(\frac{24 - 24\cdot\mu + 12\cdot\mu^2 - 4\cdot\mu^3}{\mu^7\cdot\left(e^{\mu} + e^{-\mu}\right)}\right) \right\} +\\ & + K_z\cdot F_x\cdot\ell^3\cdot\frac{1}{3} \qquad (4.I.7)\end{aligned}$$

For most practical cases the value of μ will be large enough to allow for simplification of this expression.This will yield the result as given in expression (4.21). For relatively short plate-springs the complete solution may be used. It should however be noted that it is doubtfull whether the mathematical model is adequate for short plate-springs where $\ell \leq b$. In that case other factors may have a relatively large influence upon the deformations of the plate-spring.

Following the process described in paragraph 4.3 the solution for $\theta(s)$, expression (4.I.2) can be used to determine the angular deformation , $\phi(s)$, and the deflection $w(s)$ of the plate-spring. This results in the following expressions

$$\begin{aligned}\phi(s) \simeq\ & F_z \cdot K_x \cdot \ell^2 \cdot \left(\xi - \frac{\xi^2}{2} \right) + \\ & + F_z \cdot K_y \cdot u(\ell)^2 \cdot \{ a_1 \cdot \left(-\frac{3}{2} \cdot \xi^2 + \xi^3 \right) + a_2 \cdot \left(-\xi^3 + \frac{3}{4} \cdot \xi^4 \right) + \\ & \quad a_3 \cdot \left(-\frac{3}{4} \cdot \xi^4 + \frac{3}{5} \cdot \xi^5 \right) + a_4 \cdot \left(-\frac{3}{5} \cdot \xi^5 + \frac{1}{2} \cdot \xi^6 \right) \\ & \quad + A \cdot \left(-3 \cdot \xi + \frac{3}{2} \cdot \xi^2 \right) + \\ & \quad + B \cdot \frac{1}{\mu} \cdot \left(-3 + \frac{3}{\mu} + e^{-\mu \cdot \xi} \cdot \left(3 - 3 \cdot \xi - \frac{3}{\mu} \right) \right) + \\ & \quad + C \cdot \frac{1}{\mu} \cdot \left(3 + \frac{3}{\mu} + e^{\mu \cdot \xi} \cdot \left(3 \cdot \xi - 3 - \frac{3}{\mu} \right) \right) \} \end{aligned} \qquad (4.I.8)$$

and

$$\begin{aligned} w(s) \simeq\ & F_z \cdot K_x \cdot \ell^3 \cdot \left(\frac{\xi^2}{2} - \frac{\xi^6}{6} \right) + \\ & F_z \cdot K_y \cdot u(\ell)^2 \cdot \ell \cdot \{ a_1 \cdot \left(-\frac{\xi^3}{2} + \frac{\xi^4}{4} \right) + a_2 \cdot \left(-\frac{\xi^4}{4} + \frac{3 \cdot \xi^5}{20} \right) + \\ & \quad a_3 \cdot \left(-\frac{3 \cdot \xi^5}{20} + \frac{\xi^6}{10} \right) + a_4 \cdot \left(-\frac{\xi^6}{10} + \frac{\xi^7}{14} \right) + \\ & + A \cdot \left(-\frac{3}{2} \cdot \xi^2 + \frac{1}{2} \cdot \xi^3 \right) + \\ & + B \cdot \frac{1}{\mu} \cdot \left(-3 \cdot \xi + \frac{3 \cdot \xi}{\mu} + \frac{3}{\mu} - \frac{6}{\mu^2} + e^{-\mu \cdot \xi} \cdot \left(\frac{3 \cdot \xi}{\mu} + \frac{6}{\mu^2} - \frac{3}{\mu} \right) \right) + \\ & + C \cdot \frac{1}{\mu} \cdot \left(3 \cdot \xi + \frac{3 \cdot \xi}{\mu} + \frac{3}{\mu} + \frac{6}{\mu^2} + e^{\mu \cdot \xi} \cdot \left(\frac{3 \cdot \xi}{\mu} - \frac{6}{\mu^2} - \frac{3}{\mu} \right) \right) \} \end{aligned} \qquad (4.I.9)$$

These expressions may be used to obtain the following estimates for the deflections of the end of the plate-spring

$$\begin{aligned}\phi(\ell) \simeq\ & \frac{1}{2} \cdot F_z \cdot K_x \cdot \ell^2 + \\ & + F_z \cdot K_y \cdot u(\ell)^2 \cdot \{ \frac{1}{4} + \frac{21}{4 \cdot \mu^2} + \frac{18}{\mu^4} + \frac{18}{\mu^6} - \left(\frac{3}{2 \cdot \mu} + \frac{12}{\mu^3} + \frac{18}{\mu^5} \right) \cdot \left(\frac{e^{\mu} - e^{-\mu}}{e^{\mu} + e^{-\mu}} \right) + \\ & \quad - \frac{36 + 18 \cdot \mu^2}{\mu^6 \cdot \left(e^{\mu} + e^{-\mu} \right)} \ \} \end{aligned} \qquad (4.I.10)$$

and

$$\begin{aligned} w(\ell) \simeq\ & \frac{1}{3} \cdot F_z \cdot K_x \cdot \ell^3 + \\ & F_z \cdot K_x \cdot u(\ell)^2 \cdot \ell \cdot \{ \frac{1}{7} + \frac{21}{5 \cdot \mu^2} + \frac{24}{\mu^4} + \frac{36}{\mu^6} + \\ & \quad - \left(\frac{1}{\mu} + \frac{12}{\mu^3} + \frac{36}{\mu^5} - \frac{36}{\mu^7} \right) \cdot \left(\frac{e^{\mu} - e^{-\mu}}{e^{\mu} + e^{-\mu}} \right) + \\ & \quad - \frac{72 + 12 \cdot \mu^2}{\mu^6 \cdot \left(e^{\mu} + e^{-\mu} \right)} \ \} \end{aligned} \qquad (4.I.11)$$

For most practical cases where the length of the plate-spring is large compared to the width these expressions may be simplified leading to the results presented in expressions (4.21) and (4.22).

With the iterative-analytical method it is possible to derive relatively simple expressions to estimate the main deformations of the plate-spring. Application of this method is based upon a number of elementary mathematical operations. The most important are multiplication and integration of polynomials which may contain exponential parts. Allthough the operations are elementary the multitude of them renders the analysis tedious and time-consuming. Fortunately computer programs exist that can perform the analytical operations on the expressions that were described here. The derivation of the expressions in this annex was performed with the "MUSIMP" program installed on a micro-computer at the Department of Mathematics of the Delft University of Technology.

Chapter 5.

Plate-spring parallel guidings.

5.1 Introduction.

The most widely used plate-spring mechanism is the plate-spring parallel guiding (see figure 5.1). In this mechanism two plate-springs are connecting the slide with the surrounding environment. As each plate- spring determines the position of the slide in respect of three degrees of freedom the two plate-springs together are determining the position of the slide in six degrees of freedom. The plate-springs however are mounted with their planes parallel and so both plate-springs allow motion of the slide in the direction of the x-axis. Thus allowing a parallel motion of the slide, the plate-springs are twice determining the rotation of the slide about the x-axis. The influence of this over-determination of the slide position will be discussed later in this chapter.

There are two distinct types of construction of plate-spring parallel guides as shown in figure 5.1. In the construction I two plate-springs are used. To obtain a reasonable stiffness of the mechanism with respect to displacement in the direction of the z-axis and rotations about the x- and y-axis the width of the springs has to be relatively large (typically from $\frac{1}{2}$ to $\frac{1}{4}$ of the length).

In construction II four plate-springs are used and are supporting the slide as the four legs of a table. This construction has a relatively high stiffness against rotation about the x-axis. To avoid problems due to the over-determination of the slide position, (twelve degrees of freedom fixed), the width of the plate-spring will in this case generally be small with respect to the length (from 1/5 to 1/10 of the length).

Applications of the plate-spring parallel guidings are found in different fields,

- Conversion of force-displacement or displacement-force in measurement systems.
- Accurate and reproducible generation of parallel motion, applied in optical systems where loading forces are small.
- Guiding of parts of machines over small displacements while the position of the slide should not be disturbed by relatively high, possibly dynamic, loading forces.

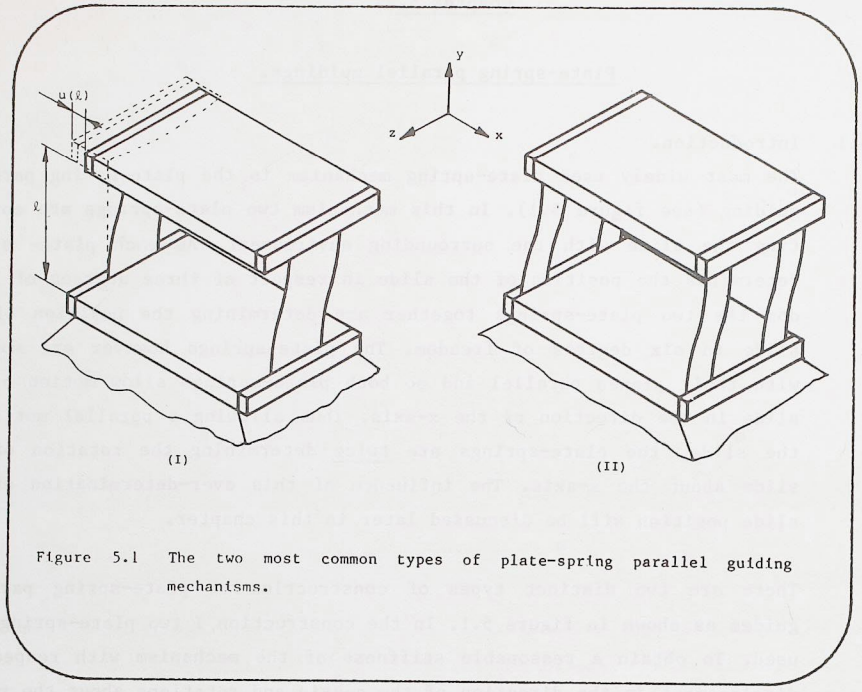

Figure 5.1 The two most common types of plate-spring parallel guiding mechanisms.

Different characteristic properties are making application advantageous in each field. In the first the integration of the guiding mechanism and the linear transducing element combined with the absence of friction are important. For the second the possibility to obtain a very good reproducibility and high quality parallel motion with cheap and simple parts is important. And in the last field of application the absence of "play" and friction together with a reliable operation under even extreme environmental conditions are important properties.

In this chapter many of the properties of plate-spring mechanisms will be discussed. This discussion is started with a description of the "nominal" behaviour of the plate-spring parallel guide. Nominal in this case includes the basic properties such as stiffness in direction of motion, motion in unloaded cases, stresses, allowable loading forces in respect of plate-spring instabilities, deviations from the ideal motion due to production inaccuracies and the dynamic stability of the plate-spring. Most of this information has been obtained in previous research at different places.

The following section will focus on the relation between driving force and displacement. Due to the deformation of the plate-spring deviations from the linear relation will occur. Different factors influencing the linearity will be discussed. Also the effect of loading forces and moments applied on the slide on this relation will be indicated. Most of the information in this and the following section is derived with the mathematical model and the iterative analytical method as presented in chapter 4.

In the next section the deviation from the desired position resulting from loading forces and moments wil be determined. An equivalent physical model of the plate-spring consisting of a combination of three springs will be introduced. With this model and the expressions supplied to determine the its parameters the behaviour of the slide under static and dynamic loading may be determined.

5.2 Nominal behaviour.

When a driving force, F_x, is exerted upon the slide of a plate-spring parallel guiding a certain displacement, u, of the slide will result. In figure 5.2 it is shown that this force should be applied at the center of the construction to arrive at a symmetrical loading of the plate-springs. As indicated in figure 5.2 the relation between F_x and u can most easily be determined through calculations of the deformations of one half of the plate-spring. For each plate-spring this yields:

$$F_x \cdot K_z \cdot \ell^2 \simeq 12 \cdot \frac{u(\ell)}{\ell} \qquad (5.1)$$

The total force needed for the parallel guide displacement, u, should be obtained by addition of the forces for each plate-spring (two springs for construction I and four in construction II).

This relation may be used to predict the stiffness of the parallel guide. This prediction will in general not be very accurate. As the thickness of the plate-spring becomes smaller the uncertainty in the determination of the compliance factor K_z becomes larger. Apart from the uncertainty about the Young's modulus of the material, (about 5-10%), the influence of inhomogenities in the material and small differences between the measured thickness and the actual, active thickness renders the prediction of the stiffness rather inaccurate. Another inaccuracy is due to the uncertainty about the stress-distribution at the clamped-ends. As suggested by different authors, (see lit. S1), a correction for deformation of the clamping can be made by increasing the length by a certain amount, for instance by half the thickness, for each clamped end.

These considerations lead to the conclusion that the uncertainty of the prediction ranges from about 25% for thin plate-springs, (0,1 mm thickness), to about 5% for thick plate-springs, (0,6 mm). Another factor that might influence the stiffness of the plate-springs is the orientation of the y-axis to the direction of rolling of the plates. To obtain an impression of this influence different plate-springs with dimensions of 100x20x0,18 mm were cut from one sheet of material under different orientations. The stiffness of plate-spring parallel guidings made with these springs was measured and the result is shown in figure 5.3.

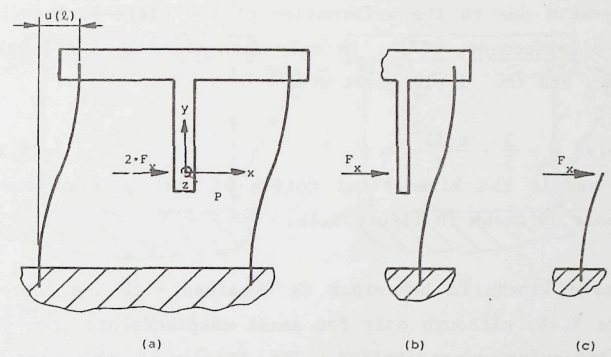

Figure 5.2 To avoid the occurence of extra loading components on the plate-springs the driving force should preferably be applied at the point of symmetry of the mechanism. In this chapter it is assumed that driving and loading forces are applied at this point, P, of the slide.
In this case the loading of one plate-spring is as shown in (b) and, on the basis of symmetry calculations may be performed on one half of the plate-spring loaded only by the driving force, F_x (c).

Angle (degrees)	0	22,5	45	67,5	90	112,5	135	157
Measured (A)	94,9	95,5	95,3	95,1	96,8	94,3	94,7	95,1
values (N). (B)	94,7	95,9	95,1	95,4	95,9	92,7	94,9	95,8

Figure 5.3 In order to determine the influence of the orientation of the plate-spring with respect to the direction of rolling of the sheet material measurements of guiding stiffnesses for parallel guidings were performed. With the nominal dimensions of 80x20x0,18 mm a guiding stiffness of about 96 N/m would be expected.
From the table it may be concluded that no noticeable influence of the orientation upon the plate-spring stiffness is found.
In the table results from two series of measurements are given to indicate the reproducibility of the mounting and measurement process.

Connected with the displacement u the slide will move in the direction of the y-axis due to the deformation of the plate-springs. The magnitude of this displacement, $v(\ell)$, is only determined by the length of the plate - springs and the displacement $u(\ell)$

$$v(\ell) = -\frac{3}{5} \cdot \frac{u(\ell)^2}{\ell} \qquad (5.2)$$

As a result the kinematical motion of each part of the slide follows a parabola as shown in figure 5.4a.

The same kinematic behaviour is obtained with the four-bar mechanism of figure 5.4b, although only for small displacements ,($\frac{u(\ell)}{\ell} < 0{,}1$), and as a first-order approximation. The length of the bars should be equal to $\frac{5}{6} \cdot \ell$.

Deviations from the parallel motion may occur due to geometrical inaccuracies. When the length of the plate-springs differs by an amount $\Delta\ell$ a rotation of the slide around the z-axis will occur as a function of the displacement $u(\ell)$. For the magnitude of the rotation can be derived

$$\Delta\phi \simeq \frac{3}{5} \cdot \left\{\frac{u(\ell)}{\ell}\right\}^2 \cdot \frac{\Delta\ell}{a} \qquad (5.3)$$

where a is the distance between the plate-springs (fig. 5.4).

Similar undesired rotations occur when the distance, a, between the plate-spring differs at the two ends. When a difference of Δa occurs the magnitude of the rotation is estimated as

$$\Delta\phi \simeq \frac{6}{5} \cdot \frac{u(\ell)}{\ell} \cdot \frac{\Delta a}{a} \qquad (5.4)$$

In order to avoid this effect different authors (H1, J1) have suggested to minimize the geometrical inaccuracies by simultaneous machining of the surfaces used to clamp the plate-springs. When the plate-springs are subsequently mounted with care accurate guiding mechanisms can be obtained. An example of such a mechanism is discussed by van der Hoek (H3). In this construction both $\Delta\ell$ and Δa are adjustable and consequently both the first and the second order deviations of ϕ may be eliminated.

Another example of a geometrical error is shown in figure 5.5. Here the surfaces used to mount the plate-springs are not parallel, a relative rotation of the slide around the y-axis will occur upon displacement in

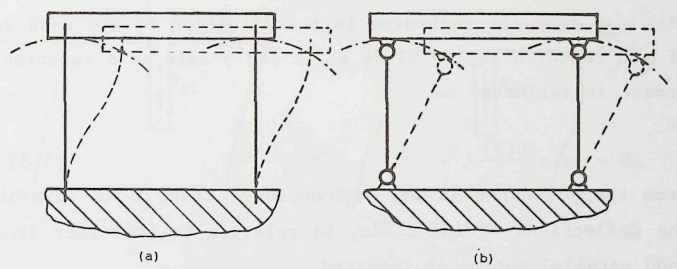

Figure 5.4 When the slide of the parallel guiding is displaced every point of the slide will move along a parabola. A motion with the same curvature is obtained with the four-bar link mechanism (b) where the two bars have a length ,ℓ', equal to $^5/_6 \cdot \ell$.

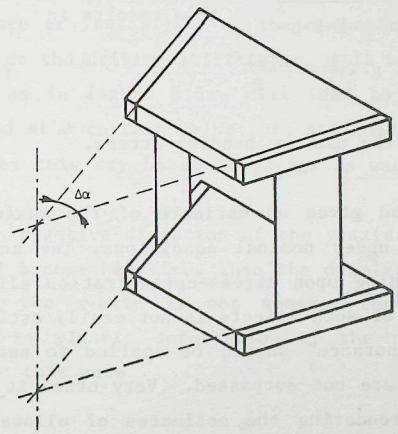

Figure 5.5 Due to manufacturing inaccuracies the two planes of the undeformed plate-springs may intersect each other. As a result the motion of the slide will be a rotation about the section line. The magnitude of the rotation at a given slide displacement depends upon the angle $\Delta\alpha$.

the x-axis direction. When the angle between the mounting surfaces is $\Delta\alpha$, the mechanism can be treated as a torsion-hinge with the center of rotation far from the mechanism in the direction of the z-axis. The magnitude of the rotation of the slide about the y-axis as a function of the displacement is estimated as

$$\Delta\theta \simeq \Delta\alpha \cdot \frac{u(\ell)}{\ell} \qquad (5.5)$$

From these remarks it may be concluded that it is advisable to minimize the deflections of the slide, in relation to the other dimensions, when a good parallel motion is required.

Another reason to reduce the ratio from displacement to length is, in many cases, the magnitude of the bending stress in the material of the springs. The magnitude of the maximum bending moment and thus of the bending stress is easily determined from figure 5.2 as

$$M_x = \frac{1}{2} \cdot \ell \cdot F_x = 6 \cdot \frac{u(\ell)}{K_z \cdot \ell^2}$$

and with $K_z \simeq \frac{12}{E \cdot b \cdot h^3}$ this results in

$$\sigma_{max} \simeq 3 \cdot E \cdot \frac{h}{\ell} \cdot \frac{u(\ell)}{\ell} \qquad (5.6)$$

where σ_{max} is the maximum bending stress.

This expression gives an estimate of the maximum bending stress in the plate-springs under nominal conditions. The actual maximum stress level will be depending upon stress-concentration effects in the clamped ends. The magnitude of such effects is not easily estimated and a certain "coefficient of ignorance" should be applied to ascertain that the allowable stress-levels are not surpassed. (Very often it will not be clear what is "allowable", rendering the estimates of allowable deflections even more uncertain).
The magnitude of stresses in the plate-springs will also be influenced by the loading of the plate-springs. As will be shown the magnitude of the loading forces is limited in order to avoid instability of the plate--springs. Therefore the maximum bending stress due to the desired displacements will in most cases be the most important stress-component.

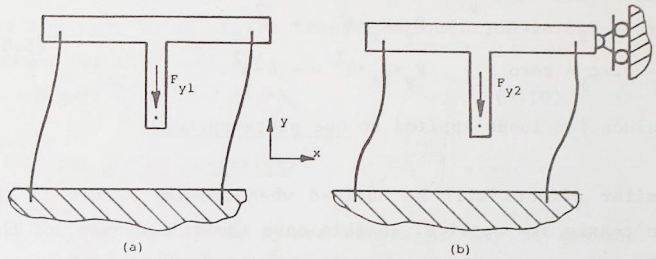

Figure 5.6 Due to loading forces applied to the slide instability of the mechanism may occur. The first form of instability occurs when the driving stiffness c_x of the mechanism becomes equal to zero (a). When the displacements of the slide in the direction of the x-axis are somehow limited the force F_y may be further increased. The next limit is imposed by the occurrence of instability of the plate-spring (buckling) where the guiding stiffness c_y of the plate-spring becomes equal to zero (b).

Limits to the loading capacity of plate-spring mechanisms are imposed by the possible occurrence of instability of the mechanism. When a force F_y is applied to the slide the driving stiffness c_x will be influenced. Negative values for F_y, as in figure 5.6a, will lead to a decrease of the driving stiffness. and at a certain value this stiffness will become equal to zero. In some cases this may be an advantage as was used in lit. (T2) and (E2).
When the force in the negative direction of the y-axis exceeds this value the stiffness c_x will become negative. When the displacement of the slide in the direction of the x-axis is not somehow controlled very large deflections, leading to plastic deformation of the plate-springs, will theoretically occur in this case.

When the displacement of the slide is controlled, for instance by a cam-mechanism, servoed actuator, end-stops etc., the negative value of F_y may be further increased without damage to the operation of the mechanism. This will be allowable upto the limit of instability of the individual plate-springs. For a certain magnitude of the force the stiffness of the plate-spring in the direction of the y-axis will be equal to zero and a small increase of the force will lead to large deflections.

The limit values for the loading force F_y for these two cases can be estimated as

$$\text{a. } c_x \to \text{zero}: \quad F_y \cdot K_z \cdot \ell^2 \simeq -\pi^2$$
$$\text{b. } c_y \to \text{zero}: \quad F_y \cdot K_z \cdot \ell^2 \simeq -4 \cdot \pi^2 \qquad (5.8)$$

(Values for loads applied to one plate-spring.)

Similar effects will be noticed when loading forces in the direction of the z-axis are applied. In this case the stiffness c_x of the mechanism and the stiffness c_z of the plate-spring may become equal to zero.
When the force F_z is applied to the slide at the center of the mechanism (point P in fig. 5.2) the following estimate for the force at which the driving stiffness c_x will be equal to zero can be used (lit.L1)

$$F_z \cdot \ell^2 \cdot \sqrt{K_z \cdot K_y} \simeq \pm 16$$

(value for one plate-spring)

As discussed in chapter 4 such results are applicable only for long and slender beams. For plate-springs where the width is not small compared to the length the influence of the "constrained warping" at the clamped ends will have a considerable influence. Expressions which describe the magnitude of this influence are not readily available. The influence of the constrained warping may be accounted for by including a multiplication factor λ in the corresponding expressions which have been derived for long and slender beams. Thus the following expressions are obtained

$$\text{a. } c_x \to \text{zero}: \quad F_z \cdot \ell^2 \cdot \sqrt{K_z \cdot K_y} \simeq \pm 16 \cdot \lambda_1$$
$$\text{b. } c_z \to \text{zero}: \quad F_z \cdot \ell^2 \cdot \sqrt{K_z \cdot K_y} \simeq \pm 28 \cdot \lambda_2 \qquad (5.9)$$

(values for one plate-spring)

The coefficients, 16 and 28, have been derived by Prandtl (P1). Expressions for the factors λ_1 and λ_2 are not available. For a plate-spring loaded at its free end (see fig.4.4) Timoshenko (T1) has derived an expression for λ . His result may be used to obtain the following table of approximations for λ_1 (for a plate-spring material with Poisson's constant equal to 0,3)

$\frac{\ell}{b} =$	20	10	8	6	4	2
$\lambda_1 \simeq$	1,05	1,10	1,12	1,16	1,29	1,6

Application of the loading torque M_x may also lead to instability in the mechanism. In this case the stiffnesses c_x and c_ϕ will both become equal to zero at the same value of the loading torque. The folowing expression may be derived for this case

$$M_x \cdot \ell \cdot \sqrt{K_z \cdot K_y} \simeq \pm 2 \cdot \pi \cdot \lambda_3 \qquad (5.10)$$

(values given for one plate-spring)

No expressions for the factor λ_3 are known. It may be assumed that the order of magnitude of the influence of the constrained warping is similar to the one observed for application of the force F_z. Derivation of more accurate expressions for the magnitudes of the critical loads may be an interesting subject for further research.
As was mentioned it may in some cases be desirable to obtain mechanisms with driving stiffness c_x equal to zero. This may be realized by loading of the slide. When a force F_y is used the required load is only 25% of the load at which the mechanism will collapse (c_y equal to zero). In case of application of F_z about 55% of the critical load should be applied and when application of the torque M_x is used the load will also lead to instability in rotation of the slide around the x-axis.
To obtain an impression of the influence of combined application of a force F_z and a moment M_x the occurrence of plate-spring instability, limit case b., has been measured at a plate-spring clamped at the two ends. The results of these measurements are shown in figure 5.7.

When the slide is loaded by a moment around the z-axis the plate-springs will be loaded by a tensile and a compressive force respectively. In this case plate-spring instability may occur when the compressive force exceeds the limit stated in expression (5.8b). Similarly around the y-axis will cause loading forces inth direction of the z-axis and instability in the mechanism may be estimated using expression (5.9).

In many cases the loading capacity of the parallel guiding will not be governed by considerations about the plate-spring instability. They are in most cases relevant only as a safety limit. During operation the allowable loading of the slide will be determined by considerations about the influence on the relation between driving force (F_x) and displacement, u, or about the deviations from the desired motion or position. Such influences of the loading forces will be studied in the following sections.

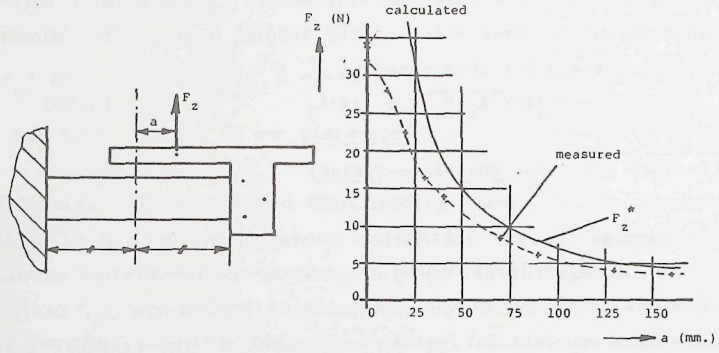

Figure 5.7 Application of a force F_z to the plate-spring at a distance a from the centre is equivalent to a force F_z and a moment $M_x = a \cdot F_z$ applied at the centre. Buckling loads F_z have been measured as a function of a for a plate-spring with dimensions 80x20x0,25 mm. The results may be compared with calculated results from expressions (5.9) and (5.10).
When the force is applied close to the center the magnitude of the limit load is best predicted by expression (5.9b). At large distances from the center the moment M_x will become most important and the limit load may be estimated as,

$$F_z^* \simeq \frac{M_{x\ crit}}{a}$$

where $M_{x\ crit}$ may be estimated using expression (5.10b)

When the guiding mechanism is subject to varying loading forces or vibrations from the surrounding structure resonance may occur. Resonance of the slide of the mechanism on the supporting plate-springs can be estimated when the stiffnesses of the plate-springs in the supporting directions can be determined. A separate resonance problem occurs for the plate-spring itself. A plate-spring clamped at two ends can exhibit a vibration in the shape as indicated in figure 5.8. A range of higher order resonance mode-shapes will exist at higher frequencies. The lowest resonance frequency, with the shape of vibration of figure 5.8, can be calculated as (lit.T3)

$$\omega \simeq 22{,}4 \cdot \left\{ \frac{1}{\sqrt{K_z \cdot m \cdot \ell^3}} \right\} \qquad (5.11)$$

where m is the mass of the plate-spring.

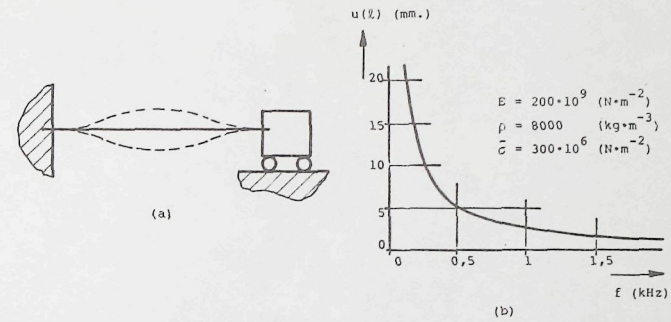

Figure 5.8 Under influence of dynamic loading forces vibrations of the clamped plate-spring may occur. Using the expressions for the lowest natural frequency, mode shape as in (a), and the maximum stress in the plate-spring of a parallel guiding an expression relating the maximum deflection of the slide and the resulting natural frequency can be obtained. From this expression, see fig. (b), it may be concluded that application of plate-spring parallel guidings will in general be restricted to small deflections.

Combination of this expression with the result for the maximum bending stress in the plate-spring mechanism leads to the following relation

$$\omega \simeq \frac{2{,}1}{u(\ell)_{max}} \cdot \frac{\sigma_{max}}{\sqrt{E \cdot \rho}} \qquad (5.12)$$

where ρ is the density of the plate-spring material.

When it is desired that this resonance frequency is above a certain value the maximum allowable deflection of a plate-spring, independent of the dimensions is determined by the three material properties, allowable stress, Young's modulus and density.
In figure 5.8 the resulting maximum deflection for a certain combination of material properties is shown as a function of the desired frequency limit.

5.3 Force-displacement characteristic ; -linearity.

It may be expected that the linear relation between the driving force, F_x, and the deflection of the parallel guiding is valid only for very small deflections. The following three factors responsible for noticeable deviations from the linear relation will be discussed,

- Geometrical effect.
- Anticlastic curvature.
- Internal stresses in unloaded state.

For small deflections the relation between the driving force and the displacement is described by a linear relation as given in (5.1). This expression is obtained with the linear beam theory where the displacement v of the end of the spring is neglected. When the displacement of the slide increases this movement of the end of the spring is given by expression (5.2).

This "shortening" of the plate-spring is the first factor that causes a deviation from the linear force-displacement relation. To estimate the magnitude of the non-linearity the deformation of one half of the spring loaded by a force F_x may be determined. Due to symmetry of the construction the other half will deform in a similar way. This case of loading has already been discussed in chapter 3. The equation governing the bending of the spring is

$$\frac{d\phi(s)}{ds} = - K_z \cdot F_x \cdot (\ell - s + v(\ell) - v(s)) \qquad (5.13)$$

When the first estimate for v(s) is v(s)= 0 the shape of the plate-spring can be determined. This will yield the linear-beam result and the following expression for $\phi(s)$ is found

$$\phi(s) \simeq - \frac{u(\ell)}{\ell} \cdot (3 \cdot \xi - \frac{3}{2} \cdot \xi^2) \qquad (5.14)$$

where $\xi = \frac{s}{\ell}$

With this expression a new estimate for the displacement v(s) can be obtained

$$v(s) \simeq - \frac{1}{2} \cdot \int_0^s \phi(t)^2 \cdot dt \simeq \frac{u(\ell)^2}{\ell} \cdot (- \frac{3}{2} \cdot \xi^3 + \frac{9}{8} \cdot \xi^4 - \frac{9}{40} \cdot \xi^5)$$

Substitution of this estimate in (5.13) and subsequent integration leads to the following expression for $\phi^*(s)$

$$\phi^*(s) \simeq -K_z \cdot F_x \cdot \ell^2 \cdot \{ \xi - \frac{1}{2} \cdot \xi^2 - 3 \cdot (\frac{u(\ell)}{\ell})^2 \cdot (\frac{1}{5} \cdot \xi - \frac{1}{8} \cdot \xi^4 + \frac{3}{40} \cdot \xi^5 - \frac{1}{80} \cdot \xi^6) \} \qquad (5.15)$$

To obtain a relation between the displacement $u(\ell)$ and the force F_x, $u(\ell)$ can be determined with

$$u(\ell) = - \int_0^{\ell} \sin \phi(s) \cdot ds \simeq - \int_0^{\ell} (\phi(s) - \frac{1}{6} \cdot \phi(s)^3 + \cdots\cdots) \cdot ds \qquad (5.16)$$

To obtain only the terms upto the third power of $u(\ell)$ this expression may be replaced by

$$u(\ell) \simeq - \int_0^{\ell} (\phi^*(s) - \frac{1}{6} \cdot \phi(s)^3) \cdot ds \qquad (5.17)$$

where the first estimate of the shape of the plate-spring, expression (5.14), is used to estimate the higher order term for $\phi(s)$. Substitution of (5.14) and (5.15) and integration leads to the following result

$$u(\ell) \simeq K_z \cdot F_x \cdot \ell^3 \cdot (\frac{1}{3} - \frac{9}{35} \cdot (\frac{u(\ell)}{\ell})^2) - \frac{9}{35} \cdot (\frac{u(\ell)}{\ell})^2 \cdot u(\ell) \qquad (5.18)$$

which can be written as

$$F_x \simeq \frac{3 \cdot u(\ell)}{K_z \cdot \ell^3} \cdot \{ \frac{1 + \frac{9}{35} \cdot (\frac{u(\ell)}{\ell})^2}{1 - \frac{27}{35} \cdot (\frac{u(\ell)}{\ell})^2} \} \qquad (5.19)$$

which expression can be used also for the complete plate-spring when the factor 3 is replaced by 12. Apparently there are two factors contributing to this geometrical non-linearity. The largest factor, due to the displacement v of the point of application of the force F_z, is represented in the denominator of (5.19). The other factor contributes one quarter of the non-linear effects, for small deflections, and is due to the third order term in expression (5.17). This factor is present in the numerator of (5.19).

This result is graphically represented in figure 5.9. It can be seen that the procentual increase of the required driving force is almost equal to $100 \cdot (\frac{u(\ell)}{\ell})^2$.

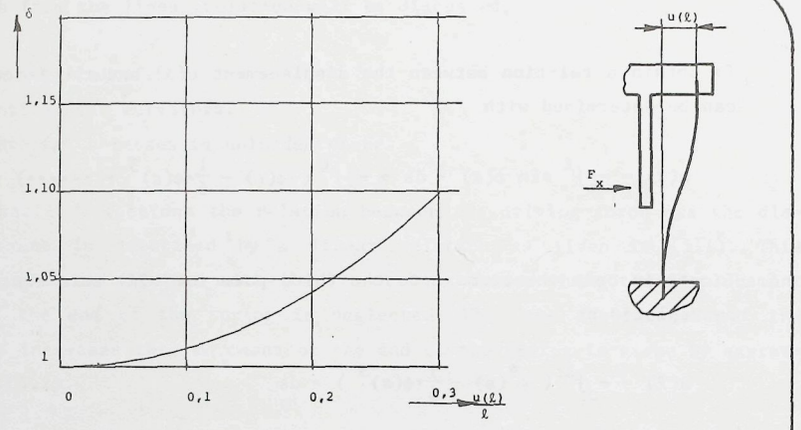

Figure 5.9 Due to the geometrical non-linear effect the driving force F_x required to obtain a certain deflection $u(\ell)$ is larger than predicted by the linear-beam theory. Expression 5.19 can be written as,

$$F_x = \delta \cdot \frac{12 \cdot u(\ell)}{K_z \cdot \ell^3}$$

In the graph the magnitude of δ as a function of $\frac{u(\ell)}{\ell}$ is shown.

The second factor influencing the linearity of the relation between the driving force and the deflection is caused by the influence of the contraction in the plate-spring material as was discussed also in chapter 3. When an element of the plate-spring is loaded by a bending moment this will result in tensile and compressive stresses. Due to the contraction effects the width of the spring will be reduced at the surface where tensile stresses are present and increased due to the compressive stresses. As a result the shape of the cross-section will change as indicated in figure 5.10.

Such contraction effects, the magnitude of which is depending on Poisson's constant, may develop fully in beams with cross-sections as shown in figure 5.10. In plates however where the width b is large compared to the thickness, h, the full development of this effect would cause a large

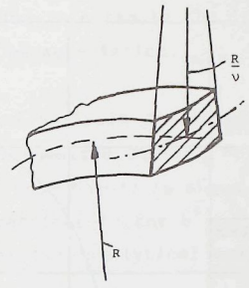

Figure 5.10 When a rectangular beam is bended to a curvature with radius R tensile and compressive stresses will be present in the upper and lower half of the cross-section. Due to the occurence of the transverse strains the cross-section will be deformed and the, originally straight, upper and lower boundary will be curved with a radius $\frac{R}{\nu}$, where ν is Poisson's constant.

change in the shape of the cross-section. Consequently the bending stiffness of the cross-section would increase considerably. As described by different authors and summarized by Dijksman (D1) this large deformation of the cross-section will not occur and the increase of the bending stiffness is limited to a factor $(1-\nu^2)^{-1}$, where ν is Poisson's constant. Dijksman describes the variation of the bending stiffness in the transition region from bending of beams to the bending of plates. It appears that the bending stiffness should be multiplied by a factor ranging from 1 to $(1-\nu^2)^{-1}$ .This factor is a function of the parameter

$$p = \frac{b^2}{h} \cdot \frac{d\phi(s)}{ds} \qquad (5.20)$$

For different values of Poisson's constant the magnitude of the multiplication factor as a function of p is shown in figure 5.11.
From the graphs it is clear that even very wide plates will have a bending stiffness equal to $\frac{1}{12} \cdot b \cdot h^3$ for very small curvatures. For the plate-spring mechanisms this will result in a low stiffness for small deflections and an increasing stiffness when the plate-springs will become more curved.

For the plate-spring parallel guiding the following relation between the maximum curvature and the deflection $u(\ell)$ can be derived

$$\left(\frac{d\phi(s)}{ds} \right)_{max} \simeq 6 \cdot \frac{u(\ell)}{\ell^2} \qquad (5.21)$$

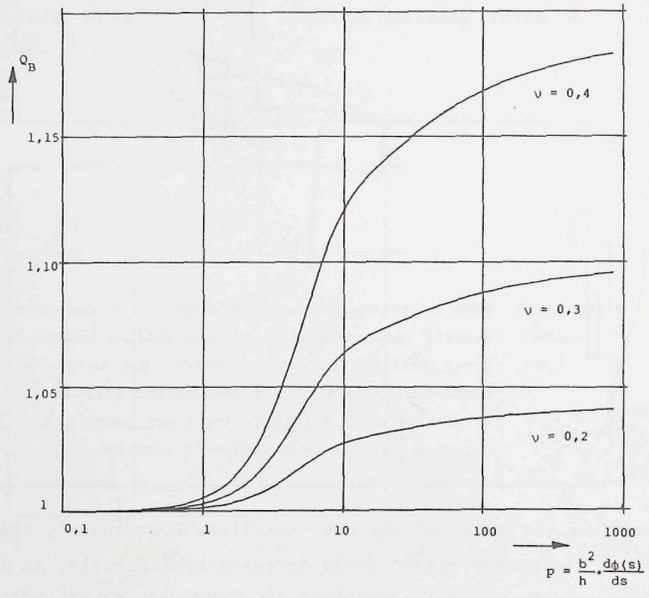

Figure 5.11 Due to the transverse stresses in bended plate-springs the magnitude of the bending stiffness B will be a function of the dimensions of the cross-section and the local curvature of the beam. The magnitude of the bending stiffness may be determined as,

$$B = Q_B \cdot E \cdot \frac{1}{12} \cdot b \cdot h^3$$

In the graph the factor Q_B is shown as a function of the parameter p for three values of Poisson's constant.
(Note : The vertical scale starts at $Q_B = 1$)
(This effect has also been discussed in para.3.4, fig.3.4)

The magnitude of the influence of the increase of the bending stiffness is related to the maximum value of the parameter p given by

$$p_{max} \simeq 6 \cdot \frac{b^2}{h \cdot \ell} \cdot \frac{u(\ell)}{\ell} \qquad (5.22)$$

The magnitude of the parameter p will be varying along the length of the plate-spring. The compliance factor K_z will thus be a function of the parameter s. This function will be governed by the complex expressions given in chapter 3 which are graphically represented in figure 5.11. The resulting differential equations will be difficult to solve analytically.

With numerical methods however it is possible to find solutions for the differential equations and to estimate the influence of the contraction on the force-displacement characteristics.

Result's of such numerical analysis are shown in figure 5.12. As in figure 5.9 the increase of the required driving force relative to the magnitude predicted by the linear beam theory is shown. Results are shown for different values of the geometrical factor $b^2 \cdot \frac{1}{h \cdot \ell}$ as a function of $\frac{u(\ell)}{\ell}$. Here the result from the iterative-analytical method, expression 5.19, is also

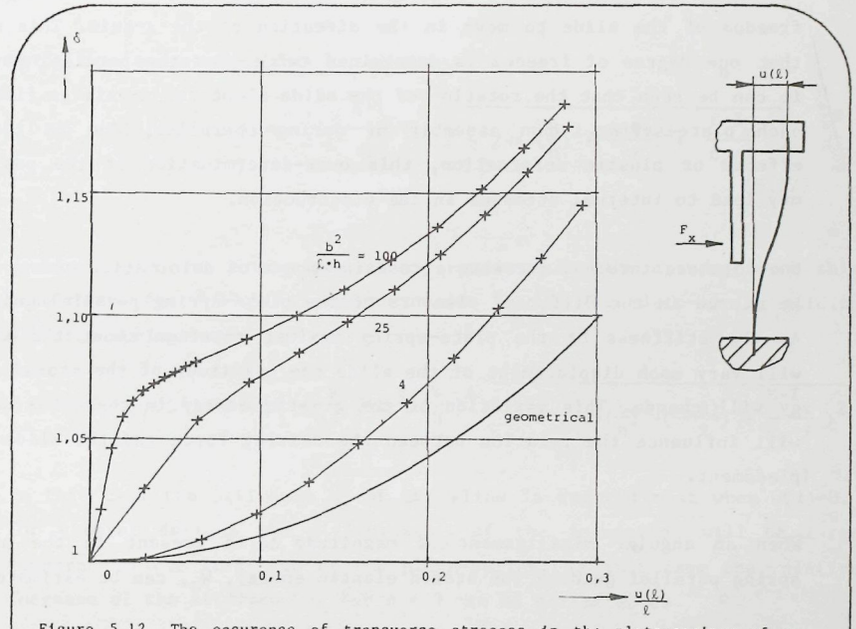

Figure 5.12 The occurence of transverse stresses in the plate-springs of a parallel guiding will give rise to an increase of the required driving force F_x.
As in figure 5.9 the magnitude of F_x is determined as,

$$F_x = \delta \cdot \frac{12 \cdot u(\ell)}{K_z \cdot \ell^3}$$

For different plate-spring geometries the magnitude of the factor δ as a function of $u(\ell)/\ell$ is shown. For very narrow plate-springs the non-linearity will approach to the effect of the geometrical non-linearity (curve A), as in figure 5.9.
(The indicated results were obtained by way of numerical integration techniques, the calculated points have been indicated).

given and it is seen that for narrow beams this gives a reasonable approximation. For wider beams however the non-linearity of the relation between F_x and $u(\ell)$ is mainly determined by the influence of the contraction effect.

The third factor influencing the linearity of the relation between the driving force and the displacement results from internal stresses in the construction when no external loads are applied. In the design shown in figure 5.1.I the two plate-springs are together determining the position of the slide in respect of six degrees of freedom. Still there exists a freedom of the slide to move in the direction of the x-axis. This means that one degree of freedom is determined twice. For the parallel guiding it can be seen that the rotation of the slide about the x-axis is fixed by each plate-spring. Upon assembly or during operation, due to thermal effects or plastic deformation, this over-determination of the position may lead to internal stresses in the construction.

Due to these internal stresses a certain amount of deformation energy will be stored in the different elements of the plate-spring parallel guiding. As the stiffness of the plate-spring against rotation about the x-axis will vary upon displacement of the slide the magnitude of the stored energy will change. This variation of the elastic energy in the construction will influence the relation between the driving force and the slide displacement.

When an angular misalignment of magnitude $\Delta\phi$ is present in the plate-spring parallel guiding the stored elastic energy, W_o, can be estimated as

$$W_o = \frac{1}{2} \cdot c_{tot} \cdot (\Delta\phi)^2$$
$$\text{where } \frac{1}{c_{tot}} = \frac{2}{c_\phi} + \frac{1}{c_f} \qquad (5.24)$$

Here c_ϕ is the stiffness of the plate-spring against rotation about the x-axis and c_f is the stiffness of the slide and foundation against this rotation. When the slide is moved along the x-axis the required driving force is changed by an amount, ΔF_x, due to the variation of W_o as a function of u. This variation can be calculated as

$$\Delta F_x = \frac{dW_o}{du(\ell)} = \frac{1}{2} \cdot (\Delta\phi)^2 \cdot \frac{dc_{tot}}{du(\ell)} \qquad (5.25)$$

The stiffness c_f of the slide and foundation can be assumed to be independent of the displacement. The stiffness of the plate-spring will be reduced when the displacement increases and therefore ΔF_x will be negative. For the parallel guiding of figure 5.1.I the stiffness, c_ϕ, of a plate-spring will be determined in paragraph 5.5. The result obtained there is

$$c_\phi \approx \frac{E \cdot I_x}{\ell \cdot (1 + a \cdot (\frac{b}{h})^2 \cdot (\frac{u(\ell)}{\ell})^2)} \qquad (5.26)$$

where $I_x = \frac{1}{12} \cdot h \cdot b^3$ and $a = \frac{(1+\nu)}{2} \cdot C_4$ is a constant depending upon the geometry of the plate-spring (see expression (5.47)).

Using this expression leads to

$$\Delta F_x \approx -2 \cdot (\Delta\phi)^2 \cdot u(\ell) \cdot a \cdot (\frac{b}{h})^2 \cdot \frac{E \cdot I_x}{\ell^3} \cdot \frac{1}{(2 + 2 \cdot a \cdot (\frac{b}{h})^2 \cdot (\frac{u(\ell)}{\ell})^2 + \frac{E \cdot I_x}{c_f \cdot \ell})^2} \qquad (5.27)$$

Combined with the linear beam theory estimate for the driving force this results in the following expression for F_x for the plate-spring guiding with two springs

$$F_x \cdot K_z \cdot \ell^3 \approx 24 \cdot u(\ell) \cdot \{ 1 - \frac{a}{12} \cdot (\Delta\phi)^2 \cdot (\frac{b}{h})^4 \cdot \frac{1}{(2 + 2 \cdot a \cdot (\frac{b}{h})^2 \cdot (\frac{u(\ell)}{\ell})^2 + \frac{E \cdot I_x}{c_f \cdot \ell})^2} \} \qquad (5.28)$$

In this case the stiffness c_x of the slide is reduced most when $u(\ell)=0$. For general designs the stiffness c_f of the foundation will be large compared to the stiffness of the plate-spring. In that case the relative decrease of the stiffness c_x for $u_\ell = 0$ can be estimated as

$$\Delta c_x \approx (\frac{a}{48} \cdot \Delta\phi^2 \cdot (\frac{b}{h})^4) \qquad (5.29)$$

For a plate-spring with length of 80 mm, width of 20 mm and thickness of 0,25 mm, the value of a is about 0,1 and a 4 percent decrease of the stiffness c_x will occur when $\Delta\phi$ equals about $0{,}7 * 10^{-3}$ rad., which is about equivalent to an internal torque of 140 Nmm. When assembly of the guide is not done carefully such values of the torque are certainly to be expected.

When the slide-displacement increases the influence of this effect will decrease rapidly which causes a marked non-lineartity of the force-displacement relation. As in figure 5.12 the effect can be shown graphically. This is done in figure 5.13 where the relative magnitude of ΔF_x compared to the driving force according to the linear-beam theory is given for the plate-spring described above. From the graph it is clear that serious non-linearity may be expected in this case.

The influence of this effect can be reduced in two ways. When the ratio of width to thickness is reduced, from wide to narrow plate-springs, the influence of an angular error $\Delta\phi$ is decreased.
Decreasing the width of the plate-spring from 20 to 5 mm reduces the maximum influence from ten percent to about one-tenth of a percent. Unfortunately this will simultaneously reduce the ratio between guiding stiffness, c_x, and the support stiffnesses c_z and c_ϕ.

Another way to reduce the influence of the over-determination of the slide position is to decrease the stiffness of the slide and foundation, c_f. From expression (5.28) it is clear that the decrease of the stiffness and the non-linearity will become very small when $c_f << EI_x$. This can be achieved by incorporating an elastic element between the clamping pieces in the slide or the foundation. Different examples of possible constructions are shown in figure 5.14. In this case the over-determination of the slide position is avoided and non-linear effects can be reduced.

The influence of the over-determination of the slide position will be even more noticable in the construction of the parallel guiding shown in figure 5.1.II. Here four plate-springs are used to guide the slide. Consequently twelve degrees of freedom of the slide are fixed which leads to a seven-fold over-determination. Such mechanisms will be hard to assemble without internal stresses. To reduce this problem the four plate-springs will generally have a relatively small width. Therefore each plate-spring will only have a large stiffness in the direction of its axis, the y-axis direction. With the four plate-springs four degrees of freedom of the slide are thus determined with a large stiffness. Unfortunately these four degrees are not independent and in this construction the rotation of the slide around the x-axis is determined twice. Such parallel guidings will generally have a relatively low stiffness in the direction of the z-axis and against rotation around the y-axis.

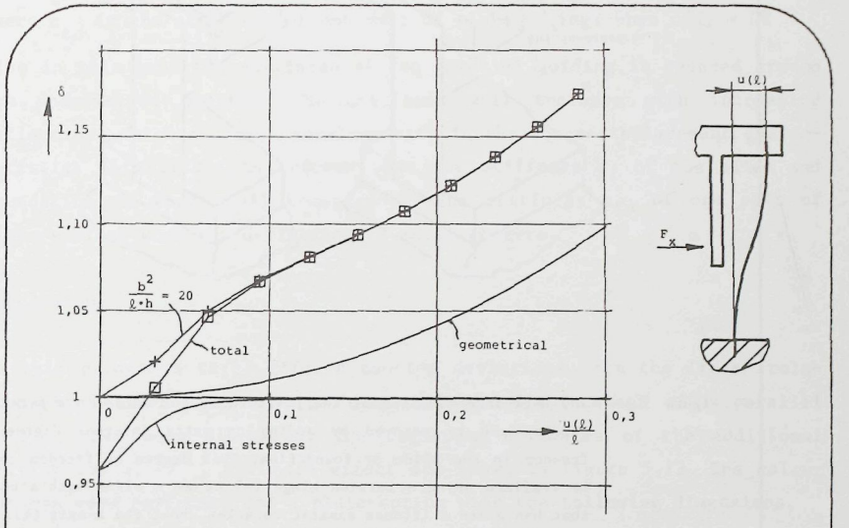

Figure 5.13 Three different factors are influencing the non-linearity in the force-displacement characteristic of a plate-spring parallel guiding. In addition to the geometrical non-linearity internal stresses in the overdetermined construction may have a large influence. For a guiding with two springs, 80x20x0,25 mm, and an internal torque of 140 Nmm at the neutral position the driving force as calculated by the linear-beam theory should be multiplied by a factor δ as shown (see fig. 5.9). It can be seen that this effect decreases the stiffness of the parallel guiding.
In combination with the result from calculations with numerical integration techniques, (see fig.5.12), the line with the +-marks, a large range of variation and non-linearity results for these dimensions.

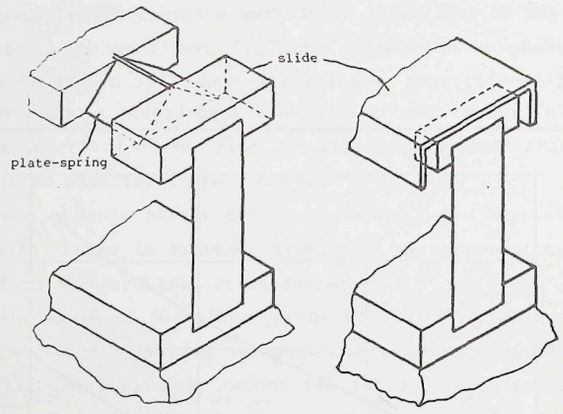

Figure 5.14 The over-determination of the position of the slide in a parallel guiding can be removed by adding an extra internal degree of freedom in the slide or foundation. This degree of freedom could be realized using a torsion hinge (a) or as a slide with a shape that has a low stiffness against rotation about the x-axis (b).

As in this case the rotation of the slide, about the x-axis is over-determined the force-displacement characteristic will be influenced by the internal stresses in the construction. Calculation of the influence of an angular error $\Delta\phi$ can be done as described for the plate-spring parallel guiding with two plate-springs.

Instead of expression (5.26) for the stiffness of one plate-spring against rotation about the x-axis the stiffness of a pair of plate-springs should be used. When a_z is the distance between the axis of the two plate-springs in the direction of the z-axis and c_y the stiffness of a plate-spring in the direction of the y-axis, this results in

$$c_t \simeq \frac{1}{2} \cdot a_z^2 \cdot c_y \simeq \frac{1}{2} \cdot a_z^2 \cdot \frac{E \cdot A}{\ell} \cdot \left(\frac{1}{\left(1 + \frac{12}{700} \cdot \left(\frac{u(\ell)}{h} \right)^2 \right)} \right) \qquad (5.30)$$

Following the same analysis as before leads to the following relation for F_x for the parallel guiding with four springs

$$F_x \cdot K_z \cdot \ell^2 \simeq 48 \cdot u_\ell \cdot \left\{ 1 - \frac{1}{232} \cdot \left(\Delta\phi \cdot \frac{a_z \cdot \ell}{h^2} \right)^2 \cdot \left(\frac{1}{\left(2 + \frac{24}{700} \cdot \left(\frac{u(\ell)}{h} \right)^2 + \frac{c_{to}}{c_f} \right)^2} \right) \right\}$$

where c_{to} is the stiffness of one pair of plate-springs when $u(\ell) = 0$.

Also in this case the stiffness of the parallel guiding is reduced around the undeflected postion. The stiffness will increase with increasing deflection, which causes a non-linearity in the force-displacement characteristic. This effect is reduced when the stiffness c_f of the slide and foundation is very small compared to the stiffness c_{to} of one pair of plate-springs when the deflection is equal to zero.

- Conclusion.

In this paragraph three effects causing deviations from the linear relationship between the driving force and the displacement of a parallel guiding have been discussed. The resulting estimates of the additional driving force, ΔF_x, for each effect are shown in figure 5.13. The calculations were performed for a plate-spring with the following dimensions,

length: 80 mm, width: 20 mm, thickness: 0,25 mm.

For the contraction effects Poisson's constant was estimated to be 0,3 and to calculate the influence of the internal stresses it was assumed that the slide and foundation have a large stiffness compared to the plate-spring. The internal torque was estimated at about 140 Nmm which is about 20 percent of the buckling load for the plate-springs.

When the three effects are combined it is clear that a noticeable non-linearity exists even for small displacements of the slide. The non-linearity is much larger than expected from the geometrical effect alone. This example may appear to give an extremely bad impression. It is of course possible to reduce the contraction effect when more narrow plate-springs are used. And similarly carefull assembly and handling will allow to reduce the influence of internal stresses. In such cases the resulting non-linearity may be about equal to the geometrical effect alone. Such narrow plate-springs will however not be desirable when a high stiffness of the guiding mechanism is required and it may be concluded that the combination of a stiff guiding mechanism and a linear transducing element is not easily achieved.

5.4 Force-displacement characteristic ; -influence of loading forces.

When the slide of the plate-spring parallel guiding is subjected to different loading components the relation between the driving force and the displacement $u(\ell)$ may be influenced. In this paragraph the nature and magnitude of these influences will be discussed.

Each plate-spring is suited to determine three degrees of freedom of the slide position. Therefore each plate-spring will be able to support the slide with respect to three loading components. For each plate-spring these loading components will be the forces F_y and F_z and the torque M_x. To determine the magnitude of these components for each spring when the slide is loaded the equations for static equilibrium of the slide can be used. A loading torque M_y acting upon the slide will thus cause loading forces F_z on each spring. Due to the over-determination of the slide position however some of the loading components cannot be distributed in this way. For the construction of figure 5.1.I (two plate-springs) it is not directly possible to distribute the loading torque M_x over the two springs. For the construction of figure 5.1.II with its seven-fold over-determination this problem occurs for every loading component. Using considerations about the symmetry of the construction and the fact that all plate-springs are having the same stiffnesses it will be possible to estimate the magnitude of the different loading components for each plate-spring.

In this paragraph the behaviour of <u>one plate-spring</u> under influence of the three loading components F_y, F_z and M_x will be discussed. The free end of this plate-spring will be displaced in the direction of the x-axis while the angular deformations of the end, $\phi(\ell)$ and $\theta(\ell)$, will be equal to zero. To describe the loading of the slide all forces and torques will be calculated as being applied at the point of symmetry of the mechanism as indicated in figure 5.2. Forces applied at other points are decomposed into torques about the axis of the coordinate-system with the origin in the point of symmetry.

The force F_y will be the loading component having the most influence on the stiffness c_x of the plate-spring. Due to the kinematic behaviour of the mechanism the free-end of the plate-spring will move in the direction of the y-axis as a function of the displacement $u(\ell)$. This relation has

been given in expression (5.2) as

$$v(\ell) = -\frac{3}{5} \cdot \frac{u(\ell)^2}{\ell}$$

When variations of $v(\ell)$ are occuring energy will be supplied to the mechanism by the force F_y. In first order approximation the displacement of the slide will not be influenced by the force F_y and thus the magnitude of the energy supplied equals

$$W = F_y \cdot v(\ell) = -\frac{3}{5} \cdot F_y \cdot \frac{u(\ell)^2}{\ell}$$

Due to the variations of this energy a variation of the driving force needed to cause a deflection $u(\ell)$ will occur.
This variation is determined as

$$\Delta F_x = \frac{dW}{du(\ell)} = -\frac{6}{5} \cdot F_y \cdot \frac{u(\ell)}{\ell}$$

And this will lead to the following relation between F_x and $u(\ell)$

$$F_x \cdot K_z \cdot \ell^2 = 12 \cdot \frac{u(\ell)}{\ell} \cdot \left(1 + \frac{1}{10} \cdot F_y \cdot K_z \cdot \ell^2 \right) \qquad (5.32)$$

For the stiffness c_x for each plate-spring this yields

$$c_x = \frac{12}{K_z \cdot \ell^3} \cdot \left(1 + \frac{1}{10} \cdot F_y \cdot K_z \cdot \ell^2 \right) \qquad (5.33)$$

(Note: The force F_y is the force applied to <u>one plate-spring</u>.)
This result derived using considerations about the energy contained in the plate-spring, may also be derived using equation (3.1). With the following estimates for u(s) and v(s)

$$v^*(s) \simeq 0$$
$$u^*(s) \simeq u_\ell \cdot (3 \cdot \xi^2 - 2 \cdot \xi^3)$$
where $u_\ell = \frac{u(\ell)}{\ell}$ and $\xi = \frac{s}{\ell}$.

This leads to the following differential equation

$$\frac{d\phi(s)}{ds} \simeq K_z \cdot \{ -F_x \cdot \ell \cdot (1 - \xi) + M_z + F_y \cdot u(\ell) \cdot (1 - 3 \cdot \xi^2 + 2 \cdot \xi^3) \} \qquad (5.34)$$

This equation can be integrated yielding an expression for $\phi(s)$. Using the

boundary condition $\phi(\ell) = 0$ the torque M_z can be eliminated and the following expression for u(s) can be obtained through integration of the expression for $-\phi(s)$

$$\frac{u(s)}{\ell} \simeq K_z \cdot \{ F_x \cdot \ell^2 \cdot (\tfrac{1}{4}\cdot\xi^2 - \tfrac{1}{6}\cdot\xi^3) - F_y \cdot \ell \cdot u(\ell) \cdot (\tfrac{1}{4}\cdot\xi^2 - \tfrac{1}{4}\cdot\xi^4 + \tfrac{1}{10}\cdot\xi^5) \} \qquad (5.35)$$

And with this expression the result given in (5.32) is again obtained by substitution of $\xi = 1$.

To determine the influence of a force F_y applied to the slide of the parallel guiding this expression is sufficient. Different measurements, see for instance lit. G1, have been performed and a good agreement has been found. When the slide is however loaded by a torque M_z each plate-spring will be loaded by equal but opposing forces F_y. The linear influence of F_y on the stiffness c_x of each plate-spring will be equal but opposite. Together their influence will be equal to zero and it is interesting to determine the second-order effect of the loading force F_y on the stiffness c_x. Therefore the result (5.35) can be used to obtain new estimates for v(s) and u(s)

$$v^{**}(s) \simeq 0$$
$$u^{**}(s) \simeq \frac{u(\ell)}{\ell} \cdot \{ (3\cdot\xi^2 - 2\cdot\xi^3) + f_y \cdot (\tfrac{1}{20}\cdot\xi^2 - \tfrac{1}{5}\cdot\xi^3 - \tfrac{1}{4}\cdot\xi^4 + \tfrac{1}{10}\cdot\xi^5) \}$$

where $f_y = F_y \cdot K_z \cdot \ell^2$

This leads to the following relation between F_x and $u(\ell)$

$$F_x \cdot K_z \cdot \ell^2 \simeq 12 \cdot \frac{u(\ell)}{\ell} \cdot \{ 1 + \tfrac{1}{10}\cdot f_y - \tfrac{1}{8400}\cdot f_y^2 \} \qquad (5.36)$$

As the magnitude of F_y should be limited to avoid the occurence of instability of the plate-springs the second-order term will generally be very small.($F_y \cdot K_z \cdot \ell^2 < 4\cdot\pi^2$)

The two remaining loading components, F_z and M_x, will not have a linear effect upon the stiffness c_x as no displacement or rotation in these directions are occurring due to the deflection of the slide. These loading components will however cause torsional deformations of the plate-spring and this will result in additional deflections of the plate-spring. In chapter 4 it has been described how the torsional deformation can be determined. Due to the effect of the constrained warping of the cross-

section the influence of this loading components will be depending upon the length to width ratio of the spring. Using the iterative analytical method the following relation between F_x and $u(\ell)$ can be derived

$$F_x \cdot K_z \cdot \ell^2 \simeq 12 \cdot \frac{u(\ell)}{\ell} \cdot \{ 1 - K_z \cdot K_y \cdot F_z^2 \cdot \ell^4 \cdot C_1 \} \qquad (5.37)$$

The coefficient C_1 is a function of the length to the width ratio of the spring and Poisson's constant for the material. The full expressions for this coefficient are presented in annex 5.I. In these expressions it appears that C_1 is a function of the parameter μ defined as

$$\mu^2 = \frac{\ell^2}{E \cdot \Gamma \cdot K_y} \text{ which may be written as}$$

$$\mu = \frac{\ell}{b} \cdot \sqrt{\frac{24}{(1+\nu)}} \qquad (5.38)$$

for plate-springs with b>h.

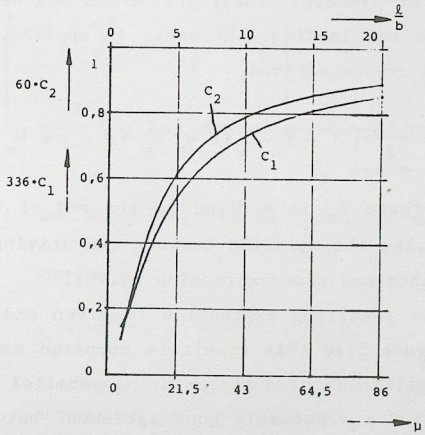

Figure 5.15 The two factors C_1 and C_2 which determine the influence of the loading components F_z and M_x upon the driving stiffness c_x of the parallel guiding, given in expressions (5.37) and (5.39), as a function of the parameter μ and the length to width ratio for a material with Poisson's constant equal to 0,3.
For extremely long plate-springs C_1 and C_2 will be equal to $\frac{1}{336}$ and $\frac{1}{60}$ respectively.

In figure 5.15 the relation between this parameter and the coefficient C_1 is shown. In this figure the relation between C_1 and the length to width ratio for a material with Poisson's constant equal to 0.3 can also be determined. It should be noted that for this loading case the force F_z is not applied at the end of the plate-spring but halfway the length of the plate spring.

When the plate-spring is loaded by a torque M_x similar results can be derived. For the relation between the driving force and the resulting displacement, for one plate-spring, it holds

$$F_x \cdot K_z \cdot \ell^2 \simeq 12 \cdot \frac{u(\ell)}{\ell} \cdot \{ 1 - K_z \cdot K_y \cdot M_x^2 \cdot \ell^2 \cdot C_2 \} \qquad (5.39)$$

Where the coefficient C_2 is equivalent to C_1 in (5.37) and can be determined using the expressions given in annex 5.I. This factor can be determined, as a function of μ or ℓ/b, from figure 5.15.

As the force F_z and torque M_x are applied at the middle of the plate-spring, the point of symmetry, their influences may be simply added when a combination of the two loading components is applied. For such cases the following relation can be derived,

$$F_x \cdot K_z \cdot \ell^2 \simeq 12 \cdot \frac{u(\ell)}{\ell} \cdot \{ 1 - K_z \cdot K_y \cdot \ell^2 \cdot (F_z^2 \cdot \ell^2 \cdot C_1 + M_x^2 \cdot C_2) \} \qquad (5.40)$$

When the loading force F_z is applied to the end of the plate-spring, as shown in figure 5.16, the relation between the driving force and the displacement can be obtained from expression (5.40).
In figure 5.16 the resulting expression is given and represented graphically. Also in figure 5.16 this result is compared with results from measurements of the stiffness of a plate-spring parallel guiding. As in chapter 4, figure 4.11.C a reasonably good agreement between both results is obtained. At larger values of the force F_z increasing differences are observed. This may be due to the contribution of higher order effects or may result from the presence of internal stresses in the over-determined construction of the guiding.

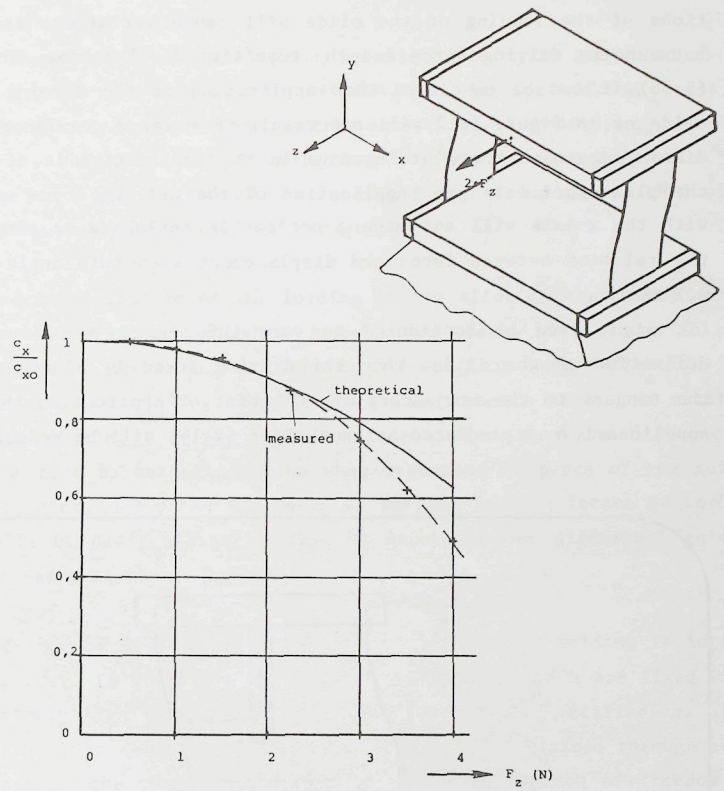

Figure 5.16 When the loading force F_z is applied to the slide at the end of the plate-spring the following relation between F_x and $u(\ell)$ is found,

$$F_x \cdot K_z \cdot \ell^2 \simeq 12 \cdot \frac{u(\ell)}{\ell} \cdot \{1 - K_z \cdot K_y \cdot F_z^2 \cdot \ell^4 \cdot (C_1 + \tfrac{1}{4} C_2)\}.$$

Measurements of this effect have been performed on a guiding with spring dimensions 80*20*0,18 mm.
The obtained results are presented together with the expected theoretical result.
The differences found for larger values of the force F_z may be due to higher order effects which were not accounted for in the derivation or may be resulting from internal stresses in the plate-springs as no steps were taken to remove the over-determination in the mechanism.

From the expressions, presented in this paragraph, it is clear that variations of the loading of the slide will cause variations in the relation between the driving force and the resulting displacement. From expression (5.36) it can be concluded that application of the driving force at the slide as in figure 5.17 will not result in a large non-linearity when the distance between the plate-springs in the x-direction is of the order of the plate-spring length. Application of the driving force under an angle with the x-axis will not have a noticeable influence on the linearity of the relation between force and displacement when this angle is less than 0,1 radian (5^{o}).
(It might even be considered to vary the angle α as a function of the deflection of the slide. When the driving force is always applied along the tangent to the trajectory of the point of application the geometrical non-linearity as predicted by expression (5.19) will be reduced.)

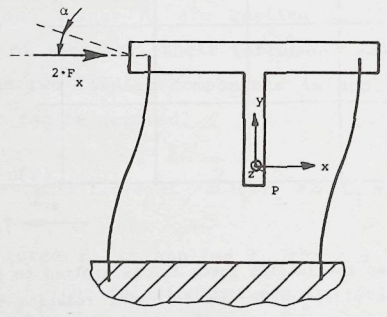

Figure 5.17 To avoid additional loading components on the plate-springs the driving force F_x should preferably be applied at the point of symmetry, P, of the mechanism. With the expressions given in this chapter the effects of application of F_x as shown here may be calculated. In most cases the resulting effects are negligible, even when the force is applied under a certain angle α with the x-axis.

5.5. Guiding stiffnesses.

When the slide of a plate-spring parallel guiding is subjected to loading forces and torques two effects will be noticed. At first the stiffness of the guiding in the direction of motion, c_x, will be changed. When a certain driving force is applied the deflection will change upon application of the loading forces and torques. This effect was discussed in the previous paragraph.

The second influence of the loading of the slide is that other deflections of the slide, not along the desired track, will occur. In accurate guiding mechanisms it will be desired that such deflections will not exceed certain limits. Therefore requirements about the stiffness of the guiding mechanism in directions other than the direction of motion must be satisfied. Also when resonance of parts of the guiding might occur, under the influence of varying loading forces or torques, it will be desirable to be able to determine the different "guiding" stiffnesses of the mechanism.

One degree of freedom of the slide in the parallel guiding is intended to be free. So there are five degrees of freedom which are fixed with a relatively high stiffness. There are five different stiffnesses of the guiding to be determined. These stiffnesses are obtained through combinations of the three stiffnesses of the three degrees of freedom that are fixed by one plate-spring. In this paragraph these three stiffnesses of one plate-spring, deformed as in the plate-spring parallel guiding, will be derived. Through combination of these stiffnesses for the two or more plate-springs the five guiding stiffnesses of the mechanism may be obtained.

Of the free end of a clamped plate-spring the deflections in y- and z-axis direction and the rotation around the x-axis are fixed with a relatively high stiffness. The behaviour of the plate-spring in these directions is similar to that of a combination of three supports with a certain stiffness. These three supports, shown in figure 5.18, are fixing the same degrees of freedom. To describe the behaviour of the plate-spring it is therefore sufficient to obtain expressions for the magnitudes of the three stiffnesses c_y, c_z and c_ψ as a function of the plate-spring dimensions and the deflection of the slide of the parallel

guiding. The two stiffnesses c_z and c_ϕ may then be combined to determine the stiffnesses and the positions of the two supports z_1 and z_2 in figure 5.18.

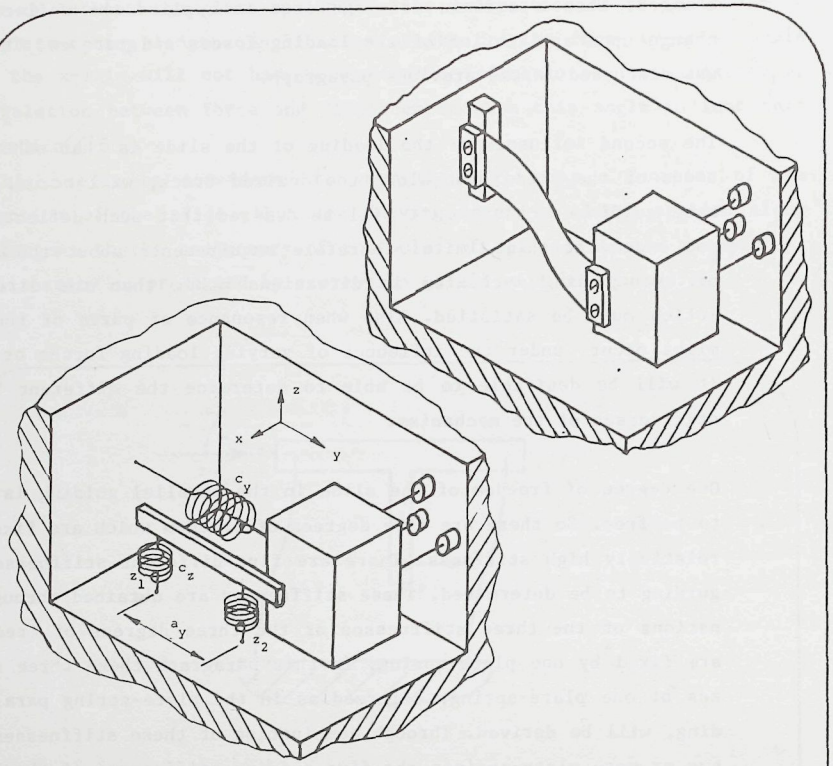

Figure 5.18 To determine the behaviour of a plate-spring parallel guiding under influence of different loading forces each plate-spring (a) may be replaced by an equivalent mechanism (b) containing three helical springs (b). The two springs z_1 and z_2 have the same stiffness and are placed at equal distances from the middle of the plate-spring. The three stiffnesses and the distance a_y may be determined with the expressions derived in this paragraph.

Determination of the stiffness c_y can be done using the differential equations given in expression (3.1). Using the iterative-analytical method solutions for these equations may be obtained. With suitable first estimates for u(s) and v(s), as in expression (5.34), an estimate of the angular deformation is obtained. A new estimate of the deflection of the end of the plate-spring in the direction of the y-axis is than obtained with

$$v(\ell) \simeq -\frac{1}{2} \cdot \int_0^{\ell} (\phi(s))^2 \cdot ds$$

When only linear terms in the force F_y are considered this leads to

$$\frac{v(\ell)}{\ell} \simeq -\frac{3}{5} \cdot \left(\frac{u(\ell)}{\ell}\right)^2 + F_y \cdot K_z \cdot \frac{u(\ell)^2}{700} \qquad (5.41)$$

The first part of this expression is the kinematical deflection as given in expression (5.2). This part is not a function of the loading force F_y. The first order estimate for the stiffness c_y would thus be

$$c_y \simeq \frac{700}{(K_z \cdot \ell \cdot u(\ell)^2)} \qquad (5.42)$$

In addition to the deflection calculated here, which is due to small variations of the bending shape of the plate-spring, a deflection due to pure tension will occur. This effect will not always be negligible. When the deflection of the slide is equal to zero the stiffness of the guiding mechanism is fully determined by the influence of the tensile stresses as the deflection v(ℓ) predicted by expression (5.41) will also be equal to zero. Thus expression (5.41) should be replaced by

$$\frac{v(\ell)}{\ell} \simeq -\frac{3}{5} \cdot \left(\frac{u(\ell)}{\ell}\right)^2 + F_y \cdot \left(\frac{1}{E \cdot b \cdot h} + K_z \cdot \frac{u(\ell)^2}{700}\right) \qquad (5.43)$$

In this case the compliance K_z can be estimated as $12/E.b.h^3$ and the following expression for c_y is obtained

$$c_y \simeq \frac{E \cdot b \cdot h}{\ell} \cdot \left\{ \frac{1}{\left(1 + \frac{12}{700} \cdot \left(\frac{u(\ell)}{h}\right)^2\right)} \right\} \qquad (5.44)$$

It is clear that for small deflections this stiffness is determined by the tensile stiffness as determined with Hooke's law. For deflections of about seven times the plate-spring thickness the bending effect will contribute an equal part to the total stiffness.

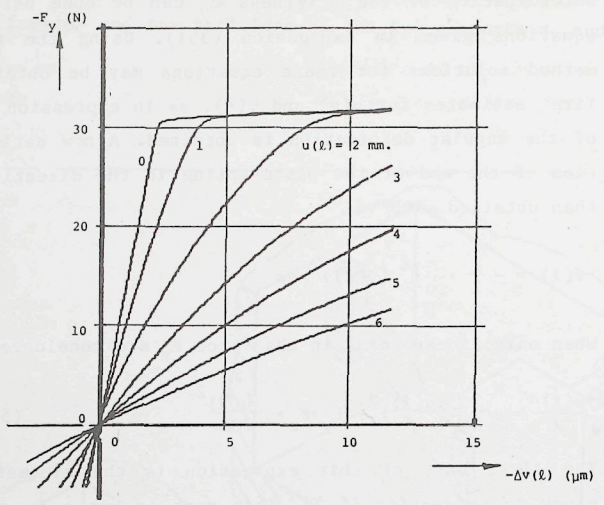

Figure 5.19 Results of measurements of the deflection v(ℓ) due to the loading force F_y applied to a plate-spring with dimensions 80*20*0,25 mm. Results are shown for different values of the deflection u(ℓ) of the plate-spring.
It can be seen that variations of this deflection does not directly influence the magnitude of the second-order buckling force.The stiffness c_y however decreases with increasing deflection u(ℓ). (The theoretical value of the second-order buckling force for this spring is -33,7 N.)

This expression for the stiffness has been obtained with different methods. The result has been experimentally verified by Grentzius (G1). To perform measurements of the deflection v(ℓ) for larger values of the force F_y a special measuring set-up has been developed. This set-up will be described in chapter 8. A resulting graph of the deflection v(ℓ) as a function of F_y is shown in figure 5.19. From this graph it is clear that expression (5.44) only gives information about the tangent to the curve for F_y equal to zero. This was to be expected as only linear terms in the loading force were considered. Depending upon the required accuracy expression (5.44) may be used to a certain magnitude of F_y.

Higher order expressions for v(ℓ) can be obtained by subsequent iterative steps in the iterative analytical method. Using terms quadratic in the loading force F_y will result in

$$\frac{v(\ell)}{\ell} \simeq -\frac{3}{5}\cdot\left(\frac{u(\ell)}{\ell}\right)^2 + F_y\cdot\left(\frac{1}{E\cdot b\cdot h} + K_z\cdot\frac{u(\ell)^2}{700}\right) - \left(F_y\cdot K_z\cdot\ell\right)^2\cdot\frac{u(\ell)^2}{42000} \qquad (5.45)$$

This result is compared with a result from measurements in figure 5.20. In this figure the result from the quasi-linear beam theory for this case is also given. Expressions for this case were derived in litt.(N1) and (E2). As discussed in chapter 3 the result from the quasi-linear beam theory is a rather complicated expression and application of this result is done with the help of graphs or tables. The expression (5.45) will in many cases be suitable to obtain an estimate of the stiffness c_y of a plate-spring in a parallel guiding.

The guiding stiffness c_ψ can best be determined about the x-axis indicated in figure 5.2 passing through the center of the plate-spring. When a force F_z is applied at the point of symmetry of the construction (figure 5.2) the symmetry of the loading of the plate-spring will assure that the rotation of the free end about the x-axis will be equal to zero. Thus the force F_z will cause only a deflection w(ℓ) of the slide and a torque M_x only a rotation, ψ(ℓ) ,about the x-axis. Determination of the stiffnesses c_z and c_ψ can be done with the iterative-analytical method. Due to the symmetry the analysis could be performed on one half of the plate-spring as in chapter 4. Analysis of the behaviour of the complete spring will yield equivalent results.

Using the methods described in Annex 4.I the following relations between F_z and w(ℓ) and between the torque M_x and the rotation ψ(ℓ) have been derived

$$F_z\cdot K_z\cdot\ell^2 \simeq 12\cdot\frac{w(\ell)}{\ell}\cdot\left\{\frac{K_z}{\left(K_x + 12\cdot K_y\cdot C_3\cdot\left(\frac{u(\ell)}{\ell}\right)^2\right)K_z}\right\}$$

$$M_x\cdot K_z\cdot\ell \simeq \psi(\ell)\cdot\left\{\frac{}{\left(K_x + K_y\cdot C_4\cdot\left(\frac{u(\ell)}{\ell}\right)^2\right)}\right\} \qquad (5.46)$$

where C_3 and C_4 are coefficients which are a function of the length to width ratio of the plate-spring and the Poisson's constant for the material. With the elementary estimates for the compliances

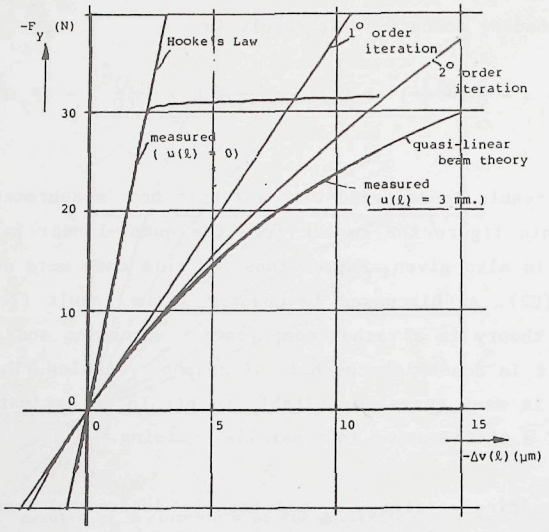

Figure 5.20 Comparison of results from measurements of the stiffness c_y of a plate-spring with different calculated results. Two graphs, for $u(\ell)=0$ and 3 mm., from figure 5.19 are shown. For $u(\ell)=0$ mm. the measured deflection can be compared with the deflection according to Hooke's law. The measured result for $u(\ell)=3$ mm. is compared with the first and second order iterative results and with the result from the quasi-linear beam theory.
For small loading forces the first order iterative result gives a reasonable estimate of the stiffness c_y. The result from the quasi-linear beam theory yields an excellent agreement with the measured result.

$$K_x = \frac{12}{E \cdot h \cdot b^3} \quad , \quad K_y = \frac{6 \cdot (1+\nu)}{E \cdot b \cdot h^3} \quad , \quad K_z = \frac{12}{E \cdot b \cdot h^3}$$

the stifnesses c_z and c_ψ are determined as

$$c_z \simeq \frac{12}{K_x \cdot \ell^3} \cdot \left\{ \frac{1}{\left(1 + 12 \cdot \left(\frac{1+\nu}{2}\right) \cdot \left(\frac{u(\ell)}{h}\right)^2 \cdot \left(\frac{b}{\ell}\right)^2 \cdot C_3\right)} \right\} \qquad (5.47)$$

$$c_\psi \simeq \frac{1}{K_x \cdot \ell} \cdot \left\{ \frac{1}{\left(1 + \left(\frac{1+\nu}{2}\right) \cdot \left(\frac{u(\ell)}{h}\right)^2 \cdot \left(\frac{b}{\ell}\right)^2 \cdot C_4\right)} \right\}$$

When the deflection $u(\ell)$ of the slide is small these stiffnesses are mainly determined by the bending deformation of the plate-spring about the x-axis. For larger deflections the stiffnesses will be reduced due to the increasing influence of the torsional deformations. As for the tensile stiffness in the expression for c_y the effect of the shear deformation of the plate-spring may be added in this expression. For relatively short plate-springs, ($\ell < 4 \cdot b$) , and small deflections this effect may become dominant and the additional deflection may be calculated with

$$\Delta w(\ell) = F_z \cdot \frac{\ell}{G \cdot b \cdot h}$$

Expressions for the constants C_3 and C_4 are given in Annex 5.I. To obtain an impression of the magnitude of these constants they are presented graphically in figure 5.21. For different shapes of the plate-springs the magnitude of the stifnesses c_z and c_ψ as a function of $u(\ell)$ is shown in figure 5.22.

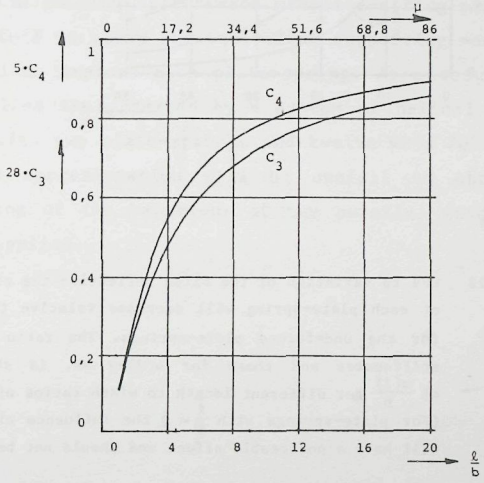

Figure 5.21 The magnitude of the factors C_3 and C_4 as a function of the parameter μ and the length to width ratio for springs of a material with Poisson's constant equal to 0,3.
For extremely long plate-springs C_3 and C_4 will be equal to $\frac{1}{28}$ and $\frac{1}{5}$ respectively.

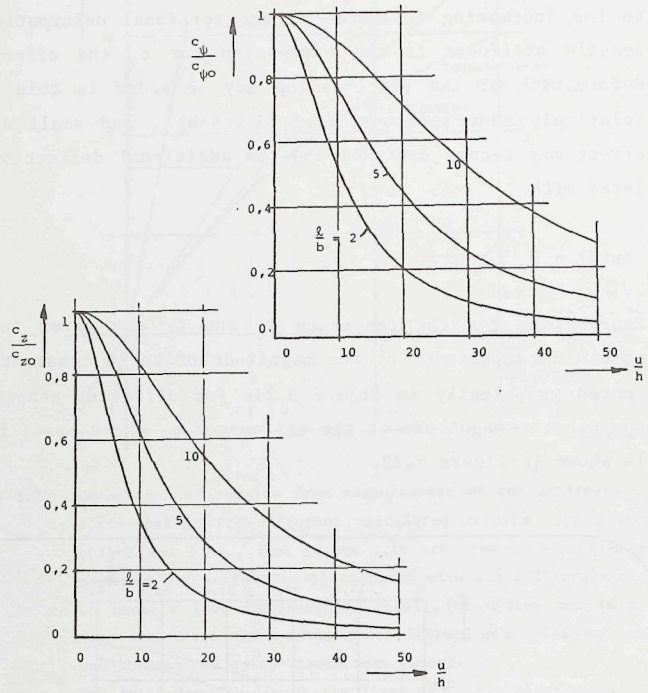

Figure 5.22 Due to variation of the slide deflection the stiffnesses c_ϕ and c_z of each plate-spring will decrease relative to these stiffnesses for the undeformed plate-springs. The ratio between the actual stiffnesses and those for $u(\ell)=0$ mm. is shown as a function of $\frac{u(\ell)}{h}$ for different length to width ratios of the plate-spring. (For plate-springs with $\frac{\ell}{b} = 2$ the influence of shear deformations will have a noticeable effect and should not be neglected.)

The expressions derived for the guiding stifnesses of the plate-spring, when deformed as in a plate-spring parallel guiding, can be used to determine the properties and the position of the three helical springs in the equivalent mechanism shown in figure 5.18. It will be clear that the stiffness of spring Y should be equal to c_y as given in expressions (5.42) or (5.45). For the springs Z1 and Z2 the sum of their stiffnesses should be equal to c_z. Due to the symmetry they should be positioned at equal distances along the y-axis from the point P at the middle of the plate-spring. The total distance, a_y, between the springs Z1 and Z2 can be determined from

$$a_y^2 = 4 \cdot \frac{c_\phi}{c_z}$$

To obtain an impression of the magnitude of a_y the resulting values for different plate-springs and as a function of the deflection $u(\ell)$ are shown in figure 5.23. It is seen that the distance a_y does not change much for different situations.

With the expressions presented in this paragraph it is possible to determine the guiding stiffnesses of plate-spring parallel guidings. It may be usefull to apply the equivalent supporting mechanism as shown in figure 5.23 to replace each plate-spring. As a result it will be seen that the slide is supported by a system of helical springs, 6 for the mechanism with two plate-springs and twelve when four plate-springs are used. This representation will be usefull to obtain a qualitative understanding of the behaviour of the parallel guiding when different loads are applied.

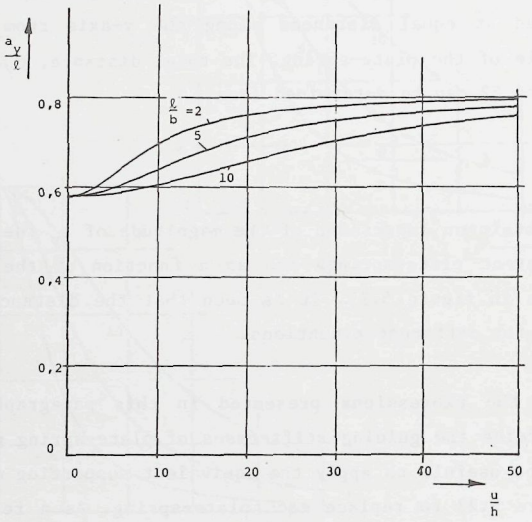

Figure 5.23 The distance a_y between the two helical springs z_1 and z_2 in the equivalent mechanism in figure 5.18 depends upon the plate-spring geometry and the deflection $u(\ell)$ of the slide. The variations of a_y for different length to width ratios and as a fuction of $\frac{u(\ell)}{h}$ are indicated.

5.6 Conclusion

On the basis of the characteristics of the plate-spring parallel guiding discussed in this chapter some remarks about its suitability in the different fields of application can be made. For application as a transducing element (either force displacement or displacement-force) the aspects of reproducibility and linearity may be of importance. As a first remark it can be stated that it is not possible to predict the stiffness c_x of the plate-spring guiding with a high accuracy. The linearity of the relation between the driving force and the slide deflection is subject to different influences. The non-linearity due to the geometrical effect is relatively small, less than 1% for $u(\ell) < 0{,}1 \cdot \ell$. The use of relatively narrow plate-springs and carefull treatment and assembly may yield guidings with such non-linearity. In most guiding mechanisms however more non-linearity, due to the anticlastic curvature and the presence of internal stresses, should be anticipated.

With modern techniques for data-handling the non-linearity of the force-displacement relation might be acceptable. The second important factor is the reproducibility. In paragraph 5.4 it was indicated that loading forces acting upon the slide may have a noticeable influence on the force-displacement relation. When good reproducibility is required care should thus be taken to avoid variations of the magnitude of the loading forces. Another factor influencing the reproducibility may be the occurence of hysteresis in the plate-spring material or in the interface between clamping and plate-spring. This effect will be briefly discussed in Appendix A. There it will be concluded that a hysteris, or uncertainty range for the position of the slide, of about 0,3% of the maximum deflection can be expected due to the internal hysteresis in the plate-spring material.

These remarks are giving some indications about the posibilities of the use of the plate-spring parallel guiding as a measuring element. In such constructions the plate-spring mechanism is both a guiding and a transducing element.

The second field of application is the generation of a motion that is reproducible and well defined. In optical systems it is common that components need to be displaced over a certain distance while no para-

sitic displacements and rotations are allowed. The motion of the slide of the parallel guiding is a combination of two displacements, yielding the curve indicated in figure 5.4. The deflection in the direction of the y-axis is in many cases acceptable. When this is not allowable a combination of two identical guiding mechanisms may be used. In these cases the quality of the resulting kinematic motion, the absence of parasitic displacements, is mainly determined by the accuracy of the production of the parts of the mechanism. Machining the different parts together and suitable jigs for mounting are helpfull in this case. With proper care it will be possible to produce high-quality guiding mechanisms, especially when the required deflection is small. An interesting example of such a mechanism is described in lit. (H2).

The kinematic motion of the unloaded slide may be good, the influence of loading forces on the slide position may cause untolerable deflections.

For such cases the quality of the guiding mechanism could be evaluated with the expressions for the different guiding stiffnesses. To obtain an impression of the quality of a guiding a suitable method is to determine the ratio between the stiffness c_x and the stiffnesses c_y and c_z of the guiding. Due to the stiffness c_x certain forces have to be applied to the slide and when equivalent forces are applied in the y- and z-axis direction the deflections should preferably be very small. As an arbitrary suggestion for the ratio between guiding and driving stiffness the value of 1000 could be used. A much lower ratio will mean that the guiding stiffnesses are very low. A higher ratio will lead to a mechanism that will show less deviations from the kinematical motion. With expressions given in this chapter the following relation between c_x and c_y and c_z can be obtained

$$\frac{c_y}{c_x} \simeq \left\{ \frac{1}{\left(\frac{h}{\ell}\right)^2 + \frac{12}{700} \cdot \left(\frac{u(\ell)}{\ell}\right)^2} \right\}$$

$$\frac{c_z}{c_x} \simeq \left\{ \frac{1}{\left(\frac{h}{b}\right)^2 + C_4 \cdot \left(\frac{1+\nu}{2}\right) \cdot \left(\frac{u(\ell)}{\ell}\right)^2} \right\}$$

The dimensions of the plate-spring will generally allow to obtain the desired ratio, 1000, for $u(\ell) = 0$. With increasing deflection this ratio will decrease. For a steel plate-spring with $\ell = 4 \cdot b$ this limit is reached for $c_y:c_x$ for $u(\ell) \simeq 0{,}24 \cdot \ell$ and for $c_z:c_x$ when $u(\ell) \simeq 0{,}09 \cdot \ell$.

This indicates that in most cases the stiffness c_z will be most critical. For accurate guiding mechanisms it is therefore suggested to minimize the deflection relative to the plate-spring length. From this consideration it can be concluded that the restriction in the different analytical methods to relatively small deflections does not interfere with reality when accurate guiding mechanisms are to be designed.

Resuming it can be stated that the plate-spring parallel guiding is a useful construction element when small relative displacements of parts are required. For small displacement a guiding mechanism with high guiding stiffnesses and a reproducible behaviour can be obtained with simple elements and without high production costs.

Annex 5.I. Analysis of plate-spring deformations.

The influence of the loading components F_z and M_x upon the driving and guiding stiffnesses is due to the torsional deformation of the plate-springs. This influence can be determined with the iterative analytical solution as was demonstrated in Annex 4.I. For the complete plate-spring of a parallel guiding the following initial estimates can be used

$$\phi^*(s) \simeq -6 \cdot u_\ell \cdot (\xi - \xi^2)$$
$$u^*(s) \simeq u_\ell \cdot (3 \cdot \xi^2 - 2 \cdot \xi^3) \qquad (5.I.1)$$

where $\xi = {}^{s}/_{\ell}$ and $u_\ell = {}^{u(\ell)}/_{\ell}$.

When the loading force and moment are applied with respect to the middle of the plate-spring ($s = \frac{1}{2} \cdot \ell$) the two loading cases may be analysed independently and the results may be directly combined afterwards. The force F_z will in this case only cause a translation of the free end of the plate-spring in the direction of the z-axis. The moment M_x will only cause a rotation of this end around the x-axis passing through the middle of the plate-spring.

- Influence of force F_z.

The initial estimates for $\phi(s)$ and $u(s)$ may be substituted in the first differential equation of figure 4.9. ,yielding

$$\frac{d\theta}{ds} - K_y \cdot E \cdot \Gamma \cdot \frac{d^3\theta(s)}{ds^3} = \simeq K_y \cdot \{ -\phi^*(s) \cdot F_z \cdot (\frac{1}{2} \cdot \ell - s) + F_z \cdot (-\frac{1}{2} \cdot u^*(\ell) + u^*(s) \} \qquad (5.I.2)$$

For this equation a solution $\theta(s)$ may be found of the following form

$$\theta(s) = F_z \cdot K_y \cdot u(\ell) \cdot \ell \cdot \{ a_1 \cdot \xi + a_2 \cdot \xi^2 + a_3 \cdot \xi^3 + a_4 \cdot \xi^4 + A + B \cdot e^{-\mu \cdot \xi} + C \cdot e^{\mu \cdot \xi} \} \qquad (5.I.3)$$

where $\xi = \frac{s}{\ell}$ and $\mu^2 = \frac{\ell^2}{K_y \cdot E \cdot \Gamma}$. For plate-spring with a rectangular cross-section and b>h this may be approximated as $\mu \simeq \frac{\ell}{b} \cdot \sqrt{\frac{24}{(1+\nu)}}$.

The boundary conditions for the solution for equation (5.I.2) are

$$s = 0 \rightarrow \theta(s) = 0 \quad \text{and} \quad \frac{d\theta(s)}{ds} = 0$$
$$s = \ell \rightarrow \theta(s) = 0 \quad \text{and} \quad \frac{d\theta(s)}{ds} = 0 \qquad (5.I.4)$$

Using these boundary conditions the following expressions for the coefficients $a_1 - a_4$ and A,B and C may be derived

$$a_1 = -\frac{1}{2} - \frac{12}{\mu^2} \quad , \quad a_2 = \frac{3}{2} + \frac{12}{\mu^2} \quad ,$$
$$a_3 = -2 \quad , \quad a_4 = 1 \quad , \quad A = -B - C \quad ,$$
$$B = \frac{a_1}{\mu \cdot (1 - e^{-\mu})} \quad , \quad C = \frac{-a_1}{\mu \cdot (1 - e^{\mu})} \qquad (5.I.5)$$

With these expressions the solution for $\theta(s)$ is determined as a function of F_z. The influence of the torsional deformation upon the bending deformation, $\phi(s)$,can be determined with the second equation of figure 4.9, yielding the following expression

$$\frac{d\phi(s)}{ds} \simeq K_z \cdot \{ \theta(s) \cdot F_z \cdot (\frac{\ell}{2} - s) + M_z + F_x \cdot (s - \frac{\ell}{2}) \} \qquad (5.I.6)$$

where it is assumed that the forces are applied halfway the length of the plate-spring.

This expression may be integrated to find the solution for $\phi(s)$. With the boundary condition at the ends of the plate-spring the magnitude of M_z can be expressed in the other loading components. Subsequent integration will lead to an estimated expression for u(s) that contains the influence F_z

$$\frac{u(\ell)}{\ell} \simeq \frac{K_z \cdot F_x \cdot \ell^2}{12} +$$
$$+ K_y \cdot K_z \cdot F_z^2 \cdot u(\ell) \cdot \ell^3 \cdot (- \frac{1}{12} \cdot A - \frac{1}{24} \cdot a_1 - \frac{1}{30} \cdot a_2 - \frac{7}{240} \cdot a_3 - \frac{11}{420} \cdot a_4 +$$
$$+ \frac{B}{\mu} \cdot (\frac{1}{\mu} - \frac{2}{\mu^2} - \frac{1}{4} + e^{-\mu} \cdot (\frac{2}{\mu^2} + \frac{1}{\mu} + \frac{1}{4})) +$$
$$+ \frac{C}{\mu} \cdot (\frac{1}{4} + \frac{1}{\mu} + \frac{2}{\mu^2} + e^{\mu} \cdot (\frac{1}{\mu} - \frac{1}{4} - \frac{2}{\mu^2}))) \qquad (5.I.7)$$

Substitution of the expressions (5.I.5) will lead to the following result

$$\frac{u(\ell)}{\ell} \simeq \frac{1}{12} \cdot K_z \cdot F_x \cdot \ell^2 + K_y \cdot K_z \cdot F_z^2 \cdot u(\ell) \cdot \ell^3 \cdot C_1 \qquad (5.I.8)$$

The coefficient C_1 is only a function of the length to width ratio of the plate-spring and the Poisson constant for the material. The following expression for C_1 may be obtained

$$C_1 = \frac{1}{336} + \frac{7}{20\cdot\mu^2} + \frac{8}{\mu^4} + \frac{48}{\mu^6} + \\ - \frac{(1+e^{-\mu})}{(1-e^{-\mu})}\cdot\left\{ \frac{1}{24\cdot\mu} + \frac{2}{\mu^3} + \frac{24}{\mu^5} \right\} \qquad (5.I.9)$$

For large values of the length to width ratio this can be approximated as

$$C_1 \simeq \frac{1}{336} - \frac{1}{24\cdot\mu} + \frac{7}{20\cdot\mu^2} - \frac{2}{\mu^3} + \frac{8}{\mu^4} - \frac{24}{\mu^5} + \frac{48}{\mu^6} \qquad (5.I.10)$$

The expression for $\theta(s)$ can also be used to determine the deflection $\Delta w(\ell)$ of the slide resulting from the torsional deformation. According to the equations in figure 4.9 this may be determined with

$$\Delta\phi(\ell) \simeq {}_0\int^{\ell} \theta(s)\cdot\frac{d\phi(s)}{ds}\cdot ds$$

$$\Delta w(\ell) \simeq {}_0\int^{\ell} \Delta\phi(s)\cdot ds$$

Using the estimates for the deformed shape , expressions (5.I.1), and the solution for $\theta(s)$, expression (5.I.3), the following expressions for the additional rotation and deflection $\Delta\phi(\ell)$ and $\Delta w(\ell)$ due to the torsional deformation of the plate-spring may be derived

$$\Delta\phi(\ell) \simeq K_y\cdot F_z\cdot u(\ell)^2\cdot\left\{ a_1 + a_2 + \frac{9}{10}\cdot a_3 + \frac{4}{5}\cdot a_4 + \right. \\ + B\cdot\left(-\frac{6}{\mu} + \frac{12}{\mu^2} - e^{-\mu}\cdot\left(\frac{6}{\mu} + \frac{12}{\mu^2} \right) \right) + \\ \left. + C\cdot\left(\frac{6}{\mu} + \frac{12}{\mu^2} + e^{\mu}\cdot\left(\frac{6}{\mu} - \frac{12}{\mu^2} \right) \right) \right\} \qquad (5.I.11)$$

and

$$\Delta w(\ell) \simeq K_y\cdot F_z\cdot u(\ell)^2\cdot\ell\cdot\left\{ \frac{a_2}{10} + \frac{a_3}{10} + \frac{3}{35}\cdot a_4 - A + \right. \\ + B\cdot\left(-\frac{6}{\mu} + \frac{18}{\mu^2} - \frac{24}{\mu^3} + e^{-\mu}\cdot\left(\frac{6}{\mu^2} + \frac{24}{\mu^3} \right) \right) + \\ \left. + C\cdot\left(\frac{6}{\mu} + \frac{18}{\mu^2} + \frac{24}{\mu^3} + e^{\mu}\cdot\left(\frac{6}{\mu^2} - \frac{24}{\mu^3} \right) \right) \right\} \qquad (5.I.12)$$

The loading force F_z will only cause a deflection of the slide which can be determined as

$$\Delta w(\ell) \simeq F_z\cdot K_y\cdot u(\ell)^2\cdot\ell\cdot C_3$$

where $$C_3 = \frac{1}{28} + \frac{21}{5\cdot\mu^2} + \frac{96}{\mu^4} + \frac{576}{\mu^6} - \left(\frac{1}{2\cdot\mu} + \frac{24}{\mu^3} + \frac{288}{\mu^5} \right)\cdot\left(\frac{1+e^{-\mu}}{1-e^{-\mu}} \right)$$

and for large length to width ratio

$$C_3 \simeq \frac{1}{28} - \frac{1}{2\cdot\mu} + \frac{21}{5\cdot\mu^2} - \frac{24}{\mu^3} + \frac{96}{\mu^4} - \frac{288}{\mu^5} + \frac{576}{\mu^6}$$

This result may be compared with the result obtained in Annex 4.I. In Annex 4.I the parameter μ is related to the length of half the plate-spring and thus the following substitutions in the expression for $\Delta w(\ell)$ should be made for this comparison

$$\mu^* = 2\cdot\mu \quad \text{and} \quad u(\ell)^* = 2\cdot u(\ell) \ .$$

With these substitutions it shows that the two results are only slightly different. This difference is due to the difference in the boundary conditions used for the two derivations.

- Influence of moment M_x.

The determination of the influence of the moment M_x applied to the plate-spring upon the deformations will be done in a similar way as for the force F_z. The initial estimates given in expression (5.I.1) will be used to obtain the differential equation for $\theta(s)$

$$\frac{d\theta(s)}{ds} - K_y\cdot E\cdot\Gamma\cdot\frac{d^3\theta(s)}{ds^3} \simeq K_y\cdot\left(-\phi^*(s)\cdot M_x + M_y \right) \qquad (5.I.13)$$

In this case the moment M_y applied at the end of the plate-spring is not equal to zero and its magnitude will be obtained using the boundary conditions.

The solution for this equation will be of the form

$$\theta(s) = M_x\cdot K_y\cdot u(\ell)\cdot\left\{ a_1\cdot\xi + a_2\cdot\xi^2 + a_3\cdot\xi^3 + a_4\cdot\xi^4 + \right. \\ \left. + A + B\cdot e^{-\mu\cdot\xi} + C\cdot e^{\mu\cdot\xi} \right\} \qquad (5.I.14)$$

The boundary conditions for this case are identical to those given in expression (5.I.4) and using these the following expressions for the coeffients a_1-a_4 and A,B and C may be derived

$$a_1 = -Q_1 \quad , \quad a_2 = 3 \quad , \quad a_3 = -2 \quad , \quad a_4 = 0 \quad , \quad A = -B - C$$

$$B = \frac{-Q_1}{\mu \cdot (e^{-\mu} + 1)} \quad , \quad C = \frac{Q_1}{\mu \cdot (e^{\mu} + 1)} \qquad (5.I.15)$$

$$\text{where } Q_1 = \frac{1 + e^{-\mu}}{1 + e^{-\mu} + \frac{2}{\mu} \cdot (e^{-\mu} - 1)} \quad .$$

The magnitude of the moment M_y may be determined from

$$M_y \simeq M_x \cdot u(\ell) \cdot (a_1 - \frac{6}{\mu^2} \cdot a_3) \qquad (5.I.16)$$

With this solution for $\theta(s)$ the influence of the moment M_x upon the deformation of the plate-spring in the x-axis direction can now be determined. The second equation of figure 4.9 yields

$$\frac{d\phi(s)}{ds} \simeq K_z \cdot \{ \theta(s) \cdot M_x + M_z + F_x \cdot (s - \frac{\ell}{2}) \}$$

Upon integration and subsequent elimination of the moment M_z an expression for the deformation $\phi(s)$ is obtained containing the influence of F_x and M_x. This expression may be integrated to obtain the following expression for the deflection $u(\ell)$ of the end of the plate-spring

$$\frac{u(\ell)}{\ell} \simeq \frac{K_z \cdot F_x \cdot \ell^2}{12} +$$

$$+ K_y \cdot K_z \cdot M_x^2 \cdot u(\ell) \cdot \ell \cdot \{ (\frac{1}{12} \cdot a_1 + \frac{1}{12} \cdot a_2 + \frac{3}{40} \cdot a_3 + \frac{1}{15} \cdot a_4 +$$
$$+ \frac{B}{\mu} \cdot (\frac{1}{\mu} \cdot (1 - e^{-\mu}) - \frac{1}{2} \cdot (1 + e^{-\mu})) +$$
$$+ \frac{C}{\mu} \cdot (\frac{1}{\mu} \cdot (1 - e^{\mu}) + \frac{1}{2} \cdot (1 + e^{\mu})) \} \qquad (5.I.17)$$

Substitution of the expressions given in (5.I.15) will lead to the following result

$$\frac{u(\ell)}{\ell} \simeq \frac{1}{12} \cdot K_z \cdot F_x \cdot \ell^2 + K_y \cdot K_z \cdot M_x^2 \cdot u(\ell) \cdot \ell \cdot C_2 \qquad (5.I.18)$$

where the coefficient C_2 may be determined as

$$C_2 = \frac{1}{10} + \frac{1}{\mu^2} - \frac{1}{12} \cdot Q_1$$

and for large values of the length to width ratio this can be approximated as

$$C_2 = \frac{1}{60} - \frac{1}{6 \cdot \mu - 12} + \frac{1}{\mu^2}$$

Due to the application of the moment M_x the free end of the plate-spring will be rotated around the x-axis passing through the middle of the plate-spring. The contribution from the torsional deformation of the plate-spring to this rotation, $\Delta\phi(\ell)$,may be determined using the estimates (5.I.5) and the solution for $\theta(s)$, (5.I.15). This leads to the following result

$$\Delta\phi(\ell) \simeq K_y \cdot M_x \cdot \frac{u(\ell)^2}{\ell} \cdot \{ a_1 + a_2 + \frac{9}{10} \cdot a_3 + \frac{4}{5} \cdot a_4 +$$
$$+ B \cdot (- \frac{6}{\mu} + \frac{12}{\mu^2} - e^{-\mu} \cdot (\frac{6}{\mu} + \frac{12}{\mu^2})) +$$
$$+ C \cdot (\frac{6}{\mu} + \frac{12}{\mu^2} + e^{\mu} \cdot (\frac{6}{\mu} - \frac{12}{\mu^2})) \} \qquad (5.I.19)$$

Substitution of the expressions given in (5.I.14) will lead to

$$\Delta\phi(\ell) \simeq M_x \cdot K_y \cdot \frac{u(\ell)^2}{\ell} \cdot C_4 \qquad (5.I.20)$$

$$\text{with } C_4 = \frac{6}{5} + \frac{12}{\mu^2} - Q_1$$

For relatively long plate-springs this may be approximated by

$$C_4 = (\frac{1}{5} - \frac{2}{\mu - 2} + \frac{12}{\mu^2}) \quad .$$

Chapter 6.

Cross-spring Pivots

6.1 Introduction.

Cross-spring pivots are plate-spring mechanisms that determine the position of a body in respect of five degrees of freedom and allow for a limited motion in the remaining degree of freedom. In this sense the plate-spring parallel guiding, allowing for the parallel motion of the slide, may be considered as a special case of the group of cross-spring pivots.
The two plate-springs of a cross-spring pivot are positioned such that their x-y-planes are parallel or coinciding. As a result the motion of the body will, in first-order approximation, be a rotation around an axis parallel to the z-axes of the springs. Under nominal operation the deformation of the plate springs is confined to bending about the z-axis, in the direction with largest compliance.
Two examples of possible constructions of cross-spring pivots are shown in figure 6.1.

In figure 6.2 the principle of operation of the cross-spring pivots is explained. When observed in the direction of the z-axis each plate-spring will fix the position of the body, or rotor, in the x-y-plane in the direction of its y-axis. This situation is similar to the one found in bar-linkage mechanisms and the observed motion of the rotor will be a rotation around the pole, P. The relative position, length and other dimensions of the plate-springs may be varied, the first order approximation of the motion of the rotor will be a rotation around the point where the two central lines of the undeformed plate-springs intersect.

As the plate-spring parallel guiding may be considered to be a special kind of cross-spring pivot many of the effects reviewed in chapter 5 will also affect the behaviour of the cross-spring pivots. The linearity in the relation between the driving torque M_z and the rotation $\phi(\ell)$ will be changed due to geometrical non-linear effects, the influence of the anti-clastic curvature and the presence of the internal stresses due to the over-determination of the rotor position. Different loading forces will both influence the stiffness c_ϕ and generate deflections of the rotor from the "nominal" track.

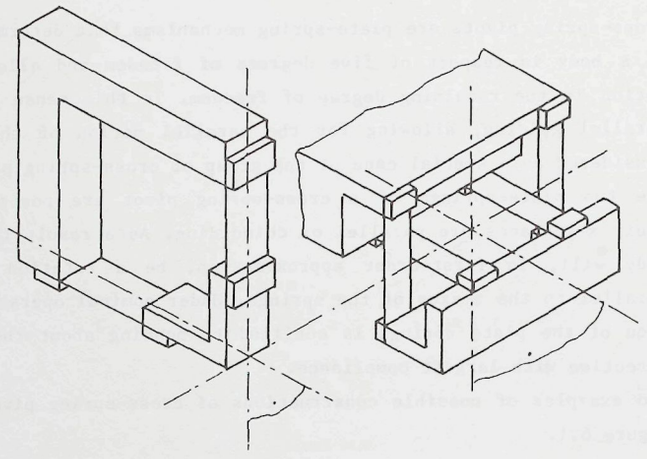

Figure 6.1

Two examples of the construction of cross-spring pivots.
For most general applications the planes of the two plate-springs will be perpendicular as in these two constructions. Such mechanisms are called "orthogonal cross-spring pivots". In most cases the two plate-springs will be equal in dimensions and properties and the initial axis of rotation will be positioned at equal distances from both the clamped ends of the plate-springs (a). These mechanisms are refered to as "symmetric orthogonal cross-spring pivots". When the initial axis of rotation, or the line falling in both of the planes of the plate-springs, divides the two plate-springs in two parts with equal length (b) the mechanism is called, "doubly symmetric orthogonal cross-spring pivot". It is this mechanism that is of most practical interest and which has received most of the attention in earlier research.
(Figure taken from litt. (D1).

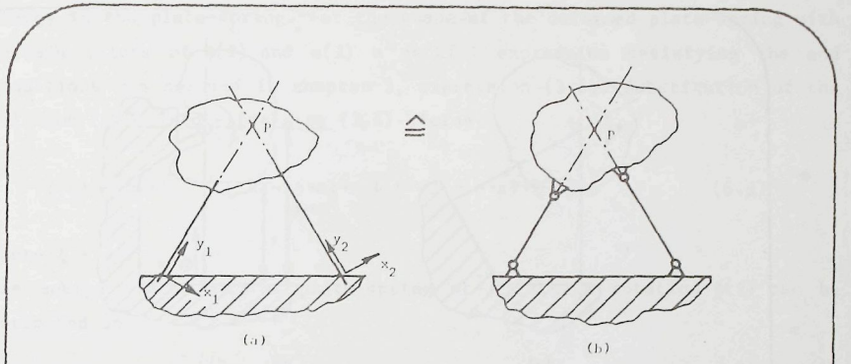

Figure 6.2

Each plate-spring will determine the position of its free end in the direction of its y-axis (y_1 and y_2 in (a)) when only the x-y-plane is considered. This situation is similar to the case of the four-bar linkage mechanism shown in (b). The motion of the both mechanisms is in first-order approximation a rotation around the z-axis through the pole, P. In both mechanisms the pole will be displaced when rotations occur.

In this chapter a number of the main properties of the cross-spring pivots will be discussed.
This discussion will begin with a derivation of the "nominal" behaviour of the cross-spring pivots. This derivation will be based upon the assumption that the cross-spring pivot is a mechanism with one degree of freedom of which the motion can, in first-order, be considered as a rotation about a known axis. Where other researches, lit. (D1) and (H1), use the equations for static equilibrium of the rotor to determine the deformations of the two plate-springs, the derivation given in paragraph 6.2 will calculate the deformation of each plate-spring separately.
Finally the combination of the deformations of the two plate-springs will yield a second-order approximation for the resulting motion of the rotor.

At the end of this chapter the influence of loading forces F_z and torques M_y and M_x upon the behaviour of cross-spring pivots will be analysed.
The emphasis will be placed upon the determination of the resulting guiding stiffnesses of the mechanism and no detailed analysis of the occurring non-linear effects will be given. As was concluded in paragraph 5.4 the combination of plate-spring guiding and the linear transducing element for measuring intsruments does not appear to be very succesfull.

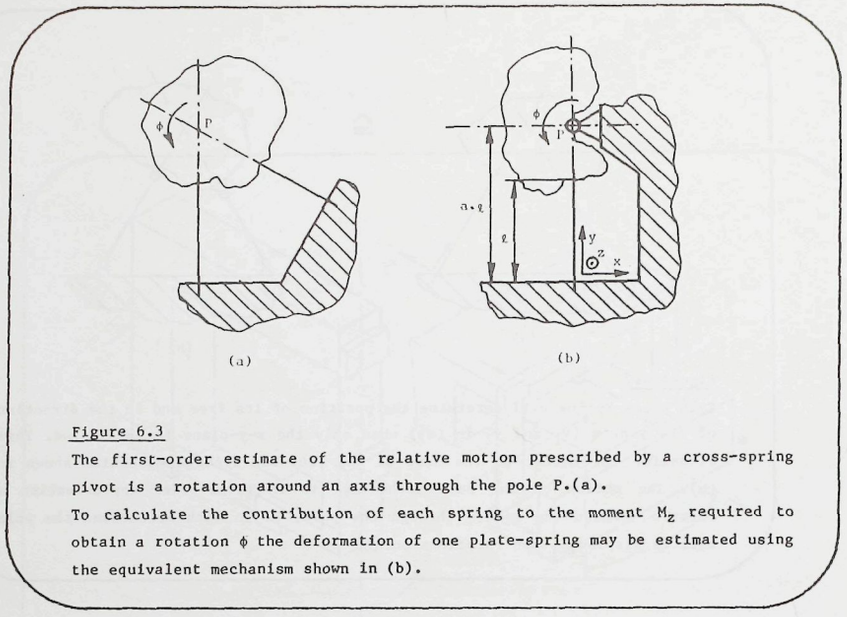

Figure 6.3
The first-order estimate of the relative motion prescribed by a cross-spring pivot is a rotation around an axis through the pole P.(a).
To calculate the contribution of each spring to the moment M_z required to obtain a rotation ϕ the deformation of one plate-spring may be estimated using the equivalent mechanism shown in (b).

6.2 Nominal behaviour of cross-spring pivots.

The first property of interest in the study of cross-spring pivots is the stiffness c_ϕ against rotation about the axis through the pole P. Both plate-springs will contribute to the stiffness. As the motion of the rotor is considered to be a rotation around the pole the contribution of each spring can be estimated with the equivalent mechanism of figure 6.3b. When the distance from the fixed end of the plate-spring to the pole is $a.\ell$, where a is positive in the direction of the positive y-axis, the relation between the angle of rotation $\phi(\ell)$ and the end deflection $u(\ell)$ will be

$$u(\ell) = (a-1) \cdot \ell \cdot \sin \phi(\ell) \qquad (6.1)$$

The equivalent mechanism will only be applicable for small values of the angle of rotation and the following approximation can be made

$$u(\ell) \simeq (a-1) \cdot \ell \cdot \phi(\ell) \qquad (6.2)$$

The relation between the driving torque M_z applied to the rotor and the resulting rotation can be derived through estimation of the stored elastic energy in the plate-spring. For the shape of the deformed plate-spring with certain values of $\phi(\ell)$ and $u(\ell)$ a general expression satisfying the end conditions was derived in chapter 3, expression (3.6). Substitution of the relation (6.2) into expression (3.6) yields

$$\phi(s) \simeq \phi(\ell) \cdot \{ (4 - 6 \cdot a) \cdot \xi + (-3 + 6 \cdot a) \cdot \xi^2 \} \qquad (6.3)$$

where $\xi = \frac{s}{\ell}$.

The energy stored in the plate-spring at a certain rotation $\phi(\ell)$ can be estimated as

$$W_{el.} = \frac{1}{2} \cdot \int_0^{\ell} \frac{1}{K_z} \cdot \left(\frac{d^2\phi}{ds^2}\right) \cdot ds \simeq \frac{1}{2} \cdot \phi(\ell)^2 \cdot \frac{1}{K_z \cdot \ell} \cdot 4 \cdot (1-3 \cdot a+3 \cdot a^2) \qquad (6.4)$$

Where K_z is the compliance factor for the plate-spring (cf. 2.1).
As $dW_{el.} = M_z \cdot d\phi(\ell)$ the following first-order estimate for the driving torque M_z due to one plate-spring can be derived

$$M_z \cdot K_z \cdot \ell \simeq 4 \cdot \phi(\ell) \cdot (1-3a+3a^2) \qquad (6.5)$$

The total stiffness of the cross-spring pivot will contain the contribution from both plate-springs. Using the indexes 1 and 2 for each plate-spring the total stiffness of the cross-spring pivot will be

$$c_\phi \simeq 4 \cdot \left\{ \frac{1}{K_{z1} \cdot \ell_1} \cdot (1 -3 \cdot a_1 +3 \cdot a_1^2) + \frac{1}{K_{z2} \cdot \ell_2} \cdot (1 -3 \cdot a_2 +3 \cdot a_2^2) \right\} \qquad (6.6)$$

This relation is valid for all geometries of cross-spring pivots, including the parallel guiding, provided that no buckling of the plate-spring will occur due to the application of the torque. It will be shown that for all possible geometries a suitable way of application of the torque can be found.

The deformation of a plate-spring in a cross-spring pivot, the rotation $\phi(\ell)$ and deflection $u(\ell)$, can be obtained through application of a force F_x and a torque M_z at the end of the plate-spring. The magnitudes of these loading components can easily be estimated as

$$M_z \simeq \frac{4 \cdot \phi(\ell)}{K_z \cdot \ell} \cdot (-\frac{1}{2} + \frac{3}{2} \cdot a) \quad \text{and} \quad F_x \simeq \frac{6 \cdot \phi(\ell)}{K_z \cdot \ell^2} \cdot (-1 + 2 \cdot a) \qquad (6.7)$$

For each of the plate-springs of the cross-spring pivots these "nominal" loading components can be determined. When the external, driving force or torque is applied to the rotor in such a way that the equations of static equilibrium for the rotor are satisfied, each of the plate-springs will be loaded according the expression (6.7). In figure 6.4 this is explained graphically. On the basis of this analysis the nominal loading condition for arbitrarily shaped mechanisms can be obtained. For symmetrical cross-spring pivots this is further illustrated in figure 6.5.

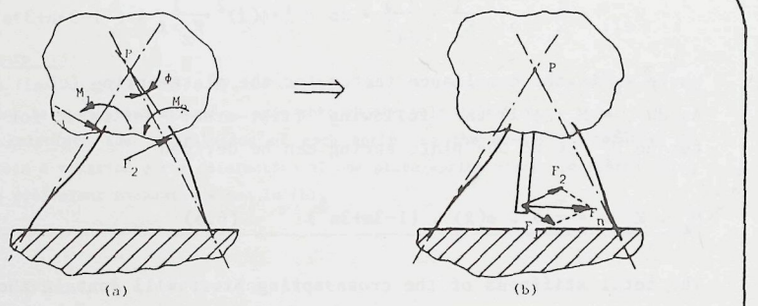

Figure 6.4

According to expressions (6.7) each plate-spring in a cross-spring pivot may be deformed into the shape resulting from the first-order description of the prescribed relative motion by a force F_x and moment M_z.(a). The two sets of loading can be combined and is statically equivalent with one force applied at a distance from the pole P. (b).

Under influence of the nominal loading forces no tensile forces, F_y, will be present in the springs. For these cases the maximum value of the internal bending moment in the plate-spring will occur at one of the clamped ends. The magnitude of the maximum bending moment can be estimated, using expressions (6.7), as

$$M_{max} \approx \frac{\phi(\ell)}{K_z \cdot \ell} \cdot (-2 + 6 \cdot a) \quad \text{for } a \geq \frac{1}{2} \quad \text{and}$$

$$M_{max} \approx \frac{\phi(\ell)}{K_z \cdot \ell} \cdot (4 - 6 \cdot a) \quad \text{for } a \leq \frac{1}{2} . \qquad (6.8)$$

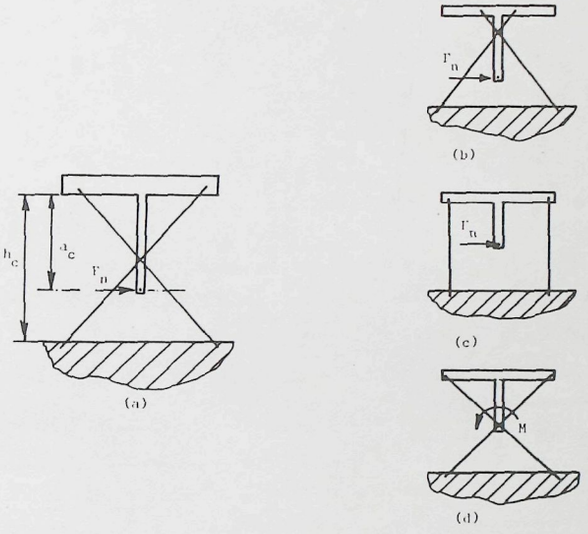

Figure 6.5

A simple expression may be obtained, using expressions (6.7) to determine the place where the nominal driving force F_n should be applied for symmetric cross-spring pivots. In such mechanisms two plate-springs have the same properties and the parameter a is the same for each spring.
For such mechanisms the distance a_c (figure a) is related to the height h_c of the mechanism by,

$$a_c = h_c \cdot (\frac{3a-1}{6a-3})$$

For the doubly-symmetric cross-spring pivot ,a = ½, the force F_n should be applied at an infinite distance. This implicates that loading by a moment M_z is the nominal loading for such mechanisms.

With these estimates the maximum bending stress occurring in the plate-spring is determined by

$$\sigma_{max} \simeq \phi(\ell) \cdot \frac{h}{\ell} \cdot E \cdot (-2 + 6 \cdot a) \qquad \text{for } a \geqslant \frac{1}{2} \quad \text{and}$$

$$\sigma_{max} \simeq \phi(\ell) \cdot \frac{h}{\ell} \cdot E \cdot (4 - 6 \cdot a) \qquad \text{for } a \leqslant \frac{1}{2} \,. \qquad (6.9)$$

As the bending deformation of the plate-spring does not directly depend upon extra loading components applied to the rotor, these estimates will for most practical cases be sufficient to estimate the stresses in the plate-springs.Only for cases where large loading components perpendicular to the x-y-plane (a force F_z or a torque M_x) are applied it is necessary to determine the shear stresses due to the torque M_y occurring in the clamped ends. The magnitude of this torque can be determined from Annex 6.I. The other loading components will generate other stresses in the mechanism which will not depend upon the angle of rotation of the pivot and can be determined with usual methods.

These considerations are based upon the first-order approximation where it is assumed that the rotor rotates around the pole P. For small angular deflections the following approximate relations are found for $u(\ell)$ and $v(\ell)$

$$u(\ell) \simeq (a-1) \cdot \ell \cdot \phi(\ell) \quad , \quad v(\ell) \simeq \frac{1}{2} \cdot (a-1) \cdot \ell \cdot \phi(\ell)^2 \qquad (6.10)$$

According to expression (6.3) the shape of the deformed plate-spring, however, is fully determined when $\phi(\ell)$ and $u(\ell)$ are known. Therefore expression (6.3) can be used to determine an estimate for the magnitude of $v^*(\ell)$ belonging to the rotation $\phi(\ell)$ and deflection $u(\ell)$.
From expression 6.3 the following expression for $v^*(\ell)$ is obtained

$$v^*(\ell) = \int_0^{\ell} (1 - \cos \phi(s)) \cdot ds \simeq - \frac{1}{2} \cdot \int_0^{\ell} \phi(s)^2 \cdot ds =$$

$$= -\ell \cdot \phi(\ell)^2 \cdot \{ \frac{3}{5} \cdot a^2 - \frac{11}{10} \cdot a + \frac{17}{30} \} \qquad (6.11)$$

The two expressions (6.10) and (6.11) for $v(\ell)$ are equivalent only for values of a given by

$$a \simeq \frac{1}{2} \pm \frac{\sqrt{5}}{6}$$

or $\quad a \simeq 0{,}127 \quad$ and $\quad a \simeq 0{,}873$.

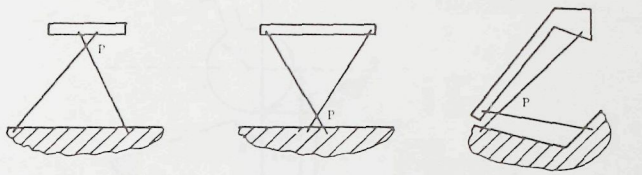

Figure 6.6
Three possible constructions of cross-spring pivots where the parameter a ≅ 1/8 or a ≅ 7/8. The second order approximation of the motion of such mechanisms is a rotation around the pole P.

The motion obtained with such cross-spring pivots, shown in figure 6.6, will in second-order approximation be a rotation around the axis through the pole P.

For all other cross-spring pivots the equivalent mechanism of a pure rotation will be only a first-order approximation. A better description of the resulting motion of the end of the plate-spring is given by expressions (6.2) and (6.11) for $u(\ell)$ and $v(\ell)$. An infinite number of mechanisms exists which will satisfy these two expressions. One of the simple mechanisms is the motion of a circle rolling along a line (see also lit. (L2)). In the undeformed state the circle, attached to the rotor, will touch the line in the point P. To describe the mechanism two parameters are available, the radius of the circle and the angle between the line and the axis of the undeformed spring. Analysis of the motion of this mechanism proves that expressions (6.2) and (6.11) will be satisfied for all mechanisms where the middle of the circle, in the undeformed state, lies on a line, AB, perpendicular to the plate-spring axis at a distance $c.\ell$ from the clamping in the foundation. The distance $c.\ell$ depends only upon the parameter a and is determined by

$$c \cdot \ell = -2 \cdot \ell \cdot \{ \frac{3}{5} \cdot a^2 - \frac{11}{10} \cdot a + \frac{1}{15} \} \qquad (6.12)$$

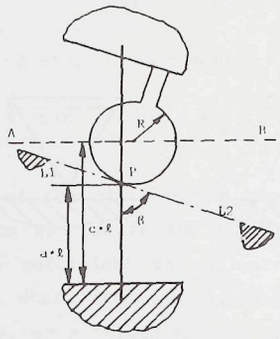

Figure 6.7

One of the mechanisms giving a second order approximation of the motion prescribed by one spring in a cross-spring pivot. The circle with radius R is connected to the rotor and is rolling along a line, L_1, L_2, connected with the stator. The diameter of the circle and the angle β may be varied, but the center of the circle should fall on the line AB in the undeformed position of the plate-spring.

This equivalent model, illustrated in figure 6.7, gives an adequate second order description of the motion of one point of the rotor, the end of one plate-spring. In the cross-spring pivot two plate-springs are present and the motions of two points are thus prescribed. As an infinite number of mechanisms as sketched in fig. 6.7 can be obtained through variation of the angle β it may be possible to obtain one mechanism that satisfies the requirements of both plate-springs. In figure 6.8 it is seen that such a mechanism, a circle rolling along a line, can be found. The center of this circle is the point where the two lines A_1B_1 and A_2B_2 intersect, the radius of the circle is equal to the distance MP and the line is perpendicular to the line MP. In this way one equivalent mechanism giving a second order description of the motion of the rotor of a cross-spring pivot can be obtained. Some examples of such mechanisms are given in figure 6.8. For symmetrical constructions as in figure 6.8 b and c the line will be parallel to the line connecting the clamped ends of the springs and the radius of the circle can be determined as,

$$R = \frac{2 \cdot \ell}{\cos(\alpha/2)} \cdot \left\{ -\frac{3}{5} \cdot a^2 + \frac{3}{5} \cdot a - \frac{1}{15} \right\} \qquad (6.13)$$

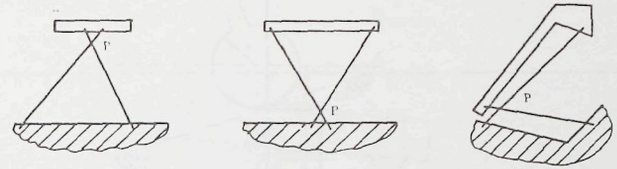

Figure 6.6

Three possible constructions of cross-spring pivots where the parameter a ≅ 1/8 or a ≅ 7/8. The second order approximation of the motion of such mechanisms is a rotation around the pole P.

The motion obtained with such cross-spring pivots, shown in figure 6.6, will in second-order approximation be a rotation around the axis through the pole P.

For all other cross-spring pivots the equivalent mechanism of a pure rotation will be only a first-order approximation. A better description of the resulting motion of the end of the plate-spring is given by expressions (6.2) and (6.11) for u(ℓ) and v(ℓ). An infinite number of mechanisms exists which will satisfy these two expressions. One of the simple mechanisms is the motion of a circle rolling along a line (see also lit. (L2)). In the undeformed state the circle, attached to the rotor, will touch the line in the point P. To describe the mechanism two parameters are available, the radius of the circle and the angle between the line and the axis of the undeformed spring. Analysis of the motion of this mechanism proves that expressions (6.2) and (6.11) will be satisfied for all mechanisms where the middle of the circle, in the undeformed state, lies on a line, AB, perpendicular to the plate-spring axis at a distance c.ℓ from the clamping in the foundation. The distance c.ℓ depends only upon the parameter a and is determined by

$$c \cdot \ell = -2 \cdot \ell \cdot \left\{ \frac{3}{5} \cdot a^2 - \frac{11}{10} \cdot a + \frac{1}{15} \right\} \qquad (6.12)$$

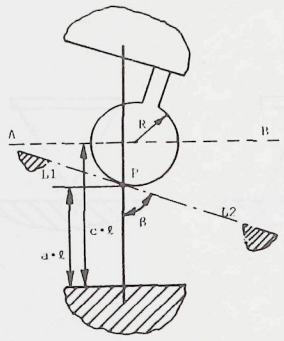

Figure 6.7

One of the mechanisms giving a second order approximation of the motion prescribed by one spring in a cross-spring pivot. The circle with radius R is connected to the rotor and is rolling along a line, L_1, L_2, connected with the stator. The diameter of the circle and the angle β may be varied, but the center of the circle should fall on the line AB in the undeformed position of the plate-spring.

This equivalent model, illustrated in figure 6.7, gives an adequate second order description of the motion of one point of the rotor, the end of one plate-spring. In the cross-spring pivot two plate-springs are present and the motions of two points are thus prescribed. As an infinite number of mechanisms as sketched in fig. 6.7 can be obtained through variation of the angle β it may be possible to obtain one mechanism that satisfies the requirements of both plate-springs. In figure 6.8 it is seen that such a mechanism, a circle rolling along a line, can be found. The center of this circle is the point where the two lines A_1B_1 and A_2B_2 intersect, the radius of the circle is equal to the distance MP and the line is perpendicular to the line MP. In this way one equivalent mechanism giving a second order description of the motion of the rotor of a cross-spring pivot can be obtained. Some examples of such mechanisms are given in figure 6.8. For symmetrical constructions as in figure 6.8 b and c the line will be parallel to the line connecting the clamped ends of the springs and the radius of the circle can be determined as,

$$R = \frac{2 \cdot \ell}{\cos(\alpha/2)} \cdot \left\{ -\frac{3}{5} \cdot a^2 + \frac{3}{5} \cdot a - \frac{1}{15} \right\} \qquad (6.13)$$

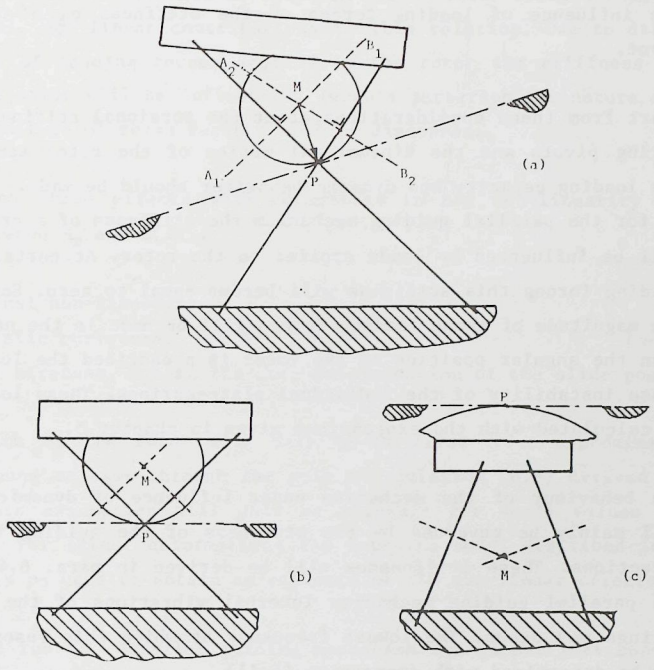

Figure 6.8

The two groups of equivalent mechanisms from figure 6.7 for the two plate-springs have one mechanism in common. This mechanism with one circle of a certain diameter connected to the rotor and rolling along a certain line through the pole P is one of the possible second-order descriptions of the motion prescribed by the cross-spring pivot.

For symmetric cross-spring pivots the line is parallel to the line connecting the two clamping points in the stator.

For negative values of R determined from expression (6.13) the center of the circle is located on the opposite side of the line (c).

where α is the angle between the axis of the two springs.
For negative values of the radius the circle, attached to the rotor, is touching the stationary line at the side of the stator (see figure 6.8b).
This improved model for the nominal motion of the rotor of the cross-spring pivot may be used in further analysis. It can be used to estimate a part of the magnitude of non-linearity due to geometrical effects and to determine the influence of loading forces on the stiffness c_ϕ of the cross-spring pivot.

Apart from these considerations about the torsional stiffness of the cross-spring pivots and the kinematical motion of the rotor some remarks about its loading capacity and dynamic behaviour should be made.
As for the parallel guiding mechanism the stiffness of a cross-spring pivot will be influenced by loads applied to the rotor. At certain values of the loading forces this stiffness will become equal to zero. Some remarks about the magnitude of these loading forces will be made in the next paragraph.
When the angular position of the rotor is prescribed the loading forces may cause instability of the individual plate-springs. These loading forces may be calculated with the expressions given in chapter 5.

The behaviour of the mechanism under influence of dynamic loading forces will mainly be governed by the stiffness of the guiding in the different directions. These stiffnesses will be derived in para. 6.4. Just like for the parallel guiding mechanism internal vibrations of the separate plate-springs may occur. The lowest frequency at which this resonance will occur can be determined with expression (5.11).
This expression may be combined with expression (6.9) for the maximum stress in the plate-spring. For a cross-spring pivot with a = ½ the following relation for the lowest natural frequency results,

$$f = \frac{1{,}03}{\phi \cdot \ell} \cdot \frac{\sigma_{max}}{\sqrt{\rho \cdot E}} \quad (\text{Hz}) \qquad (6.14)$$

For a steel plate-spring with a length of 10 mm and for a maximum angle of 0,3 rad this frequency will be about 2500 Hz.

6.3 Stiffness of the cross-spring pivot

The relation between a driving torque M_z applied to the rotor and the resulting rotation $\phi(\ell)$ will, as a first-order estimate, be governed by expression (6.6).
For larger values of the angle of rotation second-order effects will result in additional, non-linear contributions to this relation. Due to different combinations of loading forces applied to the rotor the stiffness of the cross-spring pivot will be influenced. In this paragraph the nature and the order of magnitude of these factors will be discussed.

The following three effects will contribute to the non-linearity in the relation between M_z and $\phi(\ell)$,

- Geometrical non-linearity.
- Anti-clastic curvature.
- Internal stresses, due to the over-determination of the slide position.

As the motion of the rotor will only be in first-order approximation a rotation around an axis through the pole the relation (6.6) derived on the basis of this assumption will only be adequate for small values of the angle $\phi(\ell)$. For larger deformations the improved model described in paragraph 6.2 may be used to obtain an estimate of the non-linear effects.

As described for the parallel guiding mechanism the geometrical non-linearity will not be the only or the largest non-linear effect. Due to the transition from plane-stress to plane-strain bending, the effect of the anti-clastic curvature, an important non-linear contribution may be observed for relatively wide plate-springs. Also the internal stresses in the cross-spring pivot may cause a noticeable change in the relation between the torque M_z and the angle $\phi(\ell)$. Due to the internal stresses the stiffness c_ϕ will be reduced for small values of $\phi(\ell)$. The magnitude and the influence of the internal stresses decrease with increasing angle of rotation.

The first estimate for the stiffness of the cross-spring pivot, expression (6.6) , has been derived using the assumption that the rotor performs a pure rotation around the axis through the pole P. The shape of the deformed

plate-spring was determined using the conditions at the end estimated with this model of the relative motion. The actual shape will in general differ from this shape due to the following effects,

-Due to the improved, second-order model for the motion of the rotor described in the previous paragraph the relation between the two conditions at the end of the plate-spring, as given in (6.10) should be supplemented

$$\frac{u(\ell)}{\ell} \simeq (1 - a)\cdot\ell\cdot\phi(\ell) + r\cdot\phi(\ell)^2 \qquad (6.15)$$

where the magnitude of r depends upon the radius of the circle, R, and the angle between the plate-spring and the line in the equivalent model as presented in figure 6.8. (See figure 6.9)

-The expression (3.6) relating the shape of the deformed plate-spring to the end displacements $\phi(\ell)$ and $u(\ell)$ is a first order estimate. This expression thus neglects the influence of the tensile force F_y. In the cross-spring pivot such tensile forces will be present when only a driving torque M_z is applied and therefore their influence will be noticeable in the second order part of the expressions for the stiffness c_ϕ.

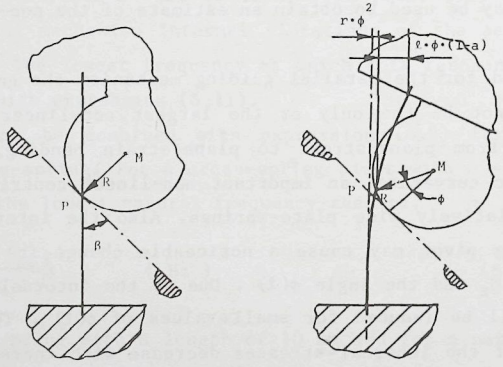

Figure 6.9
To obtain a second-order estimate of the stiffness of a cross-spring pivot the relation between the deflection $u(\ell)$ and rotation $\phi(\ell)$ of the plate-spring must be determined using a second-order mechanism describing its motion. From this figure an estimate of this relation can be obtained.

The first effect may be calculated for mechanisms where the second effect is absent. This will be the case for mechanisms where the pole P is located at the middle of both plate-springs. In that case the geometrical parameter a is equal to $\frac{1}{2}$ for both plate-springs and the tensile forces will be equal to zero.

Using expression (6.15) the elastic energy stored in the deformed plate-spring is in that case estimated as

$$W_{e1} \simeq \frac{1}{\ell\cdot K_z} \cdot \{ \tfrac{1}{2}\cdot\phi(\ell)^2 + 6\cdot r^2\cdot\phi(\ell)^4 \} \qquad (6.16)$$

The contribution of one plate-spring to the driving torque M_z will then be

$$M_{z1} \simeq \frac{\phi(\ell)}{\ell\cdot K_z} \cdot \{ 1 + 24\cdot r^2\cdot\phi(\ell)^2 \} \qquad (6.17)$$

To estimate the magnitude of this non-linear effect, only for mechanisms with $a=\frac{1}{2}$, it is necessary to derive an expression for the parameter r. From figure 6.9 the following relation is obtained

$$r \simeq \tfrac{1}{2}\cdot R\cdot\cos(\beta) \qquad (6.18)$$

Combination of the expressions (6.17) and (6.18) will allow to estimate the magnitude of the geometrical non-linearity for these cross-spring mechanisms. For the group of symmetric cross-spring pivots, where each plate-spring has the same dimensions and properties the following expression for the driving torque is thus obtained

$$M_z = \frac{2\cdot\phi(\ell)}{\ell\cdot K_z} \cdot \{ 1 + \frac{1}{6} \cdot \phi(\ell)^2 \cdot \tan^2(\tfrac{\alpha}{2}) \} \qquad (6.19)$$

For usual constructions of cross-spring pivots the geometrical non-linearity will be relatively small. For $\phi \cong 0{,}3$ rad the magnitude of the second term between the brackets is only 0.015 for the standard doubly-symmetric, orthogonal cross-spring pivot ($a = \frac{1}{2}$). It is however important to note that unexpected effects may occur when other geometries are considered. For a symmetric cross-spring pivot with $a = \frac{1}{2}$ but with increased angle α the non-linearity increases rapidly. This is shown in figure 6.10.

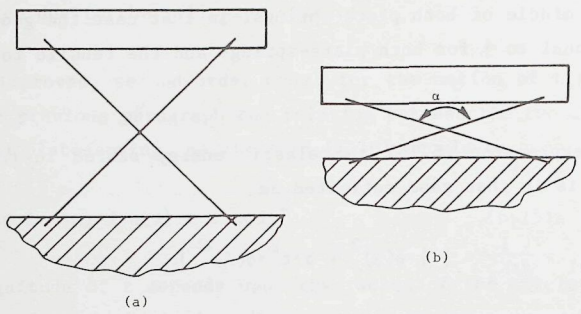

Figure 6.10
The geometrical non-linearity for cross-spring pivots depends upon the angle α between the plate-springs. For a rotation of 0,3 rad the non-linearity for the mechanism shown in (a) is about 1,5% while this is increased to about 13% for the mechanism shown in (b).

For cross-spring pivots with other values for the geometrical parameter a the influence of the tensile forces in the plate-springs should be accounted for. This might be done using the iterative analytical method in combination with the equations for the static equilibrium of the rotor. This effect has however been studied in detail by Dijksman (D1) and his results may be used to indicate the magnitude of the non-linearity for the group of orthogonal, symmetric cross-spring pivots.

In general the relation between the torque M_z and the angle $\phi(\ell)$ may be written as

$$\phi(\ell) \simeq \frac{M_z}{c_\phi} \cdot (1 + Q \cdot (M_z \cdot K_z \cdot \ell)^2) \qquad (6.20)$$

In this expression the magnitude of c_ϕ is obtained from expression (6.6). Using the expressions derived by Dijksman the parameter Q as a function of the geometrical parameter a has been calculated for the orthogonal, symmetric cross-spring pivots. The results of these calculations are shown in figure 6.11. Similar results have been obtained using the finite element method by van der Werf (lit. W2).

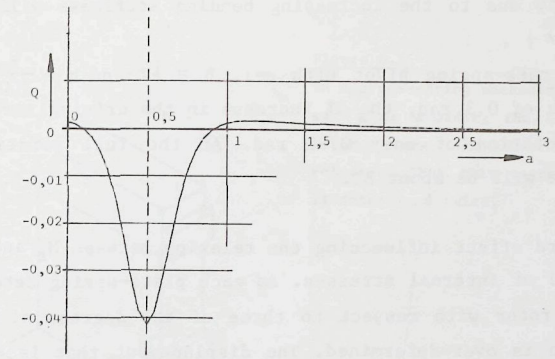

Figure 6.11
For symmetric, orthogonal cross-spring pivots the second-order estimate for the relation between the angle $\phi(\ell)$ and the torque M_z is given by relation 6.20. The magnitude of the factor Q as a function of the geometrical parameter a has been obtained using the results of Dijksman (D1).

The geometrical non-linearity is only one of the non-linear effects observed in plate-spring mechanisms. In most practical cases the contribution of the geometrical effects will be relatively small. A more important contribution may be given by the increase of the bending stiffness due to the transition from the stress distribution found in the bending of beams to the one present in the bending of plates. With the information given in chapter 5 (figure 5.11) the magnitude of this effects may be estimated. It can be seen that relatively wide plate-springs used to allow for a large angle of rotation, and thus having a small thickness, show a large non-linearity. For a doubly-symmetric orthogonal cross-spring pivot with $b \cong \frac{1}{2}.\ell$ and $h = \ell/75$ the increase of the torque M_z for a rotation of 0,3 rad will be about 4% (for a material with Poisson's constant of about 0,3).

For constructions with other values for the geometrical parameter a this influence cannot be directly calculated. An impression of the non-linearity to be expected can be obtained when the maximum curvature of the plate-spring is determined as in expression (6.8). This maximum curvature may be used to estimate the magnitude of the parameter p in figure 5.11. This parameter will allow to estimate the magnitude of the influence of the increasing bending stiffness.

As the maximum curvature increases when the parameter a is changed the

allowable thickness of the plate-spring will be reduced. Therefore the non-linearity due to the increasing bending stiffness will be more pronounced when $a \neq \frac{1}{2}$.

For a cross-spring pivot with a=1, $b \cong \frac{1}{2}\ell$ and $h = \frac{\ell}{300}$, which will allow rotation of 0,3 rad, the 4% increase in the driving torque will be expexted at a rotation of only 0,03 rad. At the full rotation of 0,3 rad the increase will be about 8%.

The third effect influencing the relation between M_z and $\phi(\ell)$ is due to the presence of internal stresses. As each plate-spring determines the position of the rotor with respect to three of the degrees of freedom, the rotor-position is over-determined. The displacement that is determined twice, is the motion of the rotor in the direction of the z-axis of the two plate-springs. Due to this over-determination internal stresses may be present in the mechanism as shown in figure 6.12 and thus an amount of elastic energy is stored in the construction. When the angle of rotation, $\phi(\ell)$, is varied the amount of this energy will vary and thus the relation between M_z and $\phi(\ell)$ will be influenced. As for the parallel guiding discussed in chapter 5 the stiffness c_ϕ will be reduced around $\phi(\ell) = 0$ and with increasing angle of rotation the effect decreases. The magnitude of this effect can be calculated using the method described in chapter 5.

The influence of the internal stresses can be eliminated by careful assembly of the plate-spring mechanism and proper care during the use of the mechanism to avoid stresses due to temperature changes or excessive loading forces. A more effective way to avoid the occurence of internal stresses is the addition of an internal degree of freedom in the mechanism. This extra degree of freedom, created in the rotor or foundation, will eliminate the over-determination of the rotor position. In this respect it is important to create a combination of rotor and foundation that yields a low stiffness in respect of loading forces applied along the axis of rotation of the cross-spring pivot. In figure 6.13 this is illustrated. To reduce the influence of the internal stresses it is important that the stiffness, c_f, is small relative to the stiffness of the plate-springs in the undeformed position, given by

$$c_z^* = \frac{1}{K_z \cdot \ell^3 \cdot \left(a^2 - a + \frac{1}{3} \right)} \qquad (6.21)$$

An example of such a construction is shown in figure 6.13. Here the addi-

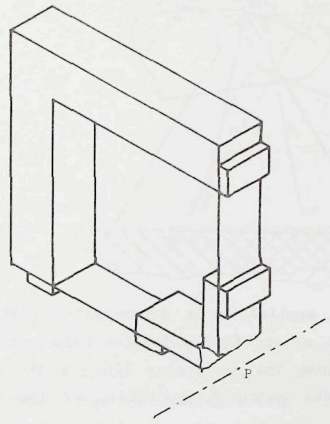

Figure 6.12
In a cross-spring mechanism each plate-spring is avoiding the motion of the rotor along the initial axis of rotation. Thus this degree of freedom is determined twice.

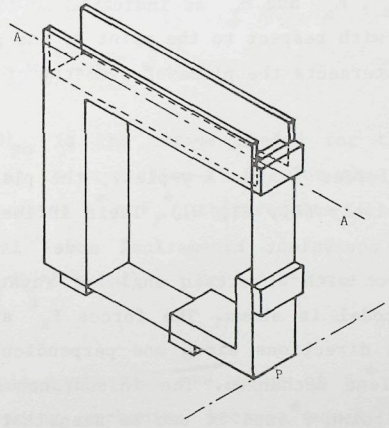

Figure 6.13
As two plate-springs in a cross-spring pivot are determine twice the relative motion in the direction of their z-axis, an extra internal degree of freedom must be created when internal stresses should be avoided. Here the stator has been modified to allow for a rotation around the line AA. As a result the relative position of the rotor along his axis of rotation is determined by the horizontal plate-spring only.

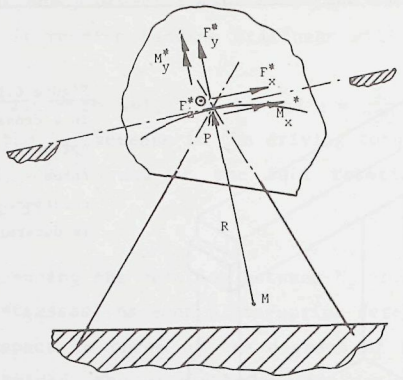

Figure 6.14

Any set of loading components applied to a cross-spring pivot can be transformed, apart from M_z, into a set of five loading components as shown here. The x^*-axis is chosen along the stationary line in the equivalent mechanism with its origin in the point P, the pole, of the undeformed mechanism.

tional degree of freedom is the relative rotation of each plate-spring clamping around the axis A-A.

The relation between the driving torque, M_z, and the angle of rotation $\phi(\ell)$ will also be influenced by the loading forces applied to the rotor. The loading forces can in all cases be replaced by an equivalent system of the loading components F_x^*, F_y^*, F_z^*, M_x^* and M_y^* as indicated in figure 6.14. These components are specified with respect to the point P, the point where the initial axis of rotation intersects the plane of symmetry of the cross-spring mechanism.

The influence of the loading forces in the x-y-plane, the plane of symmetry, has been studied extensively (D1, H1, W1). Their influence may be directly understood when the equivalent kinematical model is used. In figure 6.15 a cross-spring pivot with a certain angle of rotation, $\phi(\ell)$, together with the equivalent model is shown. The forces F_x^* and F_y^* are applied at the point P and in directions along and perpendicular to the stationary line in the equivalent mechanism. The instantaneous point of rotation for the rotor is the point P^* and it can be seen that the total moment around P^* will be

$$M_P^* = M_z + F_y^* \cdot R \cdot (\sin \phi(\ell)) - F_x^* \cdot R \cdot (1 - \cos \phi(\ell)) \qquad (6.22)$$

Thus a force perpendicular to the line along which the equivalent circle is

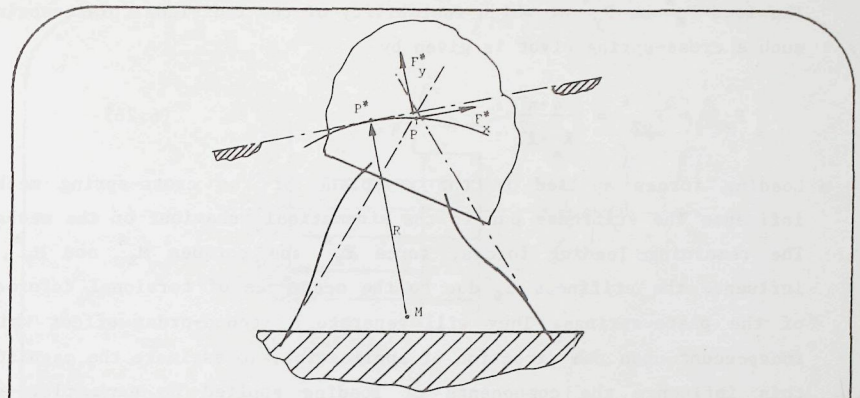

Figure 6.15

When a rotation of the rotor of the cross-spring pivot occurs its momentary point of rotation will move, to point P^*, as predicted by the equivalent mechanism. Thus the loading forces applied at the point P, the original axis of rotation, will exert a torque around the momentary axis of rotation through P^*. It is clear that the force F_y^* has a large influence and F_x^* yields only a second order contribution to the torque.

rolling, here F_y^*, has a linear contribution to the moment about the point P^* and thus directly influences the stiffness c_ϕ of the cross-spring pivot. The magnitude of the effect can be directly calculated when the radius R of the circle is known. The torque M_z needed to obtain a certain rotation $\phi(\ell)$ is calculated with

$$M_z \cong M_{zo} - F_y^* \cdot R \cdot \phi(\ell) \qquad (6.23)$$

where M_{zo} is the torque needed for the unloaded mechanism, calculated according to expression (6.5). For the orthogonal, symmetric cross-spring pivots, where $F^* = F_y^*$, this results in

$$M_z \cdot K_z \cdot \ell \simeq \phi(\ell) \cdot \{ 8 \cdot (1 - 3 \cdot a + 3 \cdot a^2) - F_y^* \cdot K_z \cdot \ell^2 \cdot \frac{2}{5} \cdot \sqrt{2} \cdot (-3 \cdot a^2 + 3 \cdot a - \frac{1}{3}) \} \qquad (6.24)$$

From this expression the value of F_y^* at which the stiffness c_ϕ of the cross-spring mechanism becomes equal to zero can be determined. For a doubly-symmetric cross-spring pivot, $a = \frac{1}{2}$, the magnitude of this load will be

$$F_{y1}^* \simeq \frac{6 \cdot \sqrt{2}}{K_z \cdot \ell^2} \qquad (6.25)$$

The load F_x^* or F_y^* at which instability of the individual plate-springs in such a cross-spring pivot is given by

$$F_{x2}^* = F_{y2}^* \simeq \frac{4 \cdot \pi^2}{K_z \cdot \ell^2} \qquad (6.26)$$

Loading forces applied in the x-y-plane of the cross-spring mechanism influence the stiffness due to the kinematical behaviour of the mechanism. The remaining loading forces, force F_z^* and torques M_x^* and M_y^*, will influence the stiffness c_ϕ due to the occurence of torsional deformations of the plate-springs. They will generate a second-order effect which is independent upon the direction of application. To estimate the magnitude of this influence the components of loading applied to each plate-spring should be determined on the basis of the equations for static-equilibrium for the rotor. In this analysis it may be assumed that each plate-spring is loaded by a force F_z and a torque M_x. As the stiffness of the plate-spring with respect to rotation about its y-axis is low no torque M_y will be absorbed by the plate-springs.
Difficulties will arise due to the over-determination of the position of the rotor. The distribution of the force F_z^* over the two springs is undetermined and considerations about the symmetry or about the relative stiffness in the direction of the z-axis should be used to estimate the magnitude of F_z for each plate-spring.

Once the two loading components for each plate-spring have been determined their influence upon the stiffness c_ϕ can be determined with the methods described in the previous chapters. The loading forces are applied to the plate-spring as shown in figure 6.16. The analysis is performed with an estimated shape of the deformed plate-spring based upon the following end-conditions

$$\phi(\ell) = \phi_\ell$$
$$u(\ell) \simeq (a-1) \cdot \ell \cdot \phi_\ell$$
$$\theta(\ell) \simeq 0$$

It is assumed that the other plate-spring will prevent the rotor to rotate around the y-axis and therefore it is assumed that $\theta(\ell)$ will be almost equal to zero. Due to the loading forces M_x and F_z a torsional deformation along the plate-spring will occur. This deformation in combination with the loading forces will then cause a variation of the stiffness c_ϕ of the cross-spring mechanism.

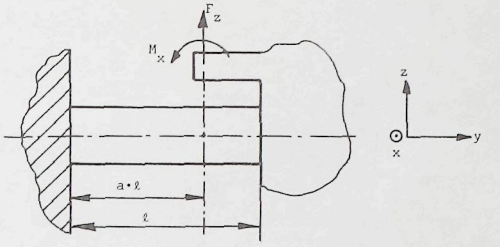

Figure 6.16
In the analysis of the influence of the loading components F_z and M_x upon the behaviour of a plate-spring in a cross-spring mechanisms it will be assumed that these components are applied at the rotor as shown here.
This selection is arbitrary, following from the general system of loading components applied to the rotor shown in figure 6.14.

In this analysis the influence of the length to width ratio of the plate-springs, caused by the effect of the constrained warping, will be accounted for. In Annex 6.I the following relation between the torque M_z, for one plate-spring, and the resulting angle of rotation ϕ_ℓ is derived

$$M_z \cdot K_z \cdot \ell \simeq \phi_\ell \cdot \{ 4 \cdot (1-3 \cdot a+3 \cdot a^2) + - K_z \cdot K_y \cdot \ell^2 \cdot (F_z^2 \cdot \ell^2 \cdot P_5 + F_z \cdot \ell \cdot M_x \cdot P_6 + M_x^2 \cdot P_7) \} \qquad (6.27)$$

where the factors P_5, P_6 and P_7 are functions of both the parameter a and the length to width ratio of the plate-spring. From this result a point on the y-axis can be determined where the application of the force F_z and the torque M_x yield independent effects.It will be shown in the following paragraph that this is the point where application of a force F_z will not cause a relative rotation ϕ of the two clamped ends. This point is located at a distance $g \cdot \ell$ from the stationary clamped end as shown in figure 6.17. The parameter g is a function of the geometrical parameter a and the dimensions of the plate-spring. When the loading components are applied at this point

expression (6.27) can be written as

$$M_z \simeq \phi(\ell) \cdot c_o \cdot \{ 1 - \frac{K_y}{K_z} \cdot \{ (\frac{F_z \cdot \ell^2 \cdot K_z}{Q_5})^2 + (\frac{M_x \cdot \ell \cdot K_z}{Q_7})^2 \} \} \qquad (6.28)$$

where $c_o = \frac{4 \cdot (1 - 3 \cdot a + 3 \cdot a^2)}{K_z \cdot \ell}$

In figure 6.17 the parameter g and the coefficients Q_5 and Q_7 are given as a function of the parameter a and the length to width ratio of the plate-spring.

This expression gives a first-order estimate of the stiffness of one plate-spring under influence of the loading components F_z and M_x. It may be used to estimate the order of magnitude of the loading components that reduce the stiffness to zero. The actual first-order buckling loads will be smaller (about 20 %). This difference is also seen between the expressions (5.9) and (5.10) and the expressions (5.37) and (5.39).

Before using this result it will be necessary to determine the loading situation for each plate-spring in the cross-spring pivot.
With expression 6.28 the magnitude of M_z for each plate-spring may be determined and thus the stiffness of the cross-spring pivot is obtained.

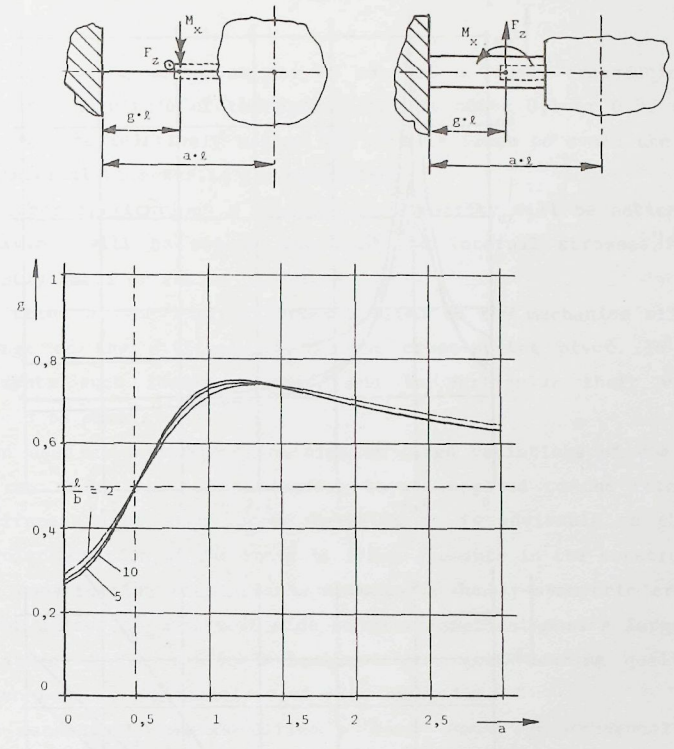

Figure 6.17

When loading components F_z and M_x are applied to a plate-spring in a cross-spring pivot the contribution of that spring to the stiffness c_ϕ is changed as indicated by expression (6.28). To determine the influence of the loading components it is advisable to apply them at a distance $g \cdot \ell$ from the stationary clamping. Application of a force F_z at this point does not cause a rotation around the x-axis of the end of the plate-spring and in this case the influences of F_z and M_x are independent.
The distance $g \cdot \ell$, shown in (a), is a function of the geometrical parameter a and the properties of the plate-spring. The presented results are calculated for plate-spring materials with Poisson's constant equal to 0,3 and for different length to width ratios.
The figures (b) and (c) show the magnitude of the coefficients Q_5 and Q_7 as a function of a.

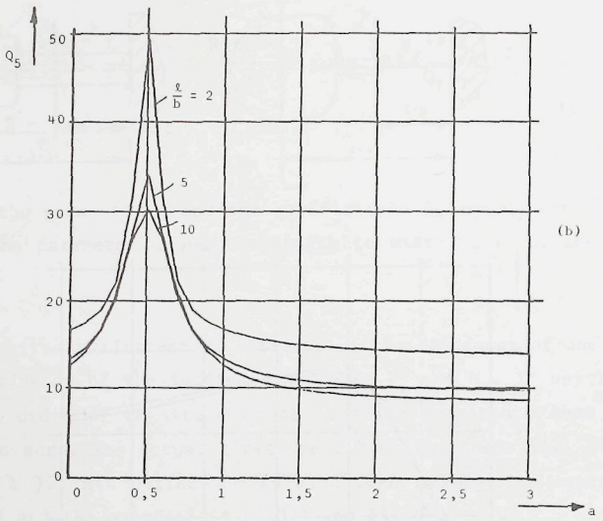

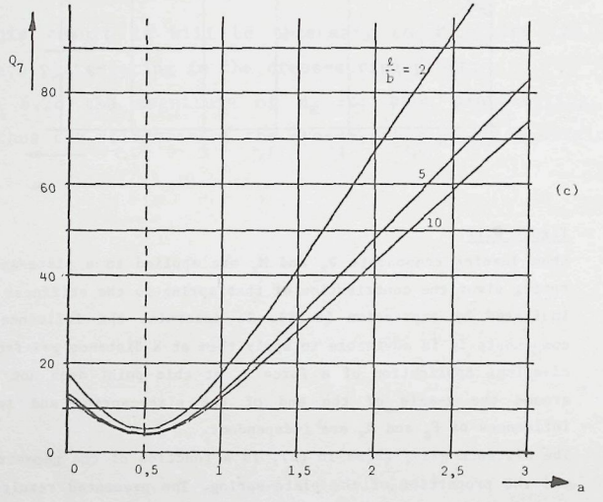

Figure 6.17 Continued.

Summarizing the contents of this paragraph the following remarks could be made,

- A cross-spring mechanism may be used as a linear transducing element when the magnitude of the parameter a is about 0,1 or 0,9, the plate-springs are relatively narrow and care is taken to avoid the occurence of internal stresses in the mechanism.
- In other applications a certain non-linearity will be noticed but the behaviour will be reproducing when the internal stresses are sufficiently small or remain unchanged.
- Variation of the loading forces applied to the mechanism will cause a change of the stiffness c_ϕ of the cross-spring pivot. In measuring elements such loading forces, and in particular their variations, should be small.
- When used as a construction element large variations of the stiffness c_ϕ may occur due to the loading forces applied to the rotor. As the stiffness might even become negative it is advisable to control the angular position of the rotor by other elements in the construction.
- For construction elements the orthogonal doubly-symmetric cross-spring pivot allows for the most wide range of applications. A large angle of rotation at low stiffness combined with good bearing qualities will often lead to the selection of this mechanism.
- For mechanisms used to define a "pure" rotation orthogonal symmetric mechanisms with a geometrical parameter a of $^1/_8$ or $^7/_8$ will be most favourable.
- The most linear transducing element is a cross-spring mechanism with symmetric and orthogonal springs with values of a around 0,1 or 0,9 as can be concluded from figure 6.11. For such cases attention should be paid to the other effects introducing non-linearity.

6.4 Guiding stiffnesses

The cross-spring mechanism is used to determine the position of the rotor in respect of five of its degrees of freedom. In the directions of these degrees of freedom the position will be determined with a certain stiffness. These guiding stiffnesses are of importance when dynamic loading forces are applied or when a well defined motion under varying loading forces is required. The stiffnesses in the five directions are determined by three stiffnesses of each separate plate-spring. As mentioned before the plate-springs have a relatively high stiffness in three directions.

In order to visiualize the guiding stiffnesses of the cross-spring mechanism it is useful, as was done for the parallel-guiding, to replace each plate-spring by a system containing three helical springs. One helical spring represents the stiffness in the y-axis direction and the other two are together generating the stiffnesses c_z and c_ψ. In figure 6.18 such an equivalent model is shown. When both plate-springs are thus replaced the rotor is supported by six helical springs while it is still free to rotate around the x-axis through the point P. It should be reminded that the stiffnesses of the helical springs will be a function of the rotation of the cross-spring pivot.

To describe the behaviour of the plate-spring, or the equivalent model, in the three directions it is necessary to determine the stiffnesses of the springs y, z_1 and z_2, the distance between the springs z_1 and z_2 and the position of these springs (see figure 6.18).

The spring y is connecting the rotor and stator while its working line coincides with the originally straight undeformed centerline of the plate-spring. The springs z_1 and z_2 have their working lines in the original y-z plane parallel to the z-axis.
Their distance along the original y-axis, a_y, depends upon the relation between c_z and c_ψ of the plate-spring. Halfway between these helical springs is the point where application of a force F_z will cause only a displacement of the end of the plate-spring in the direction of the z-axis and no rotation about the x-axis.
For symmetric constructions, as in the parallel-guide and the doubly-symmetric cross-spring mechanism, this point will be at the middle of the plate-spring. For other mechanism, and other values of the geometrical

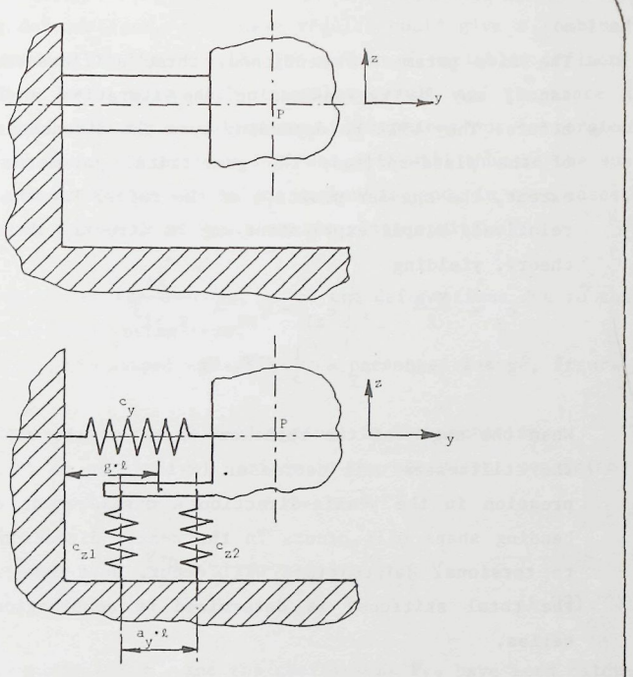

Figure 6.18.
Each plate-spring in a cross-spring pivot is determining three degrees of freedom with a high stiffness. To determine the properties of each plate-spring in these "bearing" directions it may be replaced by the equivalent mechanism (b), containing three helical springs.

parameter a, this point will be located at a distance g.ℓ from the clamping in the foundation.

The five parameters mentioned, three stiffnesses, a position and a distance, may be derived using the iterative analytical method described before. They will be depending upon the dimensions and material properties of the plate-springs, the geometrical parameter a and, to the largest extent, the angular position of the rotor. For the undeformed plate-springs relatively simple expressions may be directly obtained from the linear beam theory, yielding

$$c_y = \frac{E \cdot A}{\ell} \quad , \quad c_{z1} = c_{z2} = \frac{6}{K_x \cdot \ell^3}$$

$$g = \tfrac{1}{2} \quad \text{and} \quad a_y = \frac{1}{3} \cdot \sqrt{3} \cdot \ell$$

When the angle of the rotation, $\phi(\ell)$, of the rotor is not equal to zero, the stiffnesses will decrease. In addition to the deformation due to compression in the y-axis-direction a displacement due to variations of the bending shape will occur. In the z-axis direction extra displacements due to torsional deformations will occur. Just like for the parallel guiding the total stiffness is determined by combination of two stiffnesses in series.

The magnitude of the deflections in these three directions under influence of the loading forces being a function of the angle of rotation $\phi(\ell)$, the geometrical parameter a and the length to width ratio of the plate-springs can be determined using the iterative analytical method. For the stiffness c_y of one plate-spring is thus obtained

$$c_y \simeq \frac{E \cdot A}{\ell} \cdot \frac{1}{\left(1 + \phi_\ell^2 \cdot \left(\frac{\ell}{h}\right)^2 \cdot \left(\frac{12}{720} + \frac{12}{700} \cdot (a-\tfrac{1}{2})^2 \right) \right.} \qquad (6.29)$$

This expression may be used for small values of $\phi(\ell)$ as it is derived with linearized expressions for sin $\phi(s)$ and cos $\phi(s)$. In addition this expression will only yield the value of the stiffness for small values of the force F_y. These considerations are explained in more detail in chapter 5. Expression (6.29) is equal to the result obtained by Dijksman (D1) for orthogonal cross-spring mechanism ($\alpha = \pi/2$ rad.) .

The analysis of the deformations due to torsion in the plate-springs caused by the force F_z and the torque M_x is described in Annex 6.I. Using the

expressions derived there the extra deflection $w(\ell)$ and angular deformation $\phi(\ell)$ may be calculated. Combination of the results from the linear beam theory, the bending deformations, and these results could give a combined equivalent model according to figure 6.18. The number of variables influencing such a mechanism leads to a rather complex result and therefore a separate equivalent mechanism to calculate the deformations due to torsion will be described. The total deflections $\phi(\ell)$ and $w(\ell)$ will thus be the sum of the contributions from the two equivalent mechanisms and, in some cases, the contribution due to the shear stresses in the plate-spring.

The equivalent mechanism for the calculation of the deformations due to the torsion is described by three parameters,

- g_t, the distance from the clamped end which was presented before, figure 6.17.
- a_{yt}, the distance between the two helical springs in the mechanism.
- c_{zt}, the stiffness of the two helical springs in the equivalent mechanism. This stiffness is calculated as

$$c_{zt} \simeq \frac{P_{13}^2}{K_y \cdot \ell^3 \cdot \phi(\ell)^2} = \frac{E \cdot A}{\ell} \cdot \frac{1}{2 \cdot (1+\nu)} \cdot \left\{ \frac{P_{13} \cdot h}{\ell \cdot \phi(\ell)} \right\}^2 \qquad (6.30)$$

The magnitude of the parameter a_{yt} and the coefficient P_{13} have been calculated and the results are shown in figure 6.19.

It is clear that the stiffness c_{zt} is a function of the angle of rotation $\phi(\ell)$. For larger angles of rotation the stiffness may decrease strongly. And when a mechanism is designed to allow for larger rotations the thickness to length ratio will be smaller, leading to a further decrease of the stiffness c_{zt}.

For the stiffness of a plate-spring in the direction of the z-axis three stiffnesses in series are to be considered

- Shear deformation $\quad c_{zs} = \frac{E \cdot A}{\ell} \cdot \frac{1}{2 \cdot (1+\nu)}$
- Bending deformation $\quad c_{zb} \simeq \frac{E \cdot A}{\ell} \cdot 2 \cdot \left(\frac{b}{\ell} \right)^2$
- Torsion deformation $\quad c_{zt} \simeq \frac{E \cdot A}{\ell} \cdot \frac{1}{1+\nu} \cdot \left(\frac{P_{13} \cdot h}{\phi(\ell) \cdot \ell} \right)^2$

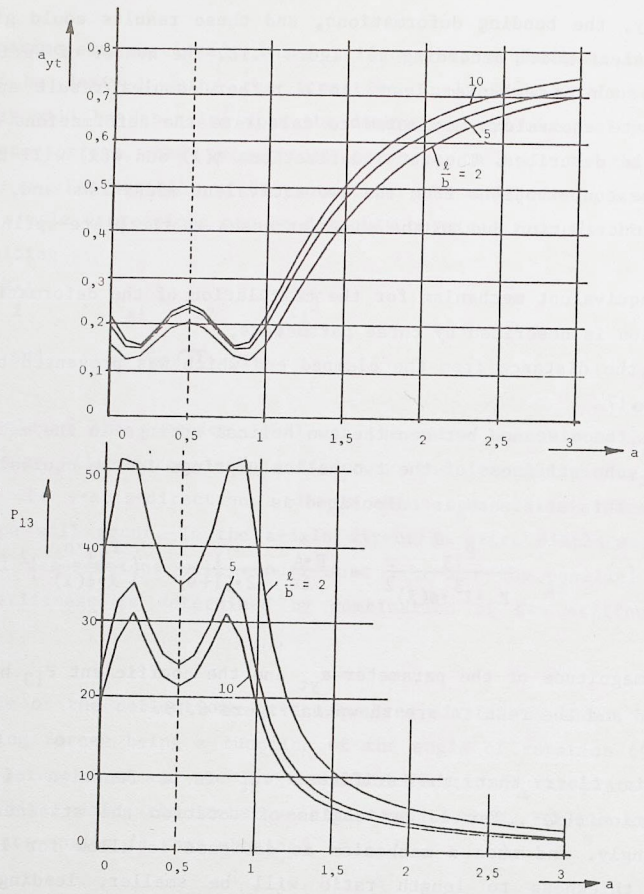

Figure 6.19

To determine the behaviour of the cross-spring pivot each plate-spring may be replaced by an equivalent mechanism as in figure 6.18. To calculate the deflections due to torsion in the plate-spring the parameter a_y can be determined from fig. (a). The stiffness of both helical springs may then be determined with expression (6.13) and the magnitude of P_{13} can be taken from fig. (b).

From these expressions the relative order of magnitude of each effect can be estimated. The shear deformation will be noticeable when the width of the plate-spring is more than half the length. The torsion deformation will be important for larger angles of rotation or for larger deflections of the end of the plate-spring. For mechanisms with values of a equal to $\frac{1}{2}$ the contribution of the torsion deformation will be noticeable for mechanisms designed for angular deformations of about 0,15 rad.

Annex 6.I

Deformation of a plate-spring by the loading components F_z and M_x

When a plate-spring in a cross-spring pivot is subjected to the loading forces F_z and M_x a torsional deformation will occur when the angle of rotation, $\phi(\ell)$, of the mechanism is unequal to zero. Due to these torsional deformation the relation between the driving torque M_x and the rotation $\phi(\ell)$ will be influenced and displacements $w(\ell)$ and $\psi(\ell)$ of the end of the plate-spring will occur. In this Annex these effects will be calculated using the iterative analytical method and the mathematical model for a plate-spring obtained in chapter 4 (figure 4.9). For the calculations it is assumed that the force F_z is applied along the initial axis of rotation of the cross-spring mechanism, thus at a distance $a.\ell$ from the fixed end of the plate-spring, see figure 6.I.1.

It is assumed that the plate-spring is a part of a mechanism and that the angular deformation $\theta(\ell)$ of the end (rotation around the y-axis) may be neglected in solving the equations. This rotation will be small as the other plate-spring in the mechanism determines this degree of freedom with a relatively high stiffness.

Thus the following displacements of the free end of the plate-spring are used as initial estimates

$$\phi(P) = \phi(\ell)$$
$$u(\ell) = -(1-a)\cdot\phi(\ell)\cdot\ell$$
$$\theta(\ell) = 0$$
$$y(\ell) = 0$$
$$v(\ell) = 0$$
$$w(\ell) = 0$$

With these end conditions the initial estimates for the shape of the deformed plate-springs will be

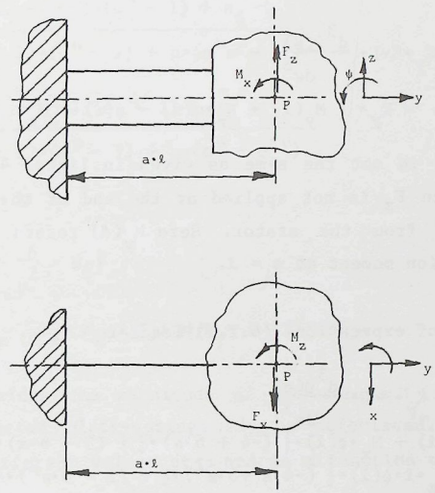

Figure 6.I.1.
To calculate the deformations of one plate-spring of a cross-spring pivot it is assumed that the different loading components are applied relative to the point P, the point where the initial axis of rotation intersects the y-axis.

$$\phi(s) \simeq \phi(\ell) \cdot \{ (4 - 6 \cdot a) \cdot \xi - (3 - 6 \cdot a) \cdot \xi^2 \}$$

and

$$u(s) \simeq -\phi(\ell) \cdot \{ (2 - 3 \cdot a) \cdot \xi^2 - (1 - 2 \cdot a) \cdot \xi^3 \} \qquad (6.I.2)$$

where $\xi = {}^{s}/_{\ell}$.

These first estimates can be substituted into the differential equation for the angular deformation $\theta(s)$, the first equation of figure 4.9, which thus becomes

$$\frac{d\theta(s)}{ds} - K_y \cdot E \cdot \Gamma \cdot \frac{d^3\theta(s)}{ds^3} \simeq \qquad (6.I.3)$$
$$= K_y \cdot \{ M_y(\ell) + F_z \cdot u(s) - \phi(s) \cdot (M_x + F_z \cdot (a \cdot \ell - s) \}$$

This equation is not the same as given in figure 4.9 because of the fact that the force F_z is not applied at the end of the plate-spring but at a distance $a \cdot \ell$ from the stator. Here $M_y(\ell)$ refers to the value of the internal torsion moment at $s = \ell$.

Substitution of expressions (6.I.1) leads to

$$\frac{d\theta(s)}{ds} - K_y \cdot E \cdot \Gamma \cdot \frac{d^3\theta(s)}{ds^3} \simeq$$
$$K_y \cdot \{ M_y(\ell) + M_x \cdot \phi(\ell) \cdot \{ (-4 + 6 \cdot a) \cdot \xi + (3 - 6 \cdot a) \cdot \xi^2 \} +$$
$$+ F_z \cdot \ell \cdot \phi(\ell) \cdot \{ (-4 \cdot a + 6 \cdot a^2) \cdot \xi + (2 - 6 \cdot a^2) \cdot \xi^2 + (-2 + 4 \cdot a) \cdot \xi^3 \} \}$$
(6.I.4)

As in Annex 5.I a solution for $\theta(s)$ in the following form may be found

$$\theta(s) = \phi(\ell) \cdot \{ a_1 \cdot \xi + a_2 \cdot \xi^2 + a_3 \cdot \xi^3 + a_4 \cdot \xi^4 +$$
$$+ A + B \cdot e^{-\mu \cdot \xi} + C \cdot e^{\mu \cdot \xi} \} \qquad (6.I.5)$$

where $\mu^2 = \frac{\ell^2}{K_y \cdot E \cdot \Gamma}$, and for $b > h$ $\mu \simeq \frac{\ell}{b} \cdot \sqrt{\frac{24}{(1+\nu)}}$.

The four coefficients $a_1 - a_4$ describe the particular solution for the differential equation and depend on $M_y(\ell)$, M_x and F_z. The other coefficients, A, B and C, and the unknown torque $M_y(\ell)$ can be determined from the four boundary conditions

$$\theta(0) = 0 \quad , \qquad \theta(\ell) = 0$$
$$\frac{d\theta(0)}{ds} = 0 \quad , \qquad \frac{d\theta(\ell)}{ds} = 0$$

On this basis all the coefficients may be determined and can be written as

$$a_4 = f_z \cdot (a - \tfrac{1}{2})$$
$$a_3 = m_x \cdot (1 - 2 \cdot a) + f_z \cdot (\tfrac{2}{3} - 2 \cdot a^2)$$
$$a_2 = m_x \cdot (3 \cdot a - 2) + f_z \cdot (3 \cdot a^2 - 2 \cdot a) + \frac{12}{\mu^2} \cdot a_4$$

With $a_5 = (a_2 + a_3 + a_4)$ and $a_6 = (2 \cdot a_2 + 3 \cdot a_3 + 4 \cdot a_4)$ it follows that

$$B = - \frac{(a_5 - \frac{a_6}{\mu}) \cdot (e^{\mu} - 1) + a_6}{2 \cdot (e^{-\mu} - 1) \cdot (e^{\mu} - 1) + \mu \cdot (e^{\mu} - e^{-\mu})}$$

$$C = - \frac{(a_5 + \frac{a_6}{\mu}) \cdot (e^{-\mu} - 1) + a_6}{2 \cdot (e^{-\mu} - 1) \cdot (e^{\mu} - 1) + \mu \cdot (e^{\mu} - e^{-\mu})}$$

$$A = -B - C$$
$$a_1 = \mu \cdot B - \mu \cdot C$$
$$m_y = \phi(\ell) \cdot \{ a_1 - \frac{6}{\mu^2} \cdot a_3 \}$$
(6.I.6)

where $f_z = F_z \cdot \ell^2 \cdot K_y$, $m_x = M_x \cdot \ell \cdot K_y$ and $m_y = M_y(\ell) \cdot \ell \cdot K_y$.

From these expressions the magnitude of the torque $M_y(\ell)$ applied at the ends of the deflected plate-springs may be calculated. Results of this calculation for different values of μ and as a function of a are presented in figure 6.I.2

To proceed expression (6.I.5) for the angular deformation $\theta(s)$, in combination with expressions (6.I.6) are substituted in the remaining equations of figure 4.9. The second differential equation of figure 4.9 delivers the base to estimate the influence of F_z and M_x upon the stiffness c_ϕ. In the calculation it will be assumed that the loading force F_y is equal to zero. As it is the relation between the torque M_z and the angle $\phi(\ell)$ that is of interest, it is assumed that the force F_x and torque M_z are applied as in figure 6.I.1. Thus the modified version of the equation for $d\phi(s)/ds$ reads

$$\frac{d\phi(s)}{ds} \simeq K_z \cdot \{ \theta(s) \cdot (M_x + F_z \cdot (a \cdot \ell - s)) + M_z + F_x \cdot (-a \cdot \ell + s) \} \qquad (6.I.7)$$

A solution for $\phi(s)$ may be obtained by direct integration and can be used to obtain an expression for u(s). The resulting expressions for the angle

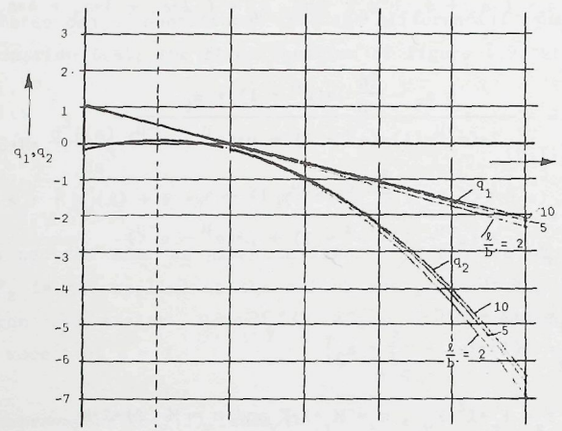

Figure 6.I.2.

In the undeflected situation the internal torsional moment $M_y(\ell)$ is equal to zero. Upon deflection this torque, due to the loading components F_z and M_x increases. The value of $M_y(\ell)$ is given by

$$M_y(\ell) \simeq (q_1 \cdot M_x + q_2 \cdot F_z) \cdot \phi(\ell)$$

The coefficients q_1 and q_2 are functions of the plate-spring properties and the geometrical parameter a. For a material with Poisson's constant equal to 0,3 these coefficients are shown as a function of a for different length to width ratios.

$\phi(\ell)$ and the deflection $u(\ell)$ are

$$\phi(\ell) \simeq m_z - f_x \cdot a + \frac{1}{2} \cdot f_x + \left(\frac{K_z}{K_y} \right) \cdot \phi(\ell) \cdot \{ (m_x + a \cdot f_z) \cdot P1 - f_z \cdot P2 \}$$

$$u(\ell) \simeq -\tfrac{1}{2} \cdot (m_z - f_x \cdot a) - \frac{1}{6} \cdot f_x - \left(\frac{K_z}{K_y} \right) \cdot \phi(\ell) \cdot \{ (m_x + a \cdot f_z) \cdot P3 - f_z \cdot P4 \} \qquad (6.I.9)$$

where $m_z = M_z \cdot K_z \cdot \ell$ and $f_x = F_x \cdot K_z \cdot \ell^2$

P1-P4 are expressions containing the coefficients $a_1 - a_4$ and A, B, C from the solution for $\theta(s)$

$$P1 = A + \tfrac{1}{2} \cdot a_1 + \frac{1}{3} \cdot a_2 + \frac{1}{4} \cdot a_3 + \frac{1}{5} \cdot a_4 + \frac{B}{\mu} \cdot (1 - e^{-\mu}) + \frac{C}{\mu} \cdot (e^{\mu} - \quad)$$

$$P2 = \frac{1}{2} \cdot A + \frac{1}{3} \cdot a_1 + \frac{1}{4} \cdot a_2 + \frac{1}{5} \cdot a_3 + \frac{1}{6} \cdot a_4 + \frac{B}{\mu} \cdot \left(\frac{1}{\mu} - \frac{1}{\mu} \cdot e^{-\mu} - e^{-\mu} \right) + \frac{C}{\mu} \cdot \left(\frac{1}{\mu} - \frac{1}{\mu} \cdot e^{\mu} + e^{\mu} \right)$$

$$P3 = \frac{1}{2} \cdot A + \frac{1}{6} \cdot a_1 + \frac{1}{12} \cdot a_2 + \frac{1}{20} \cdot a_3 + \frac{1}{30} \cdot a_4 + \frac{B}{\mu} \cdot \left(1 - \frac{1}{\mu} \cdot (1 - e^{-\mu}) \right) + \frac{C}{\mu} \cdot \left(-1 - \frac{1}{\mu} \cdot (1 - e^{\mu}) \right)$$

$$P4 = \frac{1}{6} \cdot A + \frac{1}{12} \cdot a_1 + \frac{1}{20} \cdot a_2 + \frac{1}{30} \cdot a_3 + \frac{1}{42} \cdot a_4 + \frac{B}{\mu^2} \cdot \left(e^{-\mu} \cdot (1 + \frac{2}{\mu}) + 1 - \quad \right) + \frac{C}{\mu^2} \cdot \left(e^{\mu} \cdot (1 - \frac{2}{\mu}) + 1 + \frac{2}{\mu} \right)$$

(6.I.9)

To obtain an expression relating $\phi(\ell)$ to M_z it is possible to eliminate the force F_x using the relation between $u(\ell)$ and $\phi(\ell)$

$$u(\ell) \simeq (a - 1) \cdot \phi(\ell)$$

This will yield the following expressions

$$m_z \simeq \phi(\ell) \cdot \{ (4 - 12 \cdot a + 12 \cdot a^2) - m_x \cdot \frac{K_z}{K_y} \cdot (P1 \cdot (6 \cdot a - 2) - 2 \cdot P3 \cdot (6 \cdot a - 3)) + - f_z \cdot \frac{K_z}{K_y} \cdot (P1 \cdot (6 \cdot a^2 - 2 \cdot a) - 2 \cdot P3 \cdot (6 \cdot a^2 - 3 \cdot a) - P2 \cdot (6 \cdot a - 2) \cdot (6 \cdot a - 3)) \} \qquad (6.I.10)$$

As the factors P1-P4 contain terms with M_x and F_z the expression may be

written as

$$m_z \approx \phi(\ell)\cdot\{\ (4-12\cdot a+12\cdot a^2) - (\frac{K_z}{K_y})\cdot(\ P5\cdot m_x^2 + P6\cdot m_x\cdot f_z + P7\cdot f_z^2)\ \} \qquad (6.I.11)$$

where the factors P_5, P_6 and P_7 are functions of the parameter a and the properties of the plate-spring. Using the expressions given in this chapter they can be calculated. Results of such calculations are presented in figure 6.17.

To determine the guiding stiffnesses c_z and c_y of the cross-spring mechanism the solution for $\theta(s)$ (6.I.5) can be used in the equations from figure 4.9. The deformations resulting from the torsion in the plate-spring may be added to those due to bending about the x-axis for which the stiffnesses were described in expression (6.28). For the additional angular deformation, $\Delta\phi(s)$, can be written

$$\frac{d\Delta\phi(s)}{ds} \approx \theta(s)\cdot\frac{d\phi(s)}{ds}$$

Substitution of $\theta(s)$ and $\phi(s)$ from expressions (6.I.5) and (6.I.2) and subsequent integration leads to the following result for the angle $\Delta\phi(\ell)$ at the end of the plate-spring

$$\Delta\phi(\ell) \approx \phi(\ell)^2\cdot(\ P8 + a\cdot P9\ ) \qquad (6.I.12)$$

where
$$P8 = A - \frac{1}{6}\cdot a_2 - \frac{1}{5}\cdot a_3 - \frac{1}{5}\cdot a_4 + \\ + \frac{B}{\mu}\cdot(\ 4 + 2\cdot e^{-\mu} + \frac{6}{\mu}\cdot(\ e^{-\mu} - 1)\ ) + \\ + \frac{C}{\mu}\cdot(\ -4 - 2\cdot e^{\mu} + \frac{6}{\mu}\cdot(\ e^{\mu} - 1)\ )$$

$$P9 = a_1 + a_2 + \frac{9}{10}\cdot a_3 + \frac{4}{5}\cdot a_4 + \\ + \frac{B}{\mu}\cdot(\ -6 - 6\cdot e^{-\mu} + \frac{12}{\mu}\cdot(\ 1 - e^{-\mu})\ ) + \\ + \frac{C}{\mu}\cdot(\ 6 + 6\cdot e^{\mu} + \frac{12}{\mu}\cdot(\ 1 - e^{\mu})\ )$$

A similar result is obtained for the additional displacement, $\Delta w(\ell)$, of the end of the plate-spring, yielding

$$\frac{\Delta w(\ell)}{\ell} \approx \phi(\ell)^2\cdot(\ P10 + a\cdot P11\ ) \qquad (6.I.13)$$

where
$$P10 = A + \frac{1}{6}\cdot a_1 + \frac{1}{30}\cdot a_2 - \frac{1}{105}\cdot a_4 + \\ + \frac{B}{\mu^3}\cdot(\ 12 - 10\cdot\mu + 4\cdot\mu^2 - e^{-\mu}\cdot(\ 12 + 2\cdot\mu)\ ) + \\ + \frac{C}{\mu^3}\cdot(\ -12 - 10\cdot\mu - 4\cdot\mu^2 + e^{\mu}\cdot(12 - 2\cdot\mu)\ )$$

and
$$P11 = -A + \frac{1}{10}\cdot a_2 + \frac{1}{10}\cdot a_3 + \frac{3}{35}\cdot a_4 + \\ + \frac{B}{\mu^3}\cdot(\ -24 + 18\cdot\mu - 6\cdot\mu^2 + e^{-\mu}\cdot(\ 24 + 6\cdot\mu\ )\ ) + \\ + \frac{C}{\mu^3}\cdot(\ 24 + 18\cdot\mu + 6\cdot\mu^2 + e^{\mu}\cdot(\ -24 + 6\cdot\mu)\ )$$

The factors P8 to P11 are functions of the geometrical parameter a, the loading components M_x and F_z and the properties of the plate-spring. These expressions determine the parameters describing the behaviour of the equivalent spring mechanism discussed in paragraph 6.4. The results of such a calculation have been given in figure 6.19 for different values of the length to width ratio of the plate-spring.

Chapter 7.

Different plate-spring applications, "reinforced" plate-spring elements.

7.1 Introduction

In the previous two chapters the two most common applications of plate-spring mechanisms have been discussed. Both the parallel guiding and the cross-spring pivot are guiding mechanisms using two plate-springs, "acting parallel" to each other, to determine five of the six degrees of freedom of the moving part. Also in both mechanisms the only deformation of the plate-spring in the desired motion is the bending of the plate-spring around the x-axis.

Many other usefull constructions could be made with plate-spring mechanisms. In such mechanisms either the torsional deformation of the plate-spring, plate-springs "acting in series", or special properties of plate-springs may be used. In lit. (B1) Breitinger has attempted to give a "morfological table" of the possibilities to construct mechanisms with plate-springs. Such a table will never be fully completed and will often contain many solutions which are of limited value. It illustrates, however, the vast variety of possibilities of application of plate-springs.

In the following paragraph a selection of plate-spring mechanisms will be briefly discussed. Some of these mechanisms are used to improve the properties of the parallel guiding or cross-spring pivot. Others are examples of totally different constructions.

One of the most interesting ways to improve the guiding properties, stiffness and loading capacities, of the plate-spring parallel guiding is the use of "partially reinforced" plate-spring elements. In this case one plate-spring in the parallel guiding is replaced by an element having one part with high bending stiffness and two short plate-springs at the ends (see figure 7.1).
Such mechanisms are suggested due to the fact that the central part of

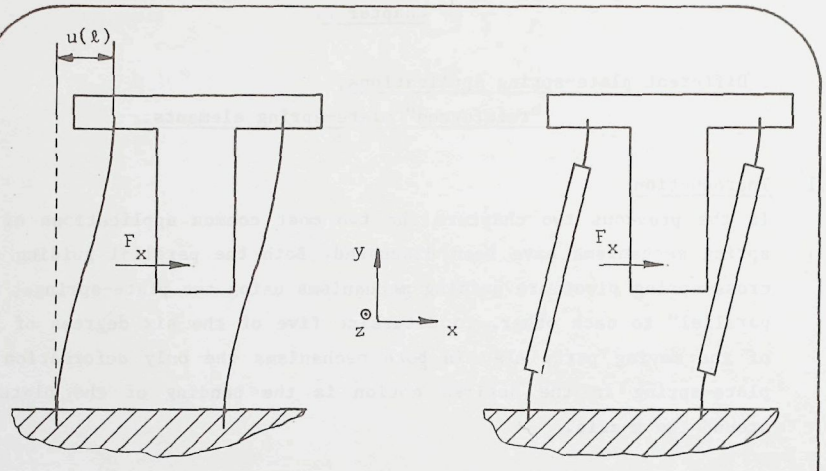

Figure 7.1

In a conventional parallel guiding (a) the central part of the plate-spring is not noticeably deformed. To increase the guiding stiffnesses and loading capacities it might therefore be helpfull to replace that part by a relatively stiff part (b).

plate-springs in conventional parallel guidings remains almost undeformed during normal operation. When loaded in other directions however the central part will be deformed and thus play a part in the guiding stiffness and the maximum loading capacity.

Different authors have suggested this change in the design of the plate-spring mechanism. To evaluate their potential advantages these mechanisms will be studied and compared with the conventional mechanism in paragraph 7.3.

7.2 A selection of plate-spring applications

7.2.1 Torsion hinges.

Probably the largest number of guiding mechanisms based on the elastic deformation is the tension strip hinge used in numerous indicating electric measuring devices (galvanometers etc.). In this mechanism two pieces of narrow, relatively long metal strip are connecting the rotor with the stator as in figure 7.2.a. A tensile force is applied to both the strips and the rotation of the rotor causes torsion of the two strips.
As the driving torques in the measuring devices are applied carefully, avoiding other loading components, the relatively low stiffnesses in the x, z, ψ and ϕ directions are acceptable disadvantages in this application.

Another, more important, disadvantage of using the torsional deformation of the strips is the relatively large non-linearity in the relation between driving torque and the angle of rotation. This non-linearity is due to the occurence of tensile and compressive stresses in the plate-spring cross-section. For a plate-spring as shown in figure 7.2.b the relation between the torque M_y and the angle of rotation $\theta(\ell)$ may, in third order approximation, be written as (litt. T1)

$$M_y \cdot K_y \cdot \ell = \theta(\ell) \cdot \{1 + \frac{1}{120} \cdot (\frac{b}{h})^2 \cdot (\frac{b}{\ell})^2 \cdot \theta(\ell)^2\} \qquad (7.1)$$

where it is assumed that b > h.
This means that for the plate-spring with dimensions 80x20x0,25 mm the influence of the non-linearity at an angular deformation of 0,2 rad. ($\simeq 10^{\circ}$) will be about 13%, due to this effect.

This relation was derived while neglecting the influence of the constrained warping of the cross-section at the end of the plate-spring. Due to this effect the nominal stiffness for plate-springs will depend upon the length to width ratio and the Poisson constant for the material. For a plate-spring clamped at both ends the stiffness may be calculated as

$$c_y = \frac{\theta(\ell)}{K_y \cdot \ell} \simeq \frac{1}{3} \frac{E \cdot b \cdot h^3 \cdot Q_t}{\ell} \qquad (7.2)$$

(under the assumption that b >h).

The magnitude of Q_t as a function of the parameter $\mu = \frac{\ell}{b} \cdot \sqrt{\frac{24}{(1+\nu)}}$ or the length to width ratio ℓ/b for Poisson constant equal to 0,3 may be taken from figure 7.2.c. This factor is calculated using the method described in chapter 4.
Measurements indicate that this method may be used for values of μ greater than 4 ($\ell > b$). For shorter plate-springs the conditions in the clampings are becoming relatively important and a smaller stiffness is measured.

Another group of guiding mechanisms where the torsional deformation of the plate-springs is used are the angle-strip hinges which were discussed, among others, by Jones (litt. J2). In these mechanisms two plate-springs connect the rotor to the stator as shown in figure 7.2.d. In addition to the effects described above such mechanisms will cause undesired rotations of the rotor around an axis in the x-z-plane. For the mechanism of figure 7.2.d. this rotation may be calculated as,

$$\alpha \simeq \tfrac{1}{2} \cdot \sqrt{2} \cdot \frac{b}{\ell} \cdot \theta(\ell)^2 \qquad (7.3)$$

This effect may be avoided when a symmetric construction of the angle-strip hinge is used. Different constructions may be made. One of them is shown in figure 7.2.e. Here the two plate-springs are each divided into two parts placed at equal distances from the axis of rotation. When the distance from the axis of rotation is increased and the plate-springs are tilted around their x-axis the vibrating bowl mechanism for parts-feeding in production automation is obtained.

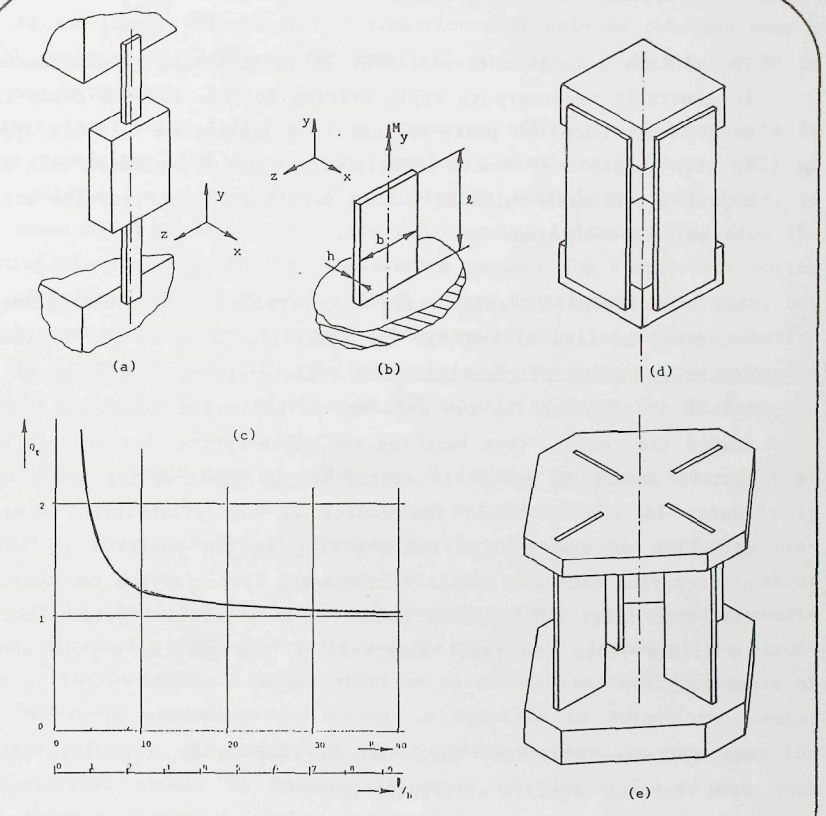

Figure 7.2 Torsion hinges.

a. Torsion hinges use two spring strips under tension to guide moving coils in measuring instruments.
b. Definition of dimensions and coordinate-system for plate-springs in torsion-hinges.
c. Due to the influence of the "constrained warping" the stiffness c_θ is a function of the length to width ratio. When both ends are clamped this influence may be estimated using the factor Q_t in expression (7.2).
d. Angle-strip hinge using two plate-springs with their planes perpendicular to each other.
e. Symmetrical design of an angle-strip hinge which will avoid the occurence of undesired parasitic rotations.

7.2.2. Plate-spring with negative and zero stiffness.

To maintain a certain displacement of plate-spring guiding mechanisms it is generally necessary to apply driving forces. In some cases the energy needed to deform the plate-springs is a limitation to their application. In such instances it would be helpfull to use a mechanism with a constant negative stiffness which is placed parallel to the positive stiffness of the guiding mechanism.

Such a mechanism for application with parallel guiding mechanisms has been described in lit. D1 and E2. The principle of operation is indicated in figure 7.3.a. An originally straight plate-spring is clamped at both ends and in the center. The two ends are moved in the direction of the y-axis toward the center, thus buckling the plate-spring. During this buckling a certain amount of energy is stored in the plate-spring and part of this energy is released when the center of the plate-spring moves in the direction of the x-axis. While moving in the positive x-direction the plate-spring exerts a linearly increasing force driving the center in this direction (fig. 7.3.b). When connected to a parallel guiding mechanism as in figure 7.3.c the total stiffness of the guiding may be considerably reduced.

The following relations have been derived to describe this plate-spring with constant negative stiffness, (D1).

Total length of undeformed plate-spring : $2 \cdot \ell$

Displacement in y-axis direction of each end: $\Delta\ell$

Negative stiffness: $c_x \simeq - 8 \cdot \pi^2 \cdot \frac{E \cdot I}{\ell^3}$

Buckling forces: $F_y \simeq - 4 \cdot \pi^2 \cdot \frac{E \cdot I}{\ell^2}$

Maximum bending stress: $\sigma_b \simeq 2 \cdot \pi \cdot E \cdot \frac{h}{\ell} \cdot \sqrt{\frac{\Delta\ell}{\ell}}$

Working range: $u \simeq \pm 2 \cdot \ell \cdot \sqrt{\frac{\Delta\ell}{3\ell}}$

In theory the first-order expressions for the stiffness of the parallel guiding and the spring with negative stiffness allow for a total compensation of the positive stiffness of the guiding mechanism.

Due to non-linear effects such a reduction will only be obtained over a small range of deflections. For practical purposes a reduction of 90 to 95% may be reached.

Another interesting factor is the occurence of increased hysteresis in these mechanisms. Due to internal damping a small part (about 0,2%) of the deformation energy in a plate-spring is lost during each cycle. In the compensated mechanism of figure 7.3.c energy is transferred from the guiding plate-springs to the compensating spring. The energy loss during one cycle is a small part of the total energy transferred internally, but may be considerable when compared to the energy supplied to the mechanism by the driving forces. Thus the hysteresis of the compensated mechanism will be about 4% when a reduction of 90% in driving forces is obtained.

To obtain a certain rate of reduction of driving force the dimensions of the plate-springs have to be calculated beforehand. In this case it is important to predict the stiffnesses of the plate-springs rather accurately. In practice this is not possible with uncertainty ranges of about 10% due to the undefined active plate-spring thickness, clamping conditions, internal stresses, Young's modulus and the influence of the structure of the material. A better solution to adjust the total stiffness of the mechanism afterwards is making it possible to rotate the center clamping piece around the z-axis of the plate-springs. In this case the plate-springs should be buckled as shown in figure 7.3.d. For such mechanisms a torque M_z should be applied to the center clamping with magnitude

$$M_z \simeq 8 \cdot \pi \cdot \frac{E \cdot I}{\ell} \cdot \sqrt{\frac{\Delta\ell}{\ell}}$$

When the central clamping piece is rotated around the z-axis, positive as indicated in figure 7.3.d, the negative stiffness will be

$$c_x = - 80 \cdot \frac{E \cdot I}{\ell^3} \cdot (1 + 0{,}24 \cdot \phi \cdot \sqrt{\frac{\ell}{\Delta\ell}})$$

(Note: In the mechanism shown in figure 7.3d the angle ϕ is negative.)

From this expression the amplitude of the rotation ϕ needed to correct an uncertainty range of 10% may be estimated. For $\ell \simeq 9 \cdot \Delta\ell$ a rotation of $\pm$ 0,12 rad. ($\simeq 7^{\circ}$) would be required.

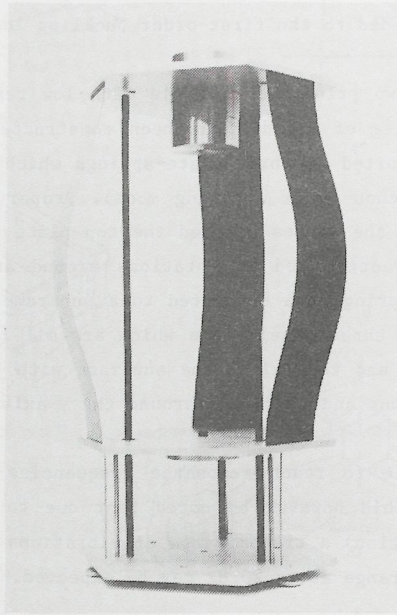

Figure 7.3.e.
Example of a construction using the low stiffnesses of elastic elements when loaded just over their buckling load.
(The length of the plate-springs is 100 mm. The mass carried at the upper table is about 15 kg.)

7.2.3 Plate-spring transmission mechanisms.

Transmissions with large transmission ratios over limited strokes may be created with different plate-spring configurations. The advantages of such mechanisms, the absense of play, high stiffnesses and good reproducibility, are of especial importance in manipulators for precision engineering applications.

The most straight forward construction is the cross-spring pivot used as a pivot for a lever. More interesting are the constructions where very high transmission ratios may be obtained. A first example is the mechanism sketched in figure 7.4a. Here a body A is connected by a parallel guiding mechanism to a body B which is connected by a similar parallel guiding to the foundation. The displacement of A relative to the foundation, u_o, is fixed by, for instance, a steel wire. The non-linear shortening of the plate-springs in y-directions can be used to generate parallel displacements of body A when body B is moved in the x-direction. For the transmission ratio may be derived

$$v = \frac{6}{5} \cdot \frac{u_o}{\ell} \cdot x$$

Thus the transmission ratio may be adjusted by adjusting u_o and large transmission ratio's (> 50) may be realized.

In this mechanism non-linear effects are combined to obtain a constant transmission ratio over a relatively large stroke. For micro-manipulators the required displacements are often very limited. In such cases non-linear effects may be used (see fig 7.4b). Here a second plate-spring is connected to the rotor B, of a cross-spring pivot such that the distance of the neutral planes of plate-springs 1 and 2 equals h. By displacement x a rotation ϕ of body B will result and thus the body A will move over the distance $v \simeq \phi \cdot h$.
Unfortunately the plate-springs 1 and 2 will shorten over a distance $\Delta\ell \simeq -\frac{1}{15} \cdot \phi^2 \cdot \ell$ each and this will influence the displacement v for larger angles of rotation.

A similar construction using the distance between neutral planes as part of a lever is shown in figure 7.4c. The body A is at one end connected to

the foundation by the two membranes 1 and 2, the part B is connected to these two membranes. A displacement x at the input causes a rotation of part B around point P1. This will cause a displacement of the end of part A, thus creating a small rotation α at the other end where part A is connected with another membrane to the foundation and rotates around point P2.

Another transmission mechanism has been used in the design of a small coining press. Such presses are in many cases using a knuckle-joint mechanism. These mechanisms have a very small stroke with large loading forces at the end of the stroke. This loading force is transmitted through the three bearings in the mechanism. The driving force is applied at the middle joint and a large transmission ratio is obtained at the end of the stroke.

The three heavily loaded joints may be replaced by one plate-spring, thus avoiding all wear and play in the mechanism. The construction shown schematically in figure 7.4d. will be able to generate compressive loads of the order of magnitude of the buckling load

$$F_{c1} \simeq \frac{4 \cdot \pi^2 \cdot E \cdot I}{\ell^2}$$

Larger magnitudes of the load may be obtained when high order buckling shapes are prescribed. More than one plate-spring may be used to increase the loading forces derived from a limited volume of the construction. A single steel plate-spring with length of 400 mm., width 100 mm. and thickness of 1,5 mm. will yield a force of about 700 N. The guiding of the slide of the press might for such cases (a small stroke) be a plate-spring parallel guiding. For a good positioning of the two parts of the tool the plane of one of these plate-springs should in such cases be coinciding with the plane where the two tools meet and accuracy is most important.

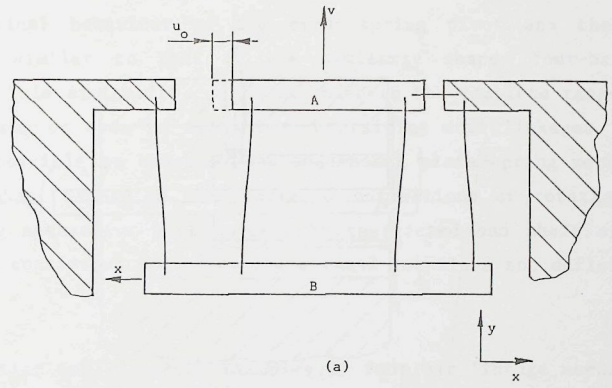

(a)

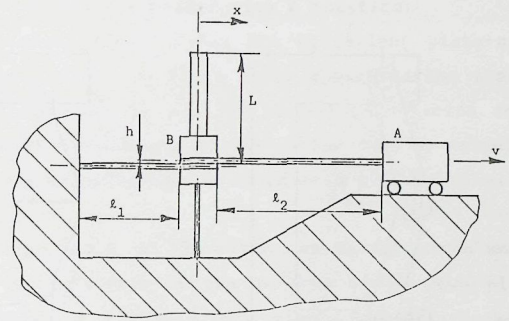

(b)

Figure 7.4 Plate-spring transmission mechanisms.

a. When the displacement, u_o, of the slide of a doubly parallel guiding mechanism is fixed in the direction of the x-axis a displacement, x, of the intermediate slide will lead to a deflection, v, of the slide in the y-axis direction. The magnitude of the linear transmission ratio may be adjusted by varying the deflection u_o.

b. For small displacements the distance between neutral lines in bended plate-springs (1) and (2) may be used as part of a lever mechanism with a large transmission ratio.

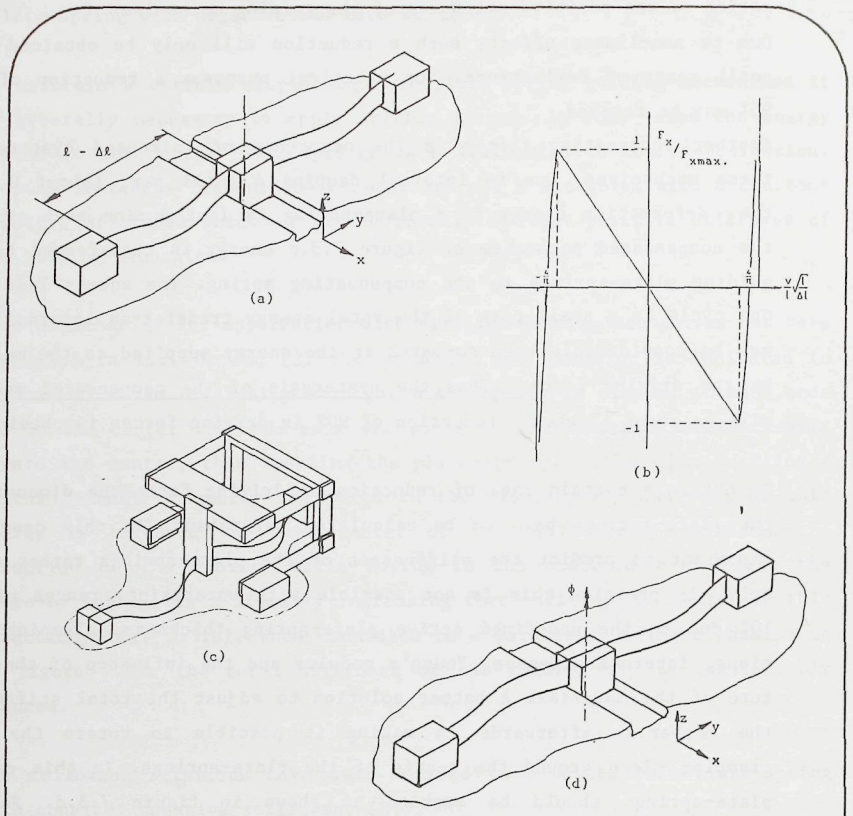

Figure 7.3 Plate-springs with constant negative stiffness.

a. The elastic energy stored in the buckled plate-spring is released when the central part moves in the direction of the x-axis. To maintain a certain positive displacement a negative force F_x should be applied to the central part.

b. In the region between the two maximum displacement a constant linear relation between a displacement in x-direction and the force F_x exists.

c. Combination of a plate-spring parallel guiding with its positive stiffness with a plate-spring with constant negative stiffness may result in a total stiffness which is small compared to the stiffness of the guiding.

d. Adjustment of the "negative spring constant" may be achieved by a rotation of the central part around the z-axis.

The special properties of the buckled plate-springs may also be used to obtain mechanisms with a very low resonance frequency. From figure 5.19 it may be seen that a plate-spring will have a very low stiffness in direction of the y-axis when it is buckled. At this point the plate-spring may carry a considerable load and the combination of low stiffness and high load allows to design mechanisms with low resonance frequency. Similarly very low stiffness in x-direction will result when a parallel guiding is loaded to the first-order buckling load.

Using these two principles a table with low resonance frequencies in all its six degrees of freedom has been constructed (figure 7.3.e). The top plate is supported by three plate-springs which are all buckled in the y-direction (second order buckling mode). Proper positioning of the center of gravity of the masses allowed the top plate to move with low stiffness in y-axis direction and in rotations around any axis in its plane. The three plate-springs are connected to a subframe which is connected to the foundation by three steel wires which are all loaded to their first-order buckling load and thus allow the subframe with the top plate to move in x and z-directions and to rotate around the y-axis.

It is possible to reach resonance frequencies below 1 Hz in all directions. It should however be noted that due to vibrations of the springs (wave propagation) a transmission of vibrations from foundation to the top plate in the range above 20 Hz may be expected.

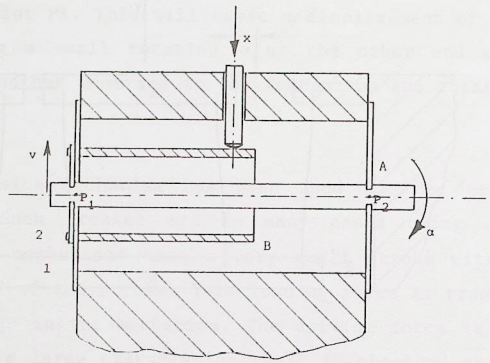

(c)

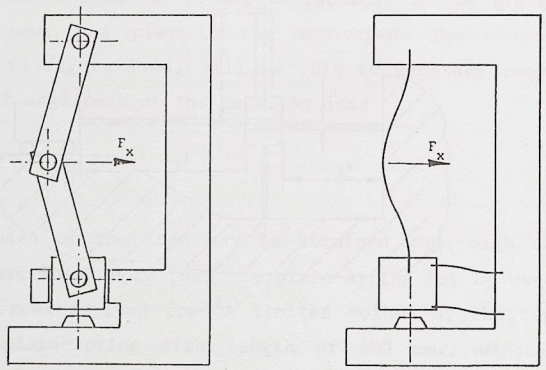

(d)

Figure 7.4. Continued,

c. The distance between the neutral planes of the rings, (1) and (2), is used to generate a lever mechanism with a large transmission ratio.

d. In the knuckle-joint mechanism as used in coining presses the three joints are heavily loaded. The same mechanism to obtain a high force and a small displacement can be made with a plate-spring to replace the three joints.

7.2.4 General four-bar linkage mechanisms using plate-springs.

The kinematical behaviour of the cross-spring pivot and the parallel guiding is similar to that of the similarly shaped four-bar linkage mechanisms. This similarity can be extended to the complete range of four-bar mechanisms or even to mechanisms containing more linkages. Therefore it may be possible to construct an equivalent plate-spring mechanism for any bar linkage mechanism. The range of deflections or rotations of the plate-spring mechanisms will however be restricted and their application may only be considered for cases where small rotations and deflections are required.

Two interesting and classical examples of four bar linkage mechanisms are the Watts' and Roberts' mechanisms. Both mechanisms cause a linear motion of one point of the slide together with a rotation.
For Watt's mechanism (figure 7.5a) the equivalent plate-spring mechanism is shown in figure 7.5c. In first order approximation the calculation of stresses and stiffnesses is similar to the calculation for the parallel guiding. The small rotation ϕ of the slide can be calculated using the expressions for the displacement $v(\ell)$ of each plate-spring.

In theory any other point on the slide may be forced to move along a line in x-direction by variation of the lengths of the two plate-springs. In the mechanism shown in figure 7.5d a simple relation between the lengths ℓ_1, ℓ_2 and distances a and b may be derived. Substitution of $b = -\frac{1}{2}a$ leads to $\ell_2 = -\ell_1$ and thus Watt's mechanism is a special case of this mechanism.

These two mechanisms are examples of plate-spring mechanisms with the kinematical properties of special four-bar linkages. Whenever four-bar mechanisms are designed for only limited strokes it may be advantageous to consider the application of plate-springs. In such cases the special advantages of plate-spring mechanisms may prove to be valuable.

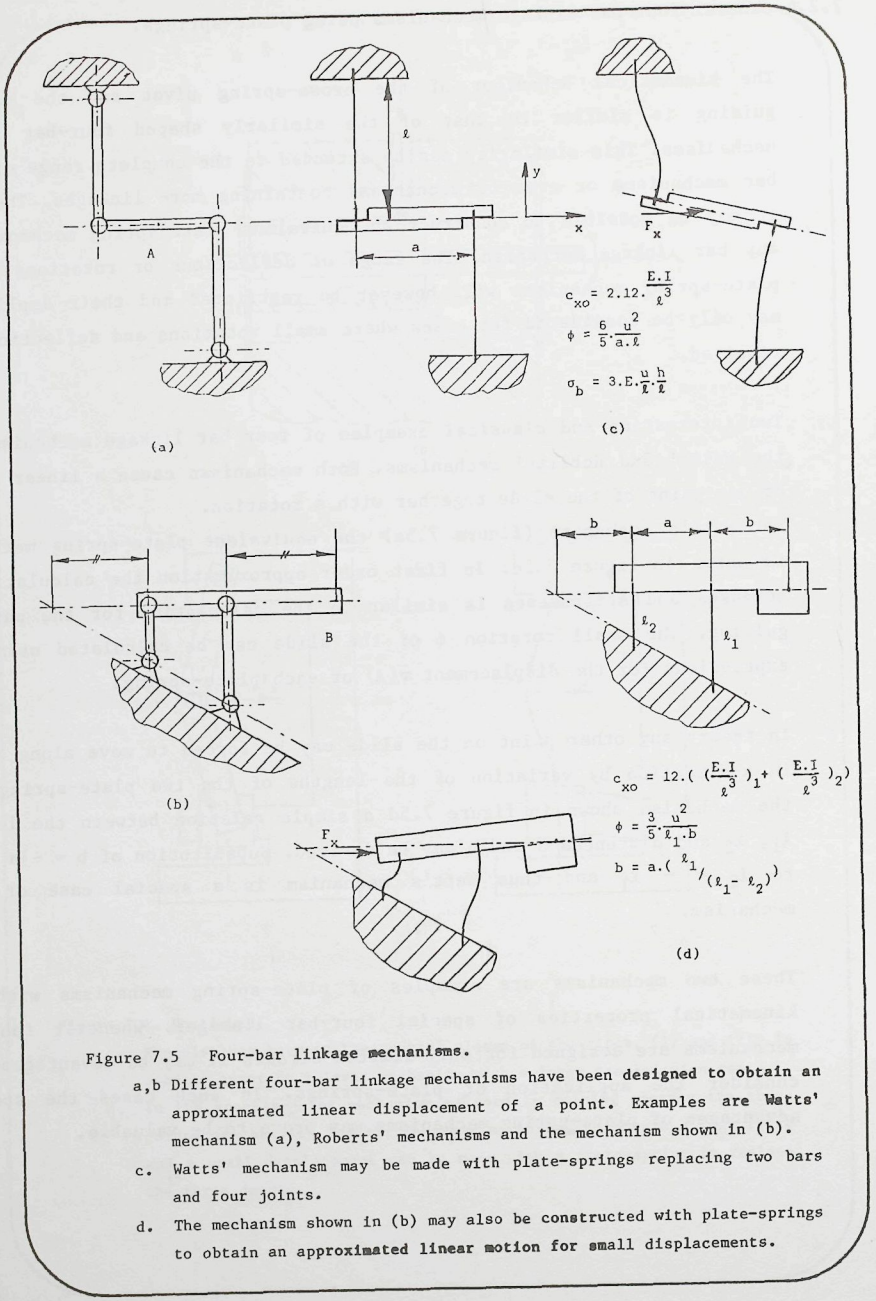

Figure 7.5 Four-bar linkage mechanisms.

a,b Different four-bar linkage mechanisms have been designed to obtain an approximated linear displacement of a point. Examples are Watts' mechanism (a), Roberts' mechanisms and the mechanism shown in (b).

c. Watts' mechanism may be made with plate-springs replacing two bars and four joints.

d. The mechanism shown in (b) may also be constructed with plate-springs to obtain an approximated linear motion for small displacements.

7.2.5 Mechanisms with five degrees of freedom ; coupling elements.

Plate-spring mechanisms discussed so far all have only one degree of freedom. Two plate-springs are used acting parallel to connect a body with the environment. Another class of mechanisms which may be of interest is formed by mechanisms with two plate-springs acting in series. In this case only one degree of freedom is fixed while the remaining five are free (i.e. having a relatively low stiffness).

An example of such a mechanism is the elastic shaft coupling shown in figure 7.6a and b. Here two plate-springs with their y-z-planes parallel are connecting part A through B with part C. Each plate-spring is determining the rotation of part B around the x-axis to either part A or part C. Thus the two plate-springs and part B are forming a shaft coupling between part A and C.All remaining degrees of freedom from part A to C are not fixed and thus this mechanism is an interesting elastic shaft coupling element that will allow for limited angular and lateral misalignments of the two shafts.

This mechanism is very similar to a plate-spring parallel guiding where the foundation is divided into the two separate parts A and C. The one degree of freedom that is determined twice in the parallel guiding is the rotation of part A with respect to part C around the x-axis. In this mechanism part B is free to move in the direction of the x-axis relative to parts A and C. This means that one internal degree of freedom remains undetermined in this mechanism.
(Note: The torque is transmitted by a pure torsional moment in part B. No extra loading forces are introduced to the bearings of the two shafts.)

Along similar lines other mechanisms with two plate-springs in series may be designed. When the z-axis of the two plate-springs are parallel such mechanisms will be resembling the cross-spring pivots discussed in chapter 6. In cross-spring pivots the translation of the rotor along its axis of rotation is determined twice. In the mechanism shown in figure 7.6c it is this translation of part A relative to part C that is fixed. In all other directions the relative motion of part A with respect to part C is, in first order approximation, free.

Such mechanisms are useful elements to couple two translating bodies. To

drive a slide guided by an accurate mechanism, for instance in optical instruments, it is desired to avoid the introduction of unknown loading forces through the driving element. The mechanism shown in figure 7.6c will allow to connect the driving element with a high stiffness in the direction of motion and low stiffnesses in all other directions The same function is obtained with a long rod with a small diameter as is also used in the measuring system described in figure 8.4.
(Note: It is advisable not to restrict the use of this sort of mechanisms only to instrument design.)

An extremely simple form of the mechanism is obtained when a plate-spring is folded over an angle of 90^{o} with as small a radius as possible (see figure 7.6d).Through combination of different coupling elements, from both types, it is possible to selectively control the different degrees of freedom of a body. Van der Hoek (H3) has described some examples of such combined constructions.

The most interesting properties of these coupling elements will be their stiffnesses in the different directions. In figure 7.7 and 7.8. expressions for these stiffnesses are given.
These elements may be compared with equivalent elastic elements performing the same function. The shaft-coupling (figure b) may be compared with the coupling using two membranes instead of the plate-springs. Such a membrane coupling will have a higher coupling stiffness relative to the stiffnesses in the other directions. However the allowable misalignment of such membrane couplings is much (about 10 times) smaller than in the case of the coupling in figure b.

The construction of figure d. may be compared to a single rod or wire. In this case the single rod will allow for smaller and simpler constructions. A disadvantage of the single rod is the kinematical displacement of the end of the rod due to rotations and deflections (similar to the kinematic deflection $v(\ell)$ of parallel guidings). The construction of figure d. does not have this disadvantage. In addition the freedom of dimensioning the plate-springs will allow to obtain larger stiffnesses c_z and larger loading capacities.

The different properties of these mechanisms have not yet been investigated in detail. Many engineering problems might however be solved when

more experience in their application is obtained. In future it may be expected that more useful mechanisms can be invented using the large ratio between in-plane and out-of-plane stiffnesses of plate-springs.

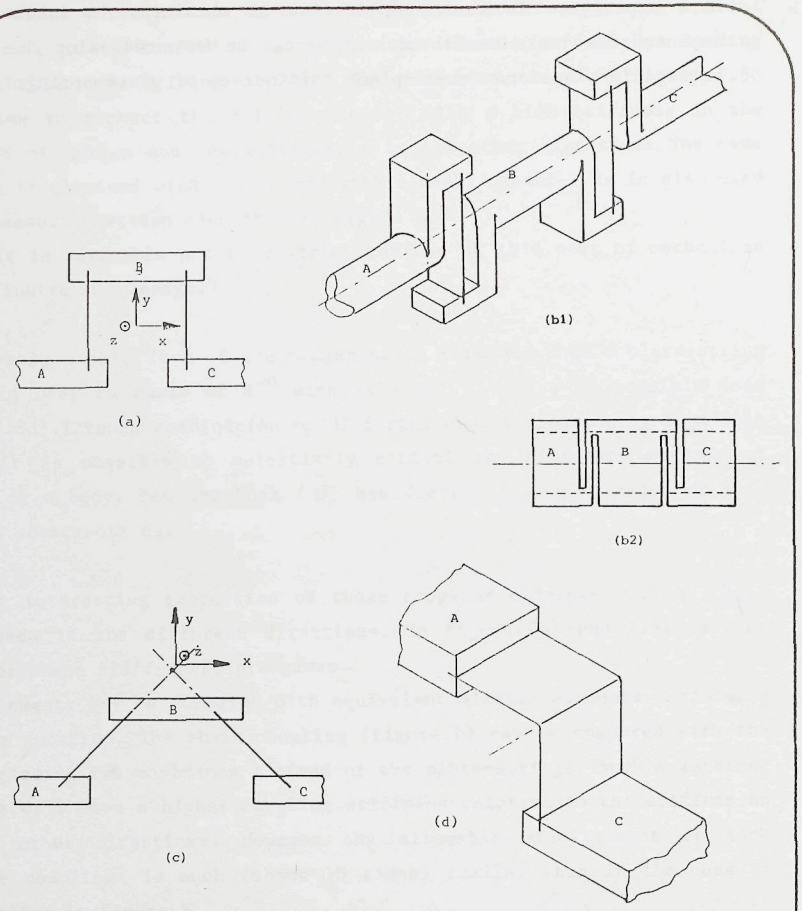

Figure 7.6 Mechanisms with five degrees of freedom.

a. The well known parallel guiding is easily transformed into a mechanisms fixing only one degree of freedom from part C relative to part A.

b. Schematic representation (b1) of an elastic shaft coupling. Against rotation around the axis a high stiffness is obtained while in all other directions relative motions are allowed for. Such a coupling may be made by the cutting of slots in a tube as indicated in (b2).

c. Based upon the geometry of cross-spring pivots a coupling element determining only one degree of freedom may be obtained.

d. The function of the cross-spring pivot shown in (c) may be performed by a single plate-spring bended over as sharp a radius as possible.

In the undeformed position the stiffnesses of part C relative to part A with respect to the pure displacements and rotations indicated are,

$$c_x \simeq \frac{E \cdot A}{\ell} \cdot \frac{1}{2} \cdot \left(\frac{h}{\ell}\right)^2$$

$$c_z \simeq \frac{E \cdot A}{\ell} \cdot \frac{1}{3 \cdot (1+\nu)} \cdot \left(\frac{h}{\ell}\right)^2$$

$$c_y \simeq \frac{E \cdot A}{\ell} \cdot \frac{1}{6} \cdot \left(\frac{h}{\ell}\right)^2$$

$$c_\theta \simeq \frac{E \cdot A}{\ell} \cdot \frac{1}{12 \cdot (1+\nu)} \cdot h^2$$

$$c_\phi \simeq \frac{E \cdot A}{\ell} \cdot \frac{1}{24} \cdot h^2$$

$$c_\psi \simeq \frac{E \cdot A}{\ell} \cdot \frac{1}{24} \cdot b^2$$

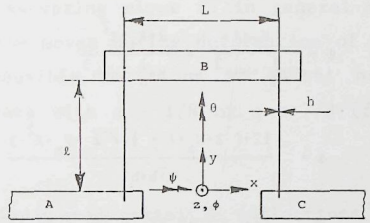

The first five stiffnesses are small of the order h^2 while the last, coupling stiffness, is large. This stiffness will in practical cases be so large that the stiffnesses of flanges and connecting parts become more important in determining the total stiffness. When the two parts A and C are not exactly aligned the plate-springs are deformed and the stiffness c_ϕ will decrease. From the earlier analysis (chapter 5 and 6) it may be concluded that the decrease will be limited (to about a factor two) when plate-spring deflections are less than 5(10) times the plate-spring thickness and angular deformations are smaller than 5(10) times the ratio of h/ℓ.

The magnitude of the driving torque leading to instability, buckling of plate-springs, may in first-order be estimated as,

$$M_{x_{crit}} \simeq \frac{2 \cdot \pi \cdot E \cdot I}{\ell} \cdot \lambda_3$$

where λ_3 is a function of the length to width ratio of the plate-spring as was discussed in chapter 5. For relatively long plate-springs $\lambda_3 \simeq 1$.

Figure 7.7. Main characteristics of elastic shaft coupling.

The different loading components will be applied to part C with respect to point P. The relations between the loading components and the deflections are,

$$\theta = \frac{M_y \cdot \ell}{G \cdot \frac{1}{3} \cdot b \cdot h^3}$$

$$\psi = \frac{M_x \cdot \ell}{G \cdot \frac{1}{3} \cdot b \cdot h^3} + \frac{2 \cdot F_z \cdot \ell^2}{E \cdot \frac{1}{6} \cdot h \cdot b^3}$$

$$\phi = \frac{12 \cdot (2 \cdot M_z \cdot \ell - \frac{1}{2} \cdot \sqrt{2} \cdot F_x \cdot \ell^2)}{E \cdot b \cdot h^3}$$

$$x = \frac{12 \cdot (\frac{5}{24} \cdot F_x \cdot \ell^3 - \frac{1}{2} \cdot \sqrt{2} \cdot M_z \cdot \ell^2)}{E \cdot b \cdot h^3}$$

$$y = \frac{F_y \cdot \ell^3}{3 \cdot E \cdot \frac{1}{12} \cdot b \cdot h^3}$$

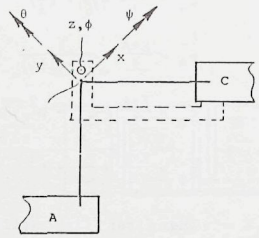

$$z = \frac{F_z \cdot \ell}{E \cdot b \cdot h} \{ 4 \cdot (1+\nu) + \frac{8 \cdot \ell^2}{b^2} \}$$

The ratio between the stiffness c_z and the stiffness c_x and c_y is of the order b^2/h^2 which will in practical cases be more than 1000.

The value of the critical value for F_z at which plate-spring instability may occur is estimated (no rigorous derivation being available) at:

$$F_{z\ crit} \simeq \frac{10 \cdot E \cdot \frac{1}{12} \cdot b \cdot h^3}{\ell^2}$$

Upon deformation of the plate-spring the stiffness c_z will be reduced. When displacements x and y remain small (less than 5(10) times the plate spring thickness) and rotations are limited (less than 5(10) times h/ℓ) the reduction is estimated to be not more than about 60%.

Figure 7.8 Alternative elastic wire support.

7.2.6 Two or more parallel guidings or cross-spring mechanisms placed in series.

The parallel guiding and cross-spring pivot discussed in chapters 5 and 6 have a number of advantages which make them attractive for machine and instrument design. One of the most important drawbacks for both mechanisms is the kinematic motion described by rotor or slide. The movement of the parallel guiding is not along a line but along the top of a parabola. The movement of the rotor of a cross-spring pivot is in general not a pure rotation but the axis of rotation moves during deformation of the plate-springs. In some cases the possible solutions of Watts' or Roberts' mechanisms and cross-spring pivots with a ≅ 1/8 or a ≅ 7/8 (figure 6.6) will be a solution.

A more general way to avoid the unwanted parasitic deflections is the use of two mechanisms in series (figure 7.9a and b).
The construction for the parallel guiding is rather common and easily understood (figure a). When the slide C is moved, quasi-statically, the part B will travel over half the deflection of C and the vertical movement of C becomes equal to zero. (More information about possible inaccuracies are given in lit. (H3).)
The same principle may be used for the cross-spring pivot (fig. b). Part B rotates over half the angle of rotation of the rotor C. As a result the axis of rotation of part C relative to the foundation A will be stationary and pass through the initial axis of rotation.

This method of placing two mechanisms in series appears to be rather attractive. However the proper operation is only assured when the proper ratio of motion of the parts C and B is obtained. In the basic design this may be statically assured by the fact that the stiffnesses of both mechanisms are equal. The accuracy of this method may be sufficient, but for general purposes the relative motion should also be assured during dynamic operation and thus the superfluous internal degree of freedom should be eliminated. This will be even more important when the mechanisms are loaded in other directions and the main stiffnesses of the two parallel mechanisms are affected differently. A possible way to eliminate the internal degree of freedom and to assure the proper ratio of movement is shown in figure c. Similar solutions might be found for constructions with two cross-spring pivots in series.

7.3 "Reinforced" plate-springs in parallel guiding mechanisms.

7.3.0 When analyzing the shape of a deformed plate-spring in a parallel guiding it becomes evident that the middle part of the plate-spring remains almost undeformed. The operation of the mechanism will thus change only very slightly when this middle part of the plate-spring is made much thicker to obtain higher stiffnesses locally. Such a mechanism, shown in figure 7.10, will behave similar to a usual parallel guiding but a relative improvement in different properties might be achieved. In this paragraph a number of these properties will be determined. With the results obtained it may be possible to indicate over what length the plate-spring should be made stiffer and whether the achieved improvements will be sufficient to justify the increased constructive complexity.

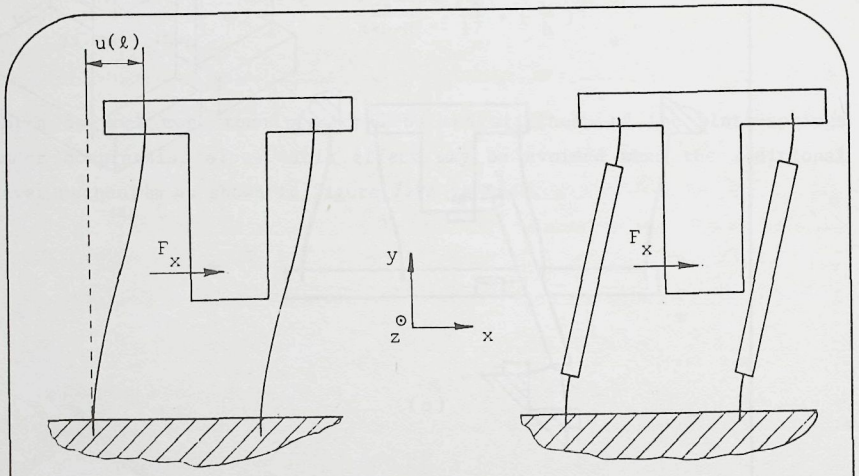

Figure 7.10
When the middle part of the plate-springs of a normal plate-spring parallel guiding (a) is reinforced to give them higher stiffnesses a parallel guiding mechanism as shown in (b) will result.

To discuss the properties of such plate-spring elements the element with a total length L is divided into two parts with a low stiffness and length ℓ and the remaining part with length $2 \cdot q \cdot \ell$. Thus the following relation between total length L and the dimension ℓ results

$$L = 2 \cdot (1 + q) \cdot \ell \qquad (7.3.1)$$

For the plain plate-spring q=0 and for the mechanism shown in figure 7.10b q is about 3.
In Annex 7.I a description of the calculation of different properties of reinforced plate-spring elements is given. The results of this analysis will be discussed here.

7.3.1 The stiffness c_x of one plate-spring element is determined as

$$c_x = \frac{12 \cdot E \cdot I}{L^3 \cdot (1 - (\frac{q}{1+q})^3)} \qquad (7.3.2)$$

7.3.2 The maximum bending stress in the plate-spring σ_b is

$$\sigma_b \simeq 3 \cdot E \cdot \frac{u(L)}{L} \cdot \frac{h}{L} \cdot (\frac{1}{(1 - (\frac{q}{1+q})^3)}) \qquad (7.3.3)$$

To compare the properties of parallel guiding mechanisms with and without reinforced part it is useful to distinguish two cases. In the first case mechanisms with equal stiffnesses c_x are compared. In this case the

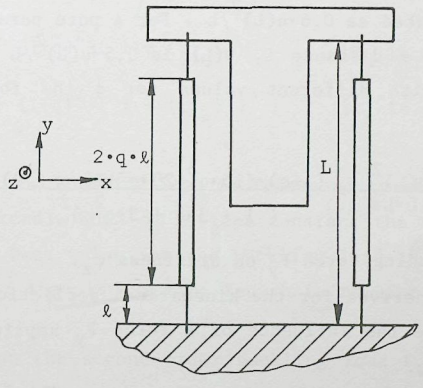

Figure 7.11
Definition of parameters used in calculation of the properties of parallel guiding mechanisms with reinforced plate-spring elements.

thickness h of the elastic part in the reinforced elements can be determined from the thickness h_o of the basic plate-spring from

$$c_x \text{ is constant} \rightarrow h = \sqrt[3]{\left(1 - \frac{q}{1+q}\right)} \cdot h_o \qquad (7.3.4)$$

In the other case the maximum value of the bending stress in the plate-spring element will be maintained. This will yield

$$\sigma_b \text{ is constant} \rightarrow h = \left(1 - \frac{q}{1+q}\right) \cdot h_o \qquad (7.3.5)$$

From these expressions it is clear that the plate-spring thickness must be reduced in both cases when a large part of the length has been reinforced. When 90% of the length of the plate-spring has been reinforced the thickness has to be chosen at about 65% of the original thickness to maintain the stiffness c_x at the same value. In order to allow the same value of the maximum bending stresses the thickness must be reduced to only 27% of the original value.

The large reduction of the thickness in this last case will cause a deterioration of some of the properties of the plate-spring guiding. When it is attemped to maintain the stiffness c_x most of the important properties of the parallel guiding will be improved.

7.3.3 Kinematical deflection, v(L).

The partial reinforcing of the plate-spring will influence the magnitude of the kinematical deflection. For a four-bar linkage parallel guiding v(L) was calculated as $0{,}6 \cdot u(L)^2/L$. For a pure parallel guiding mechanism with pivots at a distance L, v(L) is $0{,}5 \cdot u(L)^2/L$. For mechanisms with plate-springs with different values for q the following expression is obtained

$$v(L) = \frac{3 \cdot u(L)^2}{10 \cdot L} \cdot \frac{(1+q) \cdot (15 \cdot q^3 + 20 \cdot q^2 + 10 \cdot q + 2)}{(1 + 3 \cdot q + 3 \cdot q^2)^2} \qquad (7.3.6)$$

7.3.4 Influence of loading force F_y on stiffness c_x.

The expression derived for the kinematical deflection v(L) may be directly used to estimate the influence of a force F_y applied to the slide of the parallel guiding.

Using considerations of the conservation of energy the expression for the driving stiffness c_x is estimated as,

$$c_x = c_{xo} \cdot \left(1 + \frac{2 \cdot F_y \cdot v(L)}{u(L)^2 \cdot c_{xo}}\right) \qquad (7.3.7)$$

where c_{xo} is the stiffness of the guiding mechanism when $F_y = 0$ determined by expression (7.32).

As the relative magnitude of the kinematical deflection v(L) does not depend strongly upon the parameter q no noticeable change of the influence of F_y upon c_x will be found. Only when the nominal magnitude of c_{xo} decreases the influence of forces F_y will increase.

7.3.5 Buckling loads of the guiding element.

To obtain an impression of the changes of the buckling loads for the parallel guiding with reinforced plate-springs the two loading cases shown in figure 7.12 will be analysed.

The buckling load F_y for the loading case of figure 7.12a will be a force comparable with the second order buckling load given in chapter 5. For this buckling load may be derived

$$F_y = -\frac{\pi^2 \cdot E \cdot I}{\ell^2} = -\frac{4 \cdot \pi^2 \cdot (1+q)^2 \cdot E \cdot I}{L^2} \qquad (7.3.8)$$

As the thickness h will be a function of the rate of reinforcing the plate-spring (q) either expression (7.3.4) or (7.3.5) should be substituted to make a comparison. Thus the buckling load may be compared with the magnitude for a plate-spring with q = 0 by

$$F_y = F_{yo} \cdot \left[(1+q)^2 \cdot \left(1 - \left(\frac{1}{1+q}\right)^3\right)\right] \qquad (c_x \text{ is constant})$$

$$F_y = F_{yo} \cdot \left[(1+q)^2 \cdot \left(1 - \left(\frac{q}{1+q}\right)^3\right)^3\right] \qquad (\sigma_b \text{ is constant}) \qquad (7.3.9)$$

For c_x constant the buckling load is increased by about a factor 27 when q = 9 (90% reinforced). When σ_b is kept constant the increase is only about a factor 2. The best value for the buckling load is in this case obtained when about 70% of the plate-spring length is reinforced ($q \cong 2{,}5$).

A calculation for the second order buckling load F_z for the loading case shown in figure 7.12b can be made using the energy method as used also in chapter 5. To obtain an impression of the relation between the buckling load and the parameter q this calculation has been made while neglecting

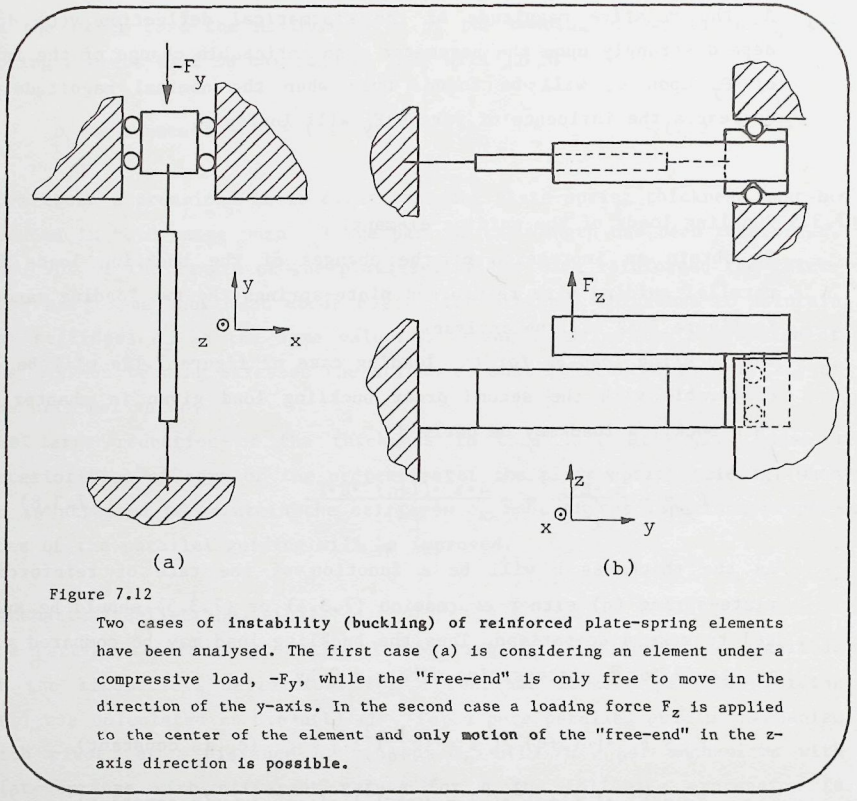

Figure 7.12

Two cases of instability (buckling) of reinforced plate-spring elements have been analysed. The first case (a) is considering an element under a compressive load, $-F_y$, while the "free-end" is only free to move in the direction of the y-axis. In the second case a loading force F_z is applied to the center of the element and only motion of the "free-end" in the z-axis direction is possible.

the effect of the constrained warping (influence of the clamping conditions upon the torsional deformation). It should be noted that the effect of the constrained warping will lead to an increase of the critical loads when the elastic part is becoming short relative to its width.
This leads to the following expression,

$$F_z^2 \simeq \frac{E \cdot I \cdot G \cdot J}{\ell^4} \cdot \left[\frac{A_1^2 + A_1 \cdot A_2 + \frac{1}{3} \cdot A_2^2}{\frac{1}{3} \cdot A_3^2 + \frac{1}{5} \cdot A_4^4 + \frac{1}{7} \cdot A_5^2 + \frac{1}{2} \cdot A_3 \cdot A_4 + \frac{1}{3} \cdot A_4 \cdot A_5 + \frac{2}{5} \cdot A_3 \cdot A_5} \right] \qquad (7.3.10)$$

where $A_1 = -2 - 6.q$

$A_2 = 6 + 12.q$

$A_3 = 2 + 8.q + 6.q^2$

$A_4 = -4 - 12.q - 6.q^2$

$A_5 = 2 + 4.q$

In the calculation of this expression a deformed shape of the plate-spring is estimated and the elastic energy in the material is then compared with the energy supplied by F_z. As the estimate for the shape is made under the assumption that a reinforced middle part is present it may not be expected that a good value is obtained for $q = 0$.

The result of this calculation is presented in figure 7.13.
In this graph is shown the factor A_0 which may be used to calculate the buckling load. Also shown are the curves that indicate how the buckling load is varied if the magnitude of q increases while either the stiffness c_x or the maximum bending stress σ_b are kept at constant values by adaptation of the thickness h. It may be concluded that no noticeable effect is obtained in the case where c_x is kept constant. In this case only the influence of the constrained warping will lead to an increase of the buckling load as the length to width ratio of the flexible part decreases.

When it is attemped to maintain the magnitude of the maximum bending stress it is seen that a drastic decrease of the buckling load is caused. In cases where the buckling load F_z may be of critical importance and σ_b should not increase it is therefore advisable not to use reinforced plate-spring elements.

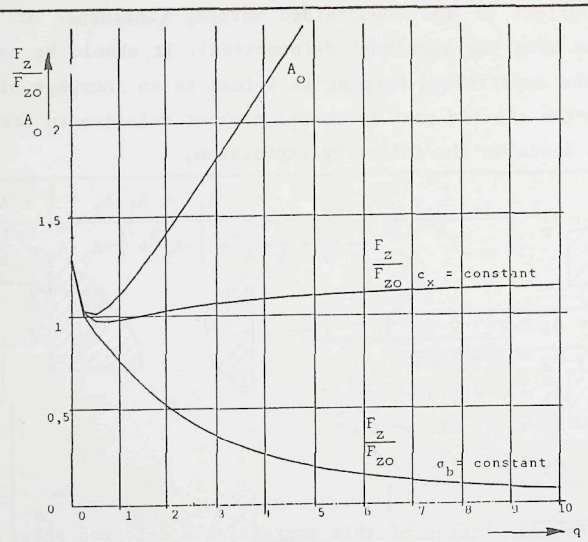

Figure 7.13

The buckling load, F_z, for the loading case of figure 7.12b, may be calculated using the expression

$$F_z \simeq A_0 \cdot 32 \cdot \sqrt{\frac{E.I_z.G.J}{L^4}}$$

where A_0 is a function of the parameter q and may be taken from this figure.

Also presented are lines indicating the magnitude of F_z as a function of q relative to the buckling load, F_{zo}, for q=0 while the plate-spring thicknesses are adjusted to maintain either c_x or σ_b constant.

In this analysis the influence of the constrained warping of the cross-section has not been taken into account. This effect will lead to higher values of the force F_z when q increases.

7.3.6 Dynamic behaviour of plate-spring elements.

In chapter 5 some remarks were made with respect to the natural frequencies of the plate-spring elements. When the plate-spring element is partially reinforced three natural modes of vibration with relative low frequencies may be expected for the relatively heavy middle part.

These modes will be a translation in the x-direction, a rotation about the y-axis and a rotation around a z-axis through the middle of the reinforced part.

When the mass of the reinforced part is equal to m the natural frequency for the first mode may be estimated as

$$\omega_x \simeq \sqrt{\frac{24 \cdot E \cdot I}{m \cdot \ell^3}} \qquad (^{rad}/_{sec}) \qquad (7.3.11)$$

The value of the natural frequencies will depend strongly upon the design of the reinforced part of the plate-spring.

When the mass of the reinforced part is of the same order of magnitude as the part of the original plate-spring it replaces, an increase of the lowest natural frequency will be obtained. This increase will be small when the maximum value of the bending stress is kept constant, the parameter q being varied. But when the stiffness c_x is maintained a noticeable increase, of factors from 5 to 10, in the magnitude of the natural frequency may be obtained.

7.3.7 Guiding stiffness, c_y.

As for the normal plate-springs the stiffness of a reinforced plate-spring element can be considered as a series of two stiffnesses, the compressive stiffness according to Hooke's law and the contribution of the varying bending shape.

The compressive stiffness is independent of the deflection, u(L), of the end of the plate-spring element. The contribution of the elastic part of the reinforced element can be calculated using the expressions for the plate-spring thickness (7.3.4) and (7.3.5). From these expressions it follows that an increase in the compressive stiffness of the elastic parts with a factor of about 6 and 2,7 respectively for c_x and σ_b constant may be obtained for $q \cong 9$ (90% reinforced).

The contribution of the reinforced part depends upon the design of this part. In this respect it is advisable to design a symmetrical construction of the reinforced part. In the a-symmetric construction as is shown in

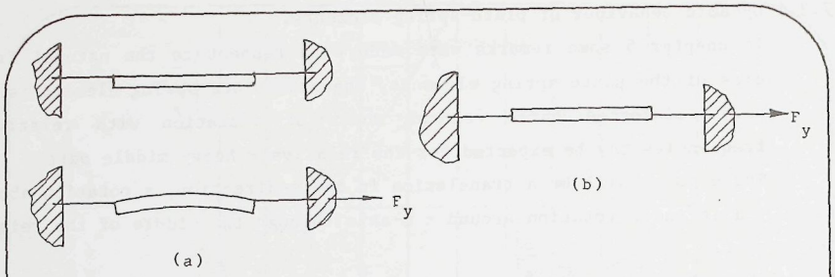

Figure 7.14

When the reinforced part of the plate-spring element is not designed symmetrically (as in (a)) a loading force F_y applied through the flexible part will cause bending deformation in the reinforced part. This will reduce the stiffness of this part in the direction of the y-axis.

figure 7.14a the compressive stiffness of the reinforced part is four times less than for the construction shown in figure 7.14b.

For the calculation of the influence of variation of the deformed bending shape on the stiffness c_y again the contribution of both the elastic and the reinforced part should be considered. In order to keep the influence of the reinforced part small it should have a high bending stiffness around the z-axis. When making the reinforced part out of a massive part with the same width and material as the elastic part the thickness, h_r, should be about (1+q) times the thickness in the elastic parts. In that case the contribution of the change in the shape of the elastic part will be dominant.

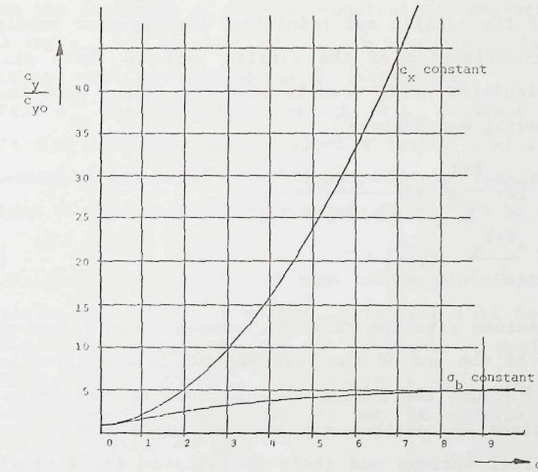

Figure 7.15

The relative increase of the part of the stiffness c_y which is due to the variation of the deformed bending shape of plate-spring elements with increasing rate of reinforcement (q) for the two different cases, c_x is constant or σ_b is constant.

For the contribution of the bending deformation of the elastic parts upon the stiffness the following first order estimate is derived in Annex 7.I

$$c_{yb} \simeq 700 \cdot \frac{E \cdot I}{L^3} \cdot \left(\frac{L}{u(L)}\right)^2 \cdot \frac{(1+q)\cdot(1 + 3\cdot q + 3\cdot q^2)^3}{1 + 10\cdot q + 45\cdot q^2 + 105\cdot q^3 + 105\cdot q^4} \qquad (7.3.12)$$

For the two cases of interest, c_x or σ_b constant, this result may be compared with the result for the normal plate-spring (q = 0). The result of this comparison is shown in figure 7.15. When σ_b is constant the increase in stiffness c_{yb} is limited to about a factor 5. When c_x is constant the increase may well be over a factor 50.

Especially when a plate-spring element is designed for a relatively large deflection u(L) the use of reinforced plate-springs will allow for an increase of the total stiffness of the guiding in the direction of the y-axis.

3.7.8 Guiding stiffnesses c_z and c_ψ.

In the undeformed position the stiffness c_z and c_ψ are determined by the stiffness of the elastic and reinforced part against bending around the x-axis. The contribution of the elastic part to these stiffnesses may be directly calculated using results from the linear beam theory. This leads to the following expressions

$$c_{zo} \simeq 12 \cdot \frac{E \cdot I_x}{L^3} \cdot \frac{(1+q)^3}{1 + 3 \cdot q + 3 \cdot q^2}$$

$$c_{\psi o} \simeq \frac{E \cdot I_x}{L} \cdot (1+q) \qquad (7.3.13)$$

These expressions give the relation between force F_z and torque M_x and the deflections of the end of the plate-spring in the direction of the z-axis and rotation around the x-axis when the load is applied as shown in figure 7.16. The given expressions may be used to determine the stiffnesses of the two helical springs and their distance in the equivalent model shown in figure 5.18. In that case the two springs have a stiffness

$$c_{zo}^{*} \simeq 6 \cdot \frac{E \cdot I_x}{L^3} \cdot \frac{(1+q)^3}{1 + 3 \cdot q + 3 \cdot q^2} \qquad (7.3.14)$$

and their distance a_y is given by

$$a_y \simeq \frac{L}{1+q} \cdot \sqrt{q^2 + q + \frac{1}{3}} \qquad (7.3.15)$$

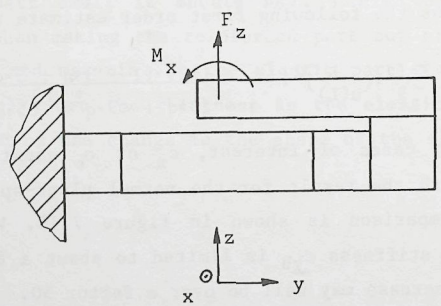

Figure 7.16

To determine the stiffnesses c_z and c_ψ of reinforced plate-spring elements the deformations due to a loading force F_z and a torque M_x have been analysed (Annex 7.I).

When the stiffnesses are compared to those for normal plate-springs it shows that the stiffness c_z remains almost unchanged when σ_b is kept constant. When the stiffness c_x is kept constant an increase of about a factor 2 to 3 for c_{zo} may be obtained for $q \cong 9$. For very large values of q a larger increase might even be obtained in this case.
The stiffness $c_{\psi o}$ will in both cases (σ_b or c_x constant) increase. For σ_b is constant a maximum increase of about a factor 3 will be obtained. For c_x is constant an increase with a factor 6 to 7 results for $q \cong 9$. For larger values of q an even larger increase in $c_{\psi o}$ may be obtained.

The contribution of the reinforced part of the plate-spring to the stiffnesses depends upon its construction. To obtain full benefit of possible improvements in the guiding stiffnesses it should be designed to have high stiffnesses in all directions. To obtain a relatively high stiffness against rotation around the x-axis it may be necessary to enlarge the width (b) of the reinforced part.

For the plate-spring element with a certain end deflection u(L) the deformations under influence of a force F_z and a torque M_x have been calculated in Annex 7.I. It should be noted that for these calculations it is assumed that the reinforced part is infinitely stiff which should be considered as the normal situation and in actual constructions should be assured by a carefull design of this part.

With the results of the calculations in Annex 7.I the magnitude c_{zt} of the two springs in the equivalent model in figure 5.18 for this case may be derived. This yields

$$c_{zt} \simeq \frac{G \cdot J}{L^3} \cdot \left(\frac{L}{u(L)}\right)^2 \cdot \frac{1}{Q_z} \qquad (7.3.16)$$

The magnitude of the factor Q_z may be estimated from the graph in figure 7.17 where results of calculations for different length to width ratios have been given. It must be realized that the calculations are taking into account the influence of the warping of the cross-section as discussed in chapter 4. Therefore the results are only estimates when the ratio of the length of the elastic part to its width is less than one. In the graph the curves are dotted in this region.

With the same remarks the influence of the parameter q upon the distance

a_{yt} between the two helical springs is shown in figure 7.18. The distance between the springs is growing with increasing q and thus the stiffness $c_{\phi t}$ is increasing relative to the stiffness c_{zt}.

To illustrate the possible increase of the stiffness c_{zt} for the reinforced plate-spring two graphs are presented in figure 7.19. Here the calculated stiffness c_{zt} is compared with the same stiffness for the normal plate-spring for the two cases, c_x = constant and σ_b = constant.
From 7.19a it is clear that some increase in c_{zt} may be obtained when c_x is constant. This increase is mainly due to the increasing influence of

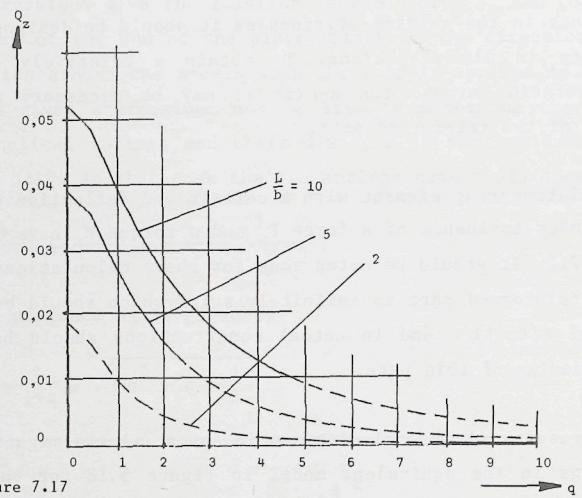

Figure 7.17

Application of a force F_z to a reinforced plate-spring element as shown in figure 7.16 will lead to torsional deformations of the elastic parts. These deformations will cause a deflection of the end of the plate-spring in the z-axis direction. The magnitude of this deflection may be calculated using the equivalent mechanism, figure 5.18, where the stiffnesses c_{zt} of the helical springs are calculated using expression (7.3.16). The magnitude of the parameter Q_z as a function of the parameter q, is shown here for different length to width ratio's (L/b) of the plate-spring element.

the "constrained warping" in the relatively short and wide elastic parts of the plate-spring elements. When σ_b is constant, 7.19b, it shows that the increasing influence of this effect does not compensate for the decreasing plate-spring thickness. In this case no noticeable increase in c_{zt} is found, for relatively large values of the length to width ratio a decrease in stiffness will even result.

One remark should be made about these calculations. When the total stiffness of a reinforced plate-spring element in the deflected position must be determined the contributions of the two equivalent models, with c_{zo} and c_{zt} respectively, should both be taken into account. This may be done by adding the deflections and rotations determined by each model. They may in fact be considered as two spring constructions acting in series as was also suggested in chapter 6. for the cross-spring pivots.

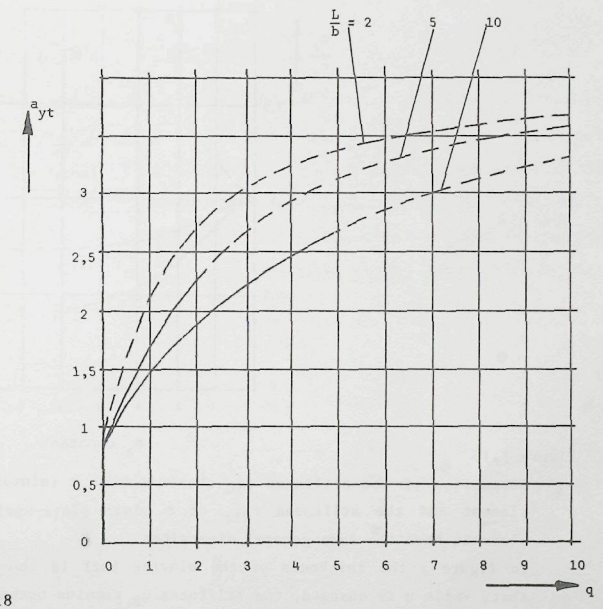

Figure 7.18

Application of a torque M_x as in figure 7.27 to a reinforced plate-spring element will lead to torsional deformations of the elastic parts. The magnitude of the resulting rotation, $\phi(L)$, of the end of the plate-spring may be estimated using the equivalent model (fig. 5.18) where the distance between the two helical springs is equal to $a_{yt}.L$. The magnitude of a_{yt} is shown as a function of the parameter q, and for different length to width ratios of the plate-spring elements.

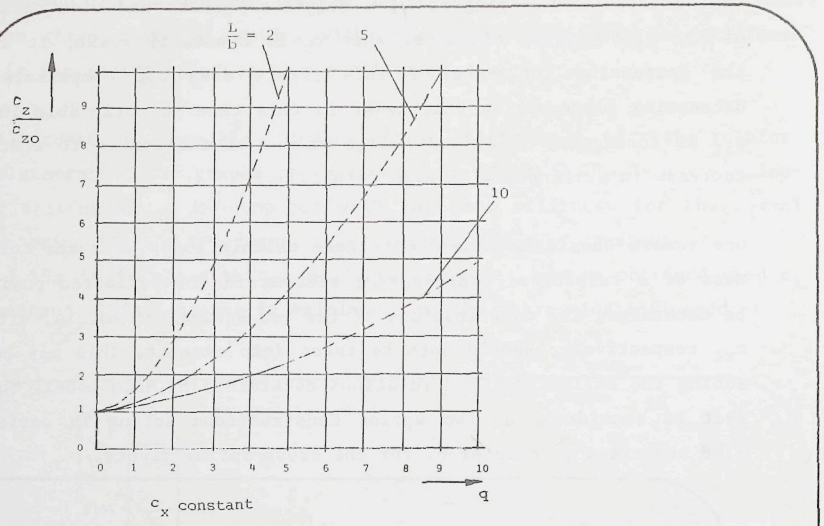

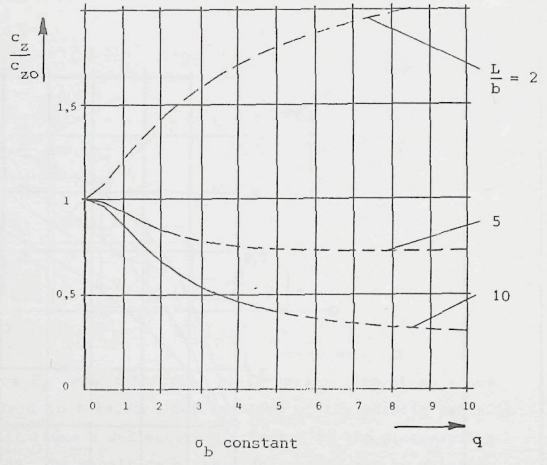

Figure 7.19

Comparison of the stiffness c_{zt} obtained with a reinforced plate-spring element and the stiffness c_{zto} of a plain plate-spring when the two elements have the same general dimensions.

In figure a the thickness of the elastic part is chosen in such a way that, while q is changed, the stiffness c_x remains unchanged.

In figure b the thickness is varied in such a way that the maximum value of the bending stress, σ_b, is constant.

The ratio between the stiffnesses is shown as a function of q for different length to width ratios.

7.3.9 Magnitude of loading stresses

In the discussion so far only the magnitude of the bending stress σ_b due to the deflection u(L) of the end of the plate-spring element has been considered. When loading forces are applied to the slide they will also cause other stresses in the elastic parts and as their cross-sectional area reduces with increasing values of q (larger part reinforced) the magnitudes of the stresses due to loading forces will increase. In many cases this will be taken into account by reducing the magnitude of the allowable bending stress σ_b. In that case higher stresses due to loading forces could be allowed.

This will however result in even smaller thicknesses of the elastic part than was predicted by expression (7.3.5). And therefore many of the properties discussed will have smaller values than suggested here.

7.3.10 Conclusion

In this paragraph a number of the properties of the reinforced plate-spring element have been discussed. Summarizing figure 7.20 gives an overview indicating whether a property is improved or not when a normal plate-spring is replaced by a reinforced plate-spring. From this figure it is clear that reinforced elements may be very useful when the bending stresses are not yet important in the normal plate-spring. In that case reinforcement will improve about all the relevant properties. Only the magnitude of other stress components due to loading forces will increase.

When the bending stresses in the normal plate-spring have reached their limit value the situation is more complex.
Now only part of the properties improve and the buckling load F_z is reduced. Also the other stress-components will become larger in this case. For this type of constructions it is therefore advisable to use plate-springs without reinforced parts. Only when the plate-spring element is used to determine only one degree of freedom (in y-direction) a slight improvement may be obtained with the reinforced element.

Another problem arises when in a certain design with plain plate-springs neither the stiffness c_x nor the stress σ_b have reached their limit values. In this case an improvement of the guiding may be obtained either by increasing the thickness of the plate-spring or by reinforcing the plate-spring. In both cases all properties are improved. Whether the largest improvement is obtained by reinforcing the plate-spring or by increasing the thickness is different for each property. In general properties in the direction of the y-axis improve most when the plate-spring is reinforced. The properties in the z-direction improve most when the thickness of the plain plate-spring element is increased.

Finally it may be concluded that partially reinforced plate-spring elements allow to improve the properties of plate-spring parallel guidings in many cases. Whether the achieved improvements are justifying a more complicated construction will depend strongly upon the particular application.
It should be reminded that in this analysis it has been assumed that the external geometry of the guiding mechanism (length and width) are fixed. Generally it will be a good method to improve properties of a plate-spring

Property	Case considered.	
	c_x is constant	σ_b is constant
Driving stiffness c_x	0	-
Bending stress σ_b	+	0
Kinematic deflection v(L)	0	0
Buckling load F_y	++	0,+
F_z (fig.7.12)	0	-,--
Lowest internal frequency	+	0
Guiding stiffnesses		
c_y ,undeflected	+	+
c_y , deflected	++	+
c_z ,undeflected	+	0
c_ψ ,undeflected	+	+
c_z , deflected	+,++	0
c_ψ , deflected	++	+
Load carrying capacity (influence of other stress components)	-	--

Figure 7.20
Comparison of some of the properties of reinforced plate-spring elements with these of normal plate-springs. Indicated is whether a property improves (+ or ++) , remains unchanged (0) or deteriorates (- or --) when the parameter q is increased.

guiding mechanism by an increasing length or width of the plate-springs. In the design of plate-spring mechanisms the selection of the length of the plate-spring should thus be given adequate attention.

Similar improvements of properties may be expected when cross-spring pivots with values of the parameter a larger than 2 and less than -1 are constructed with partially reinforced plate-spring elements. Such mechanisms are even more comparable to four-bar linkage mechanisms than the usual cross-spring pivot designs (see figure 7.21)

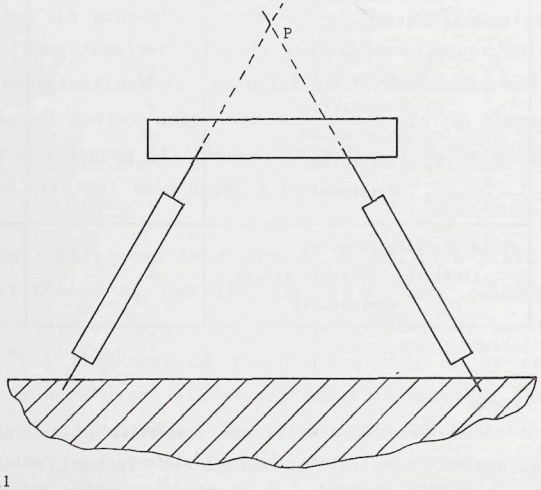

Figure 7.21

The application of reinforced plate-spring elements may also be considered for the construction of cross-spring pivots where the parameter a is more than about 2 or less than -1.

ANNEX 7.I

Derivation of expressions for some properties of reinforced plate-spring elements.

Using the iterative analytical method discussed in chapter 4 some of the main properties of reinforced plate-spring elements used in parallel guiding mechanisms may be determined. In this analysis the element shown in figure 7.I.1 will be discussed. As the element is used in a parallel guiding mechanism the rotation $\phi(L)$ of the end is equal to zero. As a result calculations may be performed on half of the element consisting of an elastic part with length ℓ and an infinitely stiff part with length $q.\ell$.

From figure 7.I.1 the following relations are obtained

$$L = 2 \cdot \ell \cdot (1 + q) \qquad (7.I.1)$$

$$u(L) = 2 \cdot (u(\ell) - q \cdot \ell \cdot \phi(\ell)) \qquad (7.I.2)$$

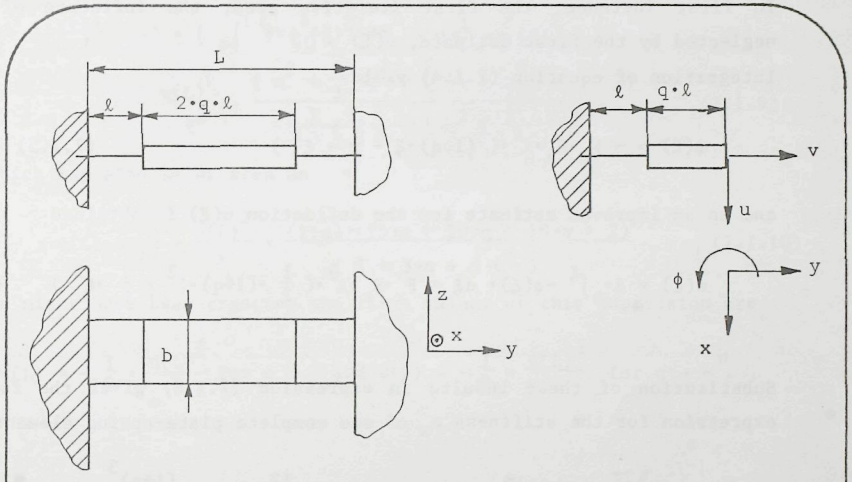

Figure 7.I.1.

In the calculations of the behaviour of the reinforced plate-spring elements the dimensions as indicated here are used. As the element is considered to be a part of a parallel guiding the calculations may, in first order approximation, be performed on one half of the element as shown in (b).

For the plate-spring element loaded by forces F_x and F_y the following equation for the curvature, $d\phi(s)/ds$, in the elastic part results (compare figure 4.3)

$$\frac{d\phi(s)}{ds} \simeq K_z \cdot [\, -F_x \cdot ((q+1)\cdot \ell - s\,) + F_y \cdot (\, \tfrac{1}{2} \cdot u(L) - u(s)\,)\,] \qquad (7.I.3)$$

(As discussed in chapter 2 and further K_z is the compliance factor of the elastic part with respect to bending around the z-axis. In most cases the expression $K_z = {}^1/_{E.I_z}$ may be used).

Introduction of the dimensionless coordinate $\xi = {}^s/_{\ell}$ leads to the expression

$$\frac{d\phi(\xi)}{d\xi} \simeq K_z \cdot \ell^2 \cdot [\, -F_x \cdot (\, (1+q) - \xi\,) + F_y \cdot (\, \frac{u(L)}{2 \cdot \ell} - \frac{u(\xi)}{\ell}\,)\,] \qquad (7.I.4)$$

Determination of c_x and $v(L)$

In first instance, the first iterative step, the influence of F_y is neglected by the first estimate, $u(\xi) \simeq 0$.
Integration of equation (7.I.4) yields

$$\phi(\xi) \simeq - F_x \cdot K_z \cdot \ell^2 \cdot (\, (1+q)\cdot\xi - \tfrac{1}{2} \cdot \xi^2\,) \qquad (7.I.5)$$

and as an improved estimate for the deflection $u(\xi)$ is obtained

$$u(\xi) \simeq \ell \cdot \int_0^{\xi} -\phi(\xi) \cdot d\xi = F_x \cdot K_z \cdot \ell^3 \cdot (\, \tfrac{1}{2} \cdot (1+q)\cdot\xi^2 - \tfrac{1}{6} \cdot \xi^3\,) \qquad (7.I.6)$$

Substitution of these results in expression (7.I.2) gives the following expression for the stiffness c_x of one complete plate-spring element

$$c_x \simeq {}^3/_{(\, K_z \cdot \ell^3 \cdot (\, 2 + 6\cdot q + 6\cdot q^2)} = \frac{12}{K_z \cdot L^3} \cdot \frac{(1+q)^3}{(\, 1 + 3\cdot q + 3\cdot q^2)} =$$

$$= \frac{12}{K_z \cdot L^3} \cdot \frac{1}{1 - (\frac{q}{1+q})^3} = \frac{12}{K_z \cdot L^3} \cdot \frac{1}{1 - p^3} \qquad (7.I.7)$$

Here the parameter p is another parameter indicating which part of the total length of the plate-spring is reinforced. The parameter p is equal to the relative length of the reinforced part. When 60% of the length L is reinforced p equals 0,6.

With expression (7.I.7) a relation between F_x and u(L) is dete ined. This relation can be used to eliminate F_x from expressions (7.I.5) d (7.I.6). Thus the following improved estimates for the deformed shape the plate-spring element are found

$$\phi^*(\xi) \simeq - \frac{u(L)}{\ell} \cdot Q \cdot (\, (1+q)\cdot\xi - \tfrac{1}{2} \cdot \xi^2\,)$$

$$\frac{u^*(\xi)}{\ell} \simeq \frac{u(L)}{\ell} \cdot Q \cdot (\, \tfrac{1}{2} \cdot (1+q)\cdot\xi^2 - \tfrac{1}{6} \cdot \xi^3\,) \qquad (7.I.8)$$

where $Q = {}^3/_{(\, 2 + 6\cdot q + 6\cdot q^2)}$

The estimate for the deformed shape of the plate-spring ay be used to derive an expression for its curvature. This expression n then be used to estimate the magnitude of the bending stresses in the p te-spring. With the approximation of $\cos\phi(\xi) \simeq (\, 1 - \tfrac{1}{2} \cdot \phi^*(\xi)^2\,)$ the inematical end deflection v(L) may now be determined using these e ressions. This results in

$$\frac{v(L)}{\ell} \simeq -2 \cdot [\, \int_0^1 \tfrac{1}{2} \cdot \phi^*(\xi)^2 \cdot d\xi + q \cdot \tfrac{1}{2} \cdot \phi^*(\xi)^2\,] =$$

$$= - \frac{u(L)^2}{\ell^2} \cdot \frac{(\, q^3 + \frac{4}{3}\cdot q^2 + \frac{2}{3}\cdot q + \frac{2}{15}\,)}{(\, \frac{2}{3} + 2\cdot q + 2\cdot q^2\,)^2} \qquad (7.I.9)$$

which may also be written as

$$v(L) \simeq \frac{3}{10} \cdot \frac{u(L)^2}{L} \cdot \frac{(1+q)\cdot(15\cdot q^3 + 20\cdot q^2 + 10\cdot q + 2)}{(\, 1 + 3\cdot q + 3\cdot q^2\,)^2} \qquad (7.I.10)$$

As might have been expected the limit values of this expression are

$v(L) \simeq - \frac{3}{5} \cdot \frac{u(L)^2}{L}$ for $q = 0$ and $v(L) \simeq - \frac{1}{2} \cdot \frac{u(L)^2}{L}$ for $q \to \infty$.

Determination of c_y

The improved estimates $\phi^*(\xi)$ and $u^*(\xi)$ may be used in the equation (7.I.4) for the curvature $d\phi(\xi)/d\xi$. The resulting equation can be integrated twice to derive expressions for $\phi(\xi)$ and $u(\xi)$ in which the first order part of the influence of a force F_y applied to the plate-spring element is taken into account. These expressions may be used to determine the influence of F_y upon the driving stiffness, c_x, of the plate-spring element. The result thus obtained is equivalent to that given by expression (7.3.7).

The obtained expressions for $\phi(\xi)$ and $u(\xi)$ may also be used to eliminate the force F_x, using expression (7.I.2) and to find new estimates for the deformed shape of the plate-spring element. The new estimate for $\phi(\xi)$ will be

$$\phi^{**}(\xi) \simeq -\frac{u(L)}{\ell} \cdot [\, Q \cdot (\,(1+q)\cdot\xi - \frac{1}{2}\cdot\xi^2\,) + F_y \cdot K_z \cdot \ell^2 \cdot \{\, Q\cdot Q_2 \cdot ((1+q)\cdot\xi - \frac{1}{2}\cdot\xi^2\,) - \frac{1}{2}\cdot\xi + Q\cdot(\,\frac{1}{6}\cdot(1+q)\cdot\xi^3 - \frac{1}{24}\cdot\xi^4\,)\,\}\,] \qquad (7.I.11)$$

where $Q_2 = \dfrac{4 + 20\cdot q + 40\cdot q^2 + 30\cdot q^3}{10\cdot(\,1 + 3\cdot q + 3\cdot q^2\,)}$

As was done in expression (7.I.9) this estimate may be used to calculate the end deflection v(L) of the plate-spring element. The resulting expression will contain a part similar to that obtained in (7.I.9) and a part that is a linear function of the force F_y. This part is the first order estimate of the deflection $\Delta v(L)$ caused by the variation of the bending shape of the plate-spring element which causes a certain contribution, c_{yb}, to the total stiffness c_y. From this analysis the expression (7.3.12) for this effect has been derived.

Determination of stiffness c_z

The contribution of the torsional deformation of the plate-spring under influence of a loading force F_z to the deflection w(L) of the end of the element in the z-direction may now be determined. As in the Annex 5.I and 6.I the torsional deformation, $\theta(\xi)$, is determined using the differential equation given in figure 4.10. Using the estimates $\phi^*(\xi)$ and $u^*(\xi)$ from expression (7.I.8) the differential equation for this case is

$$\frac{d\theta(\xi)}{d\xi} - \frac{1}{\mu^2}\cdot\frac{d^3\theta(\xi)}{d\xi^3} \simeq K_y\cdot[\, -\phi^*(\xi)\cdot F_z\cdot\ell^2\cdot(1+q-\xi) + F_z\cdot\ell\cdot(-\frac{u(L)}{2} + u(\xi))\,] \qquad (7.I.12)$$

where $\mu^2 = \dfrac{\ell^2}{K_y\cdot E\cdot\Gamma}$ is a parameter depending upon the length to width ratio of the elastic part of the element. With this factor the influence of the "constrained warping" is taken into account as discussed in chapter 4.

The end conditions for the equation are

$$\xi = 0 \rightarrow \quad \theta(\xi) = 0$$
$$\xi = 0 \rightarrow \quad \frac{d\theta(\xi)}{d\xi} = 0 \qquad \text{" constrained warping "}$$
$$\xi = 1 \rightarrow \quad \frac{d\theta(\xi)}{d\xi} = 0 \qquad (7.I.13)$$

From the differential equation with the given end conditions a solution for $\theta(\xi)$ may be found as

$$\theta(\xi) \simeq K_y\cdot F_z\cdot Q\cdot\ell^2\cdot\frac{u(L)}{\ell}\cdot [\, A + B\cdot e^{-\mu\cdot\xi} + C\cdot e^{\mu\cdot\xi} + a_1\cdot\xi + a_2\cdot\xi^2 + a_3\cdot\xi^3 + a_4\cdot\xi^4\,] \qquad (7.I.14)$$

The magnitude of the different coefficients may be determined, as was done in Annex 4.I, 5.I and 6.I, leading to the following expressions

$$a_1 = -\frac{1}{2 \cdot Q} - \frac{2}{\mu^2} \cdot (1+q)$$

$$a_2 = \frac{1}{2} \cdot (1+q)^2 + \frac{1}{\mu^2}$$

$$a_3 = -\frac{1}{3} \cdot (1+q)$$

$$a_4 = \frac{1}{12}$$

$$a_6 = 2 \cdot a_2 + 3 \cdot a_3 + 4 \cdot a_4$$

$$C = \frac{-a_6 - a_1 \cdot (1 - e^{-\mu})}{\mu \cdot (e^{\mu} - e^{-\mu})}$$

$$B = \frac{-a_6 - a_1 \cdot (1 - e^{\mu})}{\mu \cdot (e^{\mu} - e^{-\mu})}$$

$$A = -B - C \qquad (7.I.15)$$

The contribution of this torsional deformation to the angular deformation $\phi(\xi)$ and the deflection $w(\xi)$ can now be determined with the following expressions (figure 4.10)

$$\Delta\phi(\xi) \simeq \int_0^{\xi} \theta(\xi) \cdot \frac{d\phi(\xi)}{d\xi} \cdot d\xi$$

and $$\Delta w(\xi) \simeq \int_0^{\xi} \Delta\phi(\xi) \cdot d\xi \qquad (7.I.16)$$

The angular deformation $\phi(1)$ and the deflection $w(1)$ of the end of the elastic part may thus be estimated as

$$\Delta\phi(1) \simeq -K_y \cdot F_z \cdot Q^2 \cdot \ell^2 \cdot \left(\frac{u(L)}{\ell}\right)^2 \cdot \left[A \cdot (\tfrac{1}{2}+q) + a_1 \cdot \left(\frac{1}{6} + \frac{q}{2}\right) + \right.$$

$$+ a_2 \cdot \left(\frac{1}{12} + \frac{q}{3}\right) + a_3 \cdot \left(\frac{1}{20} + \frac{q}{4}\right) + a_5 \cdot \left(\frac{1}{30} + \frac{q}{5}\right) +$$

$$+ B \cdot \left(\frac{1}{\mu} - \frac{1}{\mu^2} + \frac{q}{\mu} + e^{-\mu} \cdot \left(\frac{1}{\mu^2} - \frac{q}{\mu}\right)\right) +$$

$$\left. + C \cdot \left(-\frac{1}{\mu} - \frac{1}{\mu^2} - \frac{q}{\mu} + e^{\mu} \cdot \left(\frac{1}{\mu^2} + \frac{q}{\mu}\right)\right) \right]$$

and

$$\Delta w(1) \simeq -K_y \cdot F_z \cdot Q^2 \cdot \ell^3 \cdot \left(\frac{u(L)}{\ell}\right)^2 \cdot \left[A \cdot \left(\frac{1}{3} + \frac{q}{2}\right) + a_1 \cdot \left(\frac{1}{12} + \frac{q}{6}\right) + \right.$$

$$+ a_2 \cdot \left(\frac{1}{30} + \frac{q}{12}\right) + a_3 \cdot \left(\frac{1}{60} + \frac{q}{20}\right) + a_4 \cdot \left(\frac{1}{105} + \frac{q}{30}\right) +$$

$$+ B \cdot \left(\frac{q}{\mu} - \frac{q}{\mu^2} + \frac{2}{\mu^3} - \frac{2}{\mu^2} + \frac{1}{\mu} + e^{-\mu} \cdot \left(\frac{q}{\mu^2} - \frac{2}{\mu^3}\right)\right) +$$

$$\left. + C \cdot \left(-\frac{q}{\mu} - \frac{q}{\mu^2} - \frac{2}{\mu^3} - \frac{2}{\mu^2} - \frac{1}{\mu} + e^{\mu} \cdot \left(\frac{q}{\mu^2} + \frac{2}{\mu^3}\right)\right) \right]$$

(7.I.17)

With these expressions the total deflection $\Delta w(L)$ of the end of the plate-spring due to the torsional deformation may be calculated as

$$\Delta w(L) \simeq 2 \cdot \{ \Delta w(1) + q \cdot \ell \cdot \Delta\phi(1) \} \qquad (7.I.18)$$

The result of this analysis has been used to determine the magnitude of the stiffness c_{zt} as discussed in paragraph 7.3. It should be reminded that the model used to describe the influence of the constrained warping is restricted to the case of torsion of beams. When the elastic part is relatively short compared with its width this model might not be applicable. Therefore the results of calculations where this condition is not satisfied have been shown as a dashed line in the figures in par. 7.3.

- Determination of the stiffness c_{ϕ}

When the torque M_x is applied to the end of the plate-spring element a rotation $\phi(L)$ of this part around the z-axis through the center of the plate-spring will result. Due to considerations about the symmetry of the loading of the plate-spring element no torsional deformation, $\theta(\frac{1}{2} \cdot L)$, at the middle of the plate-spring will occur.

To determine the magnitude, $\Delta\phi(L)$, of the rotation caused by torsional deformation of the elastic part of the plate-spring element the same method as discussed for the influence of F_z is followed. A differential equation as expression (7.I.12) is derived. For this equation the boundary conditions are

$$\xi = 0 \rightarrow \theta(\xi) = 0$$

$$\xi = 1 \rightarrow \theta(\xi) = 0$$

$$\xi = 0 \rightarrow \frac{d\theta(\xi)}{d\xi} = 0$$

$$\xi = 1 \rightarrow \frac{d\theta(\xi)}{d\xi} = 0$$

"constrained warping" (7.I.19)

In this case the extra boundary condition may be used to determine the unknown internal torque M_y in the plate-spring.
The obtained solution for $\theta(\xi)$ will be of the form

$$\theta(\xi) \simeq K_y \cdot M_x \cdot Q \cdot \ell \cdot \frac{u(L)}{\ell} \cdot [\, A + B \cdot e^{-\mu \cdot \xi} + C \cdot e^{\mu \cdot \xi} + a_1 \cdot \xi + a_2 \cdot \xi^2 + a_3 \cdot \xi^3 + a_4 \cdot \xi^4 \,] \qquad (7.I.20)$$

where the magnitude of the different coefficients in this case are determined as

$$a_2 = \frac{1}{2} \cdot (1+q) \quad , \quad a_3 = -\frac{1}{6} \quad , \quad a_4 = 0 \quad , \quad a_5 = a_2 + a_3 \quad ,$$

$$a_6 = 2 \cdot a_2 + 3 \cdot a_3$$

$$B = \frac{-\left(a_5 - \frac{a_6}{\mu}\right) \cdot (e^{\mu} - 1) - a_6}{2 \cdot (e^{-\mu} - 1) \cdot (e^{\mu} - 1) + \mu \cdot (e^{\mu} - e^{-\mu})}$$

$$C = \frac{-\left(a_5 + \frac{a_6}{\mu}\right) \cdot (e^{-\mu} - 1) - a_6}{2 \cdot (e^{-\mu} - 1) \cdot (e^{\mu} - 1) + \mu \cdot (e^{\mu} - e^{-\mu})}$$

$$A = -B - C$$

$$a_1 = \mu \cdot B - \mu \cdot C \qquad (7.I.21)$$

The magnitude of the torque M_y is

$$M_y \simeq M_x \cdot Q \cdot \frac{u(L)}{\ell} \cdot \left(a_1 + {}^1/_{\mu^2}\right) \qquad (7.I.21)$$

With this solution for $\theta(\xi)$ the magnitude of $\Delta\phi(1)$ may be determined as

$$\Delta\phi(1) \simeq -K_y \cdot M_x \cdot \ell \cdot \left(\frac{u(L)}{\ell}\right)^2 \cdot Q^2 \cdot [\, A \cdot \left(\frac{1}{2} + q\right) + a_1 \cdot \left(\frac{1}{6} + \frac{q}{2}\right) +$$

$$+ a_2 \cdot \left(\frac{1}{12} + \frac{q}{3}\right) + a_3 \cdot \left(\frac{1}{20} + \frac{q}{4}\right) + a_4 \cdot \left(\frac{1}{30} + \frac{q}{5}\right) +$$

$$+ B \cdot \left(\frac{1}{\mu} - \frac{1}{\mu^2} + \frac{q}{\mu} + e^{-\mu} \cdot \left(\frac{1}{\mu^2} - \frac{q}{\mu}\right)\right) +$$

$$+ C \cdot \left(-\frac{1}{\mu} - \frac{1}{\mu^2} - \frac{q}{\mu} + e^{\mu} \cdot \left(\frac{1}{\mu^2} + \frac{q}{\mu}\right)\right) \,] \qquad (7.I.23)$$

and the total angular deflection, $\Delta\phi(L)$, of the end of the plate-spring element will be

$$\Delta\phi(L) = 2 \cdot \Delta\phi(1) \qquad (7.I.24)$$

These results have been used in par. 7.3 to determine the guiding stiffnesses of the plate-spring elements.

Chapter 8

Measuring plate-spring characteristics

8.1 Introduction

To investigate whether the mathematical models used to calculate the behaviour of plate-spring mechanisms are adequate different experimental set-ups have been made. The measurements done with these installations must be accurate enough to indicate noticeable differences between theory and reality. In this chapter three different set-ups will be described. In each of these set-ups similar general considerations have been used. A number of these general remarks will be discussed first.

8.2 General observations

* Prediction of the absolute magnitude of stiffnesses.

The absolute magnitude of the stiffnesses of plate-spring mechanisms may in general be predicted with an uncertainty of about 20%. This is mainly due to the relatively large inaccuracy in the plate-spring thickness which in most cases has a cubic influence upon the stiffness. For thicker plate-springs (> 0,3 mm) the inaccuracy decreases.

Other factors contributing to the inaccuracy are Young's modulus of the material and the shape and properties of the clamping pieces. Young's modulus for thin plate-springs is varying due to anisotropy of rolled material (variations upto 5% may be found) and the molecular structure of the material. Measurements by J. Smit (S2) indicated a decrease of Young's modulus of steel plate-springs of about 5% as function of the thickness varying from 0,8 to 0,15 mm.

Elastic deformation of the clamping pieces and rounded edges thereoff render the estimate of the actual plate-spring length inaccurate. An additional length of one half of the plate-spring thickness may be added for each clamped end to account for deformation of the clamping. The additional length for the curvature at the edges of the clamping pieces depends upon

the radius of curvature. Generally 0,1 to 0,2 mm may be added for this effect.

From these remarks it is clear that no accurate measurements are needed to estimate the absolute magnitude of the stiffnesses. Variations of these stiffnesses however are all relative to the intitial values and the relative magnitude of these variations may be measured accurately. In the design of plate-spring mechanisms it will be sufficient when the relative magnitude of these variations, e.g. non-linearity or stiffnesses decreasing with deflection, are predicted. In the set-ups for measurements it is therefore attempted to relate variations to an initial value, for instance the stiffness around the undeflected position.

* Influence of internal stresses.

When a plate-spring is mounted in a measuring set-up no undesired internal stresses due to over-determination of degrees of freedom should occur. The theoretical analysis generally assumes that no such stresses are present. The different degrees of freedom of the clamping pieces at the plate-spring end must be fixed in such a way that in the experiment such stresses are avoided. In general this means that of the "free-end" of a plate-spring only three degrees of freedom (x, ϕ and θ) are to be prescribed while the plate-spring itself fixes the remaining degrees of freedom of the free-ends, see figure 8.1.
For the construction of a guiding mechanism for measurements the slide or the foundation may be made as in figures 5.14 or 6.13 to avoid unwanted stresses.

* Geometrical effects.

In the theoretical analysis it is assumed that the undeformed plate-springs are flat. This means that specimens for measurements should not be bend or twisted considerably. The presence of burrs at the sides, due to cutting for instance, is not allowable as they will lead to unpredictable effects. Dijksman (D1) discusses the influence of an initial curvature of the plate around the y-axis of the plate-spring. To avoid the resulting non-linearity it may be suggested to operate the plate-spring mechanism in a range not including the position where the plate-springs are undeformed.

* Abbe's principle.

When a body is moving the movement may have components in all six degrees of freedom. When it is necessary to measure the displacement of the body along a certain line it is necessary to place the measuring device along this line to avoid inaccuracies from other components of the motion. In some cases it is not practically possible to follow this principle and either two measuring devices are placed at equal distances from the line of interest or the measuring device is placed as close as possible to this line.

* Symmetrical clamping of plate-springs.

The clamping of plate-springs is done in such a way that both clamped surfaces are connected with similar stiffnesses to the other parts of the set-up. When a plate-spring is directly clamped with a simple clamping piece (as in figure 8.2a) this clamping piece has a relatively low stiffness in y, z and ψ directions when compared to the other half of the clamping. To avoid potential differences between theory and experiment clamping pieces as shown in 8.2b have been used. Here both sides are clamped with a clamping piece and equal stiffnesses for both surfaces are obtained.

* Direct Feedback.

While measurements are done it is important to have a direct information about the quality of the gathered data. When only "raw" numerical data are obtained and the processing of these data is performed at a later time, the progress of the experiment will generally be delayed. During processing doubts about certain results may occur but the conditions during the measurement are difficult to reconstruct. A new experiment must be done and the same risk occurs. In the experimental set-ups designed to analyse the plate-spring behaviour this problem is avoided through the use of computers for an on-line data-processing and presentation. Erronous results are detected directly and the source of this errors may be located in an efficient way. The extra time needed to connect the computing devices will, generally, prove to be a profitable investment.

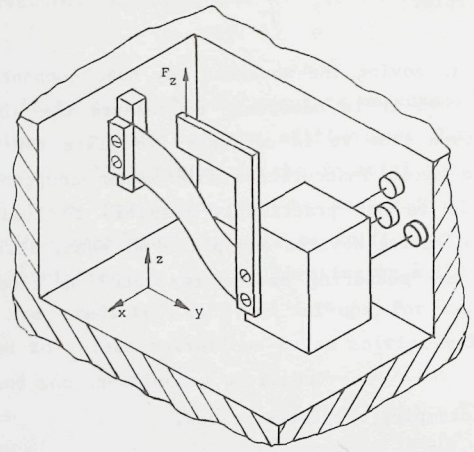

Figure 8.1

To measure plate-spring properties, for instance for stiffness c_z, the two clamped ends of the plate-spring should be mounted in such a way that internal stresses are avoided. Here three wires are used to be fix only the three "free" degrees of freedom of the free clamping piece.

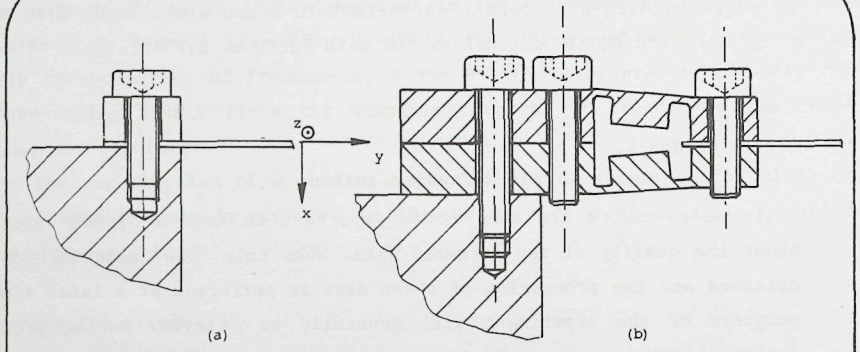

Figure 8.2

When a plate-spring is clamped as in figure (a) the upper surface is fixed to the support with a lower stiffness in y, z and ϕ directions than the lower surface.

To avoid inaccuracies in the measurements clampings of the type shown in (b) have been used. (In schematic diagrams this is not always indicated.)

* Separating the degrees of freedom.

In the design of experimental set-ups it is good to investigate the measuring process in order to see whether simplifications may be made. In many cases a causality in the process is assumed and on this basis the variables are divided into dependent and independent ones. Generally it is assumed that a plate-spring mechanism will deflect when a force is applied and the force will thus be selected as an independent variable. In the set-up for measuring guiding stiffnesses it proved to be much simpler to consider the deflection as independent variable.

Similarly many attempts were made to measure the kinematical motion of plate-spring parallel guidings. Here the deflection of the slide in the directions of the x- and y-axis should be determined. This measurement problem is not solved easily when performed as implied in the description of the problem (see figure 8.3a). However the problem may be stated as measuring the relative displacements in x- and y-axis directions of the slide and foundation. This description might lead to a measurement set-up as shown in figure 8.3b. Here the two quantities are measured at the two different parts and a much simpler measurement system results.

These two examples indicate that it may be very helpful to contemplate the description of a measurement problem. General aspects are the "inversed causality" and the "management" of the degrees of freedom.

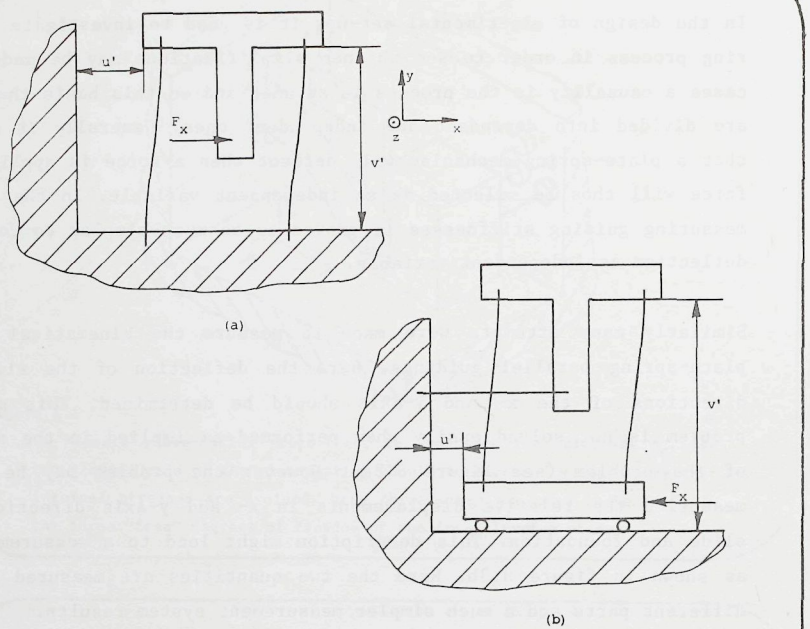

Figure 8.3

Simultaneous measurement of the two displacements, u and v, of the slide in a parallel guiding mechanism poses a difficult measurement problem. The problem may be solved more easily when the relative displacements are measured independently at the foundation and the slide as indicated in (b).

8.3 Measurement of driving stiffness c_x of parallel guidings mechanisms.

To measure the driving stiffness of a parallel guiding mechanism, its non-linearity and possibly the static hysteresis a set-up with a high resolution and small hysteresis has been made. Basically one half of the mechanism will perform a pure rectilinear movement in the x-direction. The other part is fixed in this direction while it is free to move in all other directions (as in figure 8.3b). The relative displacement in the x-direction may be measured without much difficulty. The force in the x-axis direction used to fix the other part is measured separately.

The basic lay-out of the set-up is shown in figure 8.4. Part I is moving in the x-direction along a slide guided by air bearings. A simple screw (2) is used to drive this part and any displacement measuring device may be used. This device is placed as close as possible in the center of the guiding mechanism thus reducing the influence of rotations of part (1).

Part (3) is supported in the x-direction by a long steel wire connected to the weighing system of an electronic weighing scale (4). (Sartorius 1205 M.P., max. mass 0,160 kg, resolution $1 * 10^{-5}$ kg). The principle of operation of such a weighing scale assures that the moving part of the weighing system does not move under influence of applied loads. A servo-actuator mechanism drives the moving part to its zero-position and the magnitude of the force required to maintain this situation is measured and displayed. The error in the position of the moving part has been measured and proves to be less than 2 μm.

The displacement of the slide with the part 1 is measured using a SONY-Magnescale measuring system (5). This system uses a thin rod with a magnetic waveform with a 0,2 mm pitch and a detector to measure the displacement. The rods have been made with a constant pitch and the measured displacement at 0,2 mm intervals is measured with a relative inaccuracy of ± 1 μm. The absolute inaccuracy, which is not important for the measurements, is about ± 5 μm over a measuring range of 100 mm.

Both the weighing scale and the displacement measuring system are connected to a DEC-PDP 11/10 computer. A certain displacement of part (1) is given and the operator commands the computer to accept data from both devices. The digital data are transmitted and in the computer converted to actual

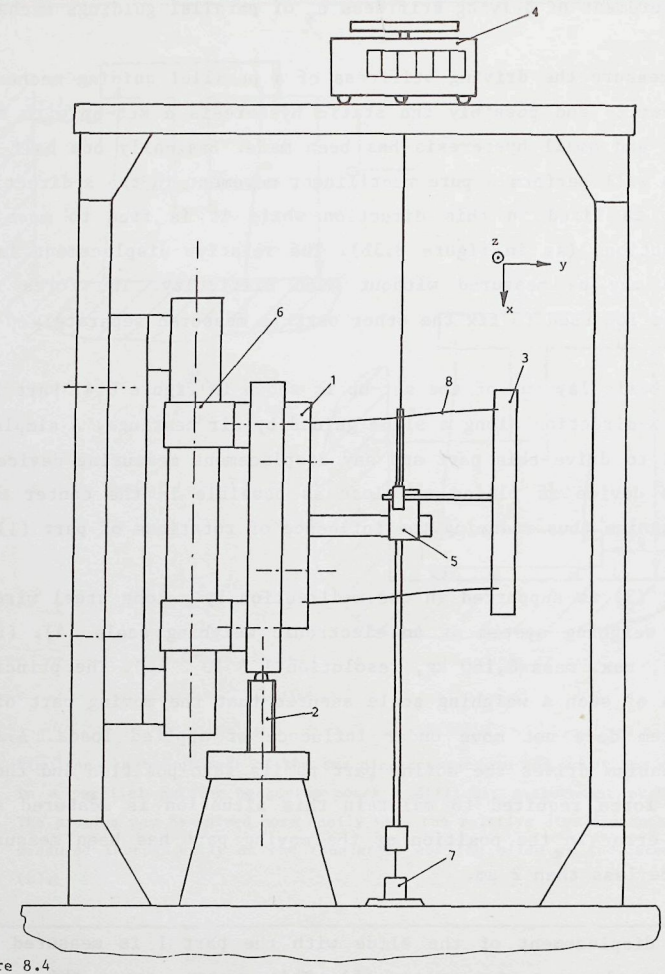

Figure 8.4

Schematic diagram of set-up used to measure the driving stiffness c_x of a parallel guiding.

1. "Foundation" of plate-spring parallel guiding mechanism
2. Screw used to drive part 1
3. "Slide" of plate-spring parallel guiding mechanism
4. Electronic weighing scale
5. Displacement transducer
6. Air bearing guiding mechanism
7. Elastic support for rod of displacement transducer
8. Plate-spring

values in millimeters and Newtons. To determine the stiffness a number of data pairs is collected and a least-square method is used to determine the tangent of the best fitting straight line. The best estimate of the stiffness is obtained when the displacements are small enough to avoid non-linear effects of the plate-springs, but large enough to avoid errors due to the resolution of the measuring apparatus. Deflections of ± 2 mm proved to be yielding good results when plate-springs with a length of about 8 mm. were used.

When the initial stiffness of the guiding mechanism was determined the computer could be used to display the difference between values calculated with this stiffness and values measured at larger deflections. In this way graphs as given in figure 3.7 could be made. While doing the measurements the measured data are directly presented. Thus deviations due to defects in the measurement set-up or the testobject can be detected immediately.

With the measuring system stiffnesses of parallel guidings as presented in chapter 3, 4 , 5 and 7 have been determined. As the resolution of both force and displacement is of the order $1{:}10^4$ non-linear effects with magnitudes less than 1% could well be determined. Although the measuring system may contain a number of sources of systematical errors (such as elastic deformation of weighing scale support and the attached steel wire and others) very good reproducible results were obtained. When a measurement was repeated the result was within a range of ± 0,1%. Disassembling and reassembling the guiding mechanism yielded differences less than ± 1%.

This repeatability is more than sufficient to determine the main effect of loading or geometrical variations upon the guiding stiffness. The resolution of the measuring set-up is even large enough to allow the measurement of static hysteresis in the guiding mechanism. An example of a measured hysteresis curve is shown in figure 8.5. From this figure it may be seen that the differences in the rest-force when the deflection is equal to zero is less than 0,2% of the maximum applied force. The hysteresis is partly due to the hysteresis in the plate-spring material, the clamping of the plate-spring and the measuring set-up itself. The last contribution is of the order of magnitude of 2.10^{-4} as was determined by Smit (S3). The magnitude of material and clamping hysteresis may be investigated with the available measuring system. A description of preliminary results of such measurements will be given in Appendix A.

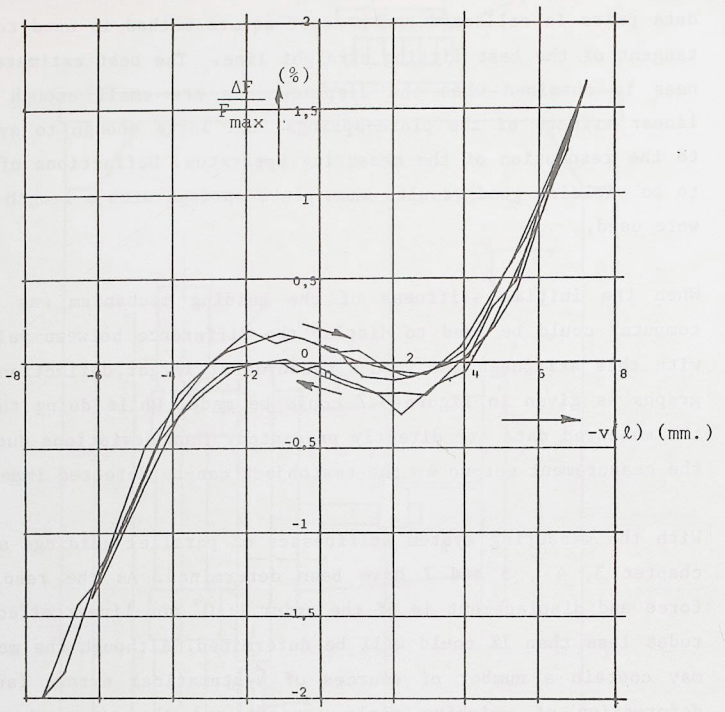

Figure 8.5

To obtain information about hysteresis in plate-spring mechanisms a modified version of the hysteresis curve may be measured. Shown is a result from a measurement with a parallel guiding with plate-spring dimensions 80*20*0,18 mm. Starting from u(ℓ)=0 two complete cycles of loading were made.

In order to present the measured hysteresis only the force difference ΔF (between the measured force and the force calculated using an estimated value for the stiffness) relative to the maximum force F_{max} predicted for the maximum deflection is shown as a function of the slide displacement. Thus the result from an ideal mechanism will be a horizontal line as ΔF is equal to zero for all deflections. Due to the non-linearity in the force-displacement relation the measured curves without hysteresis will be sloping upwards for positive and downwards for negative values of u(ℓ) (see para. 5.3). Due to hysteresis different curves will be obtained during the upward and the downward stroke. The resulting difference in this case is about 0,2% when u(ℓ) = 0. (see also Appendix A)

8.4 Measurement of stiffness c_y.

The stiffness c_y of a plate-spring as used in a parallel guiding is composed of two effects. The tensile stiffness as predicted by Hooke's Law is independent of the deflection of the guiding. In addition to this effect small changes of the bending shape of the deformed plate-spring due to forces F_y will cause a deflection in the direction of the y-axis. This effect depends upon the deflection of the guiding.

The measurement of these stiffnesses poses a measurement problem quite different from measuring the driving stiffness c_x. When a steel plate-spring with dimensions 80x20x0,25 mm is considered the stiffnesses are of the order of magnitude of 10^7 -10^6 N/m. As the loading forces are limited to 20-30 N., to avoid instability or second order effects, the deflections to be measured are in the range from 2 to 30 μm.

Measurements of the trajectory of a point of the slide carrying loading forces do not yield accurate estimates of the stiffness c_y. The kinematic deflection v(ℓ) of the slide is about 200 μm and the deflection due to the stiffnesses may only be estimated.

A better result may be expected when a plate-spring is fixed in its deformed shape and the additional deflection upon variation of the force F_y is measured (see fig. 8.7). But even in this case the experiment should be set up with great care. This is illustrated when the stiffness of the mounting plate for the plate-spring shown in figure 8.7 is estimated. The solid steel block S with dimensions 80x40x35 mm has a stiffness of about 10^7 N/m in the direction of the y-axis. It will be clear that with such a set-up no accurate measurements especially for plate-springs with small deflections in the x-direction will be obtained.

Attempting to avoid this sort of difficulties the experimental set-up shown in figure 8.8 has been made. The plate-spring (1) is clamped at both ends with symmetrical clamping pieces (2) as described in figure 8.2. The "fixed" clamping (2a) is mounted on a rotation stage build up as a four-bar linkage mechanism with elastic hinges (3). This mechanism enables the adjustment of the relative angular position of both clamping pieces. The best alignment of this angle is found by testing the similarity of the two stable buckling shapes of the undeformed specimen plate-spring (u(ℓ) = 0).

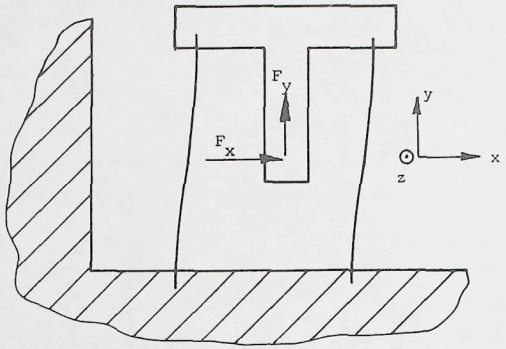

Figure 8.6

Plate-spring parallel guiding loaded by a force F_y.

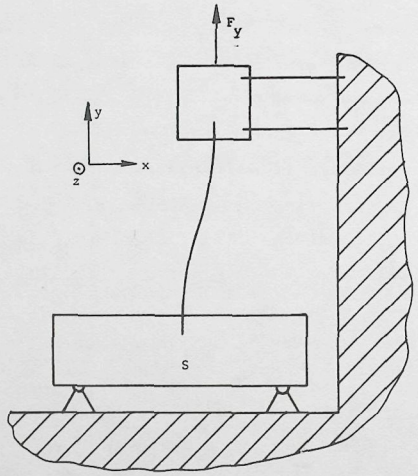

Figure 8.7

Measurement of the stiffness c_y may be done on one plate-spring of the parallel guiding which is clamped in such a way that the desired deformation is prescribed.

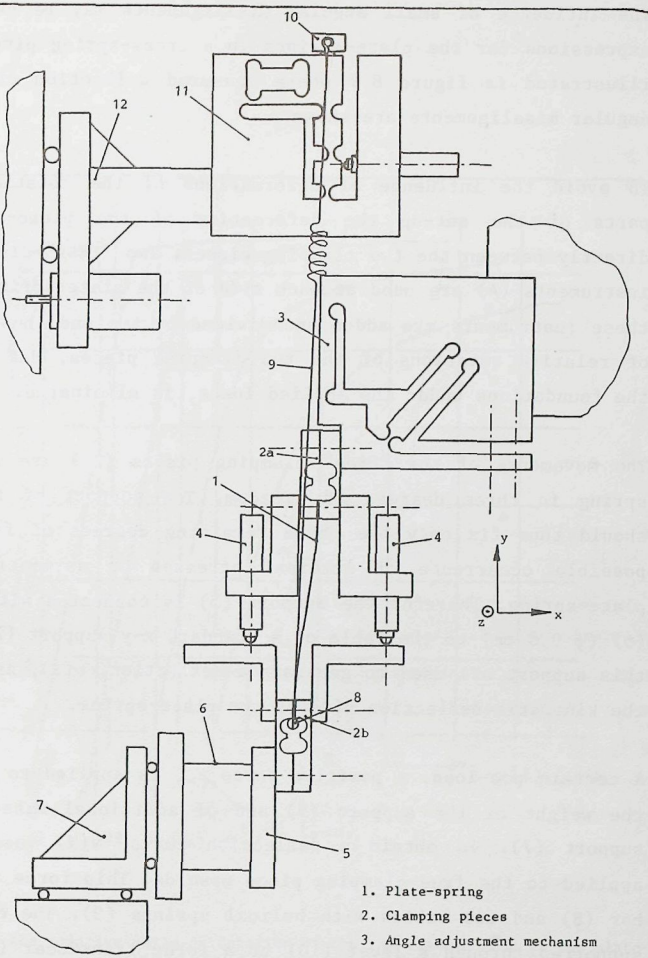

1. Plate-spring
2. Clamping pieces
3. Angle adjustment mechanism
4. Displacement transducers
5. Support for free clamping piece 2b
6. Three wires supporting no.5
7. X-Y displacement stage
8. Rod for application of force F_y
9. Cables for force application
10. Lever
11. Force transducer
12. Motor driven y-displacement stage

Figure 8.8

Schematic diagram of set-up used to measure the stiffness c_y of a plate-spring deformed as in a plate-spring parallel guiding.

The influence of small angular misalignments may be calculated using the expressions for the plate-springs in a cross-spring pivots. This effect is illustrated in figure 8.9 where measured deflection curves for different angular misalignments are shown.

To avoid the influence of deformations of the rotation stage and other parts of the set-up the deformation of the plate-spring is measured directly between the two clamping pieces. Two "TESA"-displacement measuring instruments (4) are used at each side of the plate-spring. The signals from these instruments are added and divided by two and thus the main influence of relative rotations of the two clamping pieces, due to deformations of the foundations under the applied loads, is eliminated.

The movements of the "free" clamping pieces (2b) are fixed by the plate-spring in three degrees of freedom. The support of this clamping piece should thus fix only the three remaining degrees of freedom to avoid the possible occurrence of internal stresses or asymmetric loading of the plate-spring. Therefor the support (5) is connected with three steel wires (6) (ϕ 0,8 mm) to the table of a standard x-y support (7). The movements of this support are used to generate a deflection, u(ℓ), and to compensate for the kinematic deflection v(ℓ) of the plate-spring.

A certain pre-load, a positive force F_y, is applied to the plate-spring by the weight of the support (5) and of additional masses attached to this support (7). To obtain a deflection curve, v(ℓ) versus F_y, a force is applied to the free clamping piece upwards. This force is applied through a bar (8) and two cables with helical springs (9). The end of the cables is supported through a lever (10) of a force transducer (11). When the force transducer is moved upwards by a motor driven stage (12) the loading force F_y upon the plate-spring will be reduced. The information from the force transducer and the displacement transducers is collected, transmitted to the computer (DEC-PDP 11/10) and analysed. A value for the measured stiffness c_y is determined using a least-square calculation upon about 30 data-pairs around the point where F_y equals zero.

The force transducer was designed to measure relatively small forces with a high stiffness of the transducer. In that case the deflections at the point of application are relatively small and may not be measured with standard displacement transducers. The design contains a "knuckle-joint" mechanism

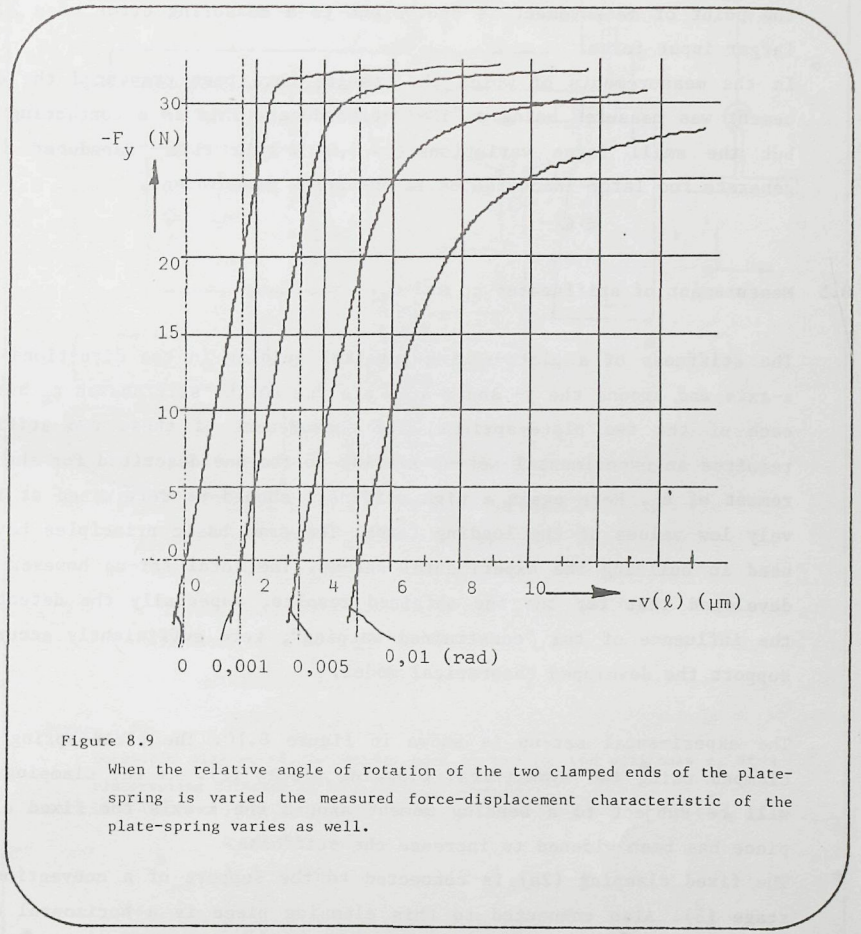

Figure 8.9

When the relative angle of rotation of the two clamped ends of the plate-spring is varied the measured force-displacement characteristic of the plate-spring varies as well.

using elastic hinges. A small deflection at the point of application of the force is transmitted to a larger deflection (20 times) at the point of measurement of the displacement. The stiffness of the mechanism is due to the stiffness of the elastic hinges. Measurement of the displacement should preferably be done without contacting the mechanism as a force applied at the point of measurement is equivalent to a measuring error of a 20 times larger input force.
In the measurements of which the results have been presented the displacement was measured using a "TESA"-transducer. This is a contacting device but the small force variations (≈ 0,01 N) in this transducer did not generate too large inaccuracies in the force measurement.

8.5 Measurement of stiffnesses c_z and c_ψ.

The stiffness of a plate-spring parallel guiding in the directions of the z-axis and around the y- and x-axis are due to the stiffnesses c_z and c_ψ of each of the two plate-springs. The measurement of these two stiffnesses requires an experimental set-up similar to the one described for the measurement of c_y. Here again a high stiffness should be determined at relatively low values of the loading force. The same basic principles have been used in building the experimental set-up. The total set-up however is not developed that far but the obtained results, especially the detection of the influence of the "constrained warping", were sufficiently accurate to support the developed theoretical model.

The experimental set-up is shown in figure 8.10. The plate-spring (1) is clamped using two symmetrical clamping pieces (2). As the clamping pieces will be subject to a bending moment around the x-axis the fixed clamping piece has been widened to increase the stiffness.
The fixed clamping (2a) is connected to the support of a conventional x-y stage (3). Also connected to this clamping piece is a horizontal bar (4) carrying two "TESA"-displacement transducers (5 and 6).
The transducer (5) rests on the surface of a bar (7) fixed to the "free" clamping piece (2b) at the center of the undeformed plate-spring. The other transducer (6) also rests upon this bar (7) but at a distance of about 100 mm in y-axis direction from the other one. The two transducers thus allow for measurement of the deflection $w(\ell)$ and rotation $\psi(\ell)$ of the free-end.

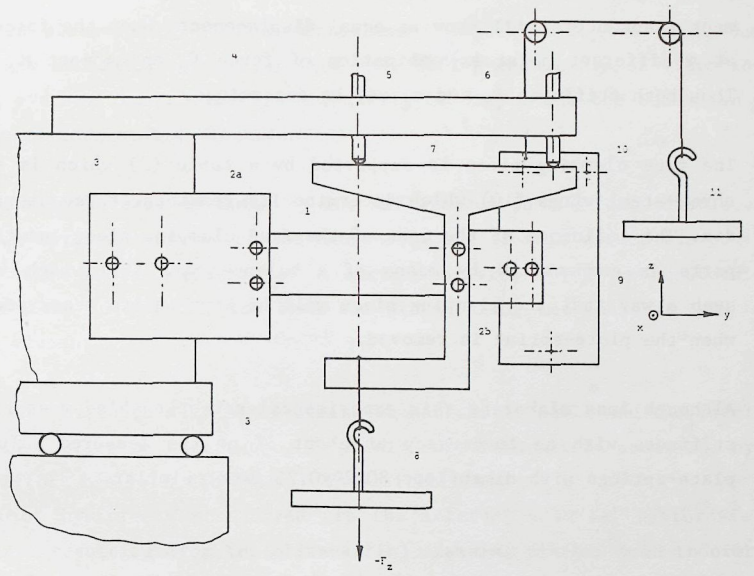

Figure 8.10
Schematic diagram of the set-up used to measure the stiffness c_z of a plate-spring deformed as in a parallel guiding.

1. Plate-spring
2. Clamping pieces
3. X-Y-stage
4. Bar
5.,6. TESA-displacement transducer
7. Bar
8. Loading table
9. Support for free clamping piece
10. Wires supporting no. 9
11. Weight for balancing of no. 9

The loading force, F_z, should be applied at the center of the plate-spring and will cause only a deflection of the free-end. The force is generated by placing weights upon the table (8) which is connected to the free-clamping piece. When the force is applied at the correct position the two displacement transducers will show an equal displacement. When the force is applied at a different point a combination of force F_z and moment M_x is applied. Thus both stiffness c_z and c_ψ may be determined.

The free clamping piece is supported by a table (9) which is supported by three steel wires (10) which determine its remaining three degrees of freedom. The influence of the mass of the free clamping piece and the connected parts is compensated by means of a balance mass (11) which is placed in such a way that the clamping piece will be kept in its measurement position when the plate-spring is removed.

Although less elaborate this experimental set-up enabled measurement of the stiffness with an inaccuracy of about 5% of the measured value for steel plate-springs with dimensions 80x20x0,25 mm or similar.

APPENDIX A

Preliminary results of measurement of hysteresis in plate-spring mechanisms.

Hysteresis in plate-spring guiding mechanisms is observed in two ways. Due to the hysteresis mechanical energy will be lost during each cycle of vibration in a vibrating system. Thus a free vibration will be damped and the mechanism will eventually come to a stable situation.

Statically the hysteresis is noted by the differences in the force-displacement curves during reversed motions of the mechanism. Due to this effect the position of the mechanism under influence of a certain driving force is undetermined. This effect leads to inaccuracies when the plate-spring mechanism is used as a transducing element.

Fortunately the hysteresis in plate-spring mechanisms is small and the resulting inaccuracy will often be acceptable. To obtain more information about the hysteresis some effort has been directed in this direction.
The sources of hysteresis considered are the internal material hysteresis and the hysteresis resulting from the plate-spring clamping pieces. Both theoretical and experimental methods were used to gain information about these effects.

The material hysteresis will depend strongly upon the magnitude of the stresses in the material during the loading cycle. For relatively low stress levels the hysteresis is relatively small, at higher values a pronounced increase of the hysteresis may occur. In many instances the fatigue stress-limit is indicating the point where this transition occurs.

The hysteresis in the clamping pieces will depend upon their design and parameters as clamping force, friction coefficient, etc. The influence of the hysteresis in clamping pieces, relative to that of the material hysteresis, will depend upon the length of the plate-spring. During the cycle with a certain stress level in the plate-spring a certain amount of energy is lost in the clamping piece. The relative magnitude of this amount of energy will be small when a long plate-spring, containing a large total amount of elastic energy, is used. Hence the efforts to reduce hysteresis must be directed to reduction of material hysteresis when long plate-springs are used (i.e. with a large length compared to th thickness). In constructions with relatively short plate-springs or when special materials are used the influence of losses in the clamping pieces will

become dominant.

As suggested in chapter 8 the measurement set-up used to measure the driving stiffness c_x of plate-spring parallel guidings may be used to estimate the static hysteresis in plate-spring constructions. The static hysteresis is of importance in the design of measuring systems. The dynamic hysteresis will in most cases be influenced by the damping influence of the surrounding air and will thus be depending strongly upon the design of the considered mechanisms.

Different examples of measured hysteresis curves are shown in figures A1 to A3. In these figures the magnitude of the difference between measured forces and forces calculated using a constant stiffness relative to the maximum applied force as a function of the displacement is shown. In figure A1 a curve as measured for a plate-spring parallel guiding is shown. In this case the length of the plate-spring is relatively large and the contribution from the hysteresis in the clamping pieces is relatively small.

The magnitude of the hysteresis may be characterized by the ratio between the force difference, ΔF, when the displacement is equal to zero on either of the two curves and the maximum applied force, F, in one direction. Using this definition the hysteresis in figure A1 is estimated as about 0,2%. This will also indicate the uncertainty range for the position of the slide when no driving force is applied. The uncertainty range will be 0,2% of 8 mm deflection, giving a 16 µm range.

In figures A2 and A3 curves measured at short plate-springs are shown. Here the plate-spring is connected with two clamping pieces as shown in figure 8.2b to the slide of the measuring set-up and a long bar. The other end of the bar is suspended at the wire connected to the weighing balance. In this case the plate-spring is subjected to a, almost, constant bending moment. Due to the short length of the plate-spring the influence of the hysteresis in clamping pieces is relatively important. In figure A2 the hysteresis is about 0,4%. It should be noted that in this case the non-linearity of the force-displacement characteristics is relatively small when compared with figure A1.

Figure A3 shows a similar hysteresis curve for a short plate-spring. Also shown here are some internal hysteresis curves obtained by making small reciprocating movements. A certain stabilizing effect during the movements may be recognized during these cycles.

To obtain an impression of the relative influences of clamping and material hysteresis contribution a series of measurements on beryllium-copper plate-springs was performed. Relatively short plate-springs, active length from 3 to 14 mm., width 6, mm and thickness 0,4 mm, were measured.
In figure A4 the magnitude of the hysteresis, in this case characterized by the absolute magnitude of the uncertainty range for the unloaded plate-spring, as a function of the active plate-spring length is shown for different values of the maximum value of the bending stress. At each stress level a certain uncertainty due to the deformations in the clamping pieces is observed. The absolute magnitude increases with increasing stress level.
In addition an uncertainty due to internal material hysteresis which increases with increasing length of the plate-spring may be noted.

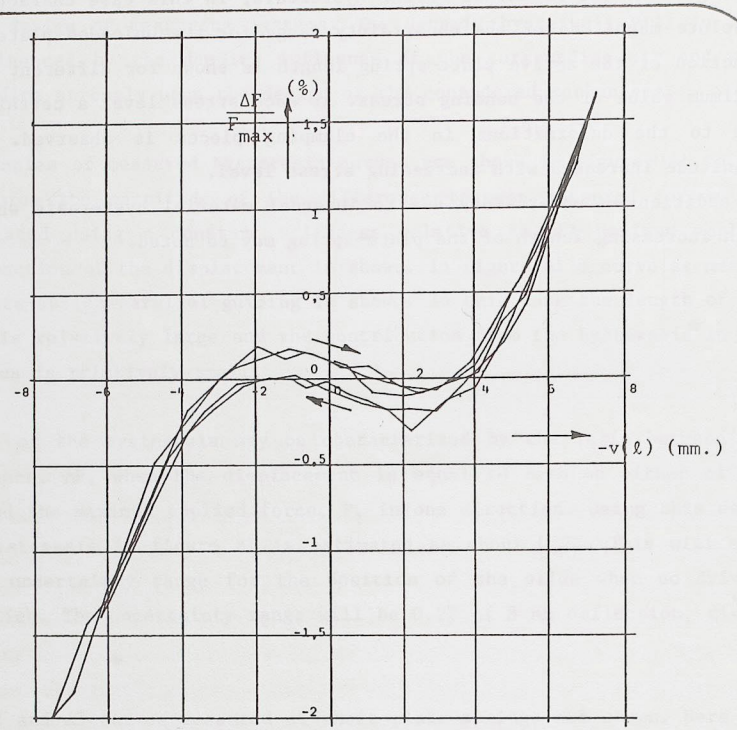

Figure A1

In first order approximation the force needed to generate a displacement of a parallel guiding is determined as, F = c.u. With the measurement set-up shown in par. 8.3 the differences, ΔF, from this relation have been measured as a function of u. The result is shown relative to the magnitude of the maximum force, $F_{max} = c.u_{max}$.

The hysteresis in the mechanism may be defined as the relative differences in $\Delta F/F_{max}$ at the loading and unloading curve for u = 0.

From the graph a hysteresis of about 0,2% is estimated. (see also fig.8.5)

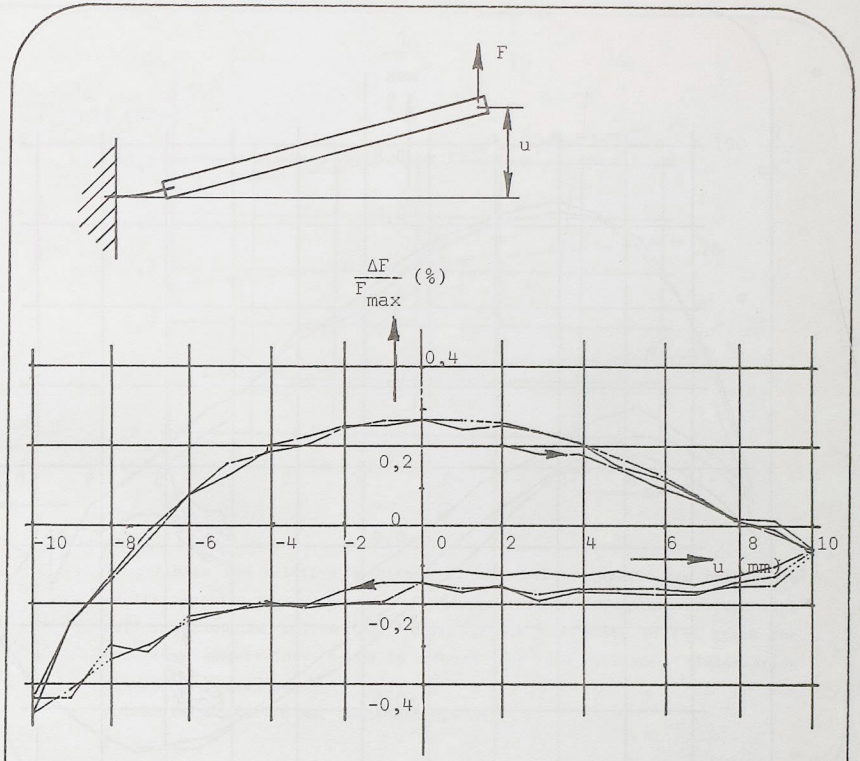

Figure A2

To estimate the influence of the hysteresis in clamping pieces the force-displacement curves of short plate-springs were measured. The result shown here was obtained with a plate-spring with dimensions of 4x6x0,4 mm. As in figure A1 only the relative magnitude of the differences from a linear relation are shown.

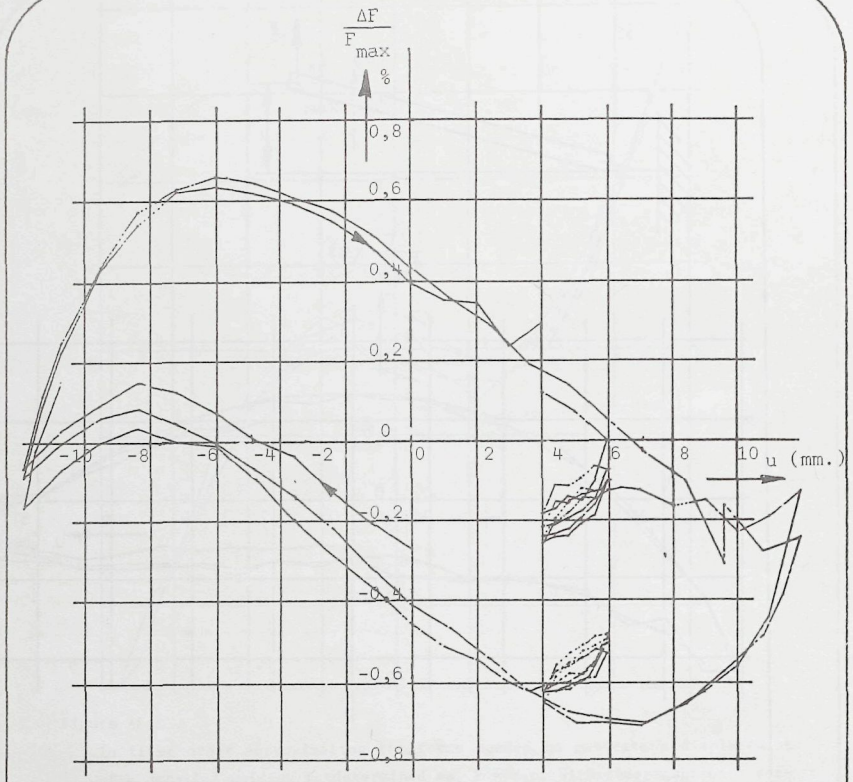

Figure A3

Hysteresis curve as measured on a short plate-spring as in figure A2. Here internal hysteresis cycles have been measured to estimate the influence of small vibrations around an equilibrium position. It is clear that the magnitude of the hysteresis depends mainly upon the maximum deflections of the plate-springs.

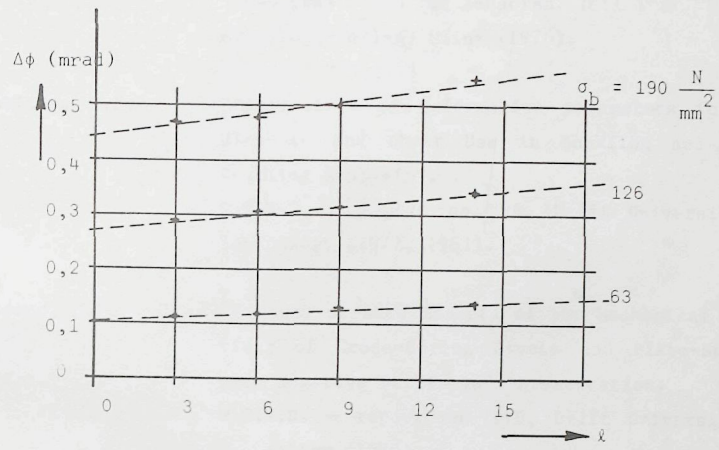

Figure A4

To estimate the relative magnitude of material hysteresis and hysteresis in the clamping pieces a serie of measurements on BeCu-plate-springs with different lengths and maximum stress levels was done. In the graph the resulting uncertainty range $\Delta\phi$ found for the unloaded plate-spring element is presented.
(Dimensions, width 6 mm, thickness 0,4 mm).

REFERENCES

(A1) Ashwell, D.G. "The anticlastic curvature of rectangular beams and plates" J. Royal Aeronautical Soc., 54 (1950) pp. 708-715.

(B1) Breitinger, R. "Losungskataloge für Sensoren, Teil I". Krauskopf-Verlag, Mainz (1976).

(B2) Besseling, J.F. "Derivatives of deformation parameters for Bar Elements and their Use in Buckling and Post-Buckling Analysis". W.T.H.D. - report no. 94, Delft University of Technology (1977, 1981).

(D1) Dijksman, J.F. "A study of some Aspects of the Mechanical Behaviour of Cross-Spring Pivots and Plate-Springs with Negative Stiffness". Dissertation. W.T.H.D. - report no. 116, Delft University of Technology (1979).

(E1) Eastman, F.S. "The Design of Flexure Pivots". J. Aero Sci 5, nov. 1937, p.p. 16-21.

(E2) Eijk, J. van "Plate-spring parallel guiding with compensated spring constant (in Dutch)". Internal report. Laboratory of Fine Mechanics, nr. 1975-E2, Delft University of Technology (1975).

(F1) Frisch-Fay, R. "Flexible bars". Butterworths London (1962).

(G1) Grentzius, W. "Loading capacity of plate-spring parallel guidings in the plane of motion (in Dutch)". Internal report, Laboratory of Fine Mechanics, Report no. 1980-G5, Delft University of Technology.

(H1) Haringx, J.A. "The cross-spring pivot as a constructional element". Appl. Sci. Res. A1 (1949, p.p. 313-332).

(H2) Hasselmeier, H. "Algemeine Untersuchungen über das Kreuzfeder Gelenk". Jenaer Jahrbuch (1954, p.p. 279-304).

(H3) Hoek, W. van der "The prediction of the dynamic behaviour and positioning accuracy of constructions and mechanism. (in Dutch) ". Textbook Eindhoven Univ. of Technology, No.4.007.1, (9th edition), 1984 (D.D.P.no. 14,63,67,69,81,89,100,101,102)

(J1) Jones, R.V. "Parallel and rectilinear spring movements". Journal of Sci. Instruments, Vol. 28 (1951, p.p. 38-41).

(J2) Jones, R.V. "Angle-spring hinges". Journal of Sci. Instruments, Vol. 32 (1955, p.p. 336-338).

(K1) Koiter, W.T. "Stijfheid en Sterkte, deel I". Scheltema & Holkema, Haarlem (1972).

(K2) Kruit, J. "Measurements of the out-of-plane stiffnesses of plate-spring parallel guidings. (in Dutch)". Internal report, Lab. of Fine Mechanics, nr.1984-K12, Delft Univ. of Technology (1984).

(L1) Love, A.E.H. "A treatise on the mathematical theory of elasticity". Fourth Edition, Cambridge University Press (1927; 1952).

(L2) Lotze, W. "Die ebene Kinematik von Biegefeder Aufhängungen" Dissertation, Dresden (1964).

(N1) Neugebauer, H.G. "Designing springs for parallel motion". Machine Design, August 7 (1980), p.p. 119-120.

(P1) Prandtl, L. "Kipperscheinungen". Diss. University of Munich. (1900). Also published in " L. Prandtl-Gesammelte Abhandelungen" Springer Verlag, 1961.

(S1) Steenbakker, "The influence of the clamping upon the bending deformation of a plate-spring (in Dutch)". Internal report, Laboratory of Fine Mechanics, nr. 1974-S7, Delft University of Technology (1974).

(S2) Smit, J.F. "Investigation of the bending stiffness of plate-springs (in Dutch)". Internal report, Laboratory of Fine Mechanics, nr. 1982-S13, Delft University of Technology, (1982).

(S3) Smit, J.F. "Measurement of hysteresis in clamped plate-springs (in Dutch)". Internal report, Laboratory of Fine Mechanics, nr. 1982-S13, Delft University of Technology (1982).

(S4) Schuller, G. "Bending of plate-springs (in Dutch)". Internal report, Laboratory of Fine Mechanics, nr. 1978-S10, Delft University of Technology, (1978).

(T1) Timoshenko S.P. and Gere, J.M. "Theory of elastic stability". Mag Grow Hill, New-York (1961).

(T2) Thorp, A.G.II. "Flexure Pivots-Design". Product Engineering, February 1953, p.p. 192-200 (1953).

(T3) Thomson, W.T. "Vibration Theory and Applications" George Allen and Unwin, London (1966).

(W1) Werff, K. van der "Large displacements of plane beam constructions applied on a cross-spring pivot (in Dutch)". W.B.T.M.-report nr. 408, Delft University of Technology, (1968).

(W2) Werf, J.J. van der "Computer Aided Design of plate-spring constructions (in Dutch)". Internal report, Laboratory of Engineering Mechanics, nr. 782. Delft University of Technology (1984).

(W3) Wang, C.Y. and Watson, L.T. "On the large deformations of C-shaped springs". Int. Jour. of Mech. Sci. Vol 22 p.p. 395-400 (1980).

(Y1) Young, W.E. "An investigation of the cross-spring pivot". J. Appl. Mech., June 1944, p.p. A113-A120.

(Z1) Zenov, P. "Untersuchung der Einwirkung von Kräften auf die dritten Ableitungen der Bewegung bei Kreuzfedergelenken". Feingeräte Technik, 19 Jg. Heft 2, (1970) p.p. 63-33.

Samenvatting

Bladveren bezitten een aantal interessante eigenschappen welke gebruikt kunnen worden voor het ontwerp van nauwkeurige geleidingen. Goed reproducerende relatieve bewegingen kunnen verkregen worden enerzijds dankzij de afwezigheid van speling en anderzijds door de grote stijfheden in de ondersteunde richtingen. In het algemeen nemen deze stijfheden af bij vervormingen van de bladveren en in de meeste gevallen zijn de toelaatbare bewegingen relatief klein.

Naast de verschillende voordelen is één van de grootste nadelen het ontbreken van een "technische infrastructuur" voor het gebruik van bladveren. De praktische ervaring in het ontwerpen van bladveermechanismen is beperkt en niet of nauwelijks in literatuur vastgelegd.
Daarnaast is de kennis over het gedrag van deze mechanismen onder invloed van belastingen niet volledig bekend en in veel gevallen niet goed toegankelijk.

In dit proefschrift wordt deze kennis uitgebreid en gecombineerd met reeds beschikbare kennis. In drie aparte hoofdstukken wordt getracht dit geheel op een toegankelijke manier te presenteren.

Voor het bepalen van het gedrag van bladveren onder invloed van drie-dimensionale belastingen wordt in hoofdstuk 2 een wiskundig model op basis van het
6 concept van de elastische lijn beschreven. In hoofdstuk 3 en 4 wordt een benaderende analytische methode beschreven waarmee oplossingen van de verkregen differentiaalvergelijkingen kunnen worden verkregen.

Bij het vergelijken van deze resultaten met meetresultaten, verkregen met de opstellingen beschreven in hoofdstuk 8, bleek dat het concept van de elastische lijn niet geheel voldoet. Een tweetal effecten moet worden toegevoegd. Het eerste is het gevolg van de overgang van de spanningstoestand bij balk-buiging naar die bij plaat-buiging. Dit effect was al eerder aangegeven door o.a. Dijksman (D1).
Het tweede effect is het gevolg van de door de inklemmingen veroorzaakte invloed op de torsie-vervormingen. Dit effect van de "belemmerde welving" van de doorsnede is toegevoegd aan het wiskundig model voor de bladveer.

In de hoofdstukken 5 tot 7 worden de belangrijkste eigenschappen van bladveermachanismen besproken. Aan de hand van het voorbeeld van de bladveerparallelgeleiding wordt een uitgebreide beschrijving van de verschillende effecten in het gedrag van bladveermechanismen gegeven. In hoofdstuk 6 wordt hieraan de informatie voor het ontwerp van kruisveerscharnieren toegevoegd. Een aantal verschillende toepassingen van bladveren worden in hoofdstuk 7 besproken. In dit hoofdstuk wordt ook de mogelijkheid tot het verbeteren van de eigenschappen van de bladveerparallelgeleiding door het toepassen van "verstijfde bladveren" onderzocht.

In een aparte appendix wordt het optreden van hysterese in bladveergeleidingen kort besproken. Algemeen wordt het als een voordeel beschouwd dat in bladveergeleidingen "bijna geen" hysterese optreedt. Om kwantitatieve informatie over de grootte van de hysterese te verkrijgen zijn een aantal verkennende metingen gedaan. De eerste resultaten van deze metingen worden in Appendix A besproken.

Stellingen behorende bij het proefschrift
On the design of plate-spring mechanisms.

1. De stap van werkelijkheid naar een theoretisch model vormt de belangrijkste barriëre voor het praktisch toepassen van beschikbare theoretische kennis. Het is daarom noodzakelijk aan het aanleren van vaardigheid in de modelvorming in het wetenschappelijk onderwijs meer aandacht te besteden.

2. Het toenemen van de abstractiegraad en de groei van het bijbehorende jargon leidt tot groeiend aanzien van een vakgebied of specialisme. In tegenstelling hiermee worden ontwerpen van mechanische constructies beter als ze eenvoudiger te begrijpen en te produceren zijn. Wellicht is dit de oorzaak van het gebrek aan aandacht en waardering die de constructieve werktuigbouwkunde ten deel valt.

3. Bij het doen van wetenschappelijk onderzoek, of dit nu op het gebied van bladveren, van kernfysica of van sociologie is, is het van wezenlijk belang dat de kwaliteit van de theoretische en experimentele bijdragen in gelijke mate wordt ontwikkeld. De kwaliteit van het onderzoek wordt namelijk eerder bepaald door het produkt van beide bijdragen dan door hun som.

4. In werktuigkundige constructies zijn de proceskrachten vaak veel groter dan de door de zwaartekracht veroorzaakte belastingen. De ontwerper dient zich te realiseren hoe de krachtwegen in de machine gesloten zijn. Het onderwijs in de sterkteleer zou hieraan een welkome bijdrage kunnen leveren door vraagstukken op andere wijze te presenteren dan gebruikelijk. Hierbij is een voorbeeld voor een alternatieve presentatie gegeven.

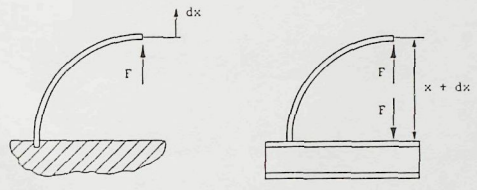

5. Het gebruik van het "Bode-diagram" in de servo-techniek en bij de analyse van dynamisch gedrag van systemen is charmant omdat door de logarithmische schalen alles wat krom is recht wordt gemaakt. De gebruikte standaard dimensieloze prestatie, (dB), leidt echter tot een ongedisciplineerd meetgedrag en spraakgebruik en, erger, tot een afname van het "begrijpend analyseren".

6. De beschikbare kennis over het gedrag van systemen met meer vrijheidsgraden zou beter overdraagbaar en toepasbaar worden indien bij het onderwijs meer aandacht wordt besteed aan het visueel begrijpelijk maken van het wiskundige verschijnsel van de "orthogonale coordinaat".

7. In tegenstelling tot de algemeen bestaande indruk vergt het vakgebied van de "aangepaste technologie" een technische inspanning van hoger niveau dan onze Westerse technologie. Het is in het belang van ontwikkelingslanden dat de hulpverlenende organisaties tijdig tot dit inzicht komen.

8. Het modelleren van een permanente magneet door een combinatie van een kortgesloten, weerstandsloze spoel en een magnetische weerstand levert een mathematisch gelijk maar energetisch beter model dan het gangbare model met een bron van constante stroom.

9. Het rechtsgevoel in onze samenleving wordt voortdurend bedreigd door de regelzucht van de wetgever. Om in deze gespannen verhouding enige ontspanning te verkrijgen is het aan te bevelen om in de verkeerslichten voor voetgangers het rode licht te vervangen door een oranje licht.

April 1985

Jan van Eijk